3.2 Run1ga - Side

The run1ga is a 30-foot impact followed by a crush impact, with the crush plate centered above the CV flange. The run1g 30-foot impact restart file was used and the crush plate was moved during the restart phase so that its centerline was approximately above the CV flange. The 30-foot impact was from time 0.0 to 0.0085 sec. The crush plate translation to center it above the CV flange was from time 0.0085 sec to 0.0086 sec. The run1ga crush occurred from 0.0086 sec to 0.027 sec. Therefore, the 30-foot impact results for this run would be the Section 3.1, 30-foot results for run1g, and the crush results for run 1ga (offset crush) are presented in this section.

Figure 3.2.1 shows the configuration of the model after the crush plate was moved above the CV flange (time = 0.0086 sec). Figure 3.2.2 shows the model configuration after the run1ga crush impact. Figure 3.2.3 through Figure 3.2.6 show enlarged views in the lid and bottom regions of the package assembly.

Figure 3.2.7 shows that the maximum strain in the CV body for the run1ga crush impact is 0.0348 in/in. The effective plastic strain in the CV lid is 0.0002 in/in and is shown in Figure 3.2.8. The CV nut ring remains elastic for the crush impact of run1ga.

The maximum effective plastic strain in the drum angle is shown in Figure 3.2.9 to be 0.1058 in/in. The maximum effective plastic strain in the drum is 0.3818 in/in and occurs in the top drum roll near the crush plate (Figure 3.2.10).

Figure 3.2.11 gives the maximum effective plastic strain in the lid to be 1.1345 in/in. This is a relatively high strain level and the maximum occurs near the stud hole at the 90° position (initially along Y axis). Another high region of strain is near the upper stud nearest the crush plate. The solid elements (used for contact bearing on the studs) around the stud holes show effective plastic strain maximum of 0.8745 in/in. The membrane effective plastic strain in the shell elements is a maximum of 0.8057 in/in and is highly localized near the stud hole at the 90° position. Some tearing of the lid could occur in the lid hole at the 90° position and at the lid hole nearest the crush plate (180°).

Figure 3.2.12 shows the effective plastic strain levels in the drum studs. The maximum is shown to be 0.5207 in/in and occurs in the stud at the 90° position. From Figure 3.2.12 it is seen that the elevated strain occurs near the outer extreme of the stud, and that the through thickness strain levels between 0.3170 and 0.3802 in/in exist.

A study of the timing of the elevated effective plastic strain levels in the lid and the drum studs shows that the lid reaches failure magnitudes before the studs. At the stud hole in the drum lid nearest the crush plate (180°), the bending strain crosses the 0.57 in/in strain at about 0.0122 seconds in the crush impact. The membrane strain in the lid elements at 180° reaches a maximum of .5295 in/in. The stud at 180° does not experience elevated strain levels (final maximum in this stud is 0.17 in/in). So at the 180° position, only the lid experiences relatively high levels of effective plastic strain.

At the 90° position in the lid, the membrane effective plastic strain exceeds the 0.57 in/in level near 0.0164 seconds in the crush impact. The surface maximum effective plastic strain exceeds 0.57 in/in at about 0.0161 seconds, slightly ahead of the membrane. At time 0.0164 seconds, the effective plastic strain levels in the stud at 90° is about 0.35 in/in maximum, with the through thickness levels between 0.104 in/in to 0.136 in/in. Therefore, at the 90° position, the lid reaches the failure level of 0.57 in/in before the stud.

From this timing data, it is shown that the lid would reach failure levels in bending and membrane before the stud effective plastic strain levels become relatively high. Therefore, it would be expected that the lid would locally tear before the bolting reached elevated effective plastic strain levels, thus possibly reducing the loadings on the studs. Due to the extent of the relatively high levels of effective plastic strain in the drum lid, it would be expected that any lid tearing would be localized and that the large washers would restrain the drum lid.

The effective plastic strain contour patterns for the other components are not shown in figures. The maximum effective plastic strain in the drum bottom is 0.2444 in/in; in the liner it is 0.2853 in/in; in the lid stiffener it is 0.1116 in/in; in the drum stud nuts it is 0.0103 in/in; in the drum stud washers it is 0.1685 in/in and in the plug liner it is 0.2181 in/in.

The kinetic energy time history for the crush plate impact is shown in Figure 3.2.13. The X velocity time history is shown in Figure 3.2.14.

The lid separation time history is shown in Figure 3.2.15 (nodes defined in Figure 3.1.30). From Figure 3.2.15 it is seen that the spike separation of just under 0.004 inches can occur with a final nominal separation of less than 0.002 inches expected.

The kaolite thickness time histories for the nodes defined in Figure 3.1.32 are given in Figure 3.2.16 for run1ga. The drum diameter time histories are given in Figures 3.2.17 and 3.2.18. The nodes defining this response are shown in Figure 3.1.34. As shown in Figure 3.2.17, the bottom head and the bottom drum roll remain at, or near 30-foot impact diameters for the crush impact. This response is expected as qualitatively shown in Figure 3.2.2. The response in the Y-direction is shown in Figure 3.2.18.

Figure 3.2.19 shows the diameter time history for various locations along the liner length. Figure 3.1.37 and Table 3.1.3 define the locations at which the diameters are obtained.

art A - Initial Design with Borobond Cylinder

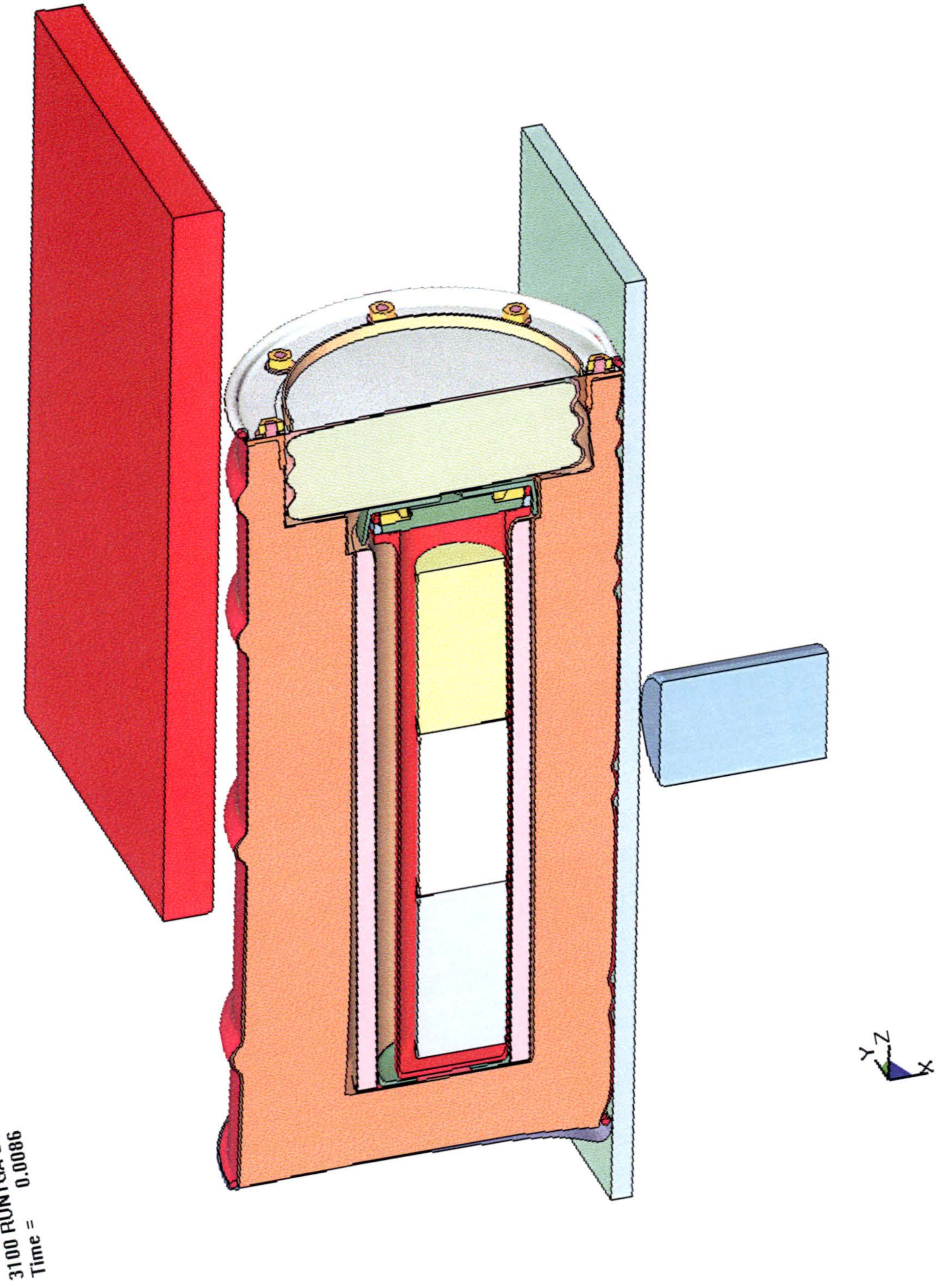

Figure 3.2.1 - Run1ga, Crush Impact, Initial Configuration for the Crush Impact

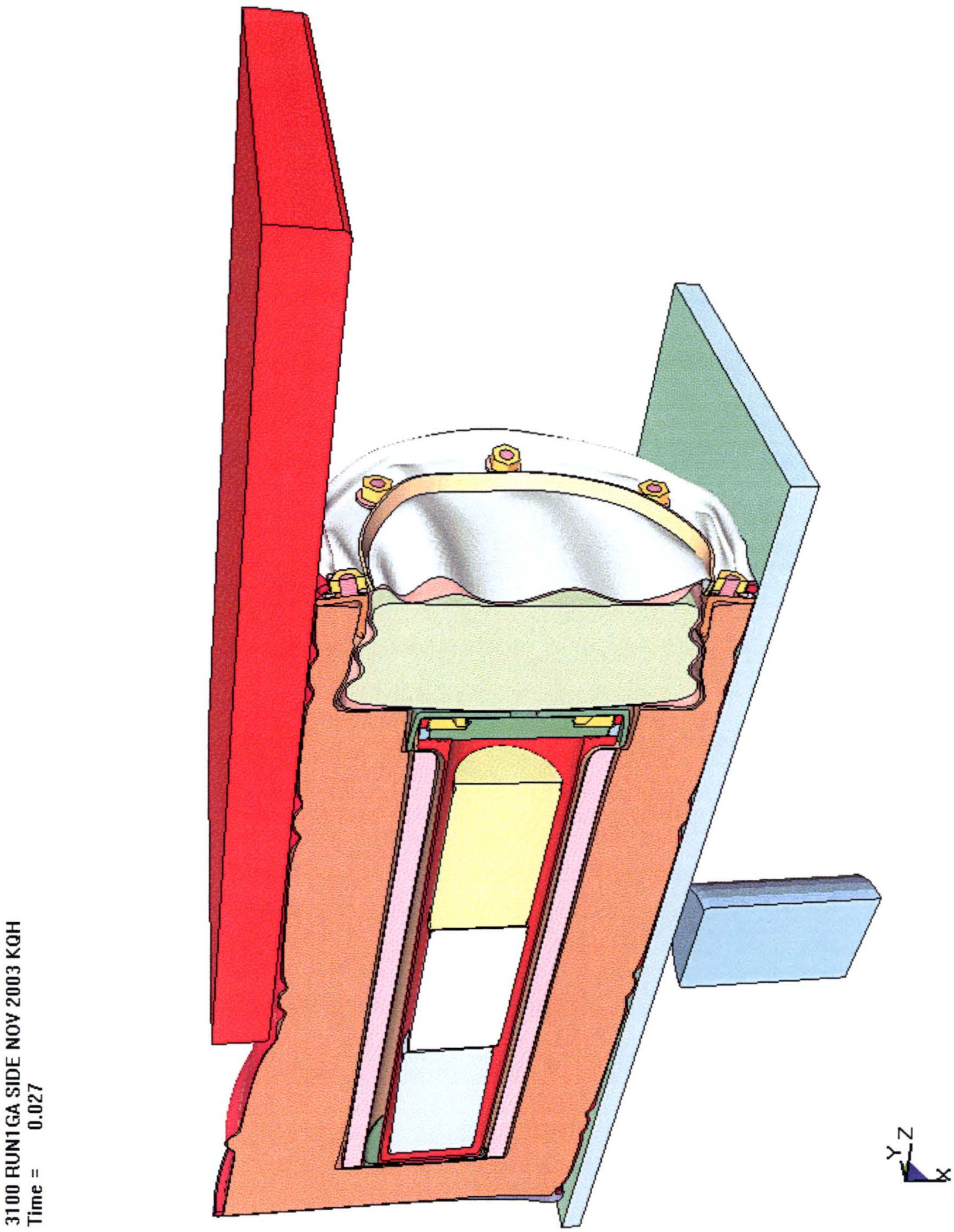

Figure 3.2.2 - Run1ga, Crush Impact, Configuration of the ES-3100 After the Crush Impact

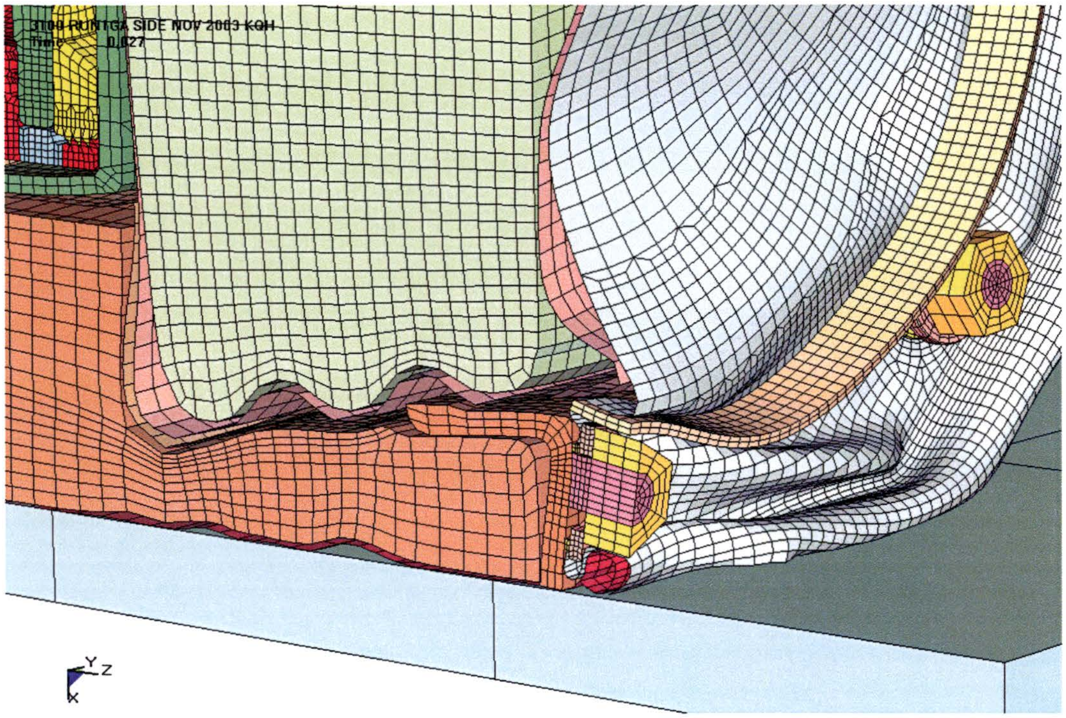

Figure 3.2.3 - Run1ga, Crush Impact, Configuration of the Lid Region Near the Rigid Plane

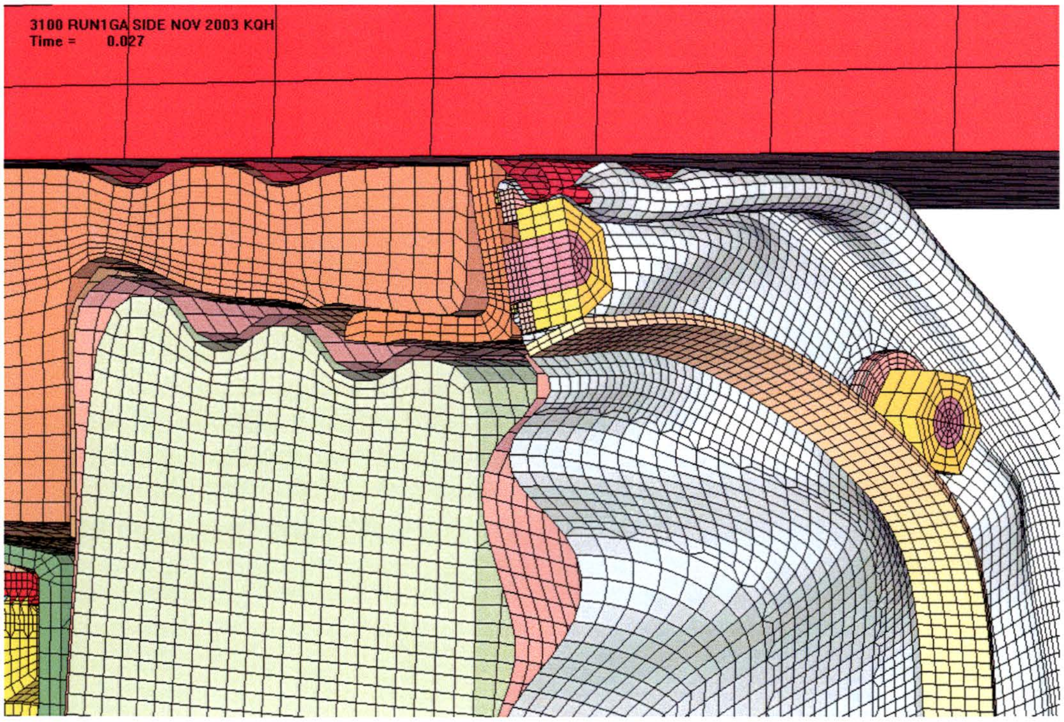

Figure 3.2.4 - Run1ga, Crush Impact, Configuration of the Lid Region Near the Crush Plate

Part A - Initial Design with Borobond Cylinder

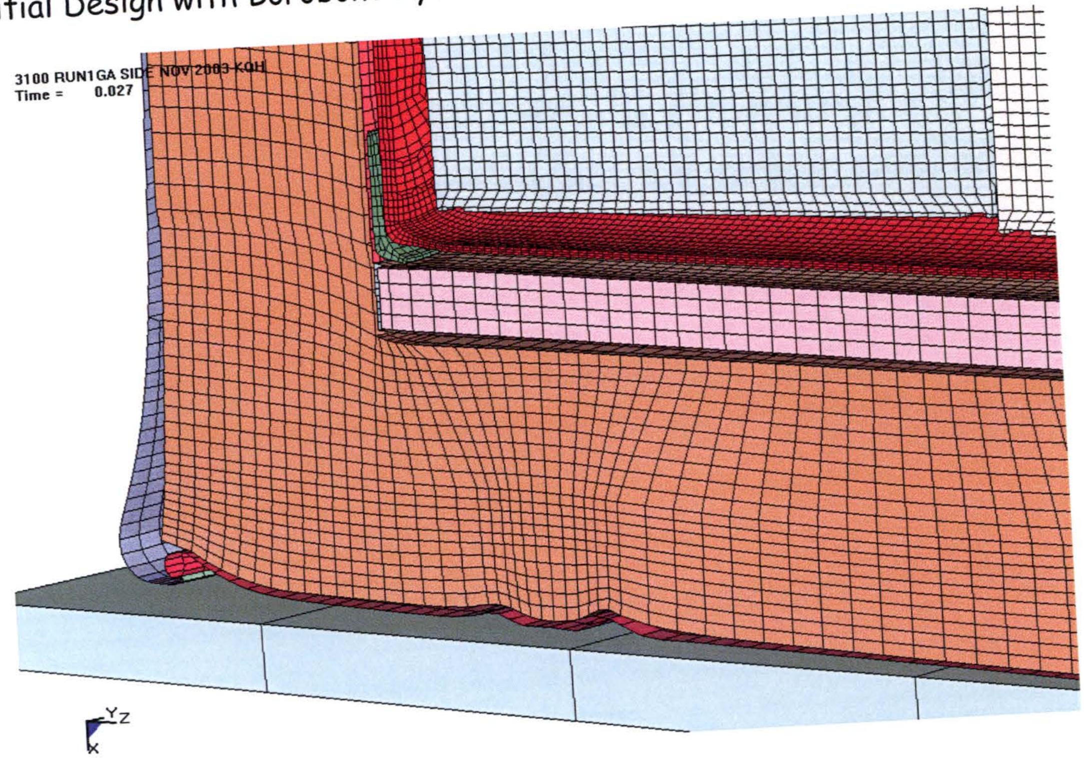

Figure 3.2.5 - Run1ga, Crush Impact, Configuration of the Bottom Near the Rigid Plate

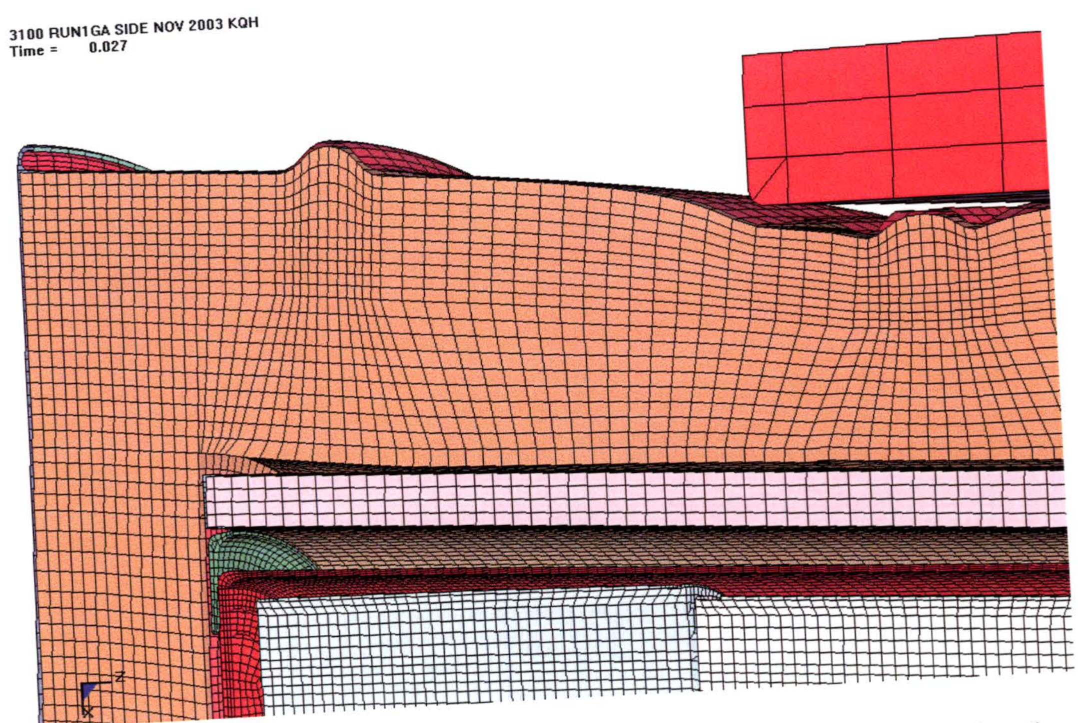

Figure 3.2.6 - Run1ga, Crush Impact, Configuration of the Bottom Near the Crush Plate

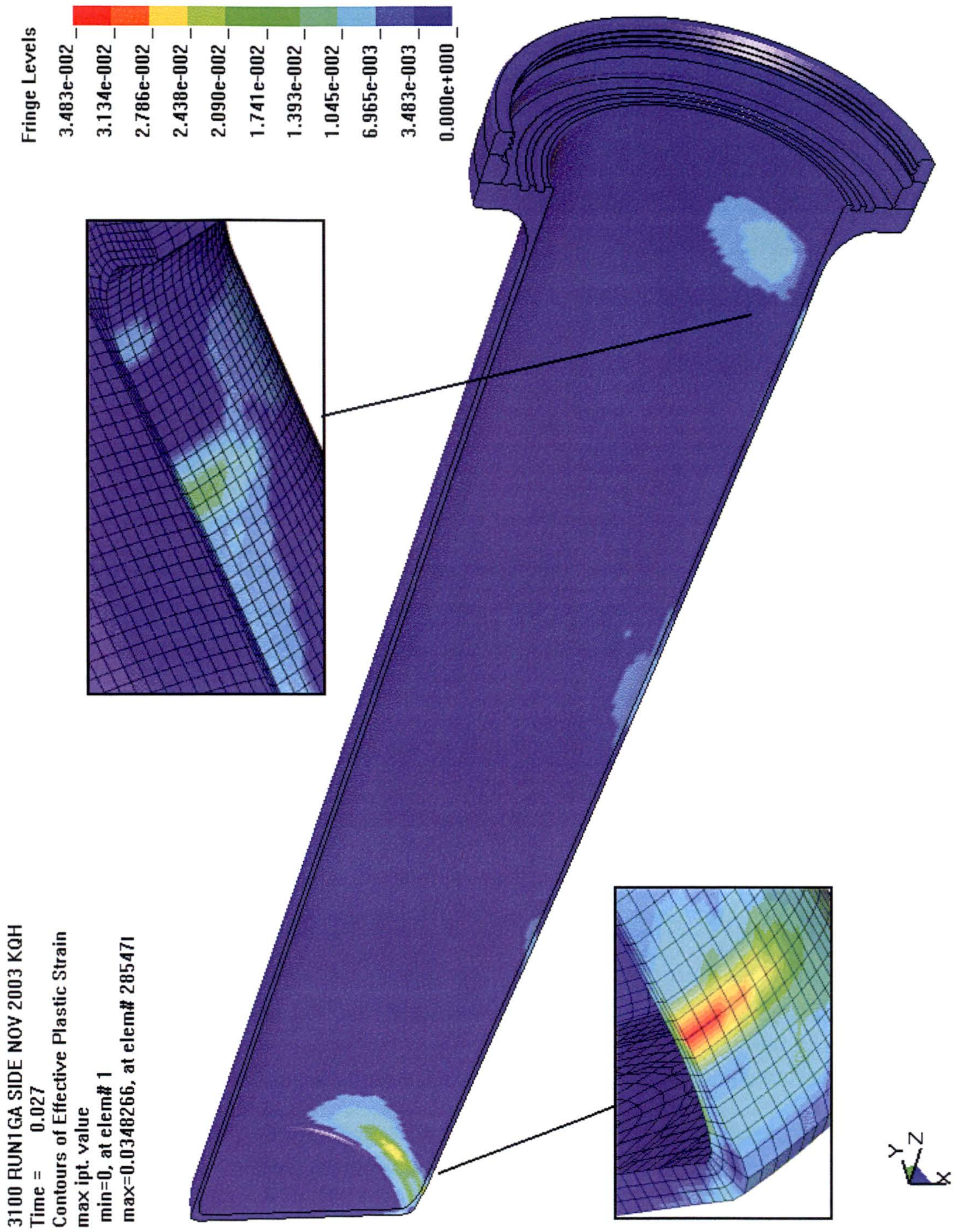

Figure 3.2.7 - Run1ga, Crush Impact, Effective Plastic Strain in the CV Body

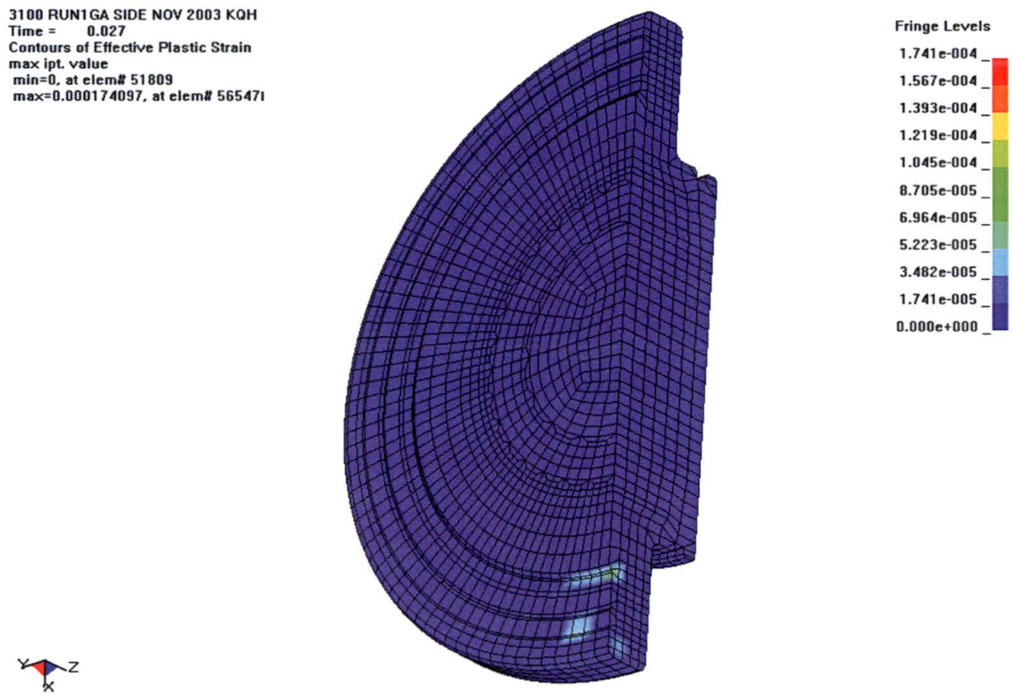

Figure 3.2.8 - Run1ga, Crush Impact, Effective Plastic Strain in the CV Lid

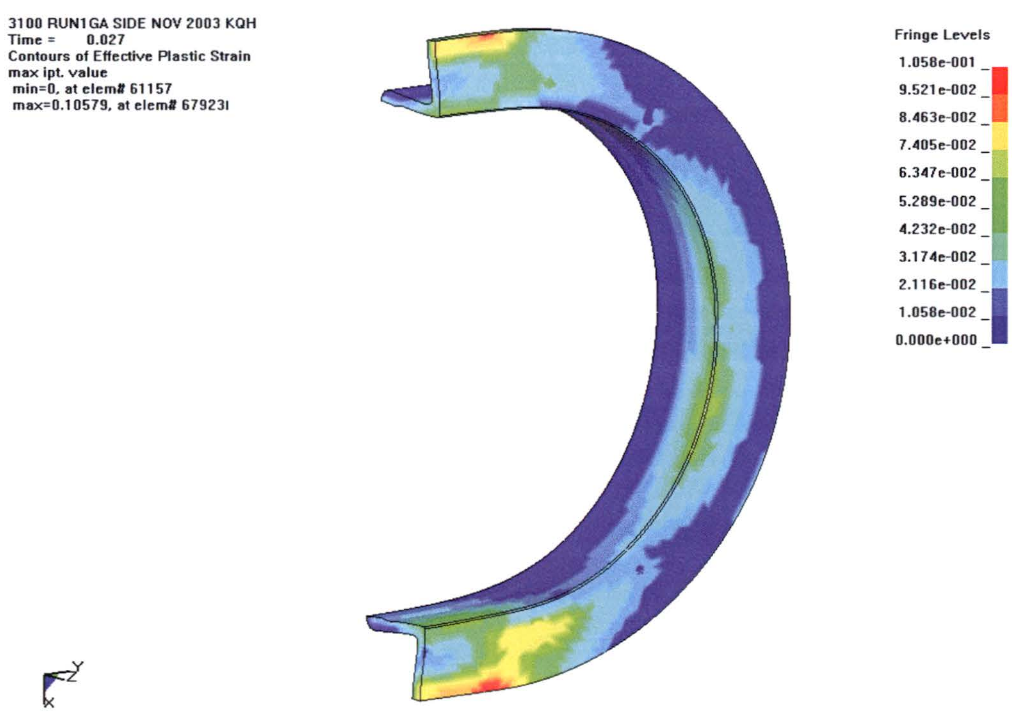

Figure 3.2.9 - Run1ga, Crush Impact, Effective Plastic Strain in the Drum Angle

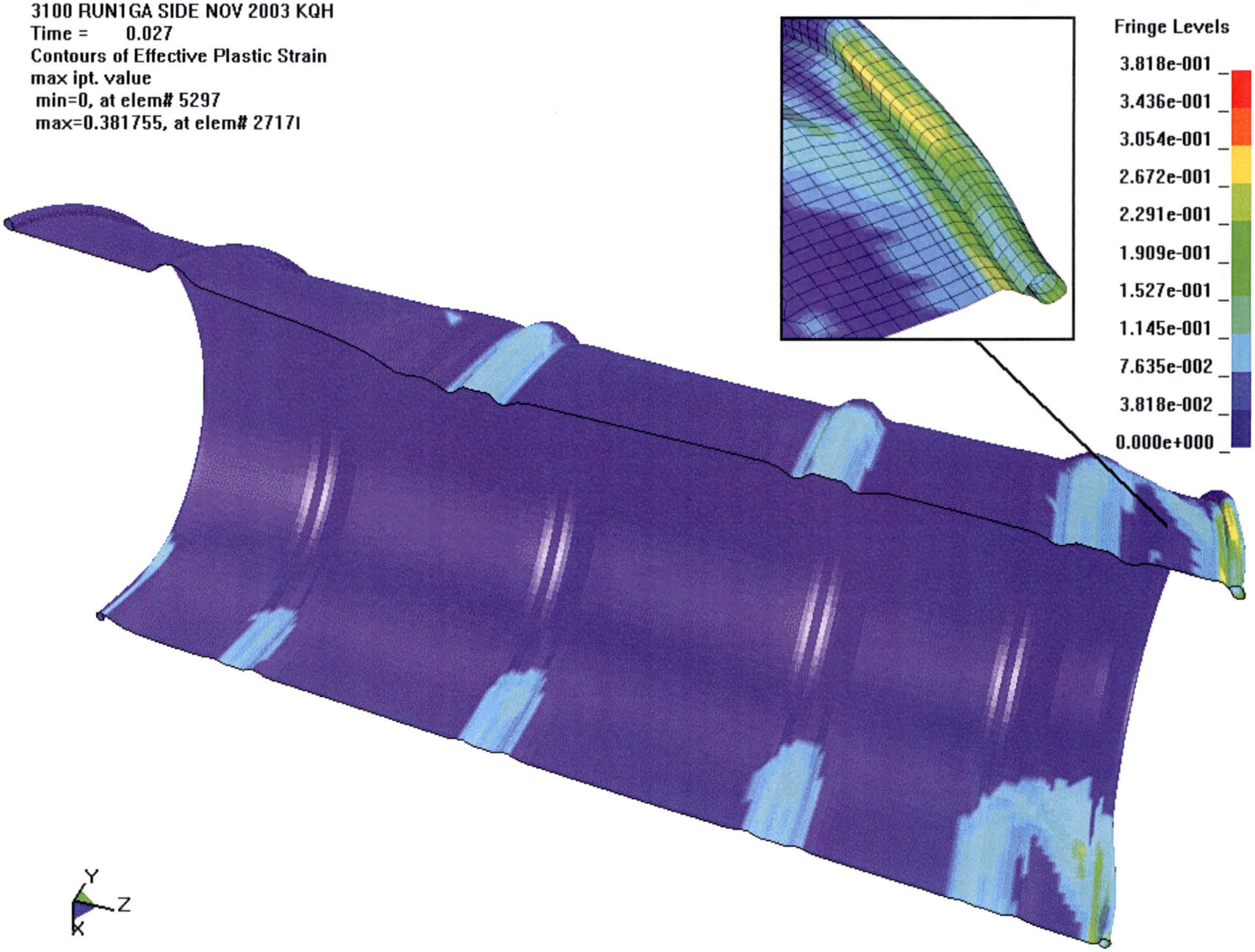

Figure 3.2.10 - Run1ga, Crush Impact, Effective Plastic Strain in the Drum

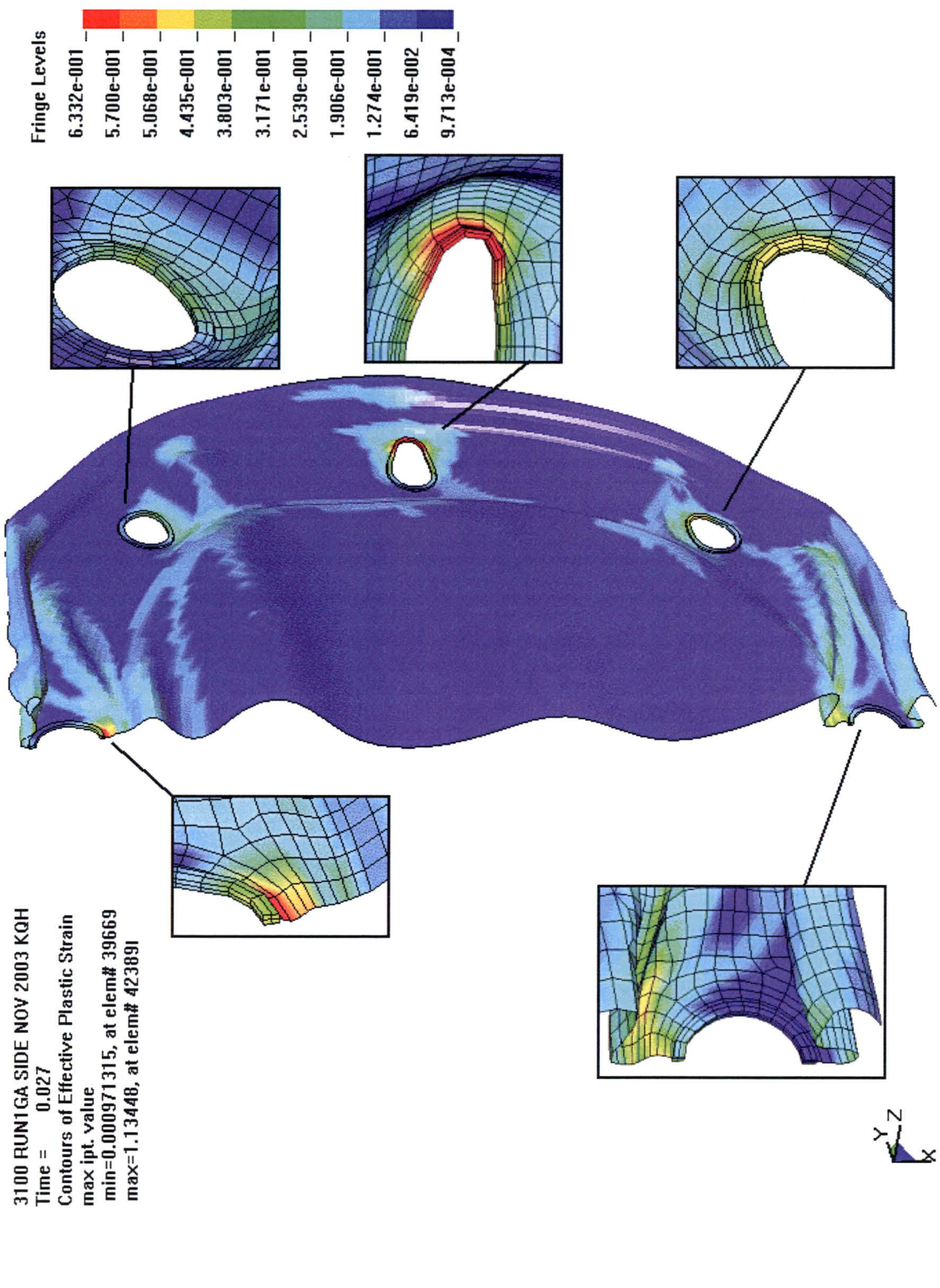

Figure 3.2.11 - Run1ga, Crush Impact, Effective Plastic Strain in the Lid

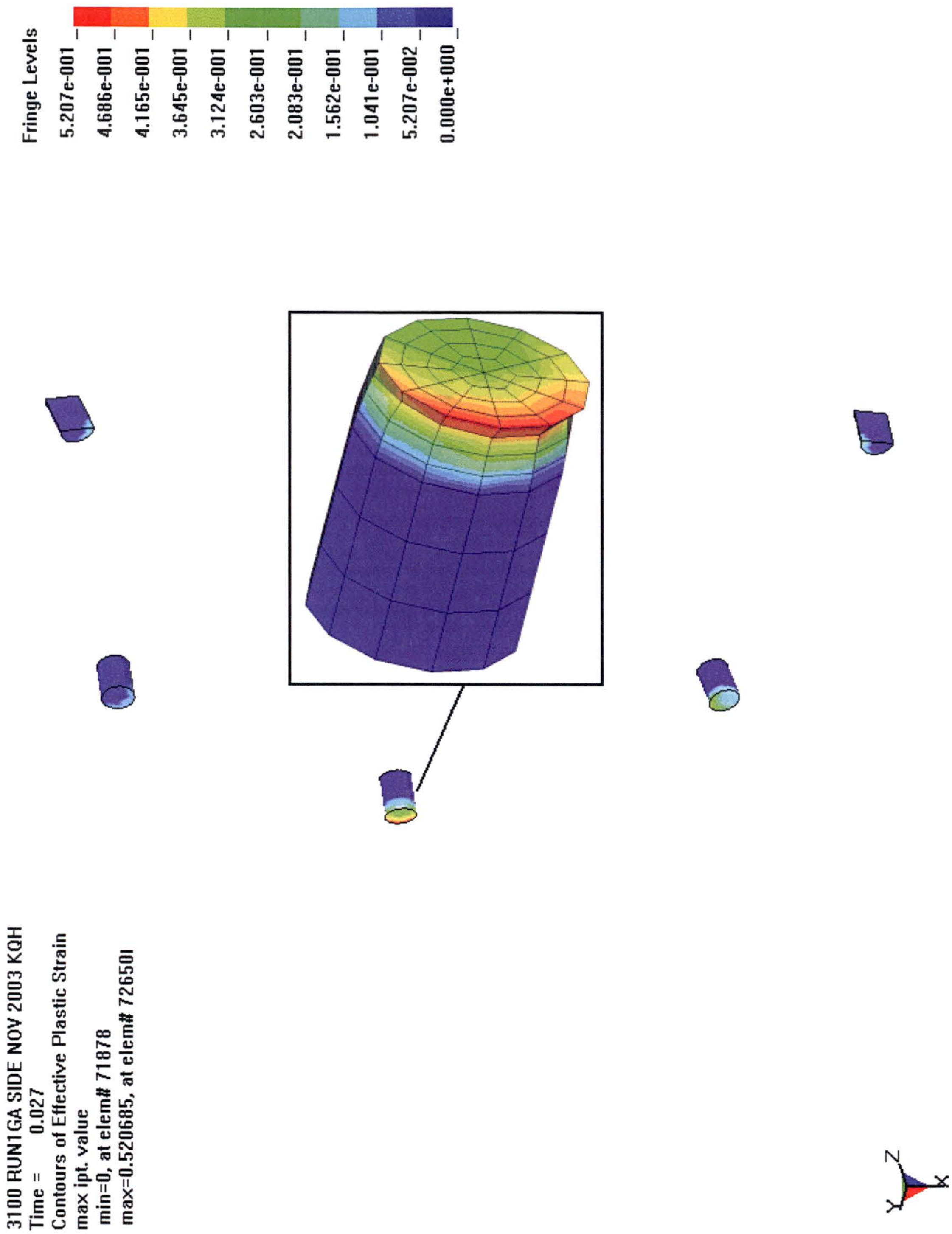

Figure 3.2.12 - Run1ga, Crush Impact, Effective Plastic Strain in the Drum Studs

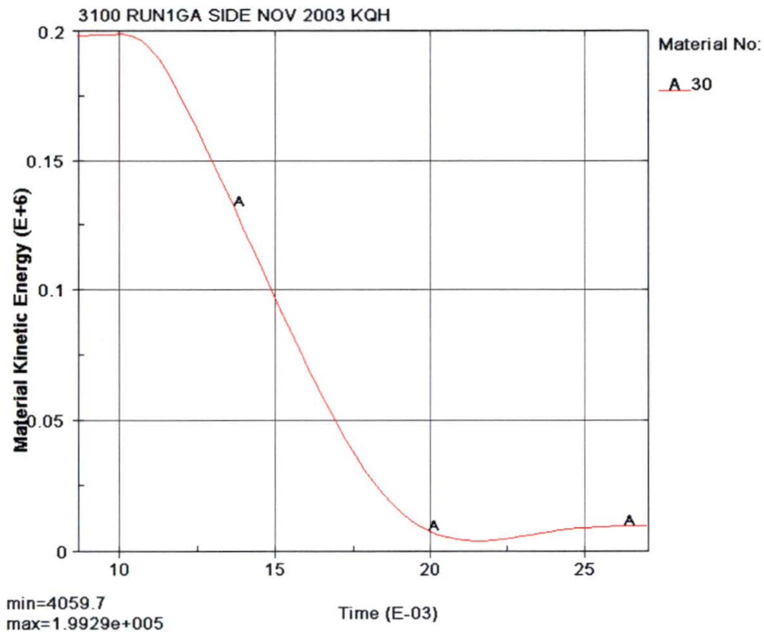

Figure 3.2.13 - Run1ga, Crush Impact, Kinetic Energy Time History

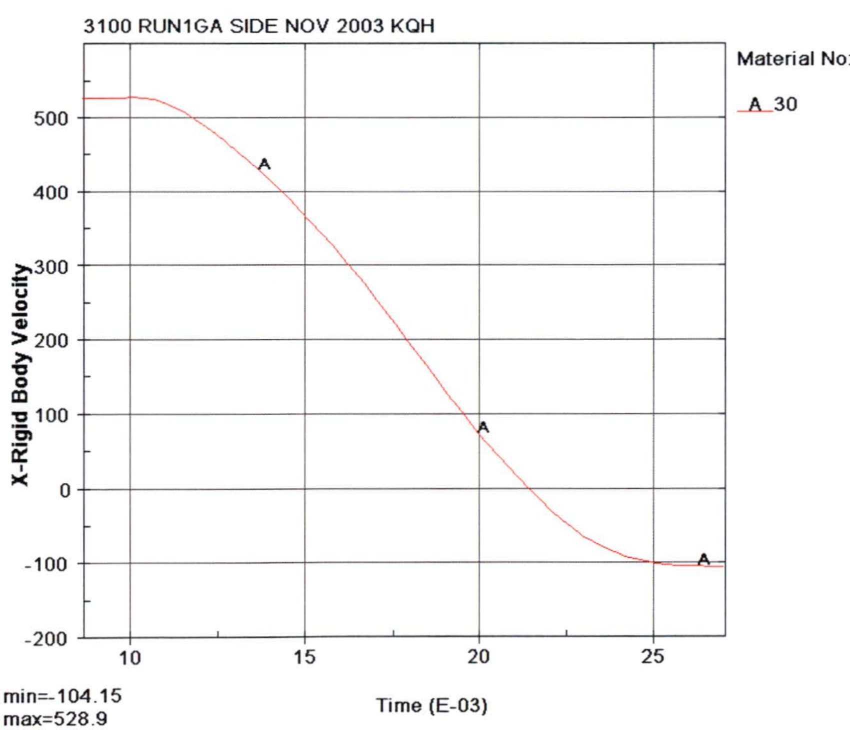

Figure 3.2.14 - Run1ga, Crush Impact, X Velocity Time History

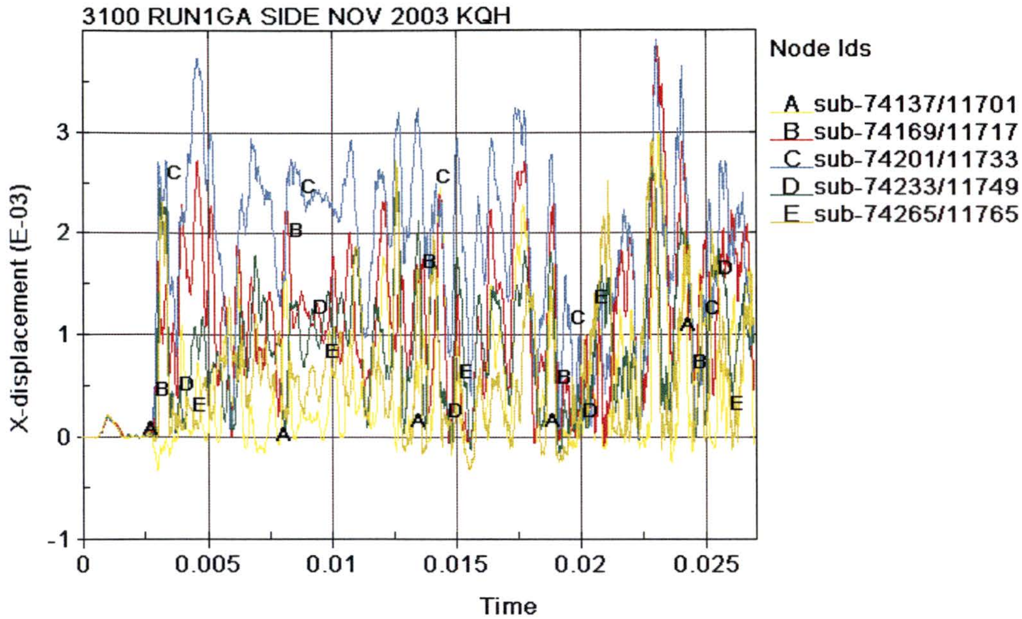

Figure 3.2.15 - Run1ga, Lid Separation Time History

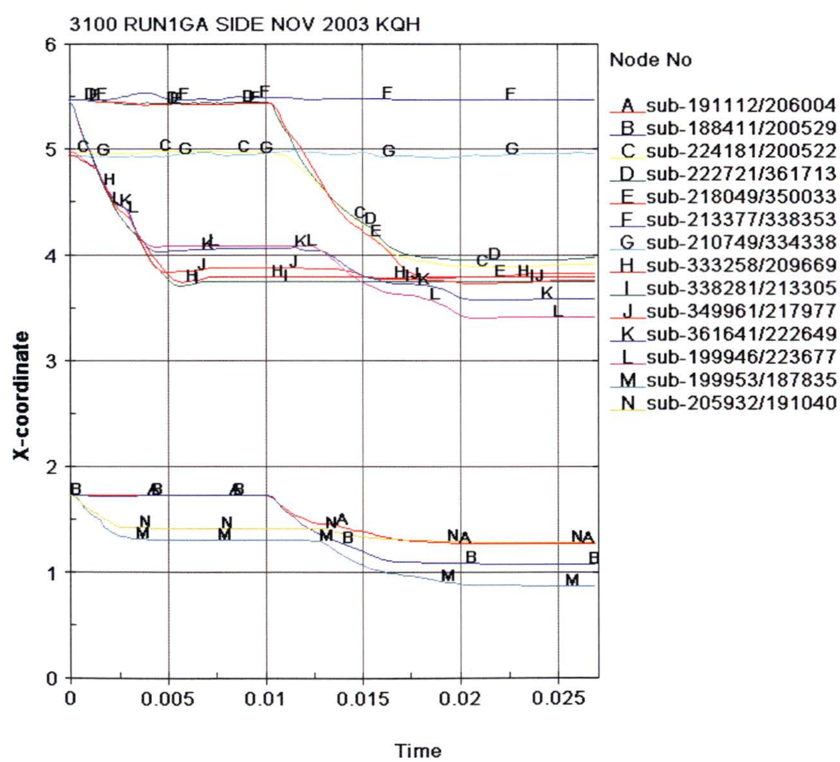

Figure 3.2.16 - Run1ga, Drum Kaolite Thickness Time Histories

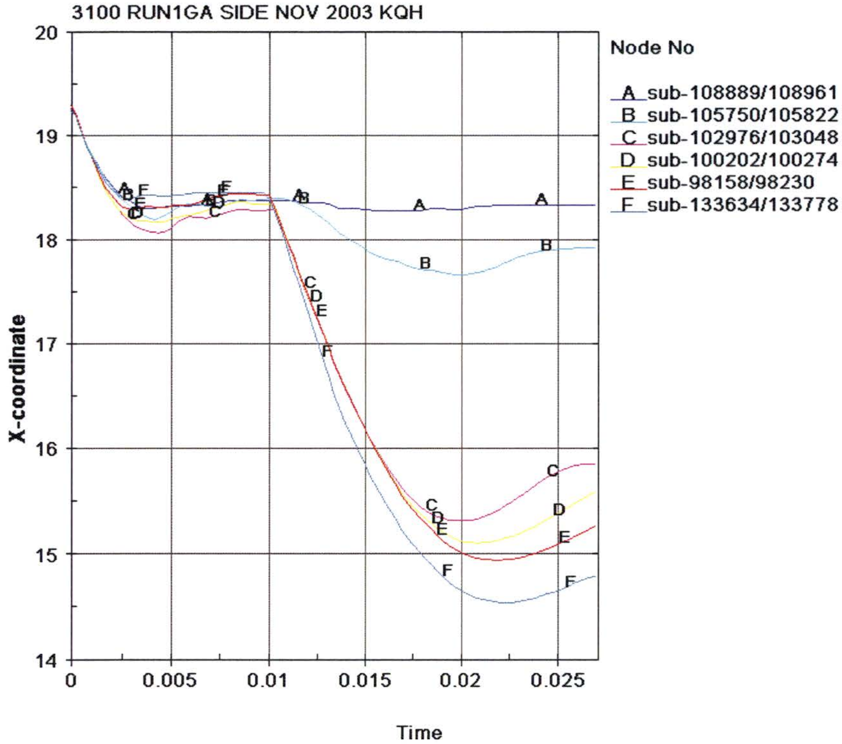

Figure 3.2.17 - Run1ga, Drum Dimension Time History in the X-Direction

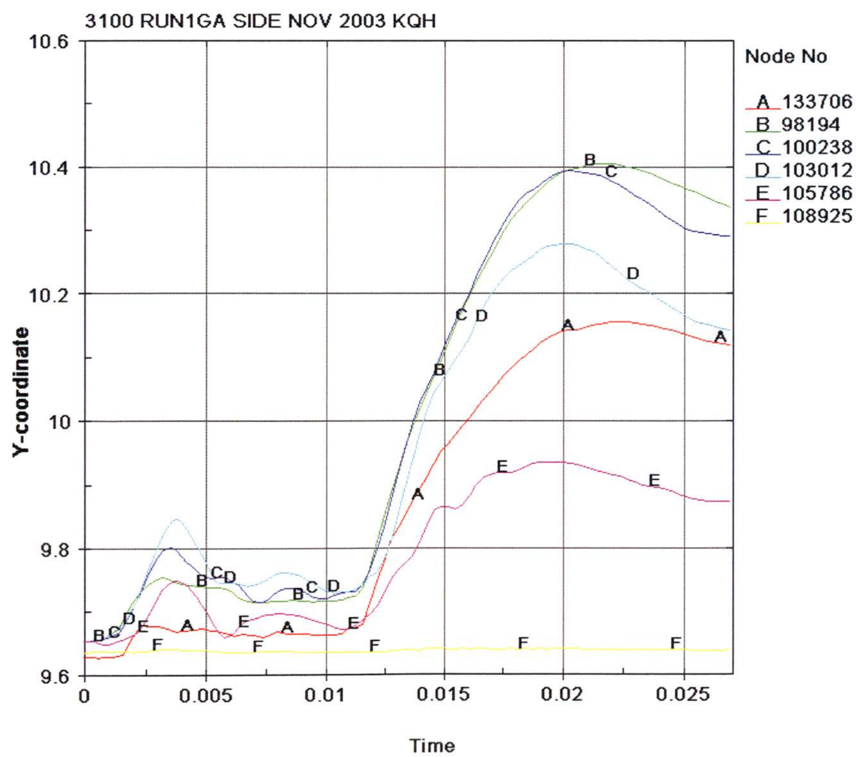

Figure 3.2.18 - Run1ga, Drum Dimension Time History in the Y-Direction

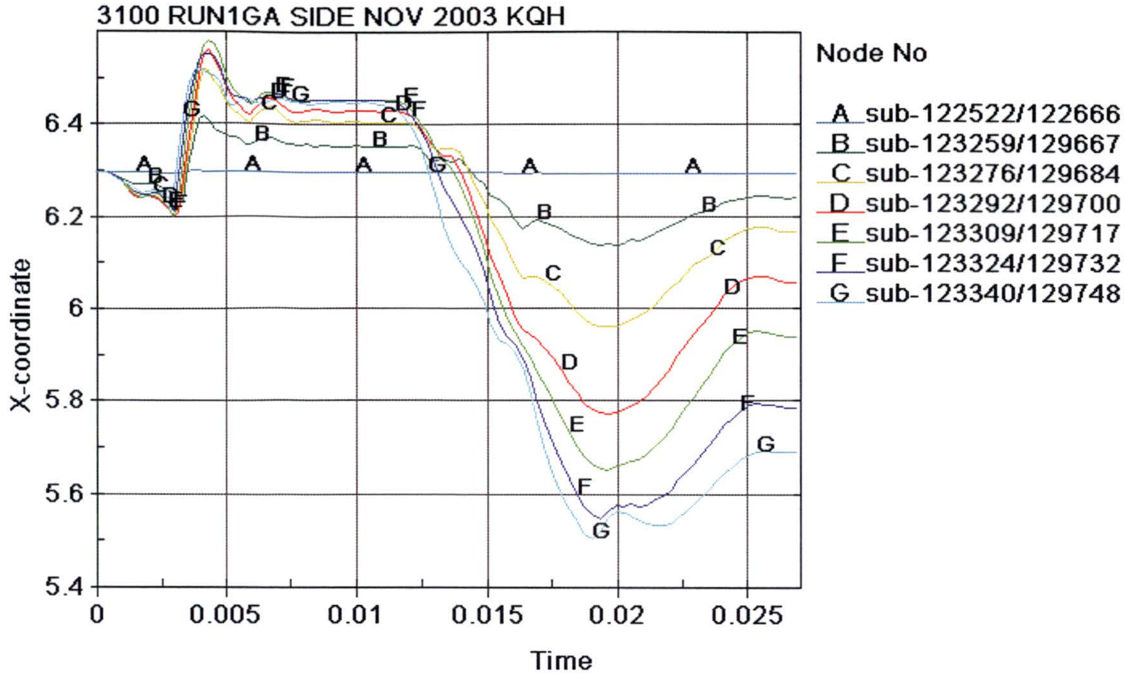

Figure 3.2.19 - Run1ga, Liner Diameter Time History

3.3 Run1hl - Side

Run1hl is the lower bounding kaolite run (100°F). It is basically the run1g model, but with kaolite properties of section 2.3.5.2. It is a run with a 4-foot impact (time = 0 to 0.01 seconds), followed by a 30-foot impact (0.01 to 0.02 seconds), followed by a 30-foot crush impact (0.02 to 0.04 seconds), finally followed by a 40-inch punch impact (0.04 to 0.055 seconds). The initial configuration of run1hl is similar to Figure 3.1.1. The configuration after the 4-foot impact is shown in Figure 3.3.1. Figure 3.3.2 and 3.3.3 show the configuration at the extremes of the package.

The CV body undergoes plastic deformation in the 4-foot impact. The effective plastic strain in the CV body is shown in Figure 3.3.4 to have a maximum of 0.0263 in/in. The elevated plastic strain levels are near the CV bottom head. The CV lid and nut ring remain elastic during the 4-foot impact. The plastic strain in other components for the 4-foot impact are given in Table 3.3.1.

Table 3.3.1 - Run1hl, 4-Foot Impact, Effective Plastic Strain Levels in Some Components

Component	Effective Plastic Strain, in/in
Angle	0.0054
Drum	0.1561
Drum Bottom Head	0.0991
Liner	0.0537
Lid	0.1320
Lid Stiffener	0.0001
Lid Studs	0.0000
Lid Stud Nuts	0.0000
Lid Stud Washers	0.0011
Plug Liner	0.0022

Figure 3.3.5 shows the final configuration for the run1hl 30-foot impact. Figures 3.3.6 and 3.3.7 show the configurations for the package extremes.

The maximum effective plastic strain due to the 30-foot impact in the CV body is 0.0287 in/in as shown in Figure 3.3.8. The maximum effective plastic strain in the drum lid is shown to be 0.5180 in/in in Figure 3.3.9. The maximum lid strain is a surface strain at the stud hole nearest the rigid surface (0°). The membrane effective plastic strain component is 0.4026 in/in in the localized region near the stud hole. Effective plastic strain levels in other components for the 30-foot impact are given in Table 3.3.2.

Table 3.3.2 - Run1hl, 30-Foot Impact, Effective Plastic Strain Levels in Some Components

Component	Effective Plastic Strain, in/in
CV Lid	0.0001
CV Nut Ring	0.0000
Angle	0.0777
Drum	0.2250
Drum Bottom Head	0.2125
Liner	0.1800
Lid Stiffener	0.0118
Lid Studs	0.1098
Lid Stud Nuts	0.0000
Lid Stud Washers	0.0225
Plug Liner	0.0956

The final configuration for the crush impact is shown in Figure 3.3.10. The configuration at the package extremes are shown in Figure 3.3.11. The maximum effective plastic strain in the CV body is 0.0287 in/in as shown in Figure 3.3.12. The maximum effective plastic strain in the drum for the crush impact is 0.5309 in/in (surface strain). The maximum in the drum occurs near the angle on the crush plate side of the drum as shown in Figure 3.3.13. The maximum membrane effective plastic strain at this location is 0.3616 in/in.

The maximum effective plastic strain in the lid is 1.2969 in/in (surface strain) and occurs just below the upper stud hole (hole nearest the crush plate, 180°) as shown in Figure 3.3.14. The maximum membrane effective plastic strain in this region of the lid is 0.8995 in/in. A time line investigation during the crush impact shows that the lid exceeds 0.57 in/in strain in bending at about 0.0228 seconds at the 180° stud hole. The crush impact started at about 0.0200 seconds, so the lid reaches failure level near the start of the crush impact. The membrane levels in the lid reach 0.57 in/in at about 0.0236 seconds.

The elevated effective plastic strain levels in the lid are localized in the region just inboard of the upper stud.

The effective plastic strain in the drum studs is 0.4159 in/in and occurs in the upper stud at the bearing of the lid onto the stud (180°). The elevated strains in the stud are localized on the inner surface. Effective plastic strain levels throughout the thickness of the stud are generally 0.25 in/in or less.

Considering the strain levels in the lid and the studs, some tearing in the lid at the 180° stud hole would be expected. But the tearing would be localized to the stud hole due to the extent of the strain patterns. Failure of the stud to restrain the lid due to this tearing is not expected. The lid stiffener would limit any tearing from the stud at 180° and the large washer would be expected to restrain the lid.

The effective plastic strain in other components due to the crush impact are listed in Table 3.3.3.

Table 3.3.3 - Run1hl, Crush Impact, Effective Plastic Strain Levels in Some Components

Component	Effective Plastic Strain, in/in
CV Lid	0.0003
CV Nut Ring	0.0000
Angle	0.1178
Drum Bottom Head	0.3342
Liner	0.2637
Lid Stiffener	0.0530
Lid Stud Nuts	0.0007
Lid Stud Washers	0.0832
Plug Liner	0.1255

The final configuration after the punch impact is shown in Figure 3.3.16. The effective plastic strain level in the CV body is shown in Figure 3.3.6. The maximum strain is 0.0299 in/in and is located near the bottom head. The effective plastic strain level in the drum after the punch impact remains at 0.5309 in/in as shown in Figure 3.3.18. The maximum effective plastic strain in the other package components for the punch impact are listed in Table 3.3.4.

Table 3.3.4 - Run1hl, Punch Impact, Effective Plastic Strain Levels in Some Components	
Component	Effective Plastic Strain, in/in
CV Lid	0.0006
CV Nut Ring	0.0000
Angle	0.1178
Drum Bottom Head	0.3345
Liner	0.2637
Lid	1.2971
Lid Stiffener	0.0530
Lid Studs	0.4221
Lid Stud Nuts	0.0007
Lid Stud Washers	0.0844
Plug Liner	0.1255

Figure 3.3.19 shows the lid separation time history for all the impacts. The CV lid separation shows a maximum spike separation of about 0.006 inches occurs during the punch. The spike is a response to the rebounding impact of the CV/weights. An average value of .003 in or less is demonstrated in the response when the solution is stopped.

Figure 3.3.20 shows the time history for the kaolite thicknesses. The nodal locations for nodes shown in Figure 3.3.20 are shown in Figure 3.1.32.

Figure 3.3.21 shows the diameter changes in the drum in the model X direction.
Figure 3.3.22 shows the radial changes in the Y direction (normal to the impact directions). The nodes are defined in Figure 3.1.34.

Figure 3.3.23 shows the liner diameter time history. The node pair locations are shown in Figure 3.1.37 and Table 3.1.3.

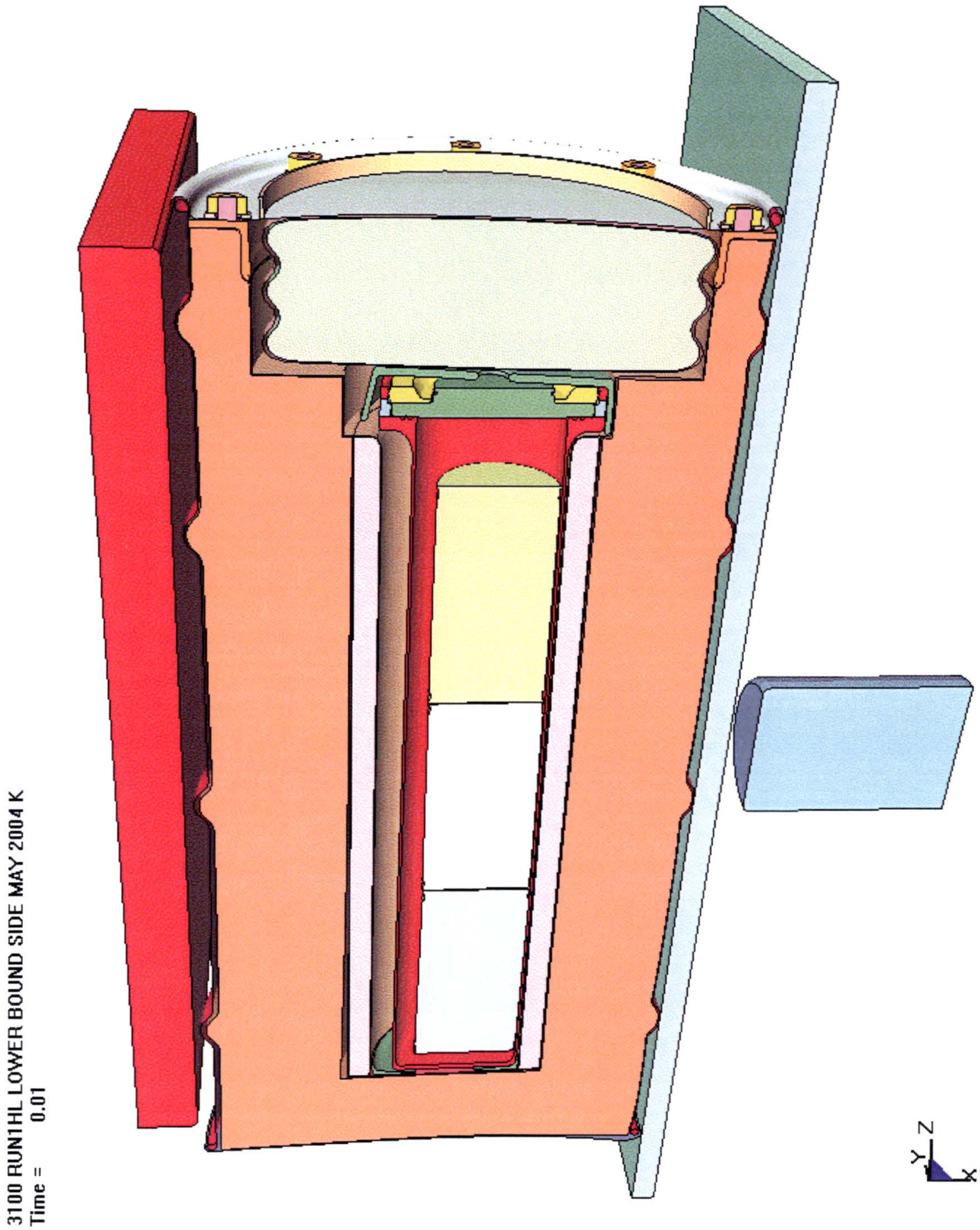

Figure 3.3.1 - Run1hl, 4-Foot Impact, Final Configuration

Part A - Initial Design with Borobond Cylinder

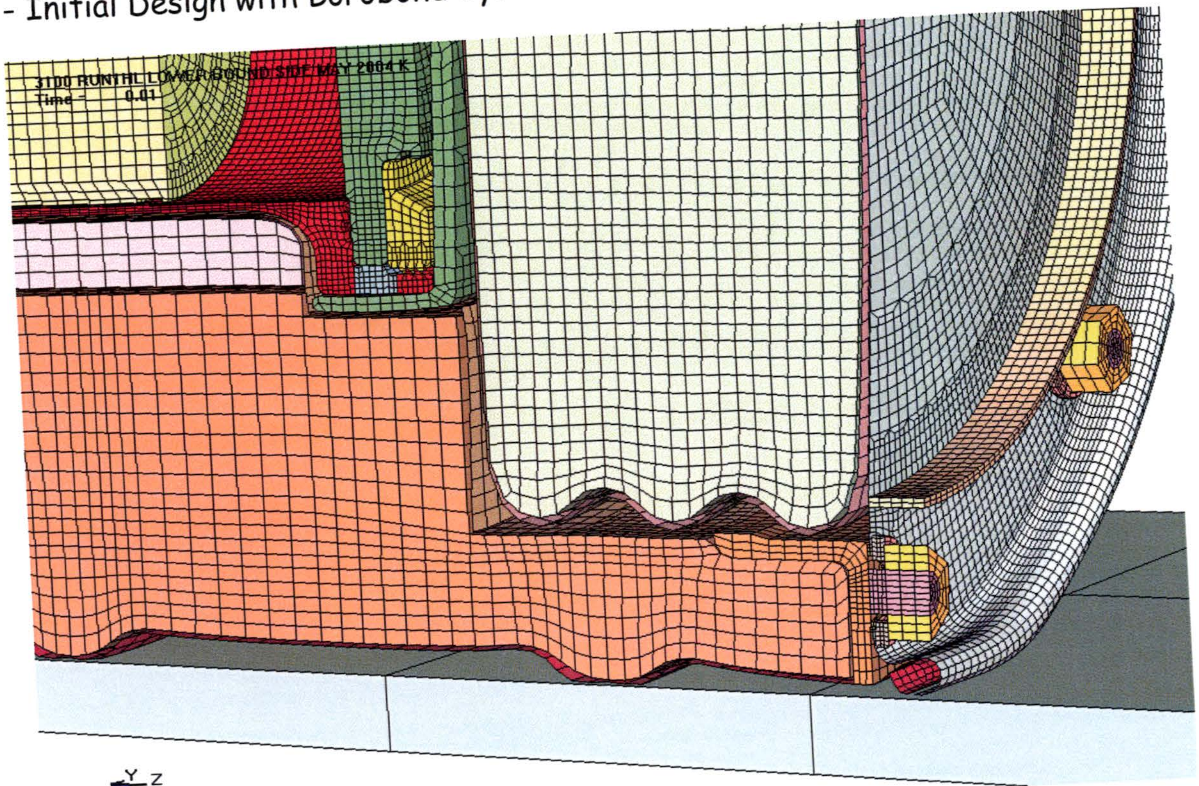

Figure 3.3.2 - Run1hl, 4-Foot Impact, Configuration in the Lid

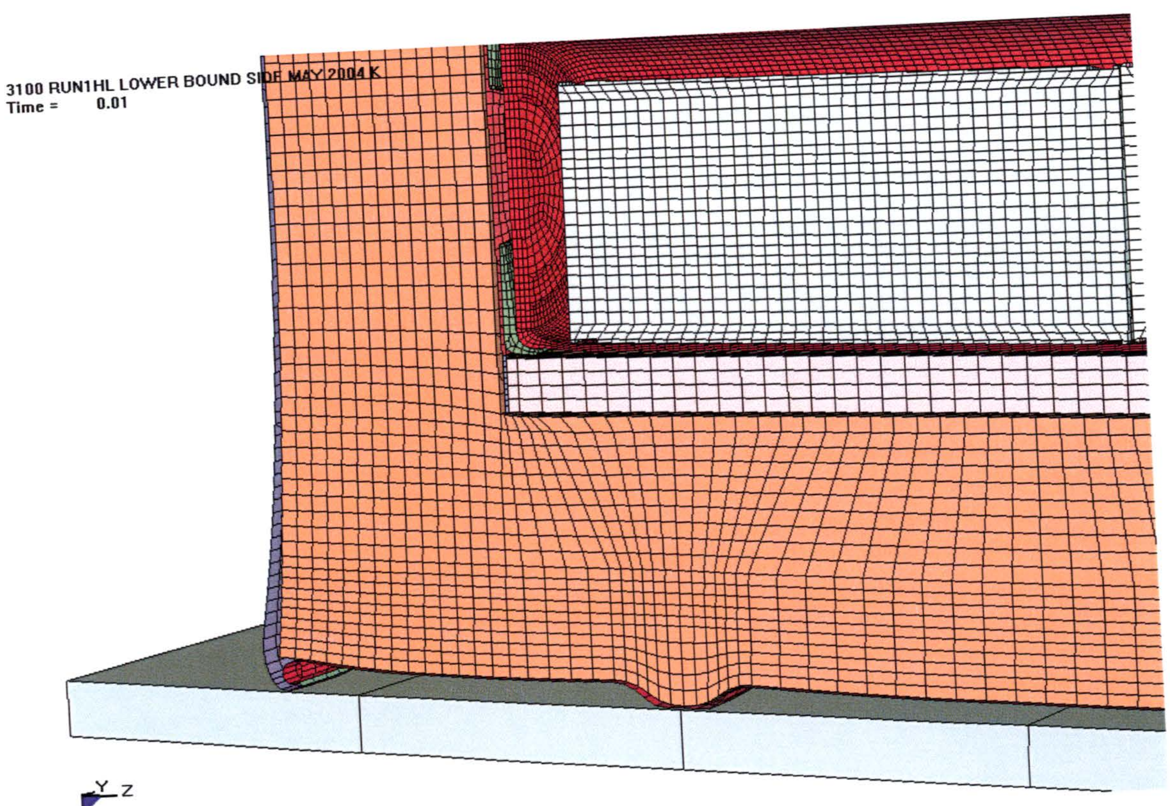

Figure 3.3.3 - Run1hl, 4-Foot Impact, Configuration in the Bottom

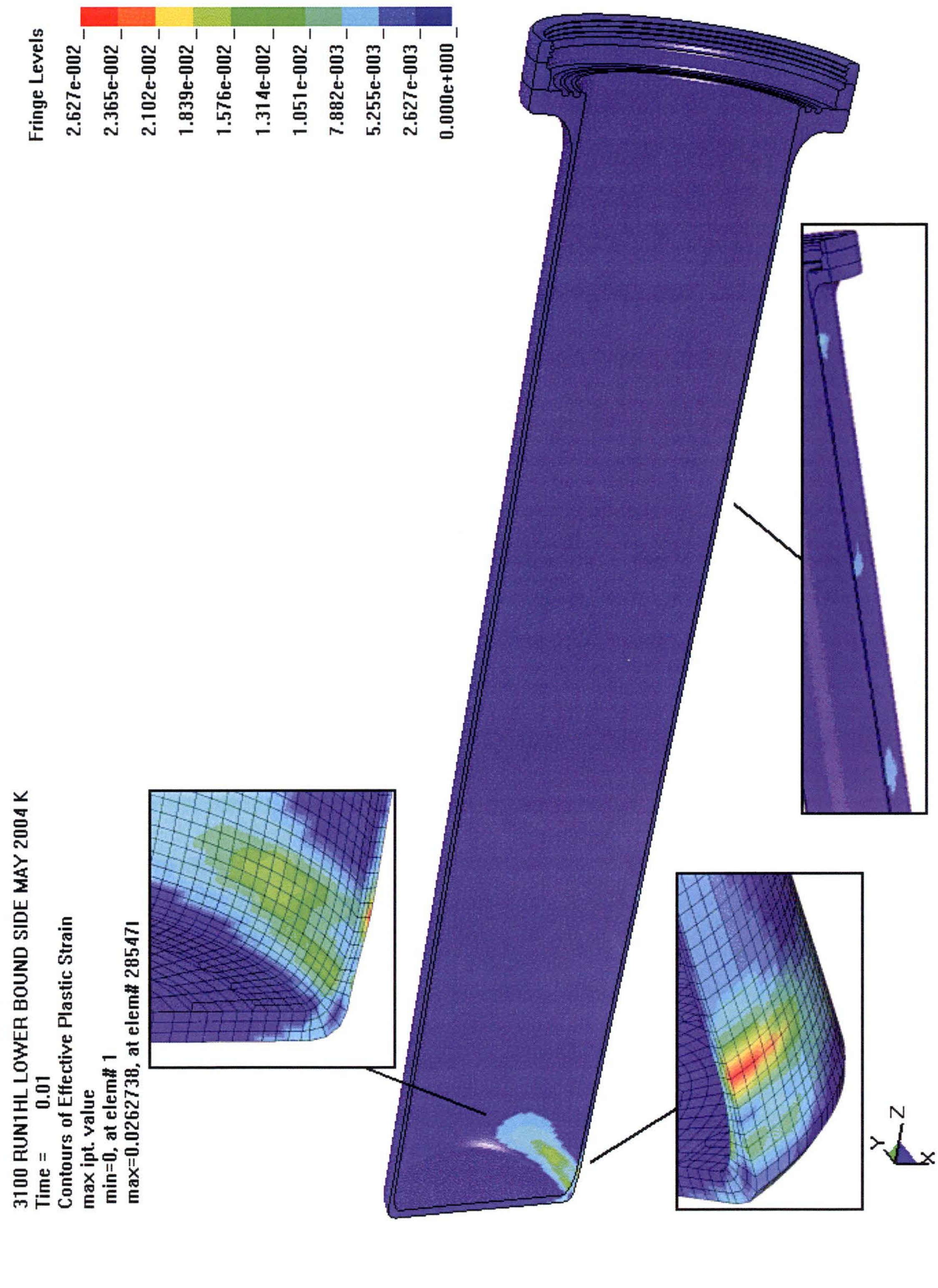

Figure 3.3.4 - Run1hl, 4-Foot Impact, Effective Plastic Strain in the CV Body

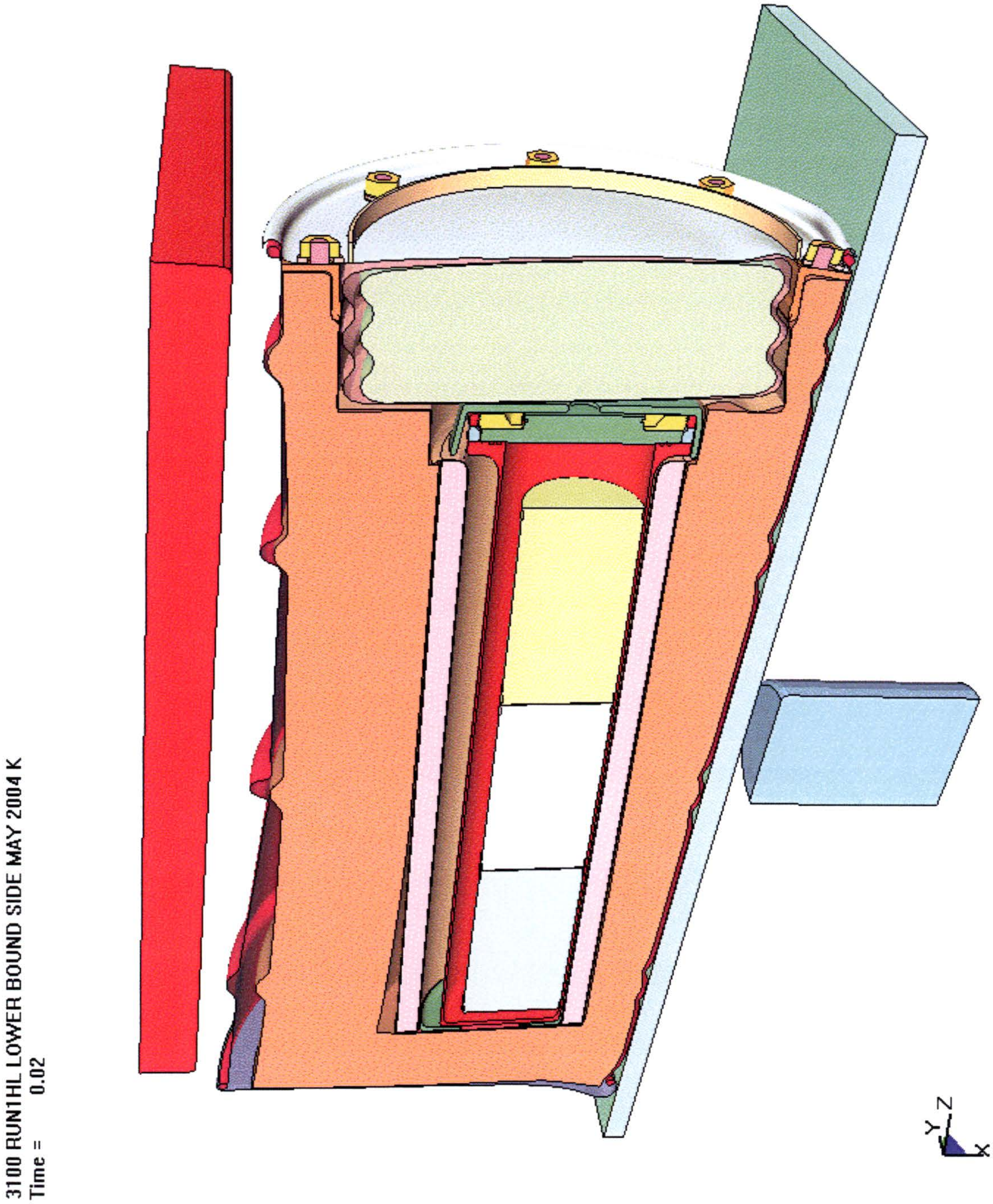

Figure 3.3.5 - Run1hl, 30-Foot Impact, Final Configuration

Part A - Initial Design with Borobond Cylinder

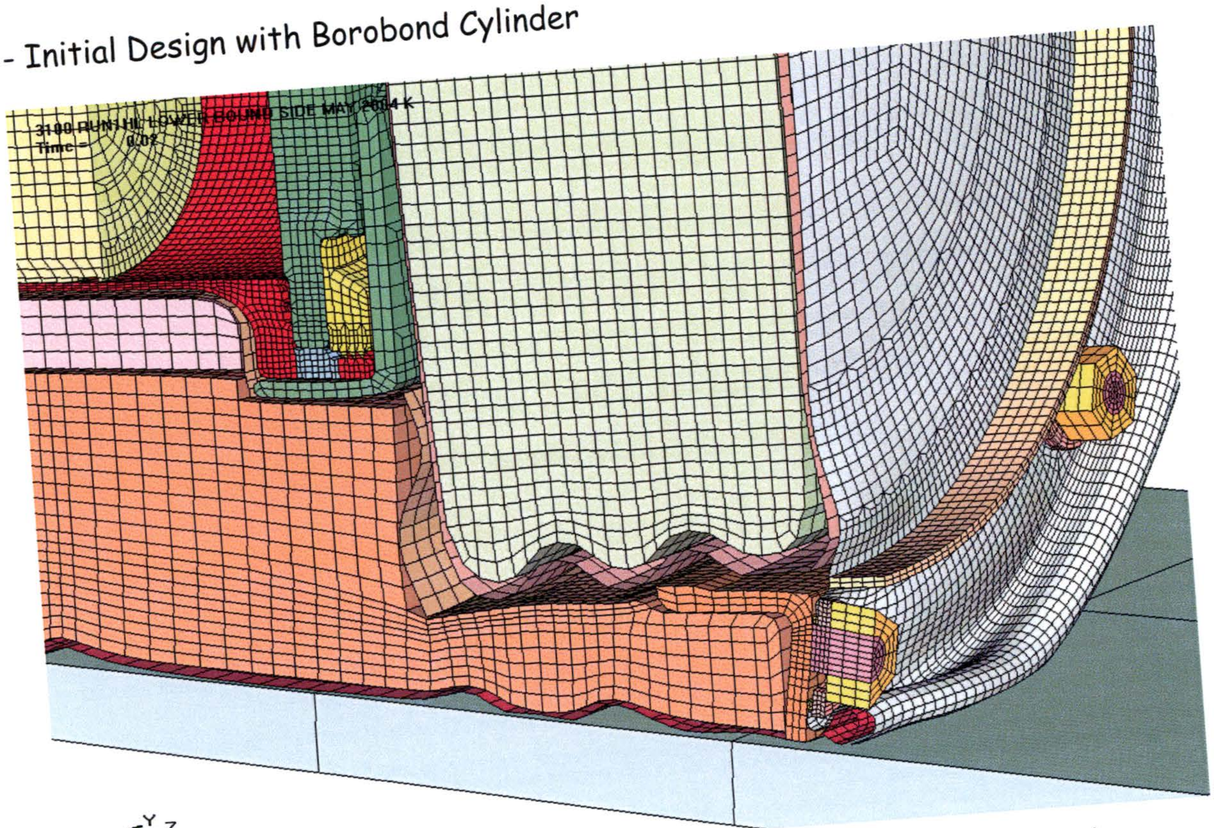

Figure 3.3.6 - Run1hl, 30-Foot Impact, Configuration of the Lid

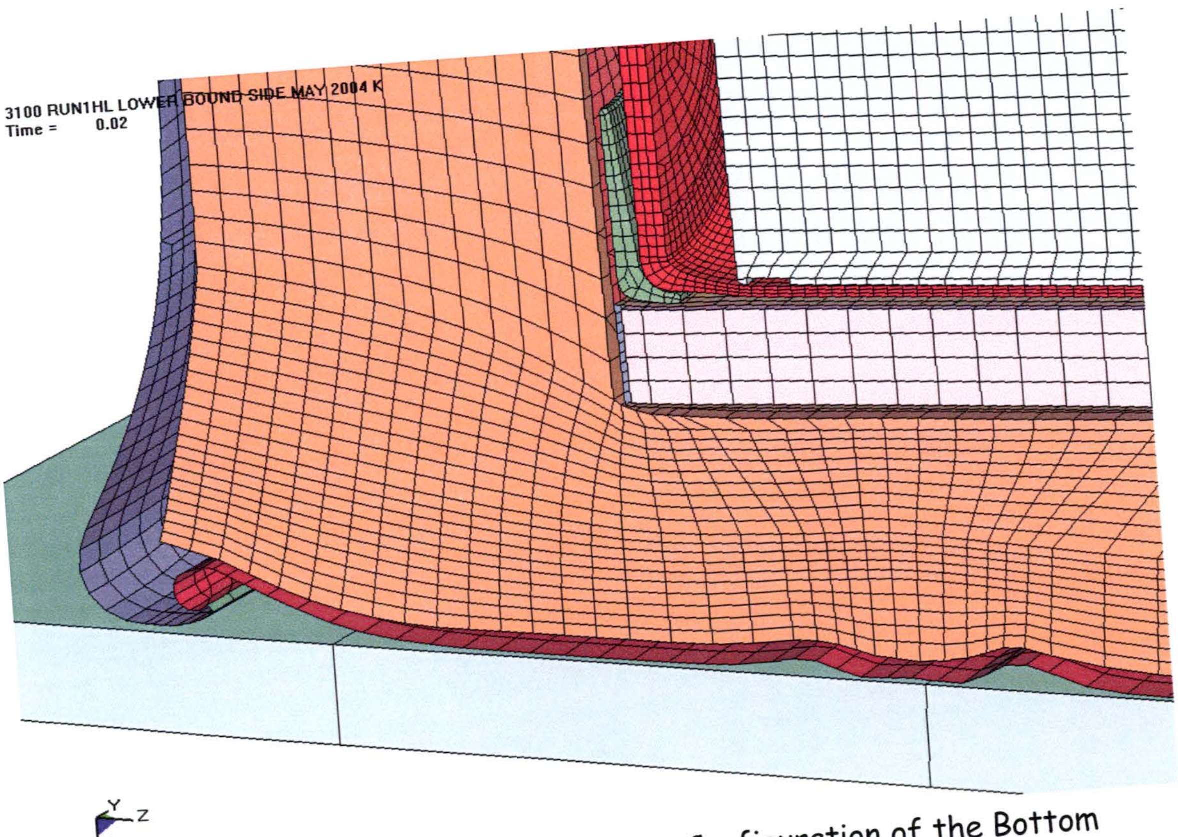

Figure 3.3.7 - Run1hl, 30-Foot Impact, Configuration of the Bottom

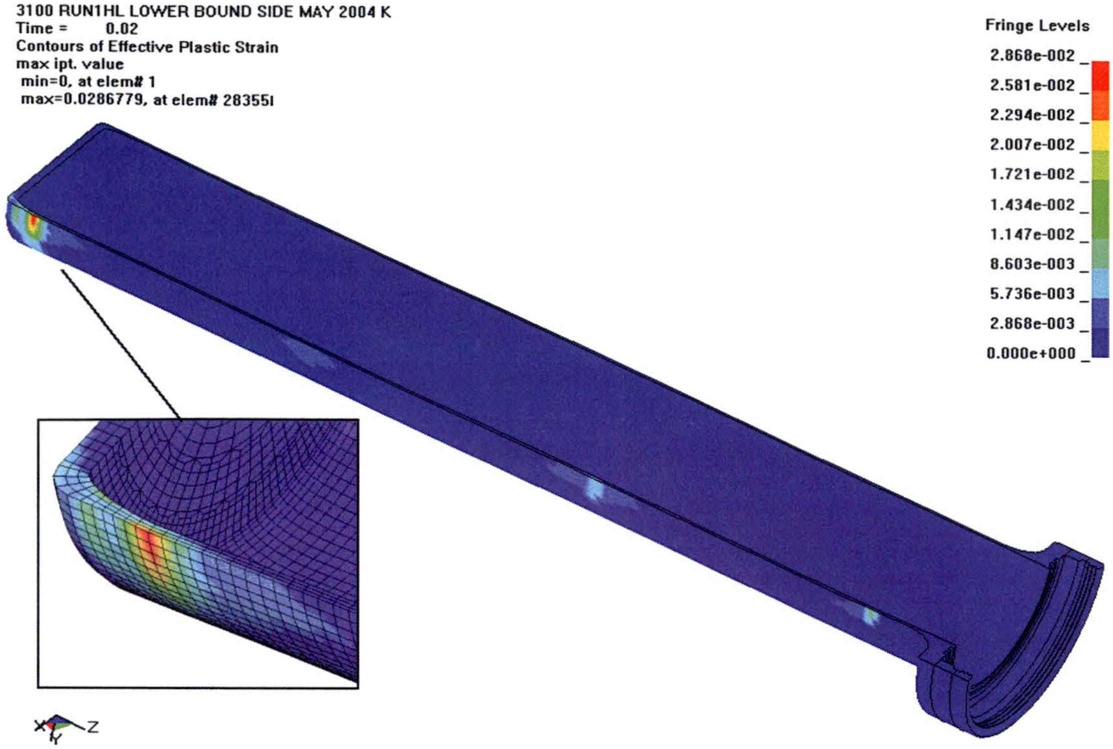

Figure 3.3.8 - Run1hl, 30-Foot Impact, Effective Plastic Strain in the CV

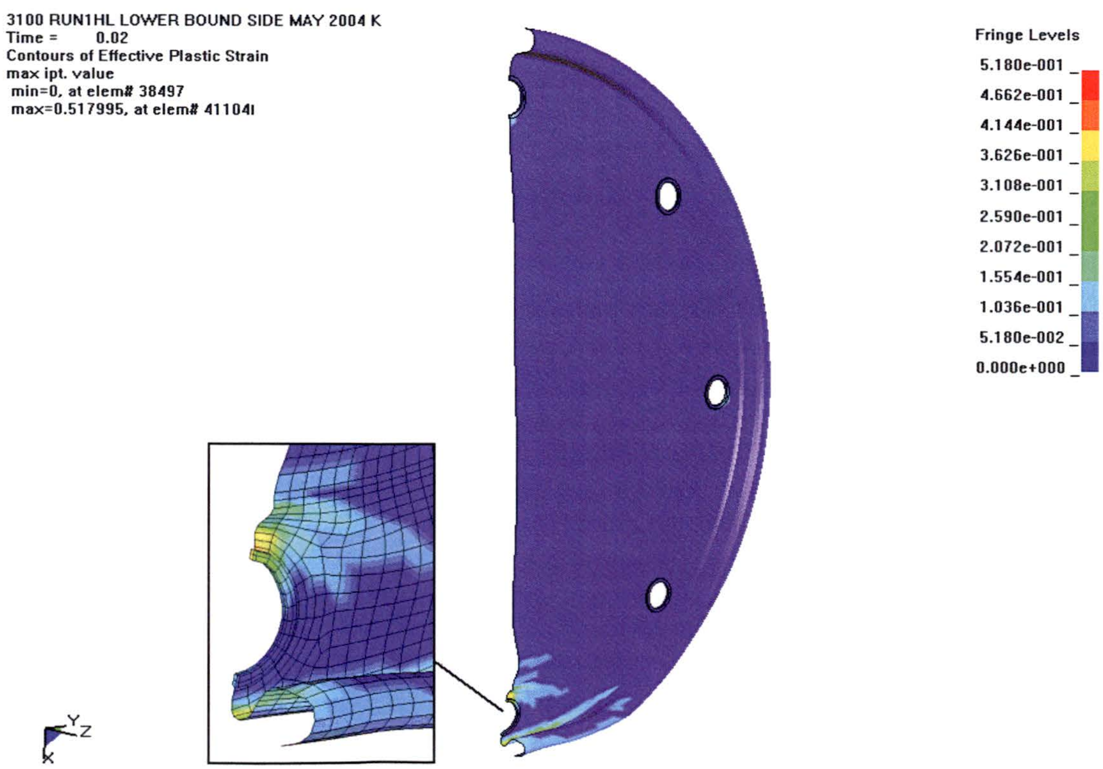

Figure 3.3.9 - Run1hl, 30-Foot Impact, Effective Plastic Strain in the Lid

Part A - Initial Design with Borobond Cylinder

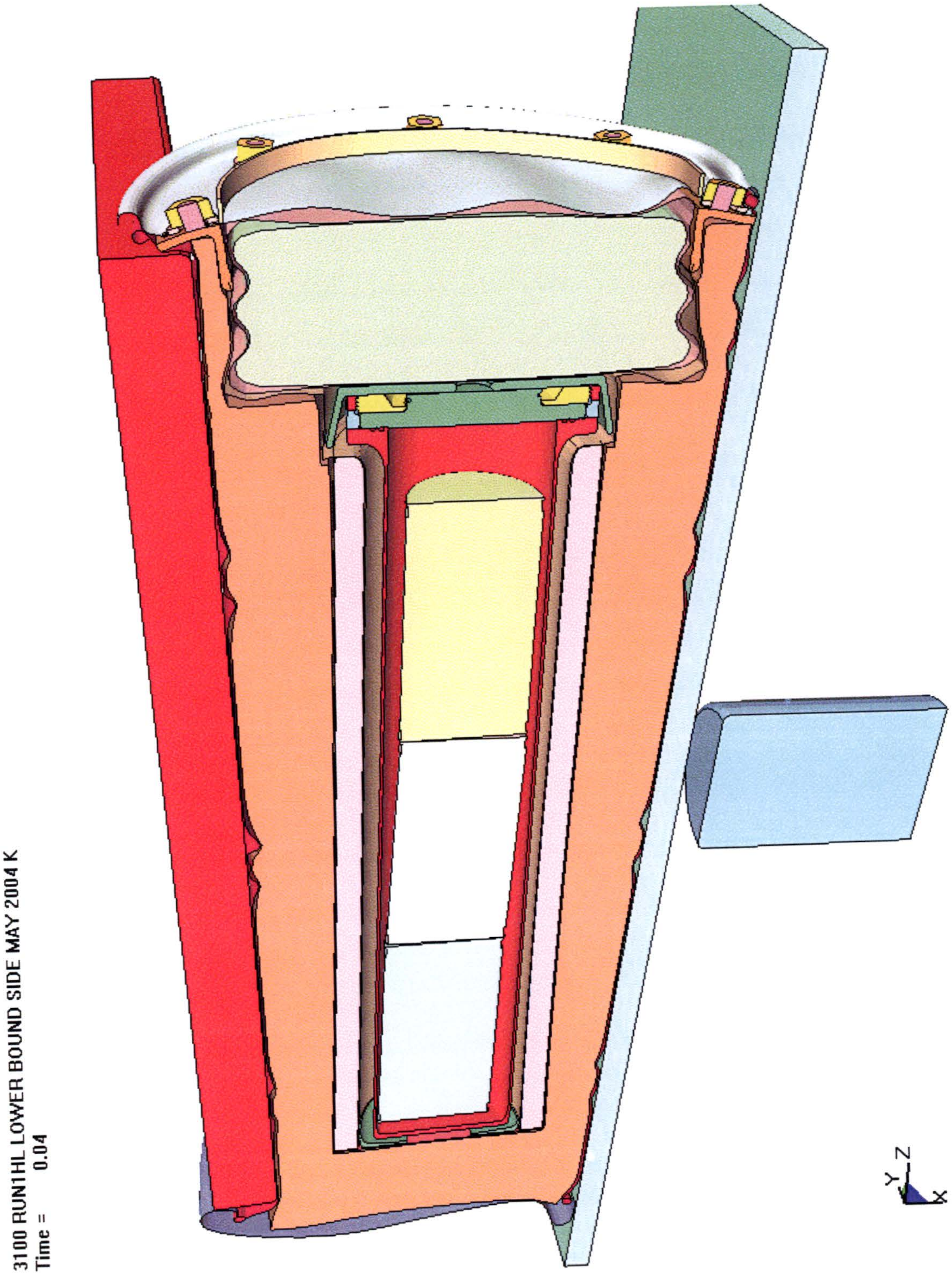

Figure 3.3.10 - Run1hl, Crush Impact, Final Configuration

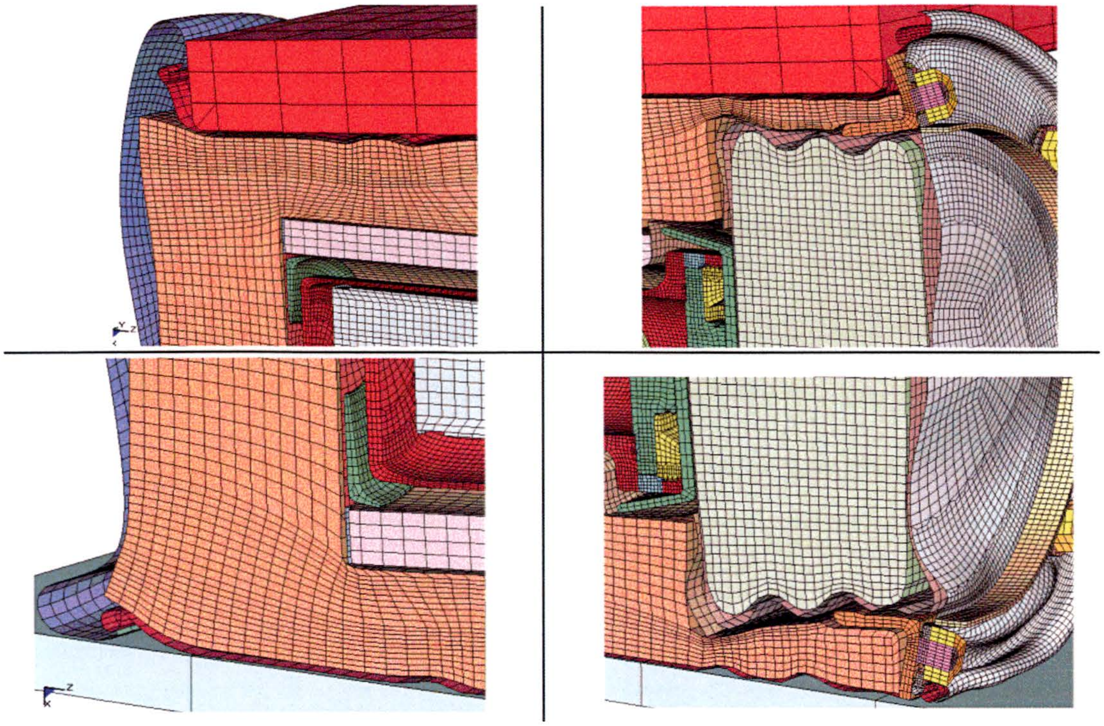

Figure 3.3.11 - Run1hl, Crush Impact, Configuration at the Package Corners

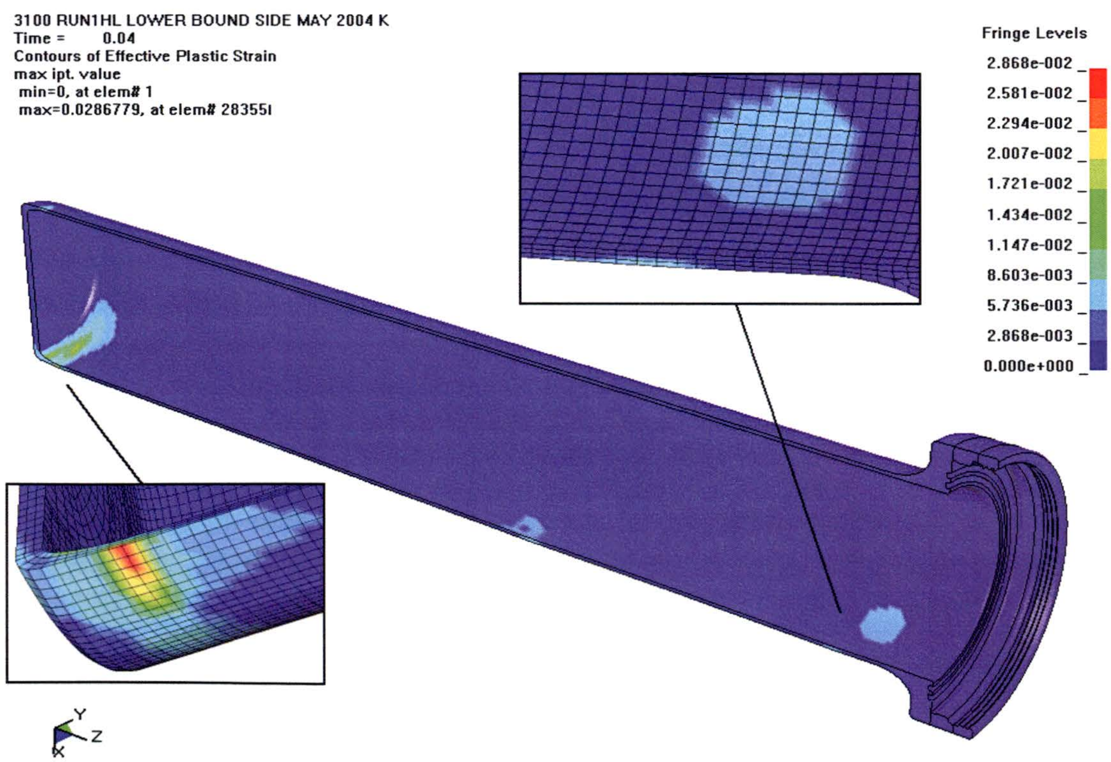

Figure 3.3.12 - Run1hl, Crush Impact, Effective Plastic Strain in the CV Body

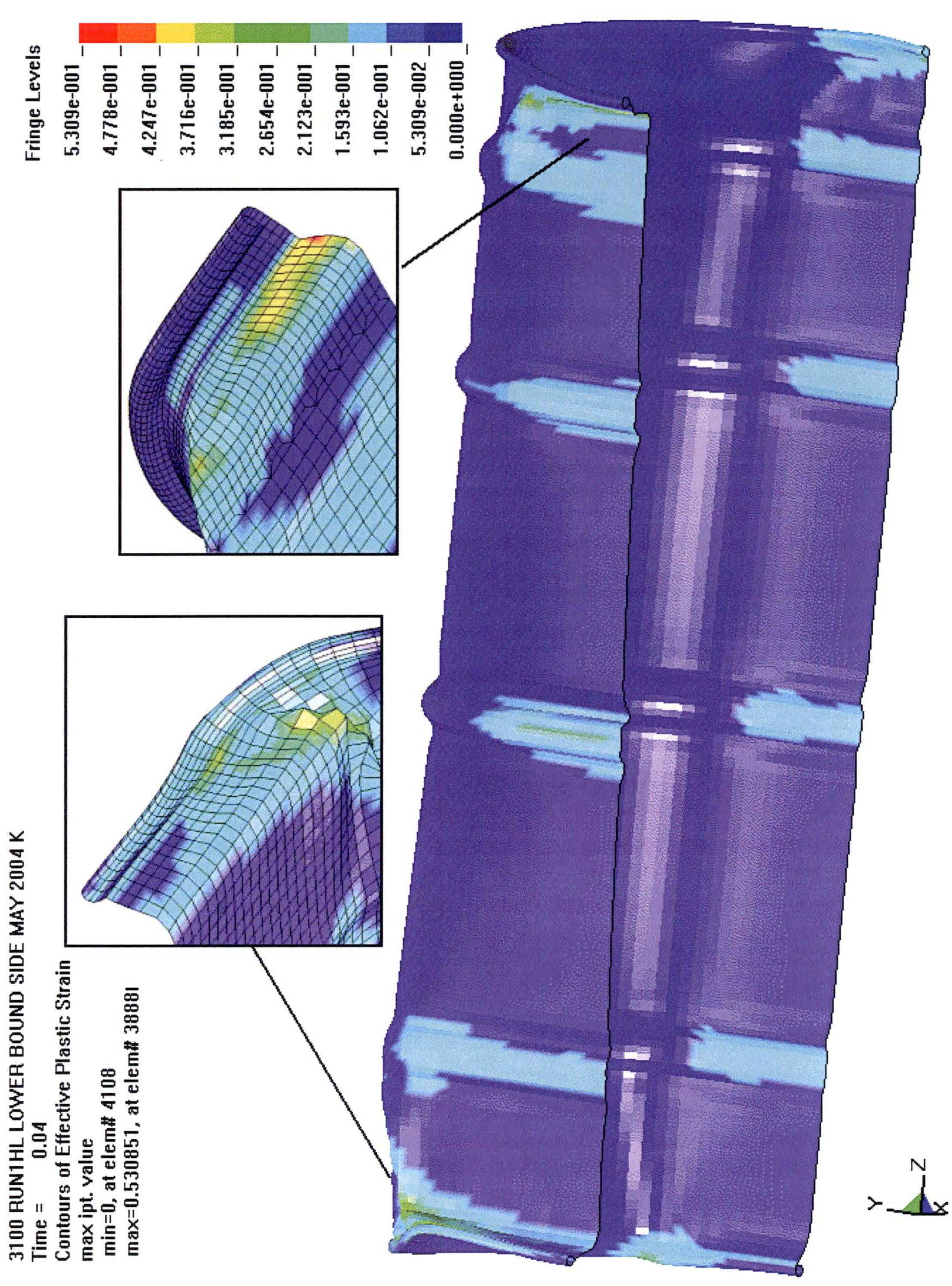

Figure 3.3.13 - Run1hl, Crush Impact, Effective Plastic Strain in the Drum

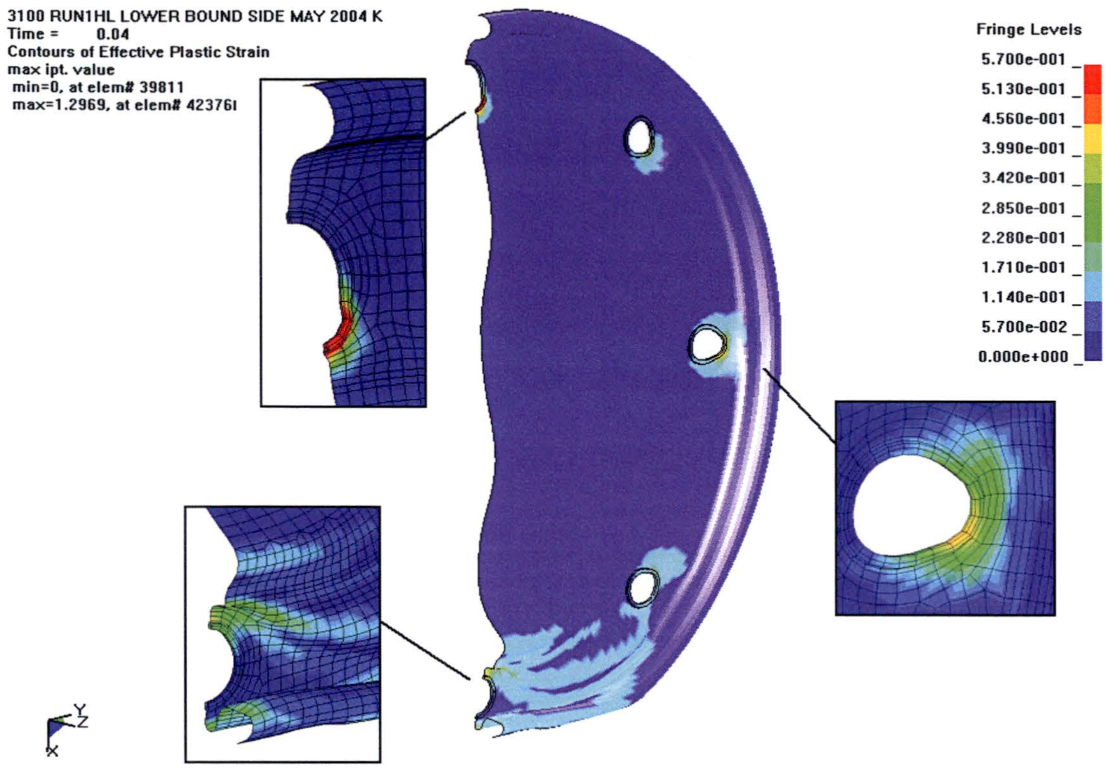

Figure 3.3.14 - Run1hl, Crush Impact, Effective Plastic Strain in the Lid

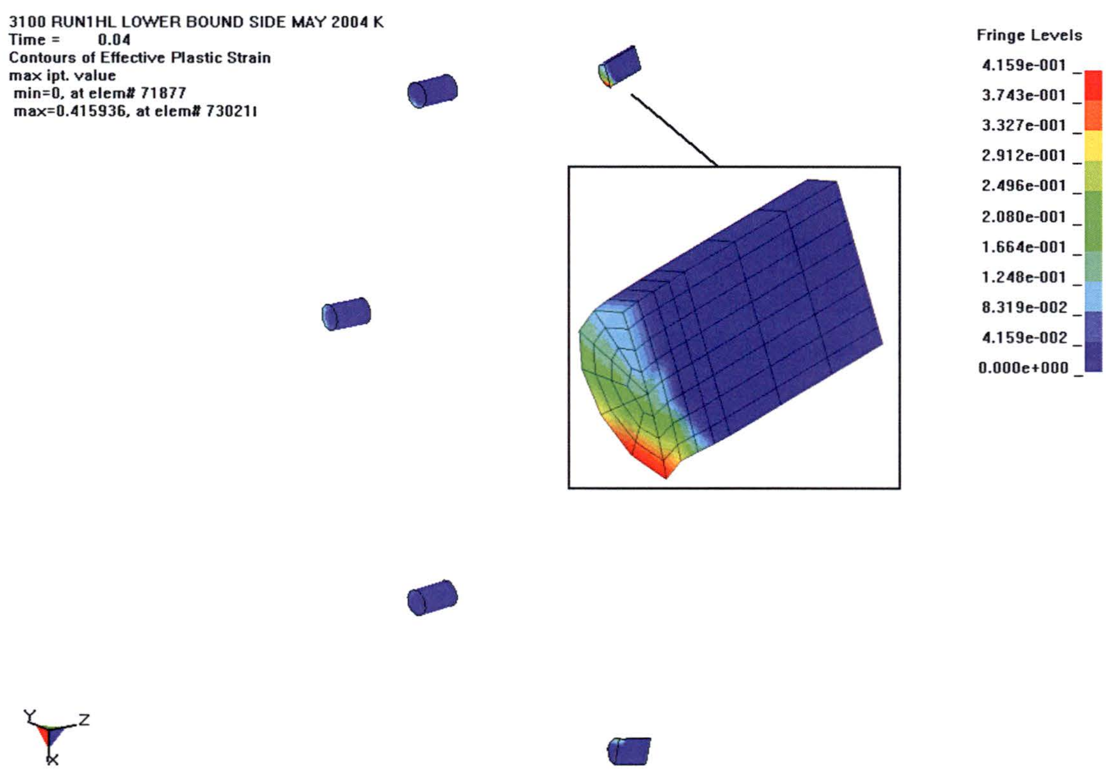

Figure 3.3.15 - Run1hl, Crush Impact, Effective Plastic Strain in the Studs

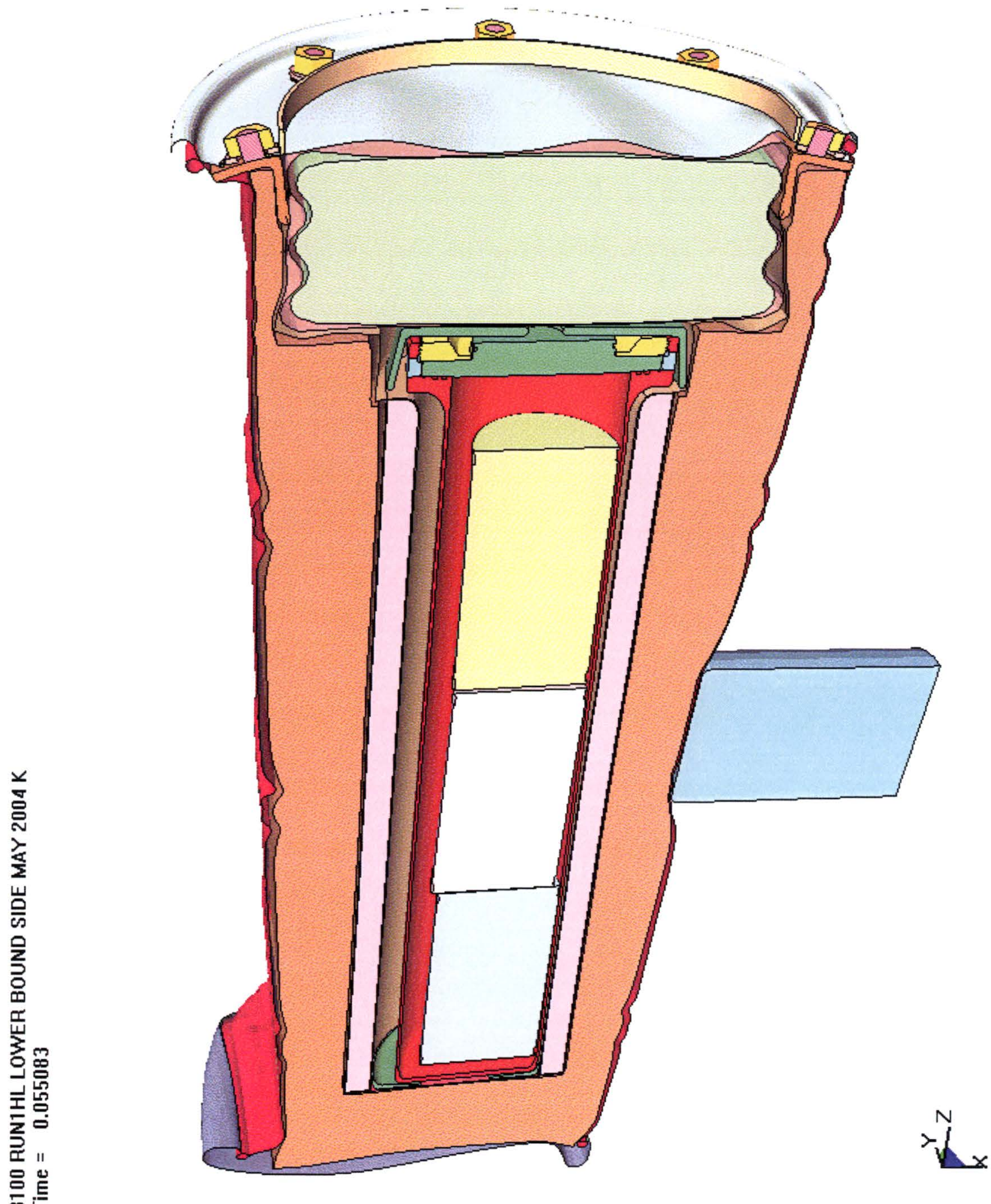

Figure 3.3.16 - Run1hl, Punch Impact, Final Configuration

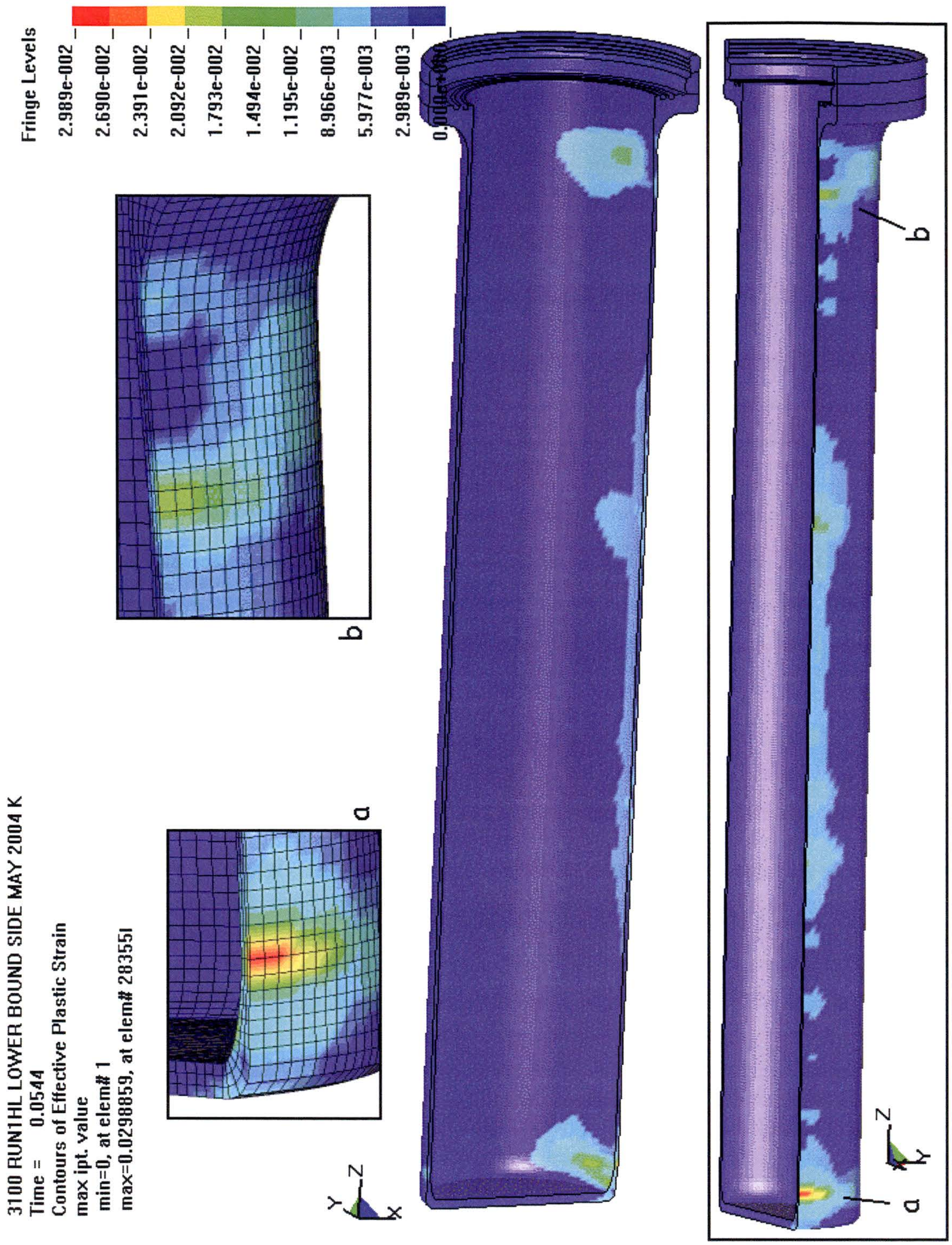

Figure 3.3.17 - Run1hl, Punch Impact, CV Effective Plastic Strain

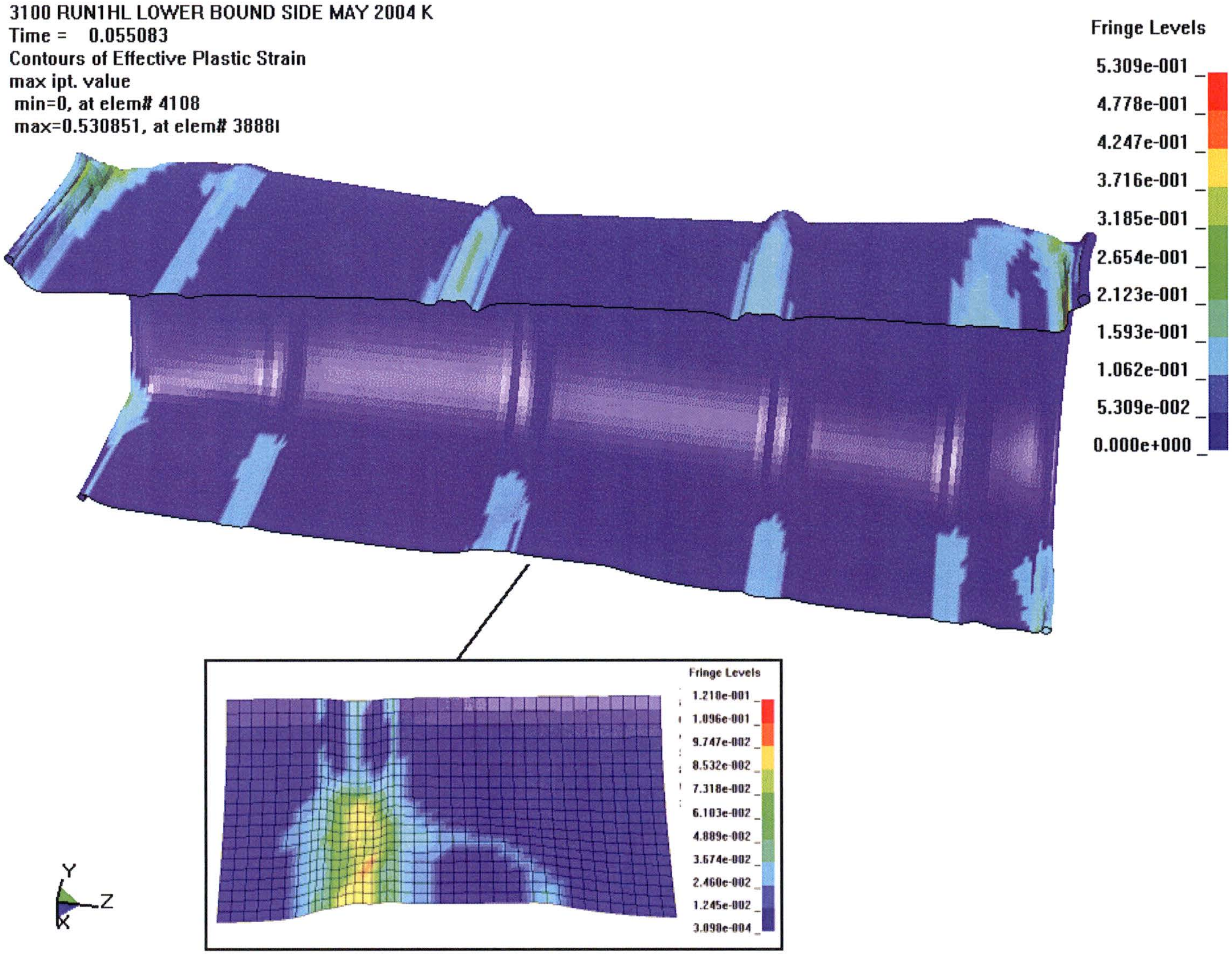

Figure 3.3.18 - Run1hl, Punch Impact, Effective Plastic Strain in the Drum

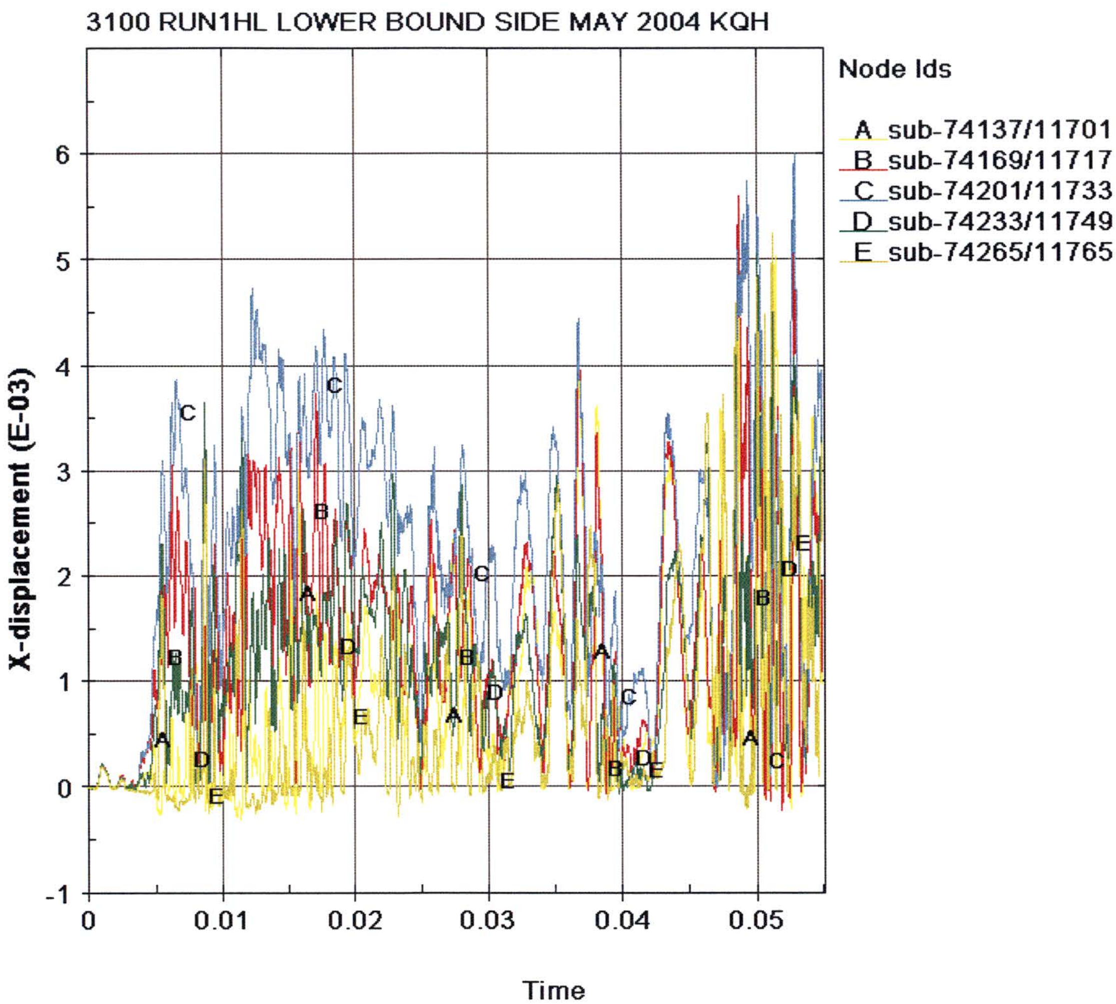

Figure 3.3.19 - Run1hl, CV Lid Separation Time History

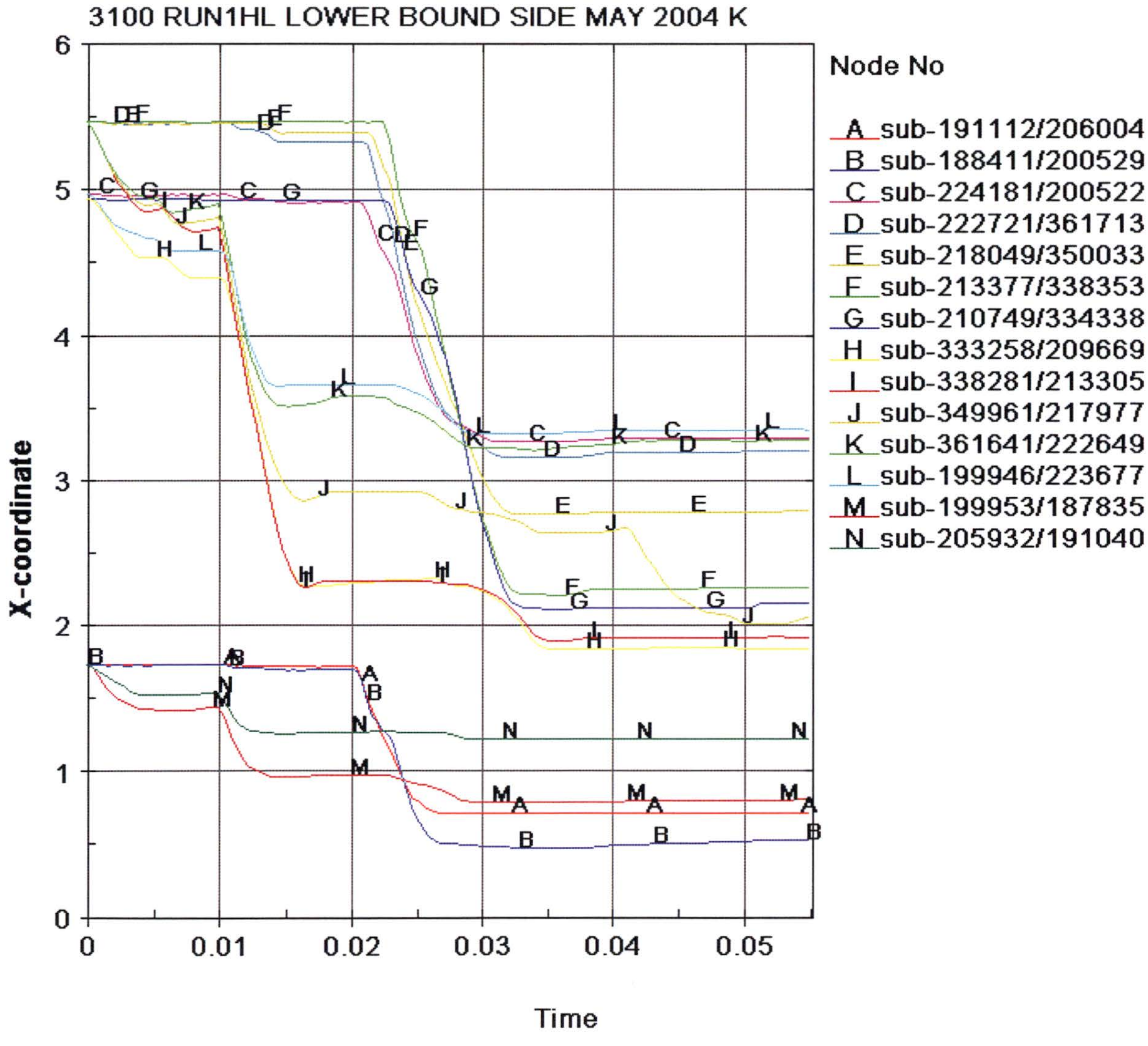

Figure 3.3.20- Run1hl, Kaolite Thickness Time History

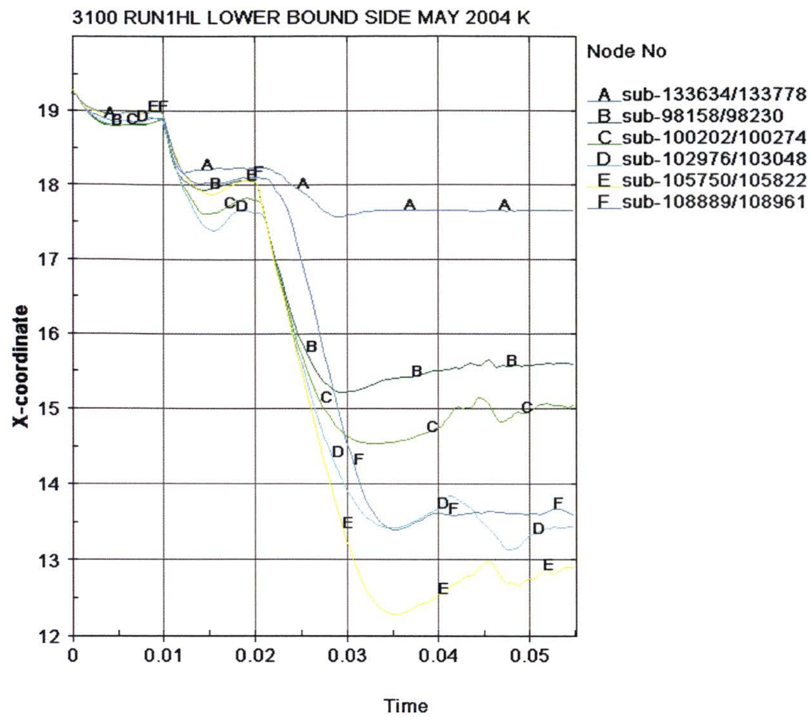

Figure 3.3.21 - Run1hl, Drum Dimension Time History in the X-Direction

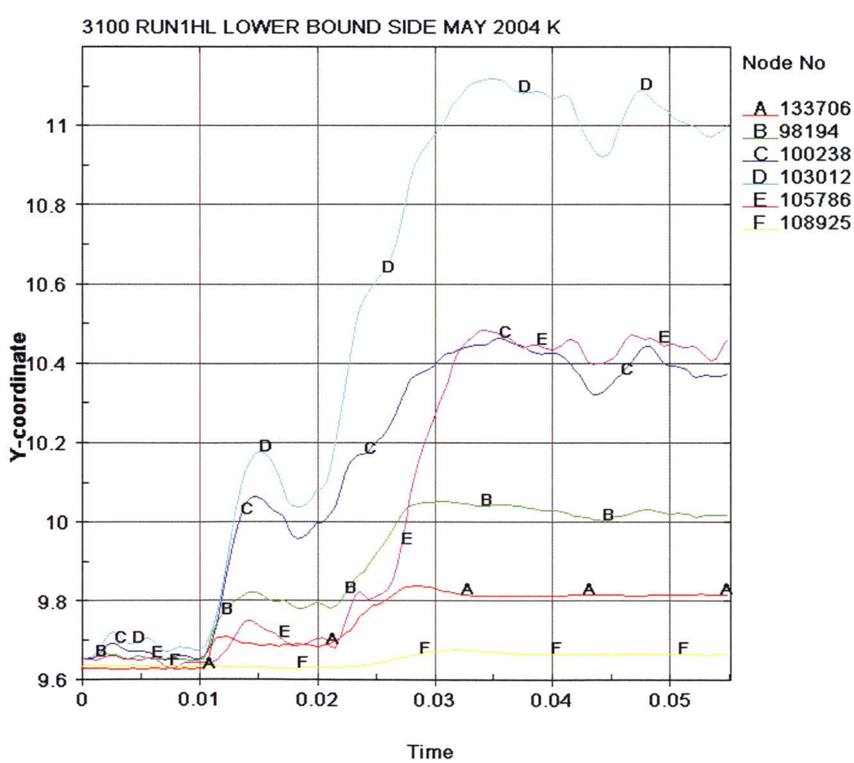

Figure 3.3.22- Run1hl, Drum Dimension Time History in the Y-Direction

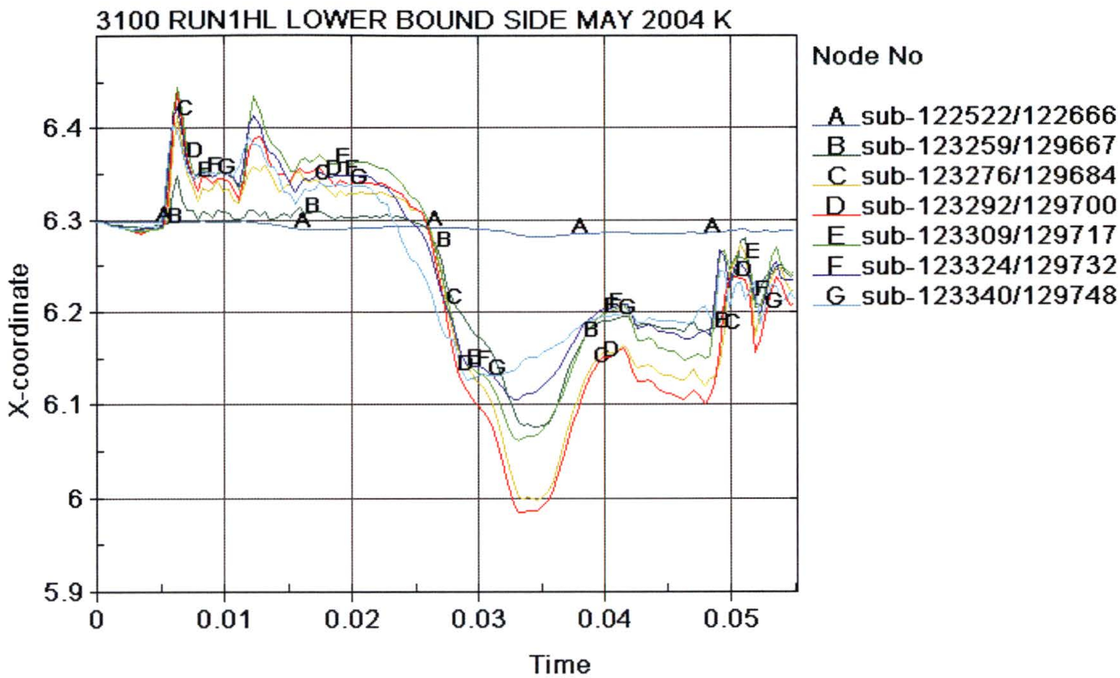

Figure 3.3.23 - Run1hl, Liner Diameter Time History

3.4 Run1hh - Side

Run1hh is the upper bounding kaolite run(-40°). It is basically the run1g model, but with the upper bound kaolite properties of section 2.3.5.3. It is a run with a 4-foot impact (time = 0 to 0.01 seconds), followed by a 30-foot impact (0.01 to 0.0188 seconds), followed by a 30-foot crush impact (0.0188 to 0.04 seconds), finally followed by a 40-inch punch impact (0.04 to 0.052 seconds).

The final configuration for the 4-foot impact is shown in Figure 3.4.1. Figures 3.4.2 and 3.4.3 show the configuration at the corners of the shipping package. The effective plastic strain in the CV body for the 4-foot impact is shown in Figure 3.4.4. The maximum effective plastic strain is shown to be 0.0298 in/in near the bottom head. The effective plastic strain in other package components for the 4-foot impact are listed in Table 3.4.1.

Table 3.4.1 - Run1hh, 4-Foot Impact, Effective Plastic Strain Levels in Some Components

Component	Effective Plastic Strain, in/in
CV Lid	0.0000
CV Nut Ring	0.0000
Angle	0.0059
Drum	0.1170
Drum Bottom Head	0.1215
Liner	0.0598
Lid	0.0860
Lid Stiffener	0.0000
Lid Studs	0.0000
Lid Stud Nuts	0.0000
Lid Stud Washers	0.0310
Plug Liner	0.0046

The final configuration for the 30-foot impact is shown in Figure 3.4.5. Figures 3.4.6 and 3.4.7 show the configuration at the corners of the package. The maximum effective plastic strain for the 30-foot impact in the CV Body is 0.0386 in/in near the bottom head. The maximum effective plastic strain in the drum lid is 0.4073 in/in near the rigid plane.

The effective plastic strain in other components for the 30-foot impact are given in Table 3.4.2.

Table 3.4.2 - Run1hh, 30-Foot Impact, Effective Plastic Strain Levels in Some Components	
Component	Effective Plastic Strain, in/in
CV Lid	0.0000
CV Nut Ring	0.0000
Angle	0.0622
Drum	0.2259
Drum Bottom Head	0.2528
Liner	0.0970
Lid Stiffener	0.0069
Lid Studs	0.1226
Lid Stud Nuts	0.0000
Lid Stud Washers	0.0951
Plug Liner	0.0995

The final configuration for the crush impact is shown in Figure 3.4.10. The configuration at the extremes of the package are shown in Figure 3.4.11. The maximum effective plastic strain for the crush impact in the CV body is 0.0462 in/in, on the crush plate side near the lid end of the top inner weight as shown in Figure 3.4.12. The maximum effective plastic strain in the drum is 0.2623 in/in near the angle and the rigid plane (Figure 3.4.13). The maximum effective plastic strain in the drum lid is 0.6411 in/in (surface strain), Figure 3.4.14. The maximum occurs at the lid hole for the stud closest to the crush plate(180°). The membrane effective plastic strain is 0.4922 in/in at this location. The effective plastic strain in the studs is 0.1753 in/in as shown in Figure 3.4.15. The effective plastic strain in other components are listed in Table 3.4.3 for the crush impact.

Table 3.4.3 - Run1hh, Crush Impact, Effective Plastic Strain Levels in Some Components	
Component	Effective Plastic Strain, in/in
CV Lid	0.0004
CV Nut Ring	0.0000
Angle	0.0816
Drum Bottom Head	0.2807
Liner	0.2005
Lid Stiffener	0.0217
Lid Stud Nuts	0.0000
Lid Stud Washers	0.1034
Plug Liner	0.1258

The final configuration for the punch impact is shown in Figure 3.4.16. The maximum effective plastic strain in the CV body after the punch impact is shown to be 0.0599 in/in in Figure 3.4.17. The maximum effective plastic strain in the drum is 0.2623 in/in (surface strain) and is located near the angle at the rigid surface. The maximum effective plastic strain in elements local to the punch impact is 0.1382 in/in (surface strain) as shown in the insert in Figure 3.4.18. The maximum effective plastic strain for the lid and other package components at the end of the punch impact are listed in Table 3.4.4.

Table 3.4.4 - Run1hh, Punch Impact, Effective Plastic Strain Levels in Some Components	
Component	Effective Plastic Strain, in/in
CV Lid	0.0004
CV Nut Ring	0.0000
Angle	0.0816
Drum Bottom Head	0.2807
Liner	0.2027
Lid	0.6411
Lid Stiffener	0.0217
Lid Studs	0.1761
Lid Stud Nuts	0.0000
Lid Stud Washers	0.1034
Plug Liner	0.1258

Figure 3.4.19 shows the CV lid separation for all the impacts. A maximum spike for the lid separation of less than 0.008 inches is found. At the end of the impacts, the maximum separation is on the order of 0.006 in, with the response being oscillatory in nature. Average separation of 0.003 inches or less is shown to be expected after the successive impacts.

Figure 3.4.20 shows the drum diameter time history response to the impacts in the X direction (direction of the impacts). Figure 3.4.21 shows the Y direction radial response (normal to the impact direction). The drum nodes are defined in Figure 3.1.34.

The Figure 3.4.22 shows the kaolite thickness time history for the four impacts. Figure 3.1.32 shows the nodal locations.

Figure 3.4.23 shows the liner diameter time history along its length. The nodal pairs are defined in Figure 3.1.37 and Table 3.1.3.

Part A - Initial Design with Borobond Cylinder

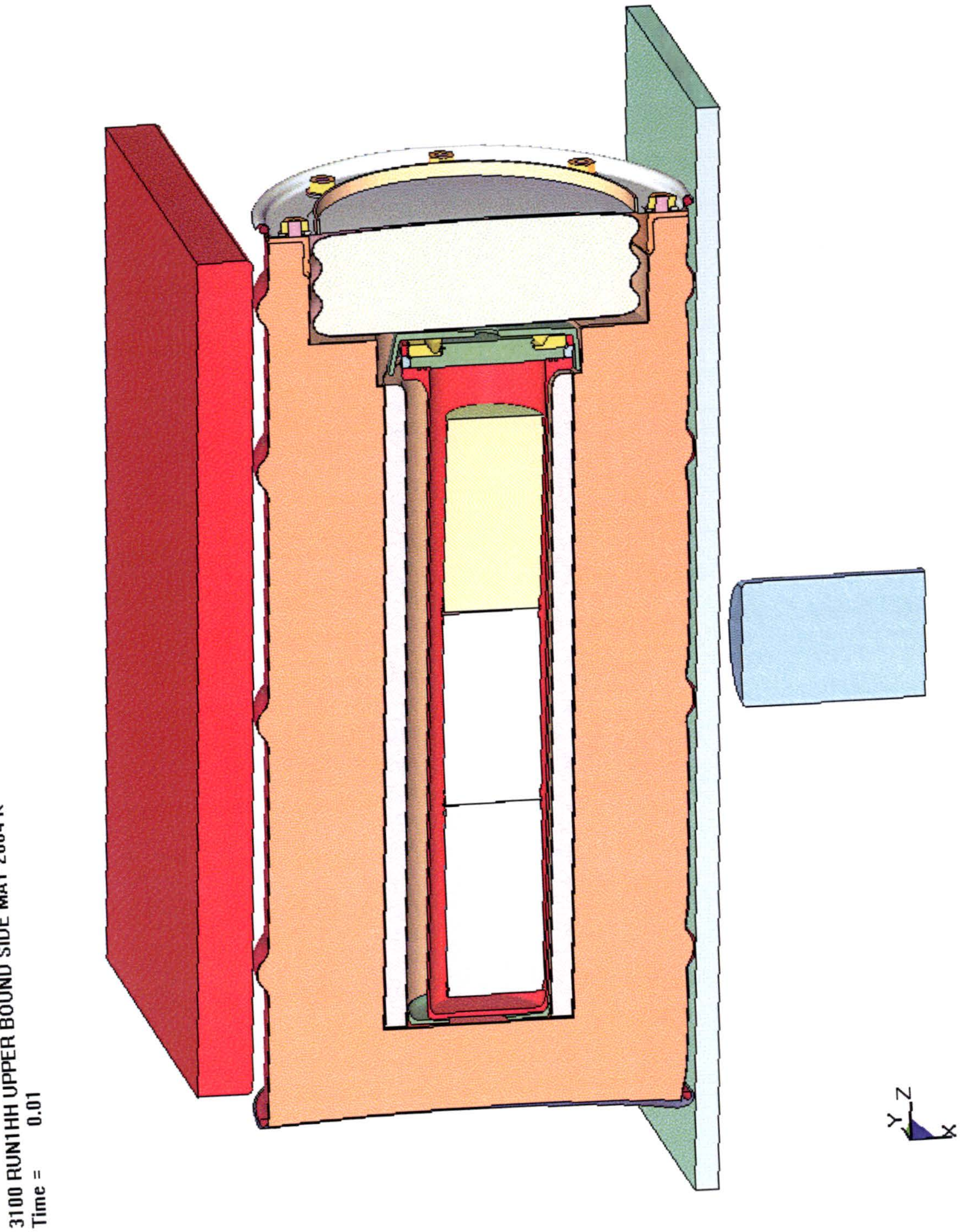

Figure 3.4.1 - Run1hh, 4-Foot Impact, Final Configuration

Part A - Initial Design with Borobond Cylinder

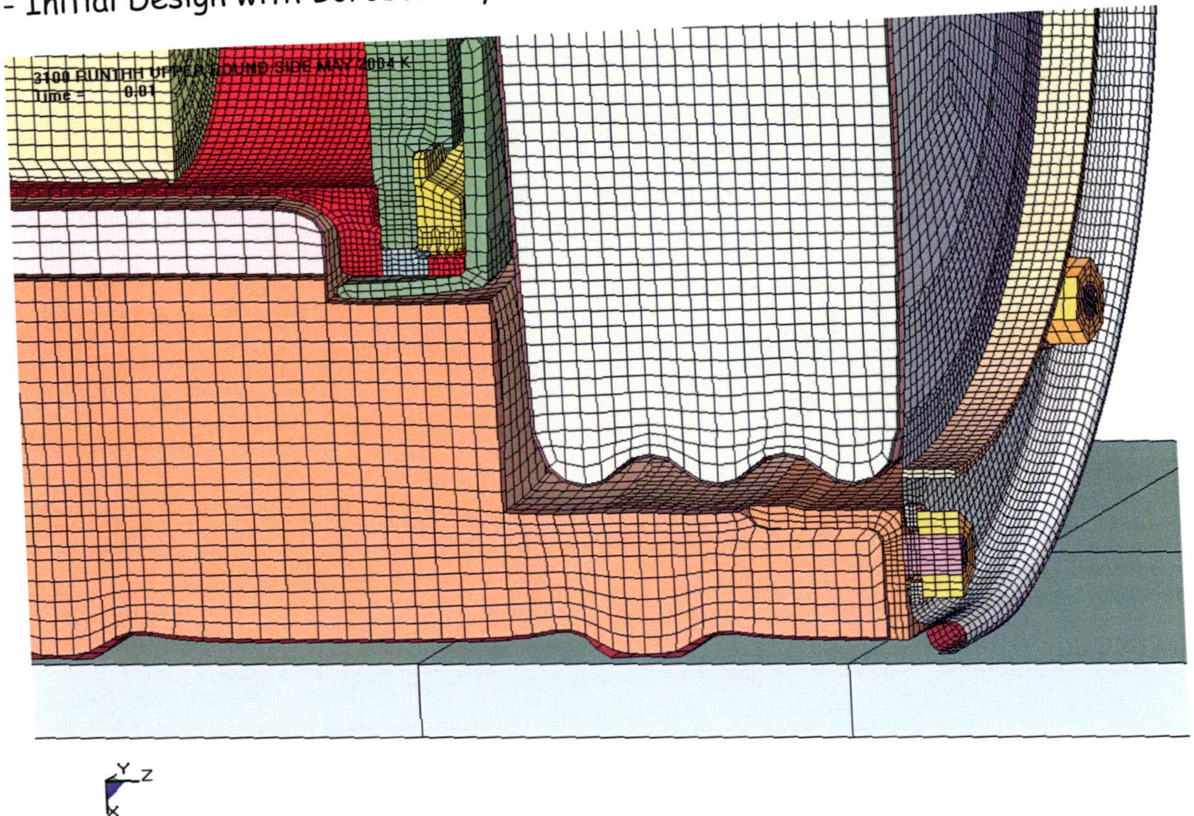

Figure 3.4.2 - Run1hh, 4-Foot Impact,

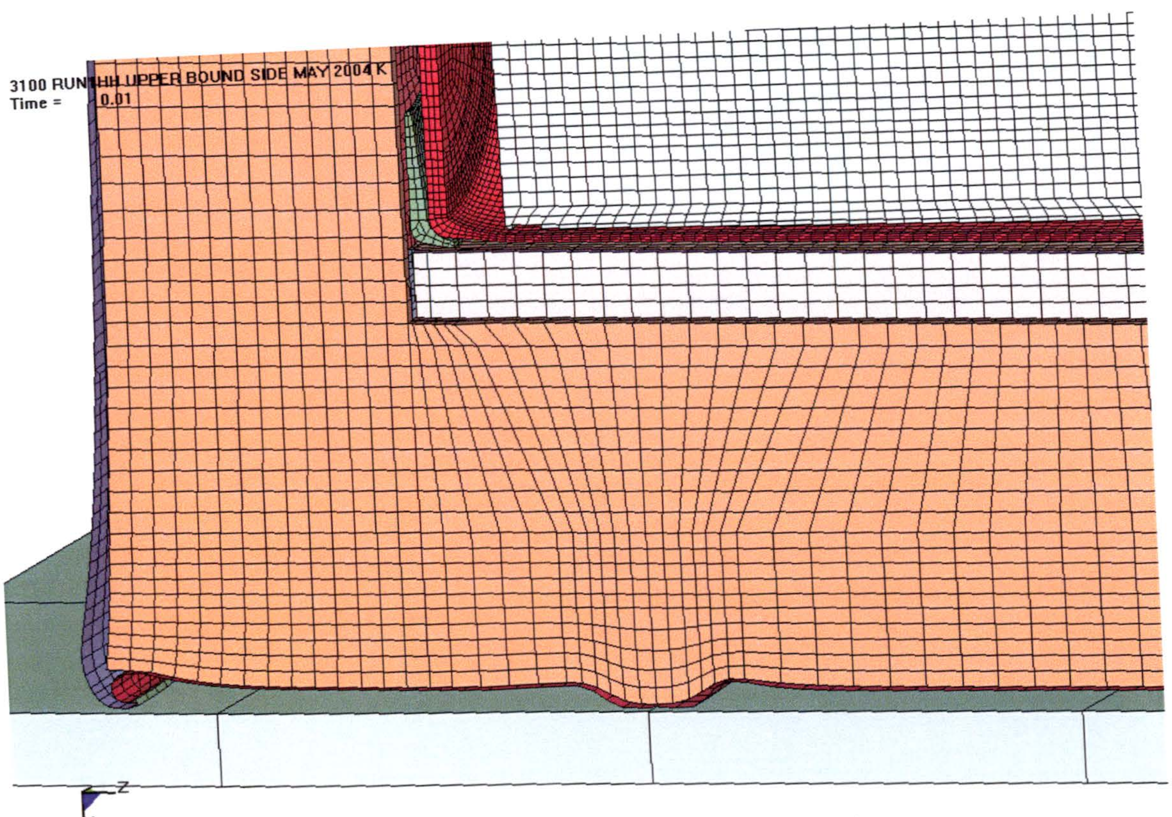

Figure 3.4.3 - Run1hh, 4-Foot Impact,

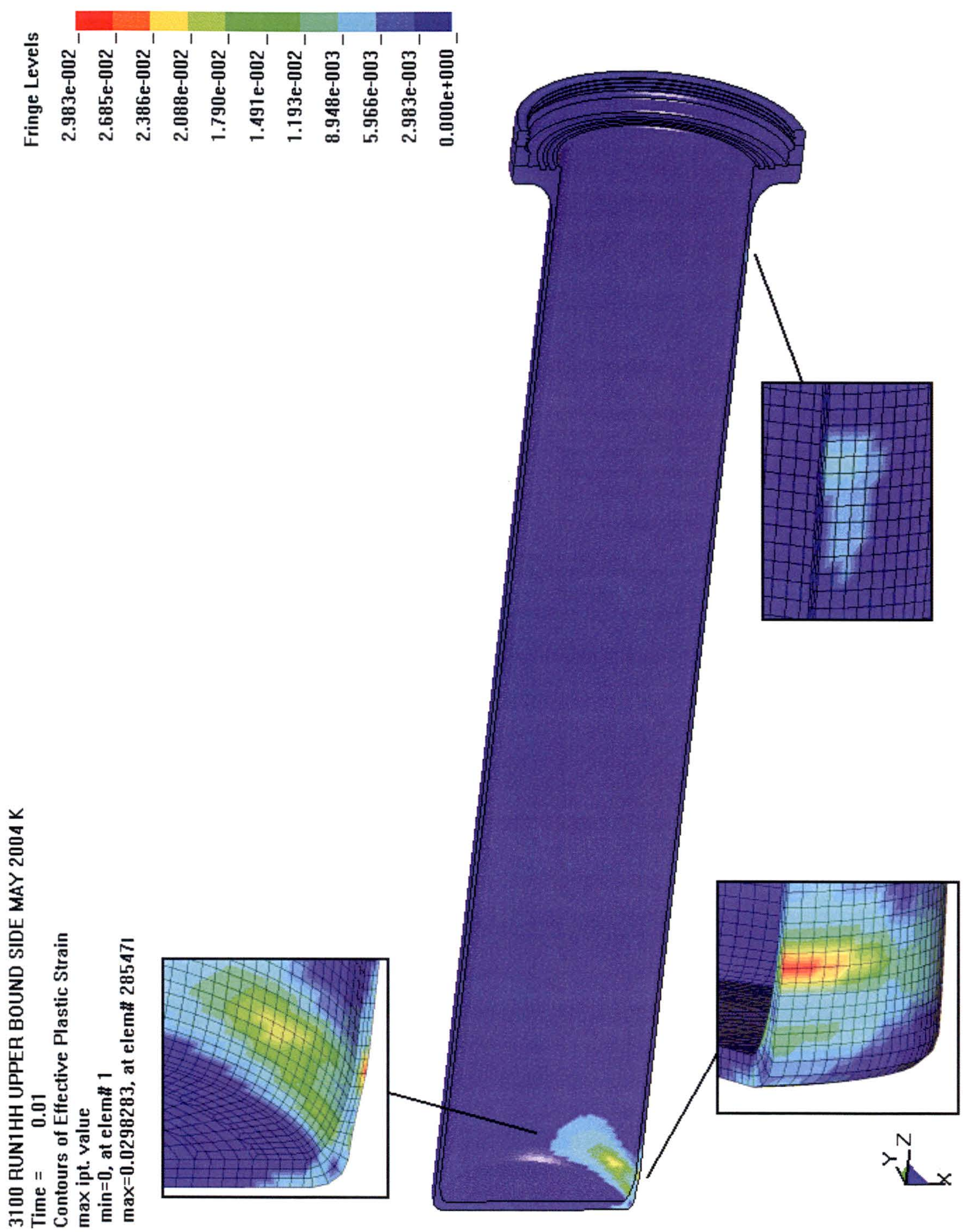

Figure 3.4.4 - Run1hh, 4-Foot Impact, Effective Plastic Strain in the CV Body

Part A - Initial Design with Borobond Cylinder

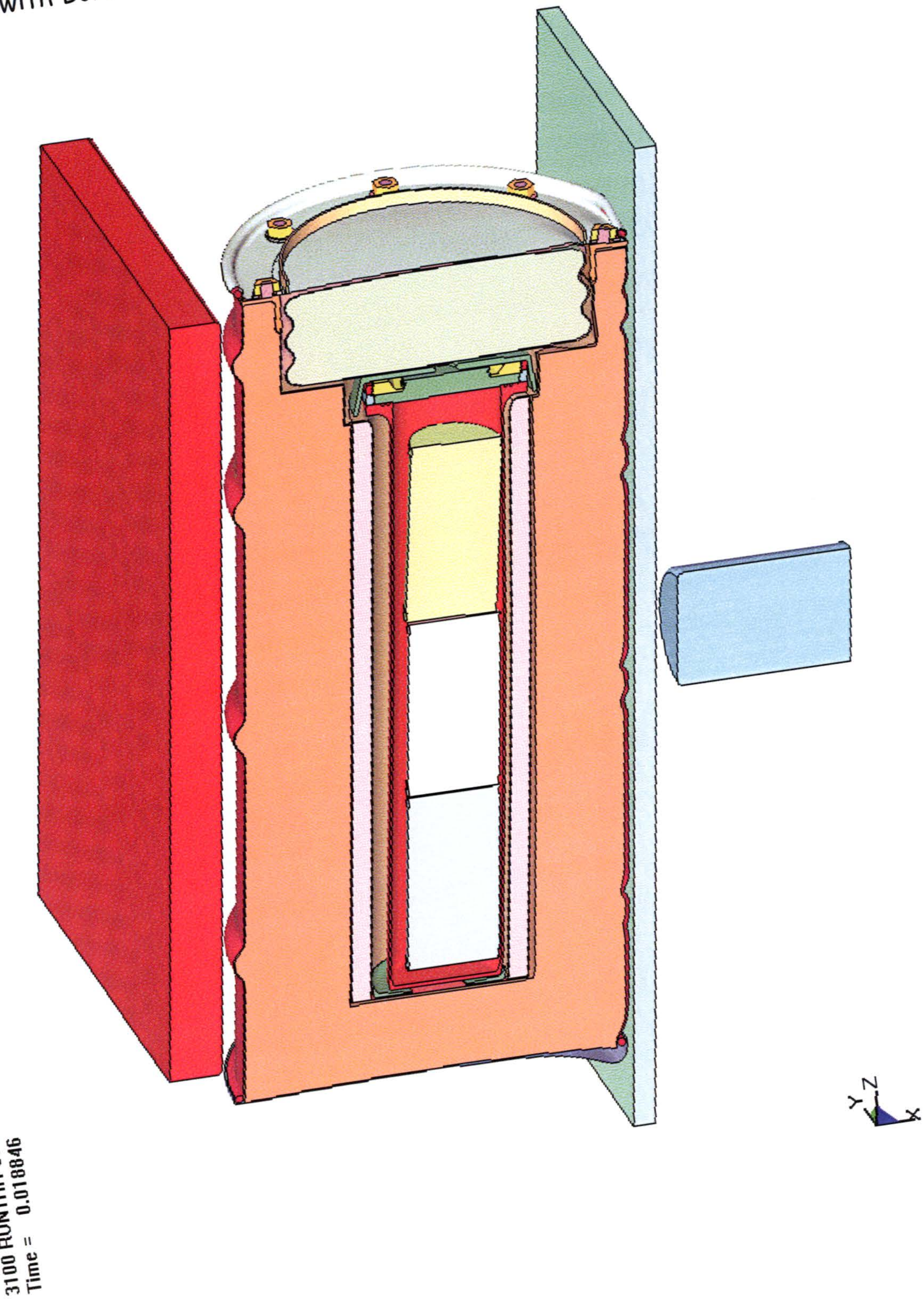

Figure 3.4.5 - Run1hh, 30-Foot Impact, Final Configuration

Part A - Initial Design with Borobond Cylinder

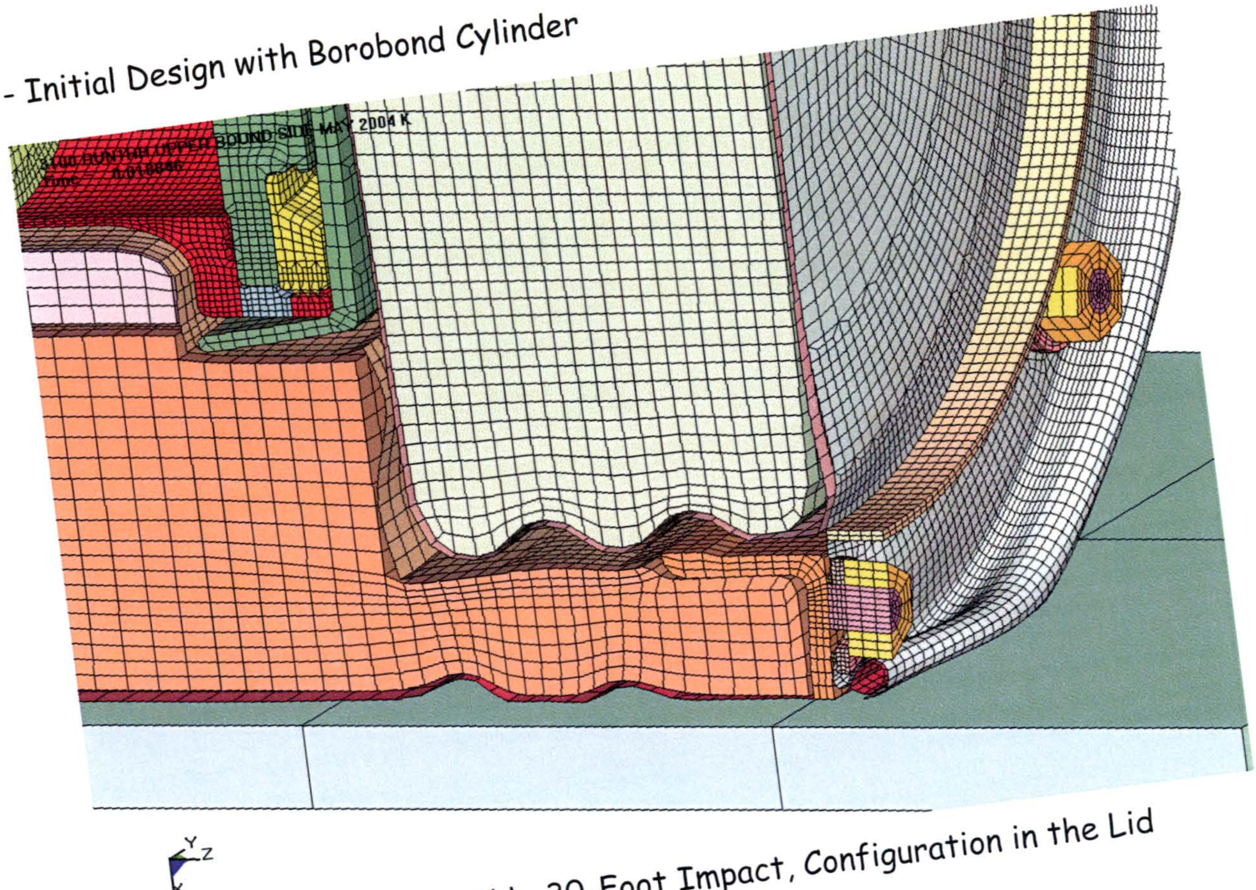

Figure 3.4.6 - Run1hh, 30-Foot Impact, Configuration in the Lid

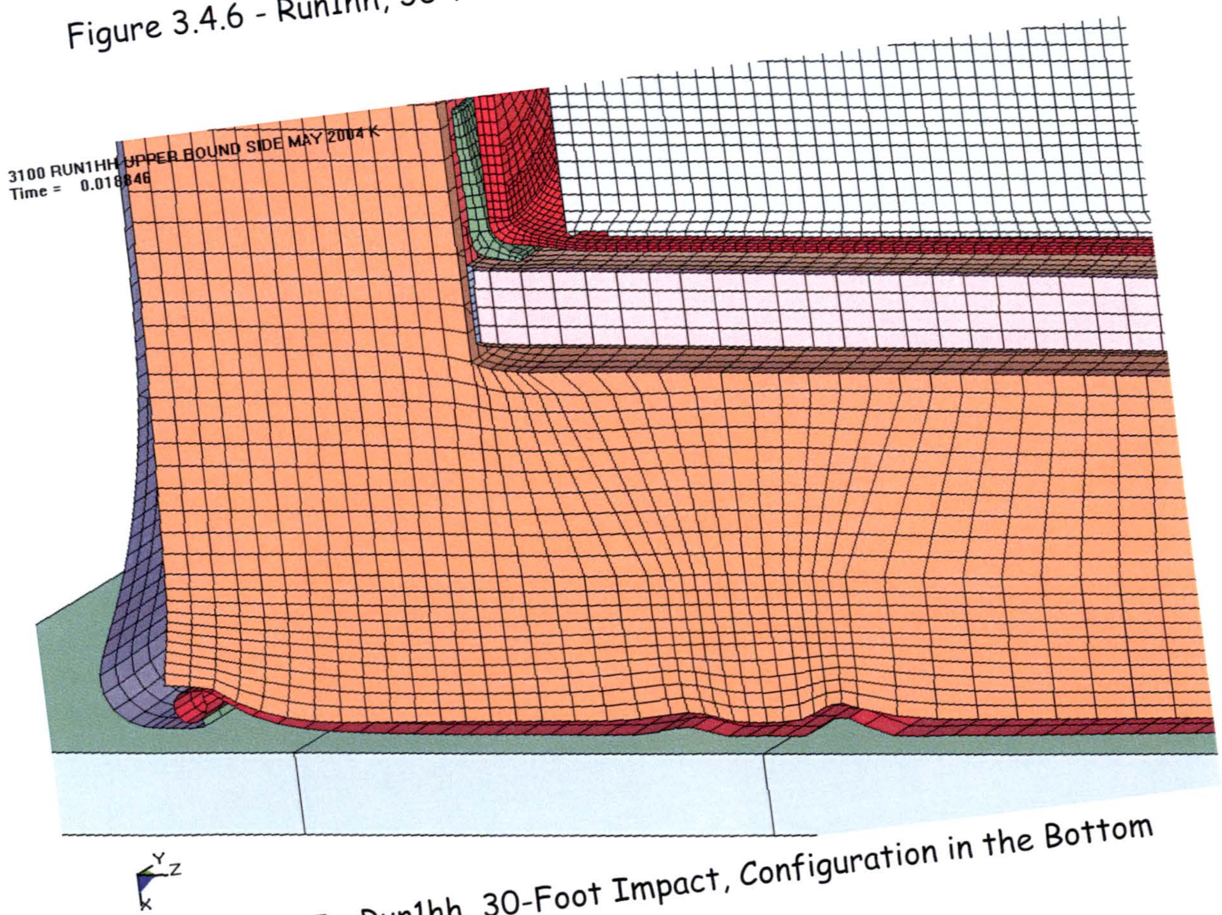

Figure 3.4.7 - Run1hh, 30-Foot Impact, Configuration in the Bottom

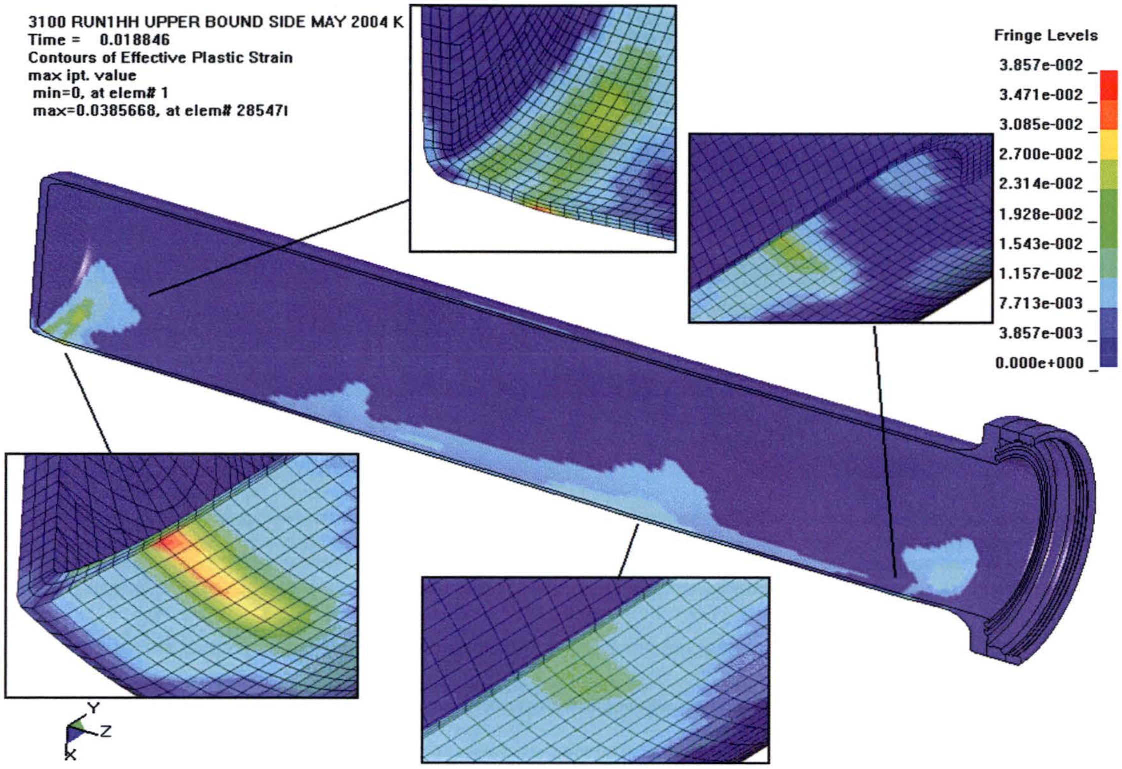

Figure 3.4.8 - Run1hh, 30-Foot Impact, Effective Plastic Strain in the CV Body

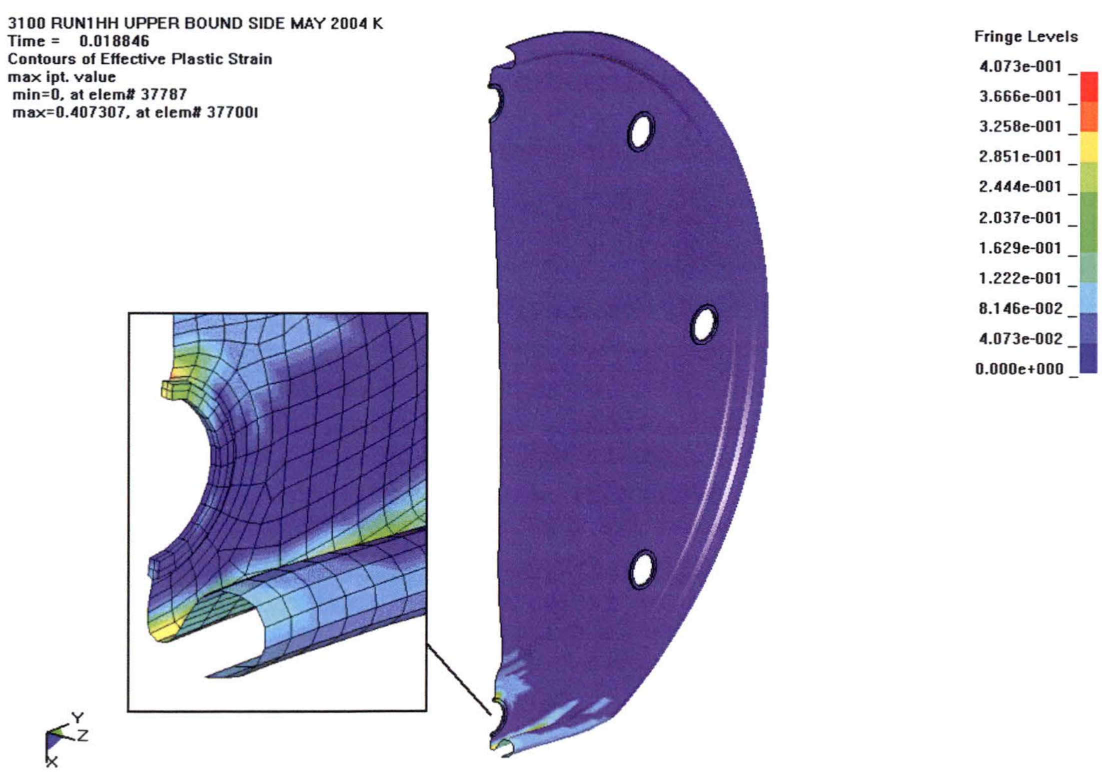

Figure 3.4.9 - Run1hh, 30-Foot Impact, Effective Plastic Strain in the Lid

Part A - Initial Design with Borobond Cylinder

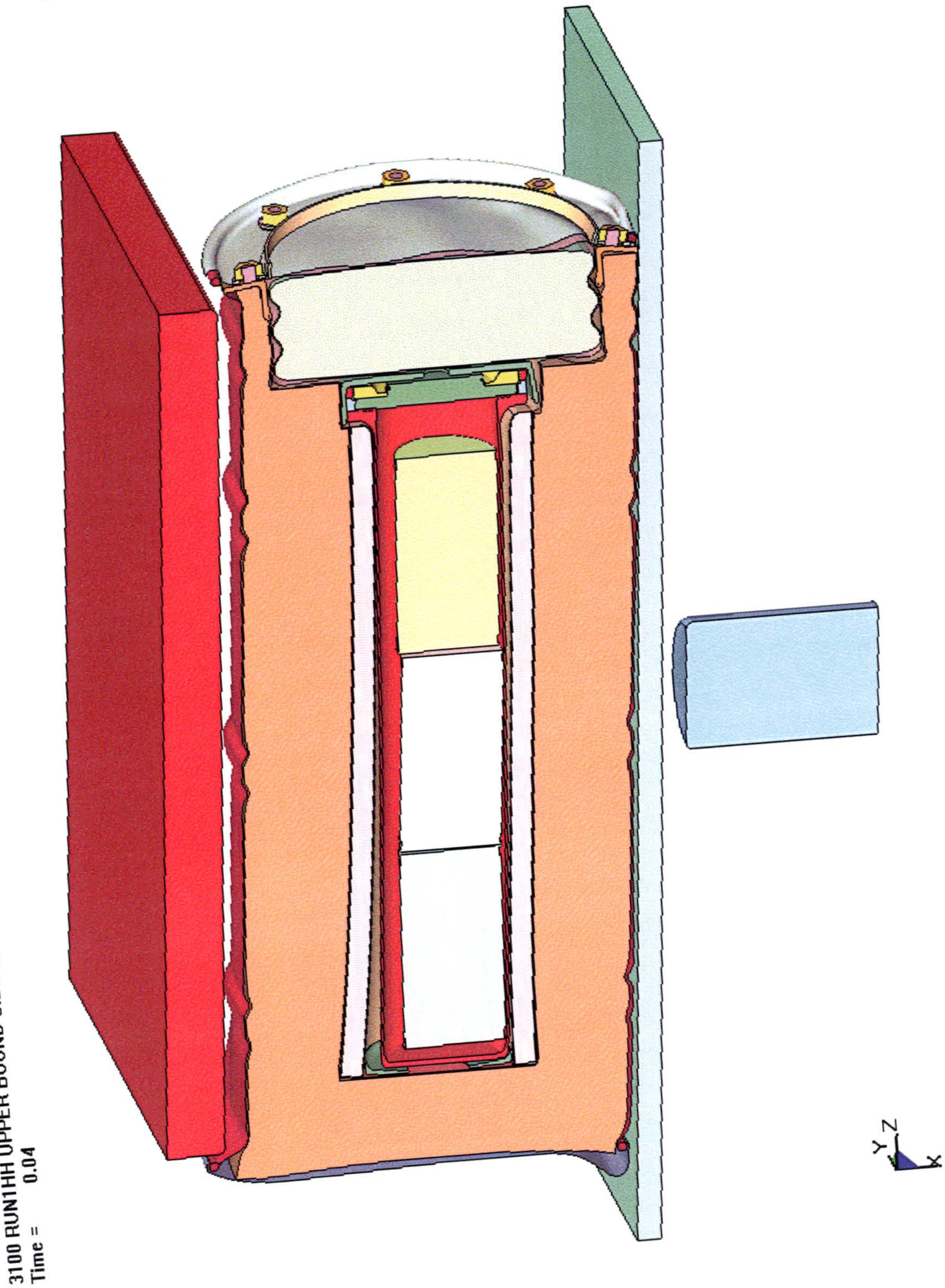

Figure 3.4.10 - Run1hh, Crush Impact, Final Configuration

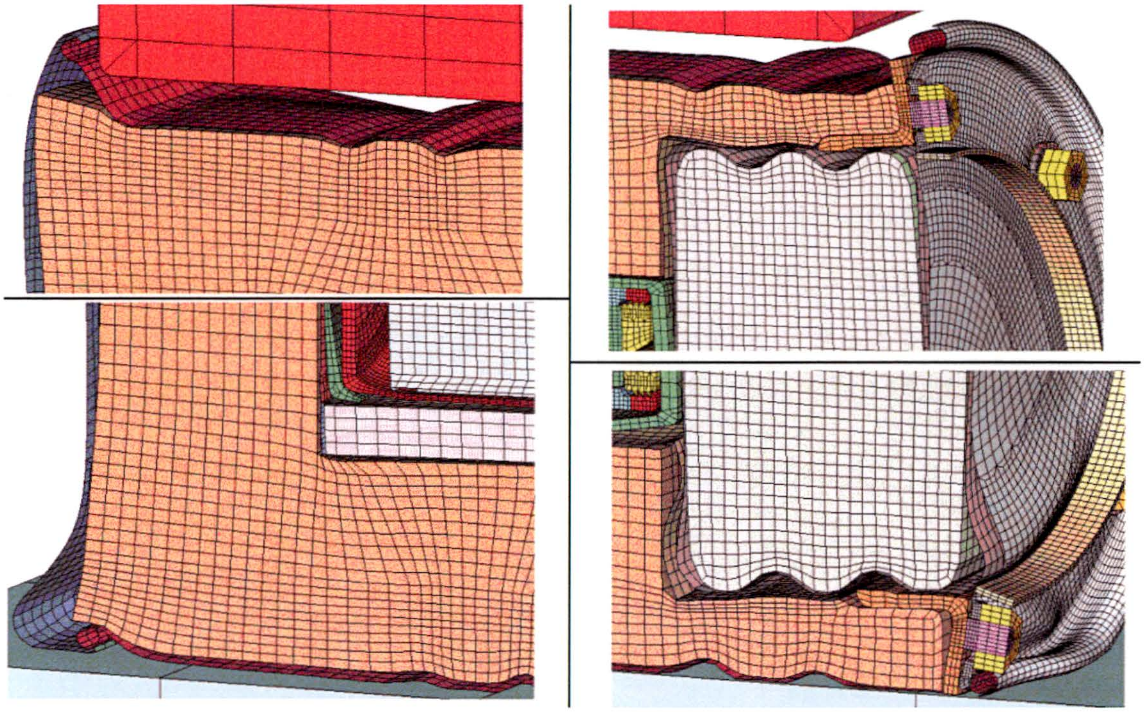

Figure 3.4.11 - Run1hh, Crush Impact, Configuration of the Package Corners

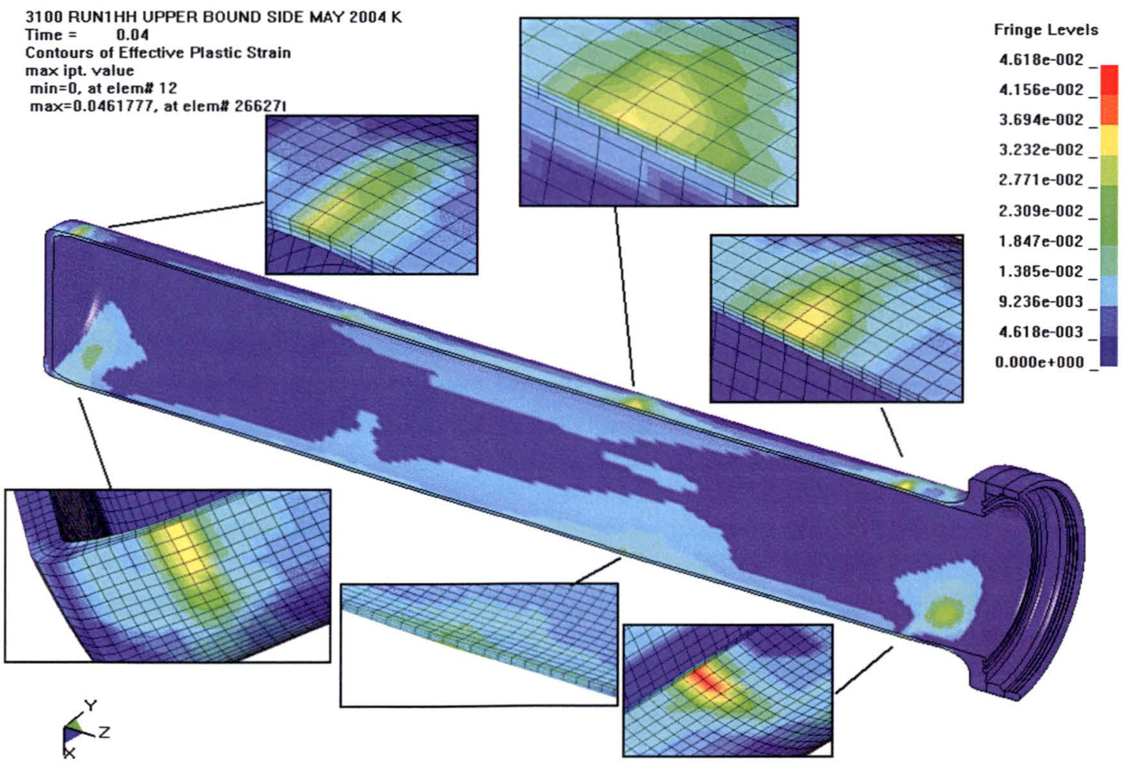

Figure 3.4.12 - Run1hh, Crush Impact, Effective Plastic Strain in the CV Body

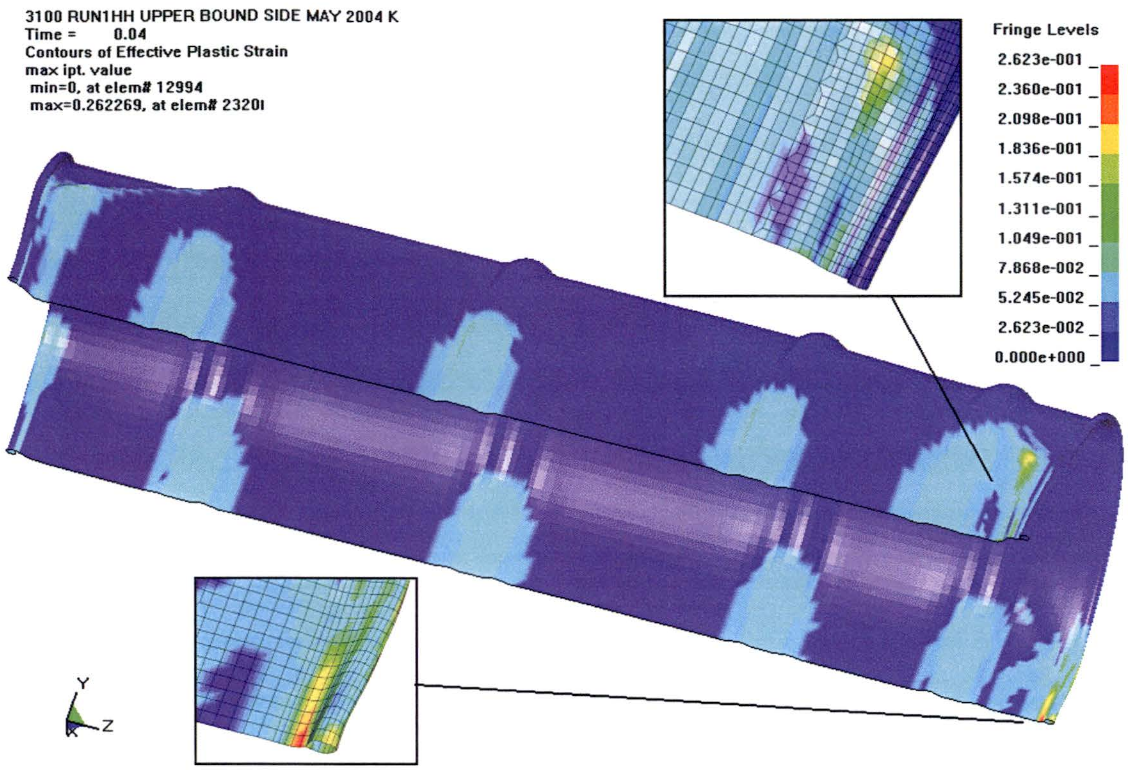

Figure 3.4.13 - Run1hh, Crush Impact, Effective Plastic Strain in the Drum

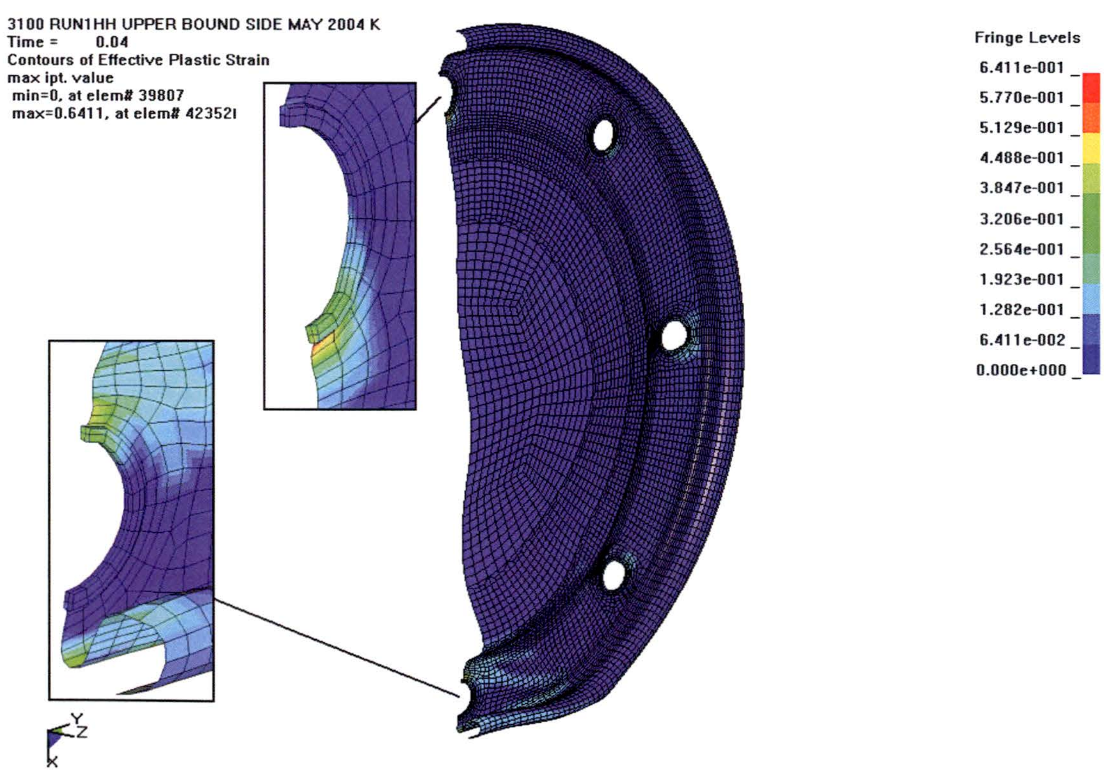

Figure 3.4.14 - Run1hh, Crush Impact, Effective Plastic Strain in the Lid

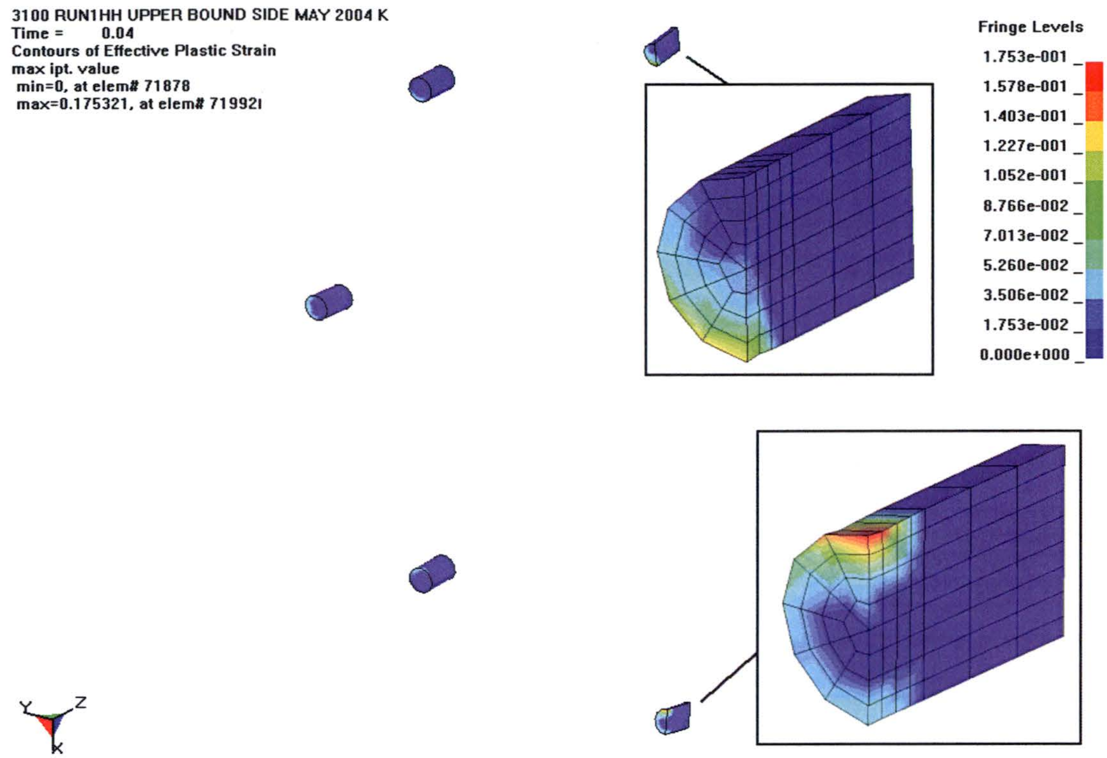

Figure 3.4.15 - Run1hh, Crush Impact, Effective Plastic Strain in the Studs

Part A - Initial Design with Borobond Cylinder

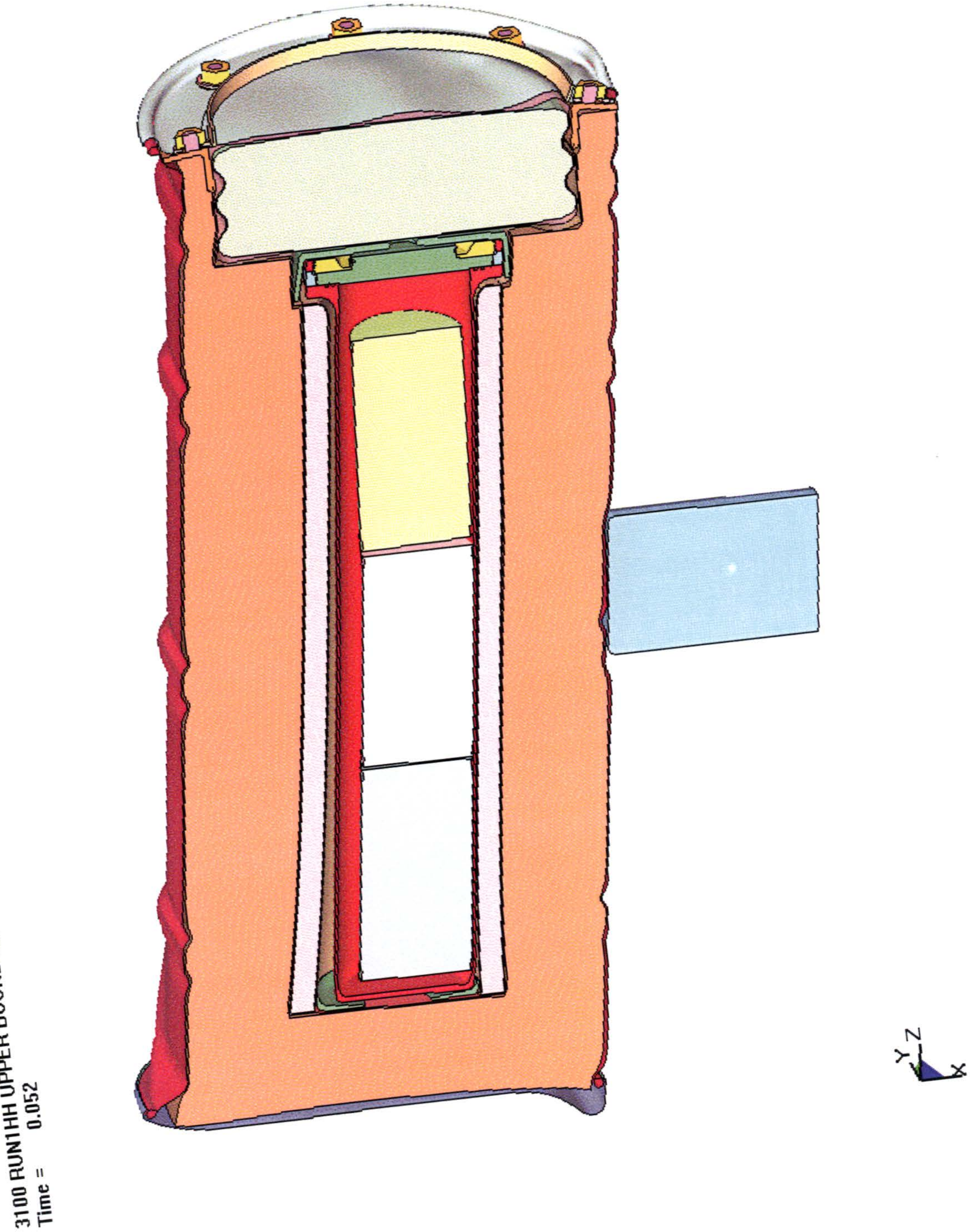

Figure 3.4.16 - Run1hh, Punch Impact, Final Configuration

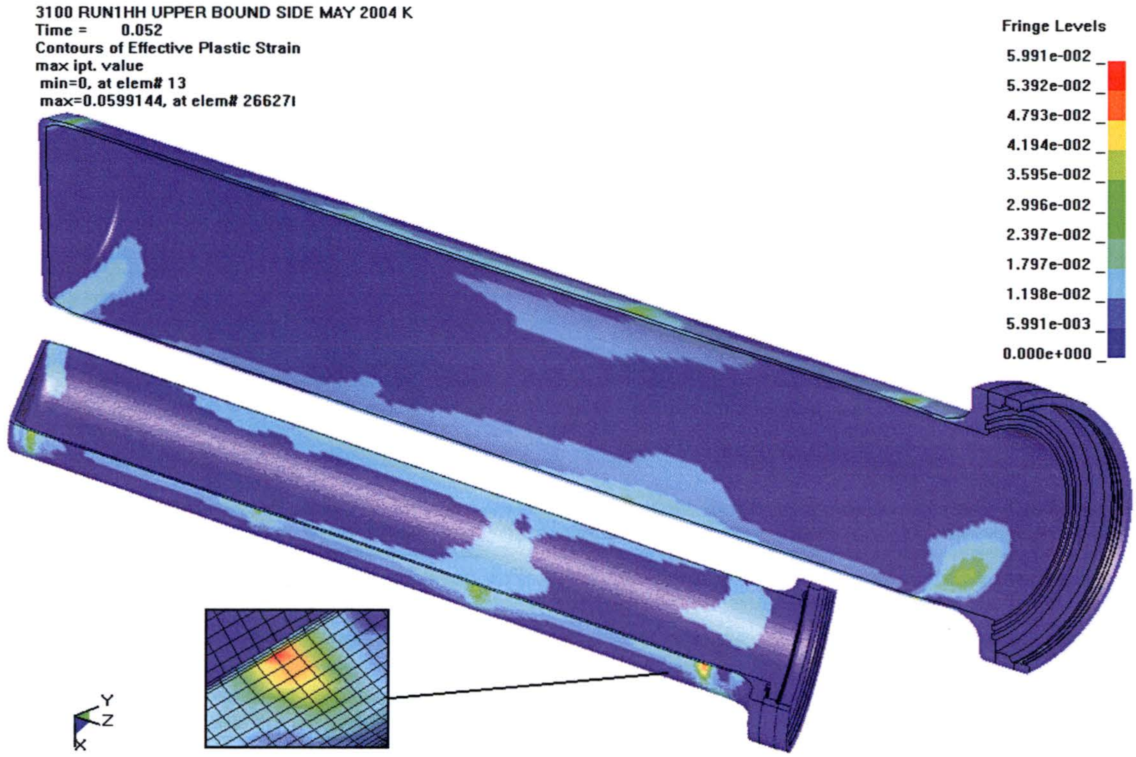

Figure 3.4.17 - Run1hh, Punch Impact, Effective Plastic Strain in the CV Body

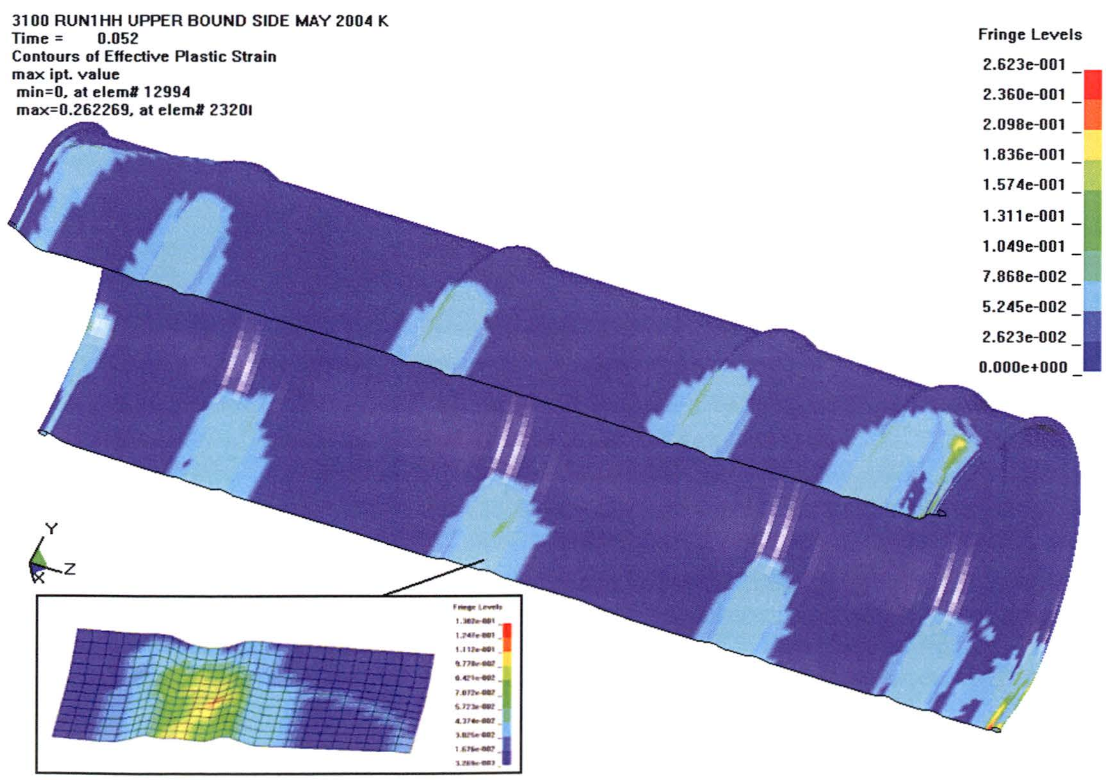

Figure 3.4.18 - Run1hh, Punch Impact, Effective Plastic Strain in the Drum

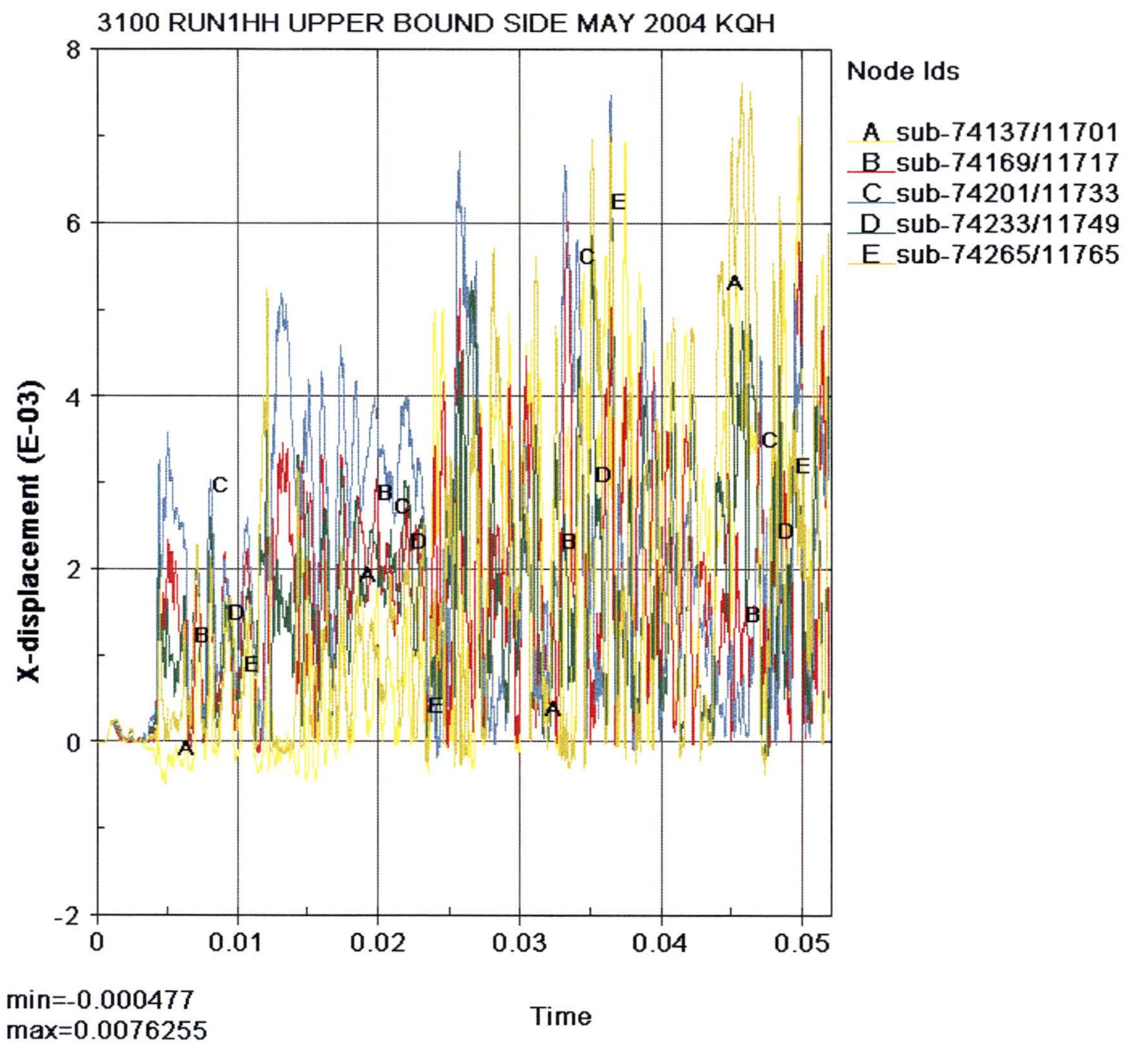

Figure 3.4.19 - Run1hh, CV Lid Separation Time History

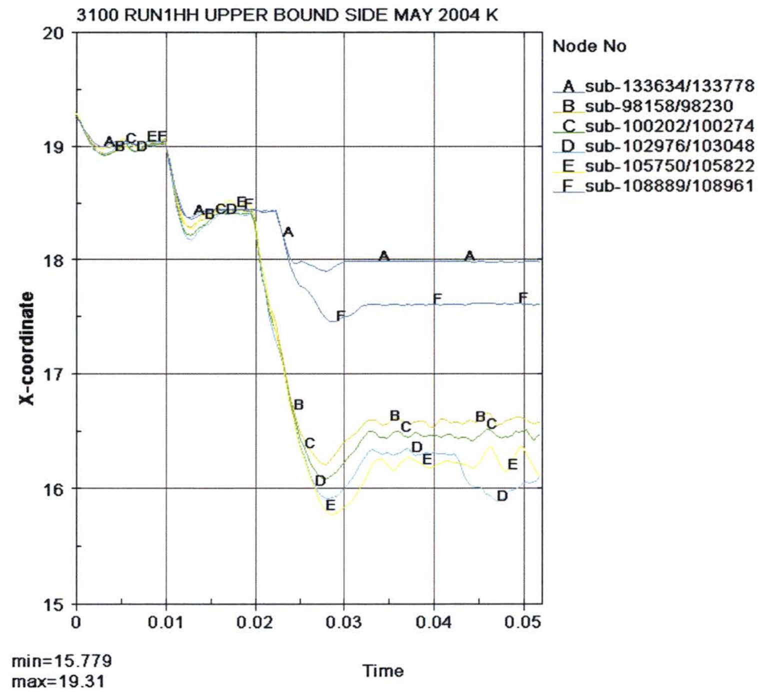

Figure 3.4.20 - Run1hh, Diameter of the Drum in the Direction of the Impacts

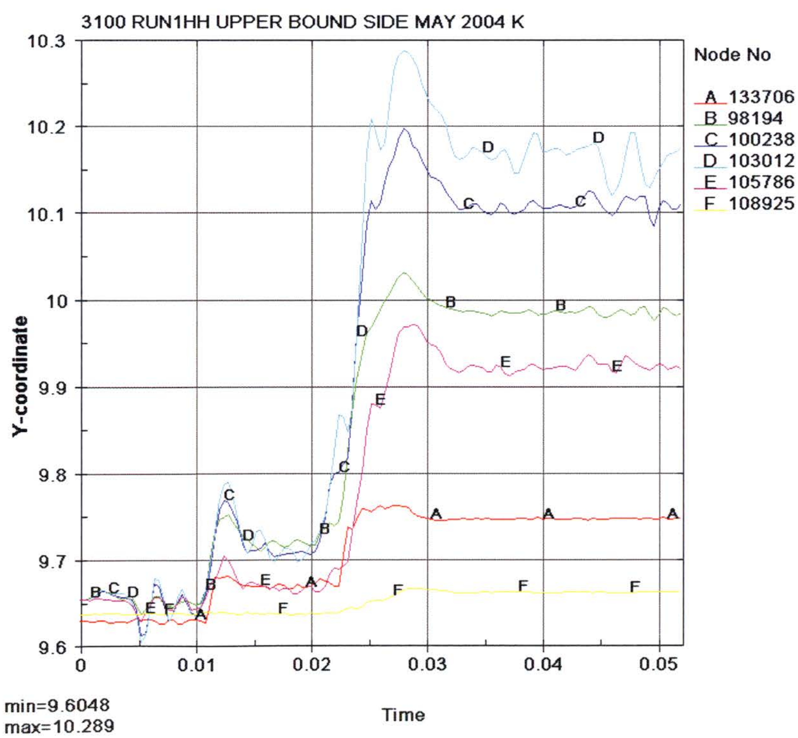

Figure 3.4.21 - Run1hh, Radius of the Drum in the Direction Normal to the Impacts

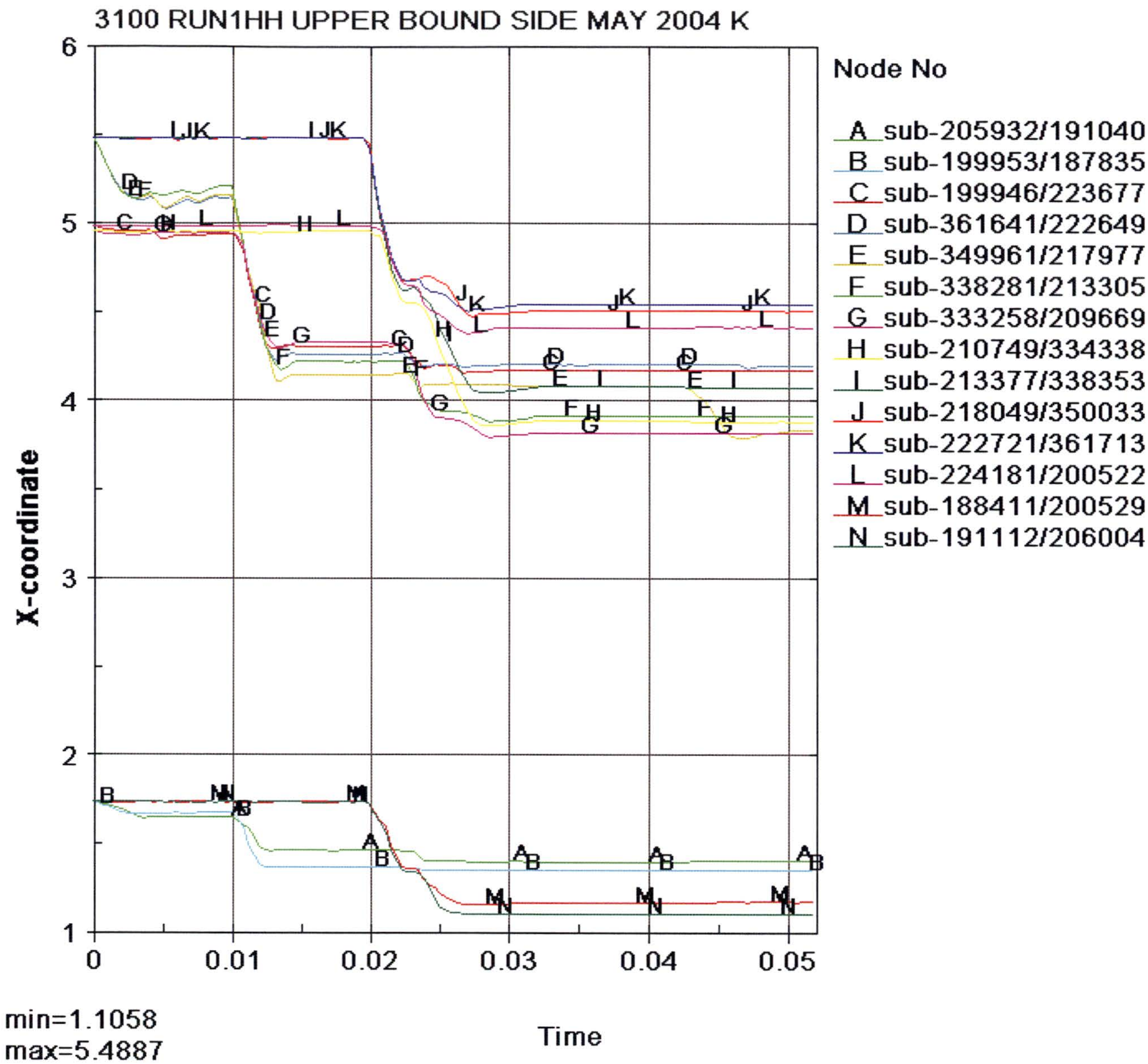

Figure 3.4.22 - Run1hh, Thickness Time History of the Drum Kaolite

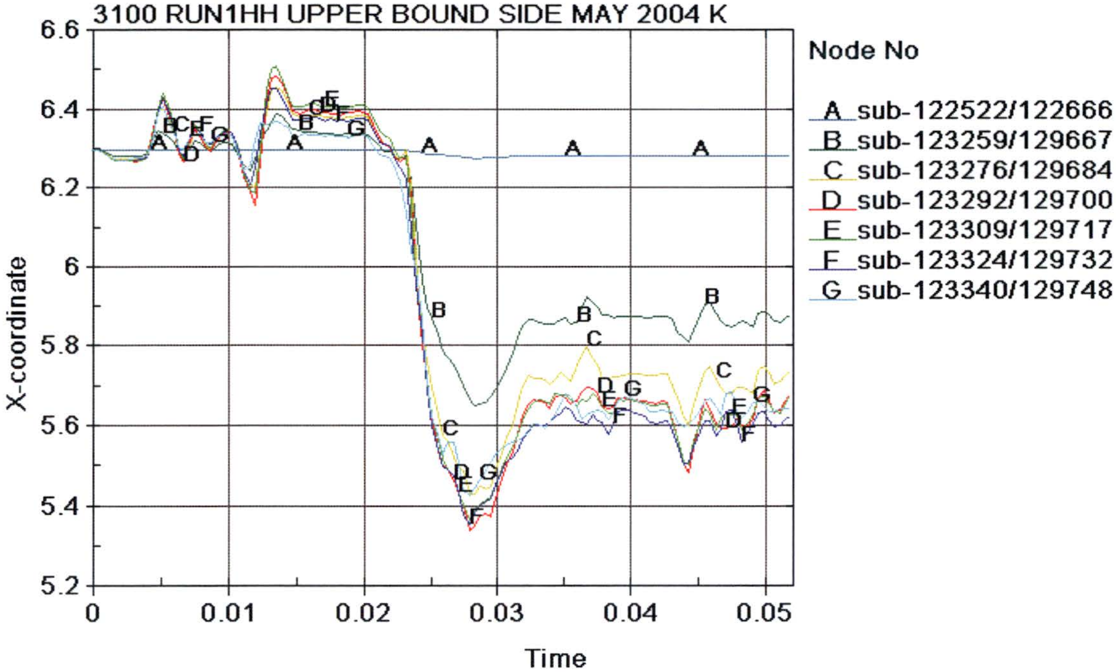

Figure 3.4.23 - Run1hh, Liner Diameter Time Histories

3.5 Run2e - Corner

Run2e is a package CG over corner impact with a 30-foot impact (time = 0 to 0.015 seconds)followed by a crush impact (0.015 to 0.05 seconds).

The configuration after the 30-foot impact is shown in Figure 3.5.1. The maximum effective plastic strain in the lid studs is in the stud at the impact with the rigid plane (0°) and is 0.5197 in/in as shown in Figure 3.5.2. It can be seen from the insert in Figure 3.5.2, that strains near the maximum exist across the thickness of the stud. Therefore, it should be noted that slight differences between the modeled length and actual length of the stud could be significant relative to possible failure of the stud. Other differences such as friction and local flexibility in the test pad armored plate (stud "digging in") could also significantly effect this stud and cause failure. The maximum effective plastic strain of other components for this impact are listed in Table 3.5.1.

Table 3.5.1 - Run2e, 30-Foot Impact, Effective Plastic Strain Levels in Some Components

Component	Effective Plastic Strain, in/in
CV Body	0.0142
CV Lid	0.0024
CV Nut Ring	0.0000
Angle	0.0393
Drum	0.3238
Drum Bottom Head	0.0000
Liner	0.3797
Lid	0.2968
Lid Stiffener	0.0271
Lid Stud Nuts	0.2252
Lid Stud Washers	0.0907
Plug Liner	0.1131

Figure 3.5.3 shows the final configuration for the crush impact. In Figure 3.5.4 the maximum effective plastic strain in the CV lid is shown to remain at 0.0024 in/in. Figure 3.5.5 shows the effective plastic strain in the liner to be a maximum of 0.5507 in/in. The maximum effective plastic strain in the drum is in the crimping as shown in Figure 3.5.6 and is a maximum of 0.3787 in/in. The maximum effective plastic strain in the drum studs

is shown to be 0.5578 in/in in Figure 3.5.7. As explained in the 30-foot impact results, slight variances in the length/configuration in this vicinity could prove significant in the test due to the relatively high level of strain through the thickness of the stud. There is a crimping of the lid and the drum roll in this local region, hence, even if the stud did shear, the lid would be held captive by the drum roll.

Table 3.5.2 - Run2e, Crush Impact, Effective Plastic Strain Levels in Some Components

Component	Effective Plastic Strain, in/in
CV Body	0.0364
CV Nut Ring	0.0000
Angle	0.0464
Drum Bottom Head	0.0731
Lid	0.3579
Lid Stiffener	0.0272
Lid Stud Nuts	0.2258
Lid Stud Washers	0.1111
Plug Liner	0.1170

The lid separation time history is given in Figure 3.5.8. A spike separation occurs in the crush impact with a maximum gap of about 0.010 inches. The run2e was extended to about 0.06 seconds so that the ringing associated with the gap at 0.05 seconds could relax. From the figure it is seen that an average value of gap would be 0.002 inches, or less due to the oscillatory nature of the gap response.

Figure 3.5.9 shows the location of the nodes used to obtain the minimum koalite thickness in the package bottom. The time history thickness is shown in Figure 3.5.10 for the bottom kaolite. A minimum thickness of about 1.8 inches is shown.

Figure 3.5.11 shows the location of the nodes used to obtain the minimum kaolite thickness in the plug. Figure 3.5.12 shows the distance time history with the minimum being about 2.8 inches.

Figure 3.5.13 shows the nodes used to obtain overall drum dimensions for the impacts. The final lengths from the bottom head to the lid are used to describe the deformations. Curve A in Figure 3.5.14 gives the length response of the crush corner to the lid. It has a final length of about 38.2 inches. Curve B in Figure 3.5.14 gives the length response from the initial 30-foot impact corner on the rigid surface to the bottom of the drum. This length has a final value of about 38.75 inches.

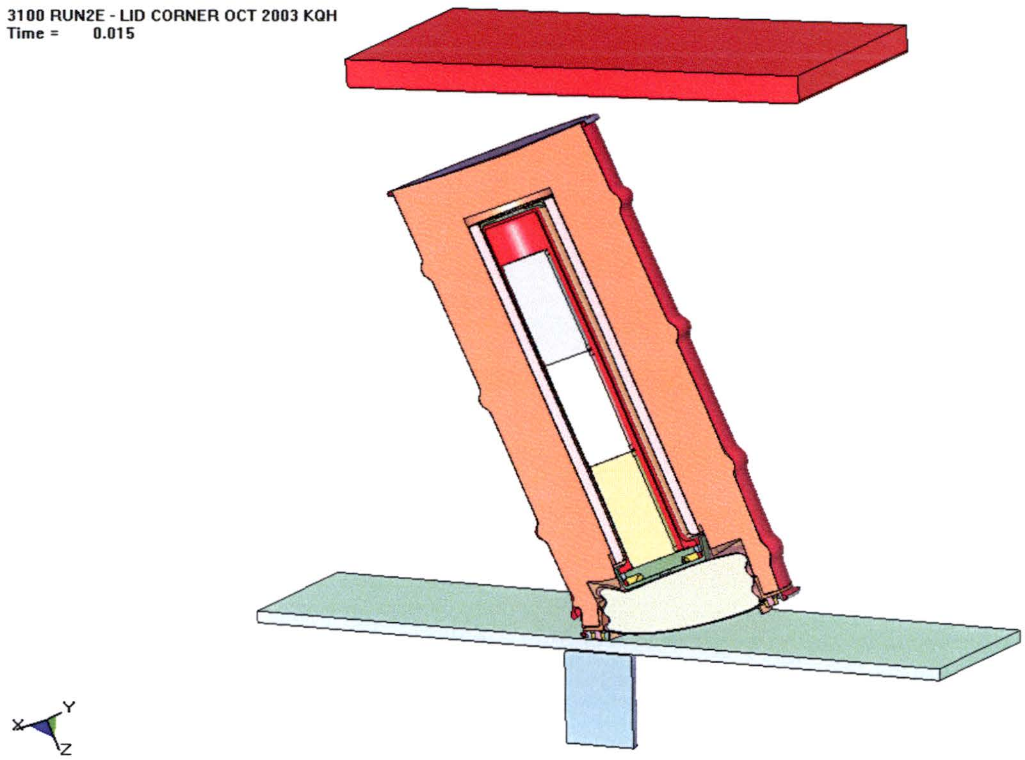

Figure 3.5.1 - Run2e, 30-Foot Impact, Final Configuration

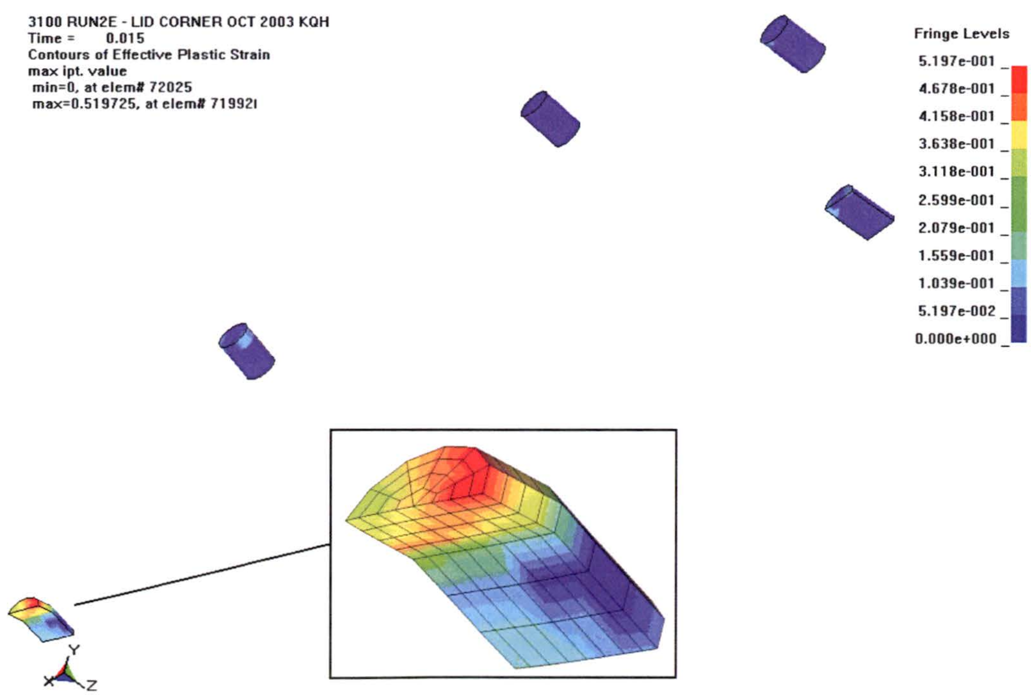

Figure 3.5.2 - Run2e, 30-Foot Impact, Effective Plastic Strain in the Drum Studs

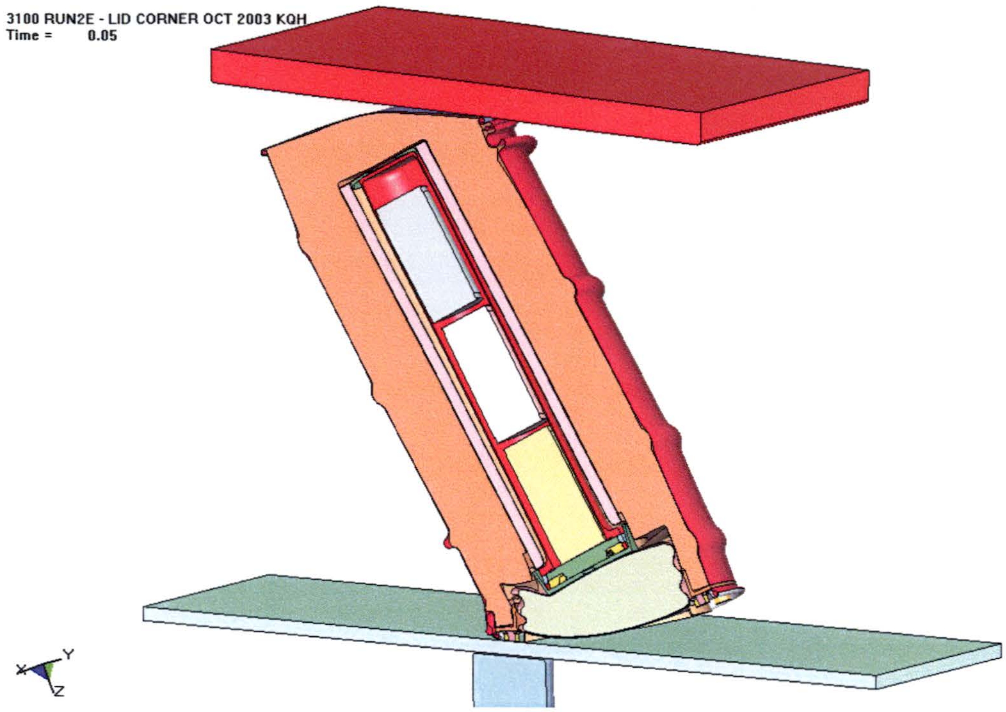

Figure 3.5.3 - Run2e, Crush Impact, Final Configuration

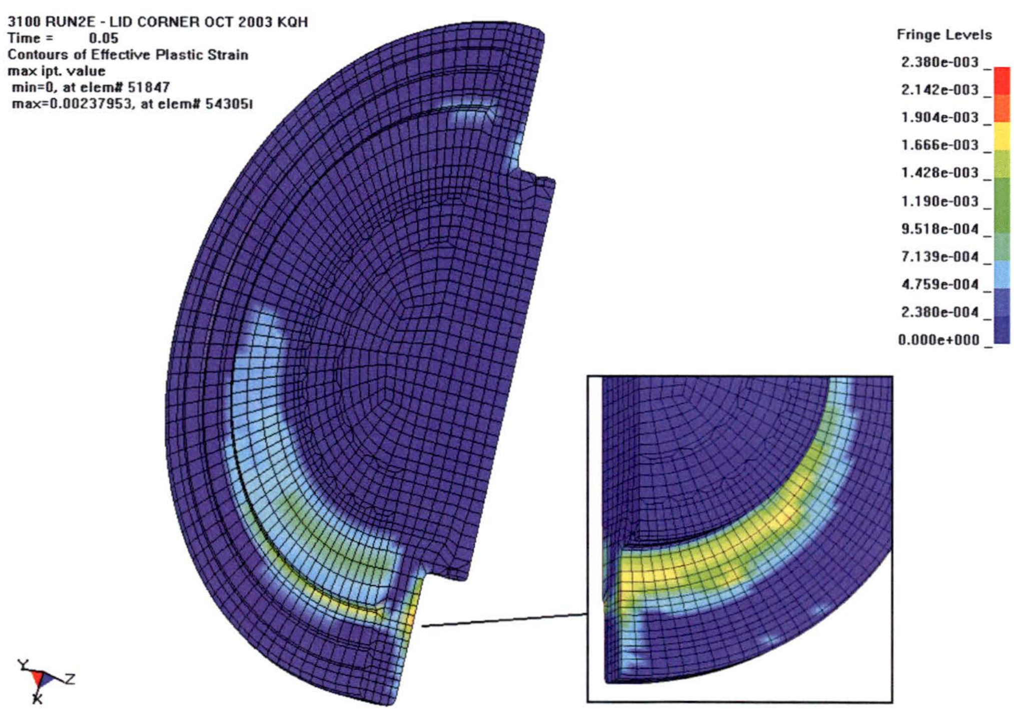

Figure 3.5.4 - Run2e, Crush Impact, Effective Plastic Strain in the CV Lid

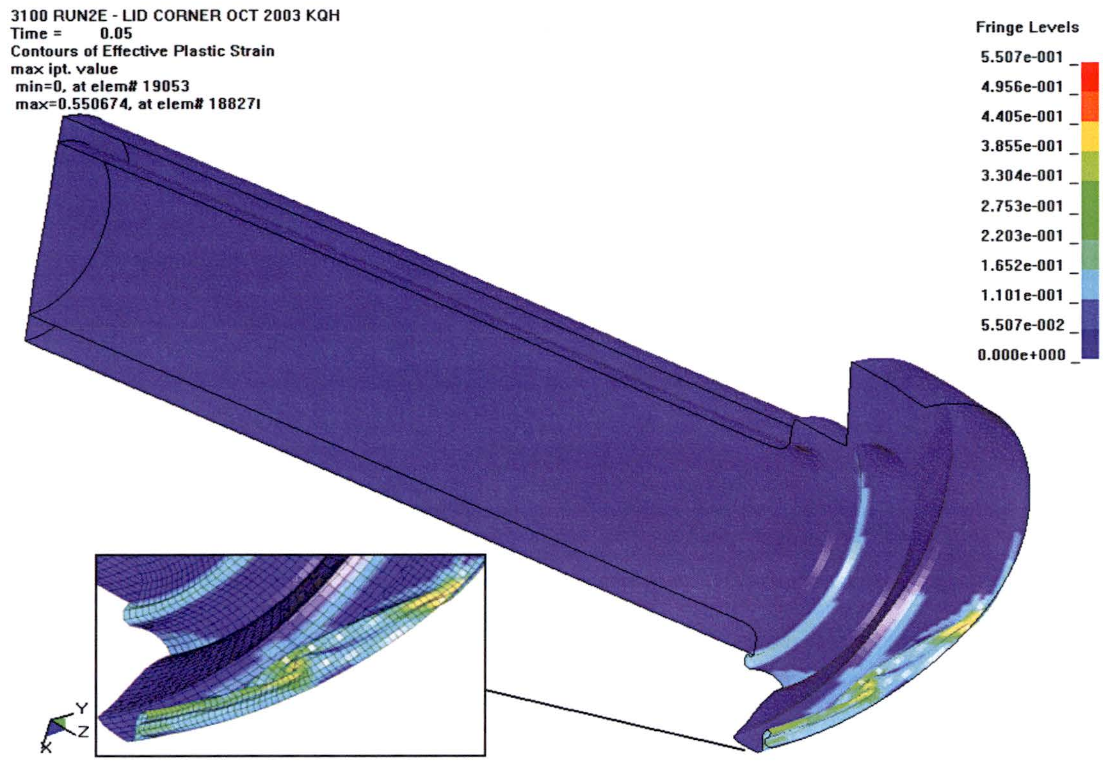

Figure 3.5.5 - Run2e, Crush Impact, Effective Plastic Strain in the Liner

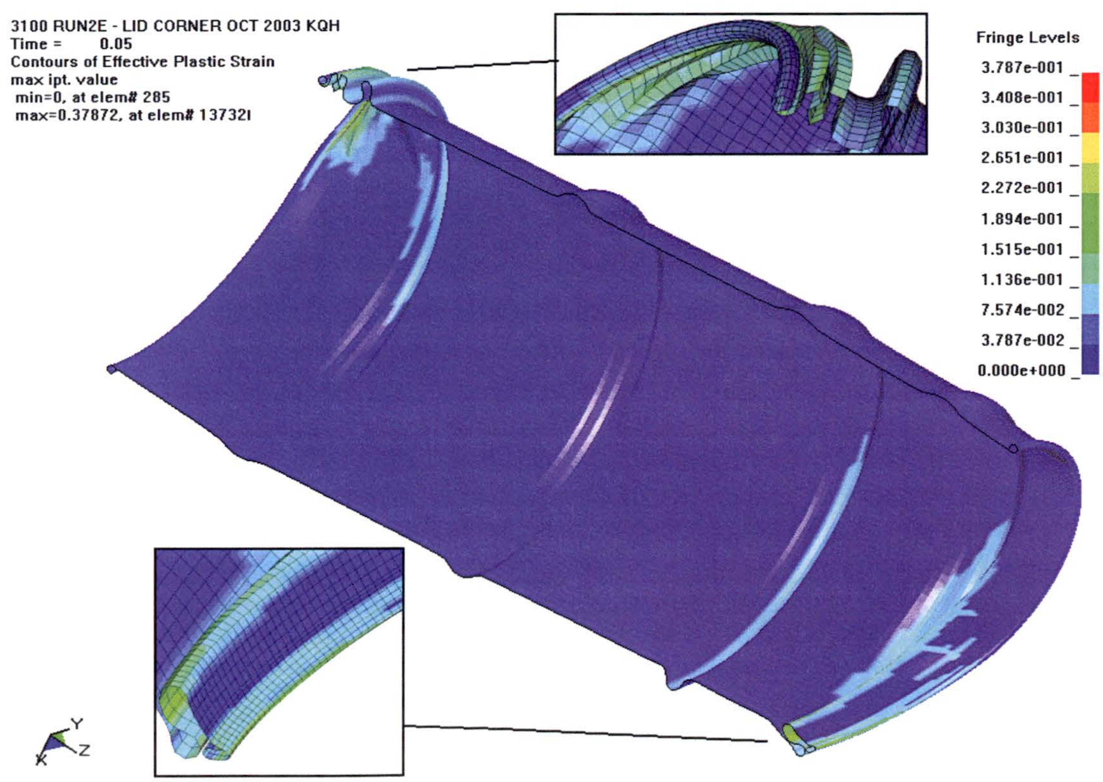

Figure 3.5.6 - Run2e, Crush Impact, Effective Plastic Strain in the Drum

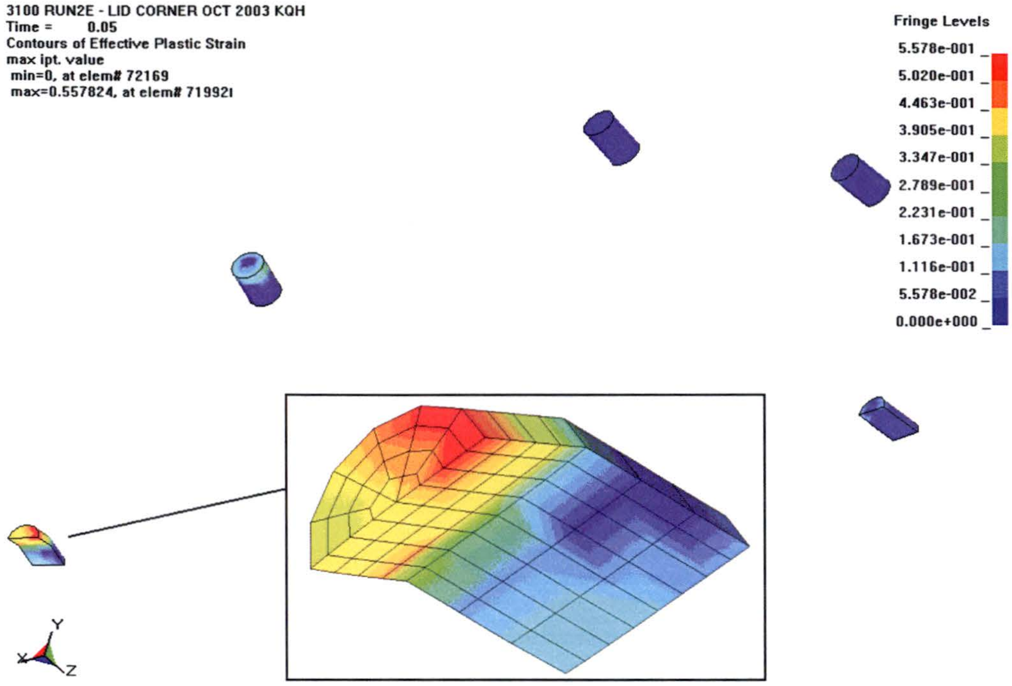

Figure 3.5.7 - Run2e, Crush Impact, Effective Plastic Strain in the Drum Studs

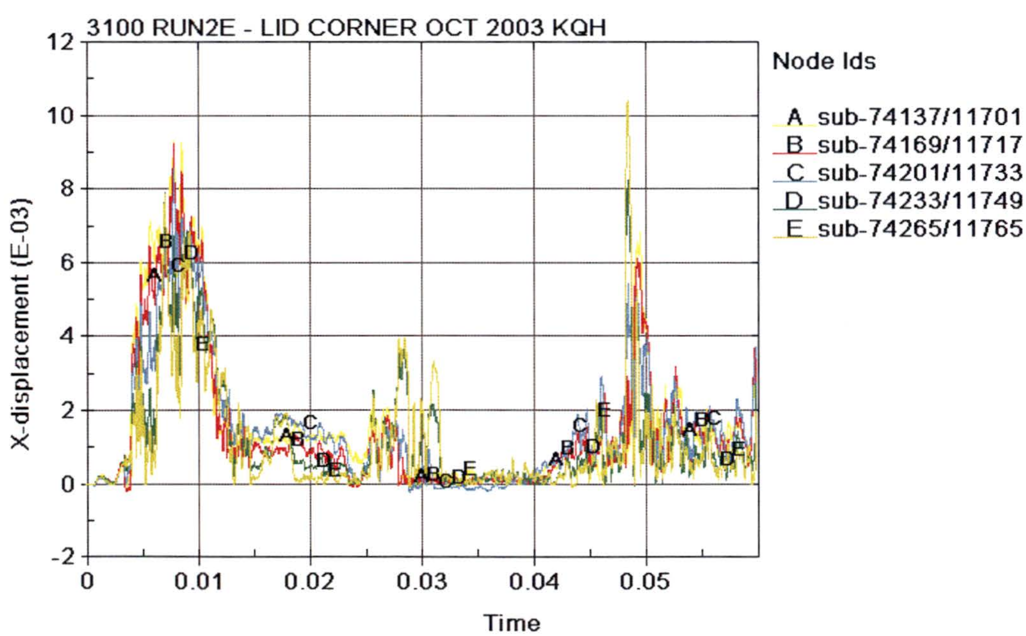

Figure 3.5.8 - Run2e, CV Lid/Body Separation Time History

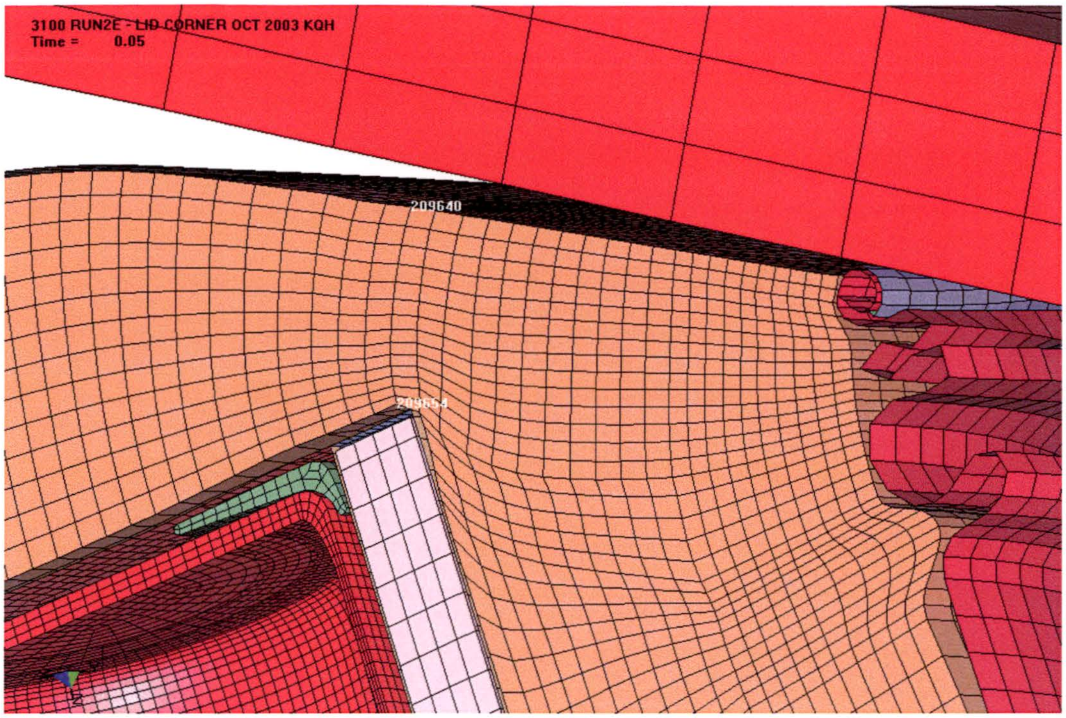

Figure 3.5.9 - Run2e, Location of Kaolite Nodes at the Bottom for Thickness Evaluation

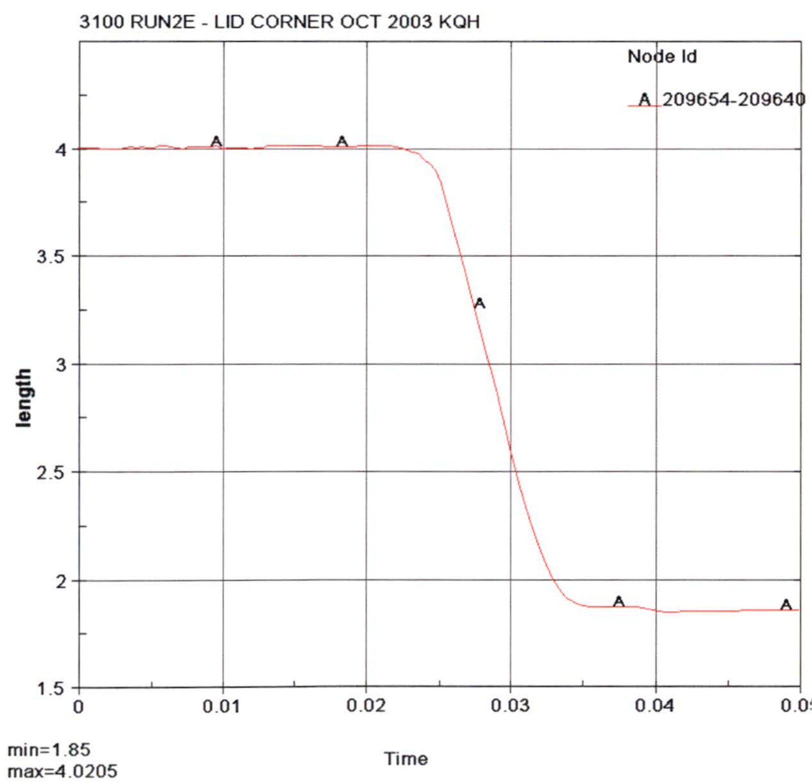

Figure 3.5.10 - Run2e, Minimum Thickness Time History for the Bottom Kaolite

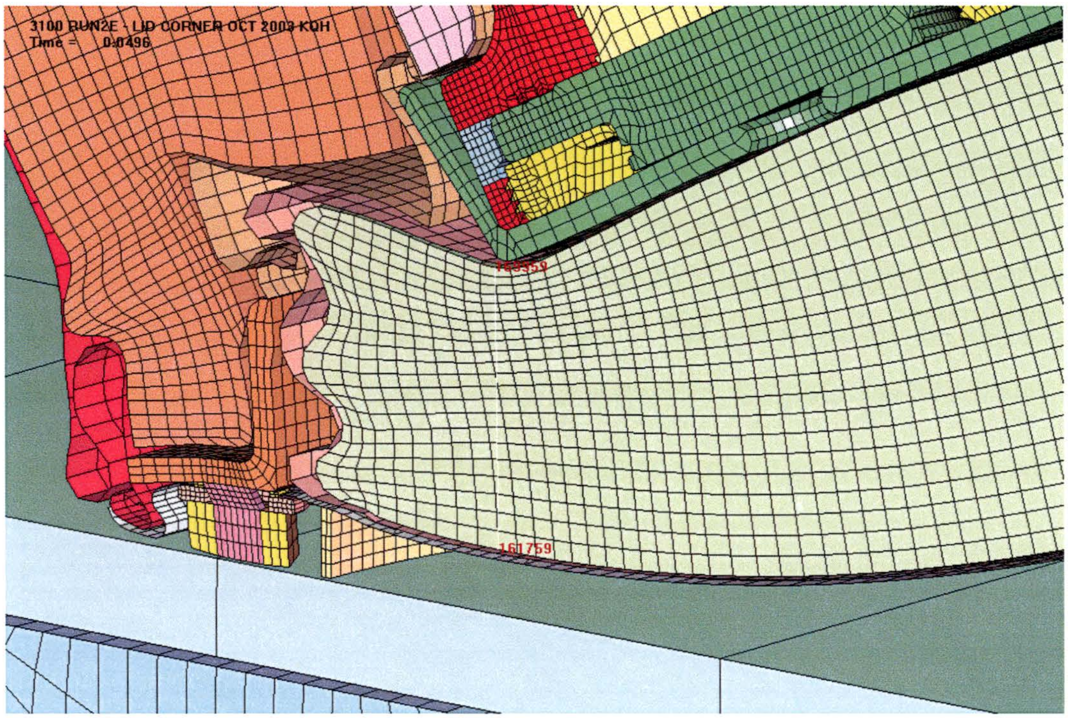

Figure 3.5.11 - Run2e, Location of Kaolite Nodes in the Plug for Thickness Evaluation

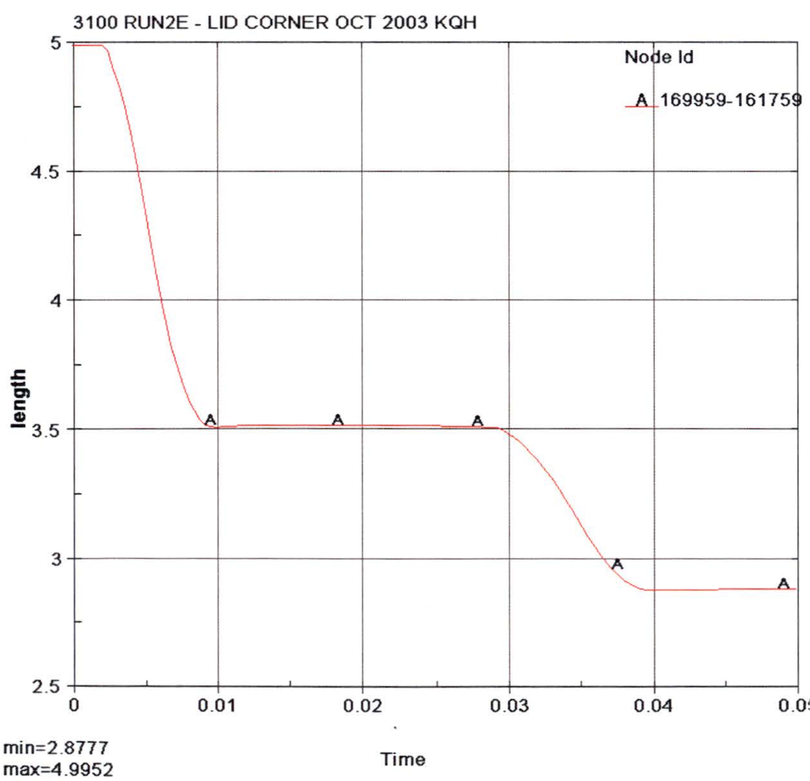

Figure 3.5.12 - Run2e, Minimum Thickness Time History for the Plug Kaolite

Figure 3.5.13 - Run2e, Length Dimensions in the Drum

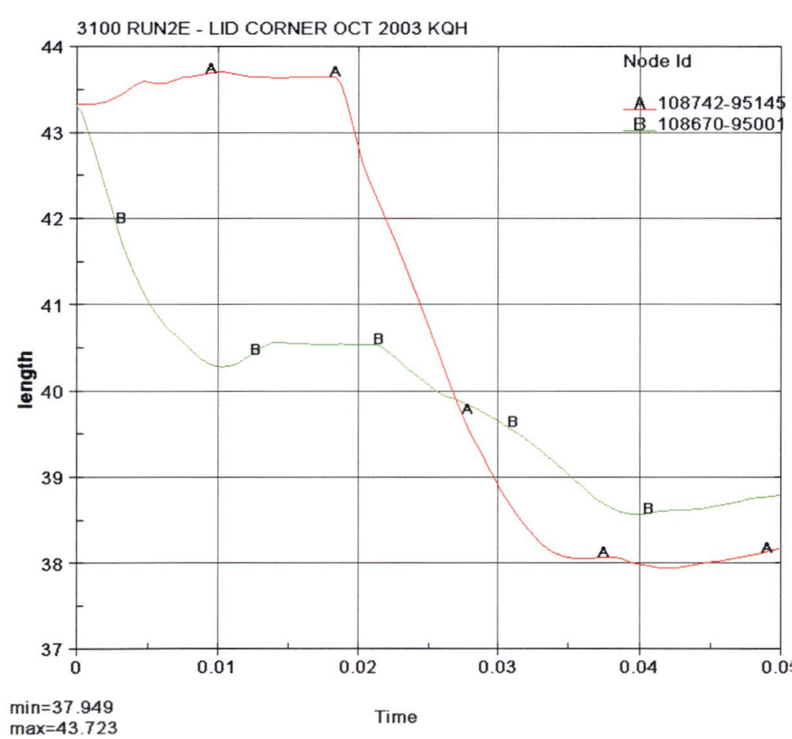

Figure 3.5.14 - Run2e, Time History of Length Dimensions in the Drum

3.6 Run3b - End

Run3b is a 30-foot lid end impact (time = 0 to 0.010 seconds) followed by a crush impact onto the package bottom (0.010 to 0.028 seconds). Figure 3.6.1 shows the final configuration for the 30-foot impact. Because of the relatively low demand placed on the components, no strain plots are presented for the 30-foot impact. Table 3.6.1 summarizes the maximum effective plastic strains in the package components.

Table 3.6.1 - Run3b, 30-Foot Impact, Effective Plastic Strain Levels in Some Components

Component	Effective Plastic Strain, in/in
CV Body	0.0012
CV Lid	0.0031
CV Nut Ring	0.0000
Angle	0.0287
Drum	0.0565
Drum Bottom Head	0.0024
Liner	0.1665
Lid	0.1094
Lid Stiffener	0.0068
Lid Studs	0.0962
Lid Stud Nuts	0.0162
Lid Stud Washers	0.0510
Plug Liner	0.0636

Figure 3.6.2 shows the final configuration for the 30-foot impact and the successive crush impact. Figure 3.6.3 shows that the maximum effective plastic strain in the CV body is 0.0053 in/in. The maximum occurs in the bearing of the body flange onto the lid (at the O-ring seals). The magnitude of effective plastic strain is questioned due to the fact that the elevated strains occur at single nodes and are not symmetric (see the insert in Figure 3.6.3). The maximum effective plastic strain in the bottom region of the CV body is found to be 0.0035 in/in and does exhibit a symmetric characteristic as is shown in Figure 3.6.3.

The CV lid effective plastic strain fringes are shown from both sides in a split image in Figure 3.6.4. The maximum effective plastic strain in the lid is shown to be 0.0034 in/in in the figure. The other components are summarized in Table 3.6.2.

Table 3.6.2 - Run3b, Crush Impact, Effective Plastic Strain Levels in Some Components

Component	Effective Plastic Strain, in/in
CV Nut Ring	0.0000
Angle	0.0304
Drum	0.1258
Drum Bottom Head	0.0312
Liner	0.3585
Lid	0.1415
Lid Stiffener	0.0098
Lid Studs	0.1541
Lid Stud Nuts	0.0170
Lid Stud Washers	0.0510
Plug Liner	0.0944

The CV lid separation time history is shown in Figure 3.6.5. The response during the 30-foot impact is a spike separation of about 0.012 inches, which relaxes to a maximum value of 0.003 inches for the remainder of the 30-foot impact. During the crush impact it is seen that separation is spikes to a maximum of about 0.004 inches, but the average remains at about 0.002 inches or less at the end of the impact.

Figure 3.6.6 shows the nodes chosen to obtain the drum height and kaolite thickness time history data. Figure 3.6.7 shows the drum height time history. From the figure it is seen that the overall height would be approximately 39 inches. Figure 3.6.8 shows the thickness time histories in the kaolite for the plug and the bottom. The curve A in the figure is for the bottom kaolite thickness, and it reaches about 2.2 inches as a final value. Curve B, is for the plug and it reaches about 3.4 inches for the final kaolite thickness.

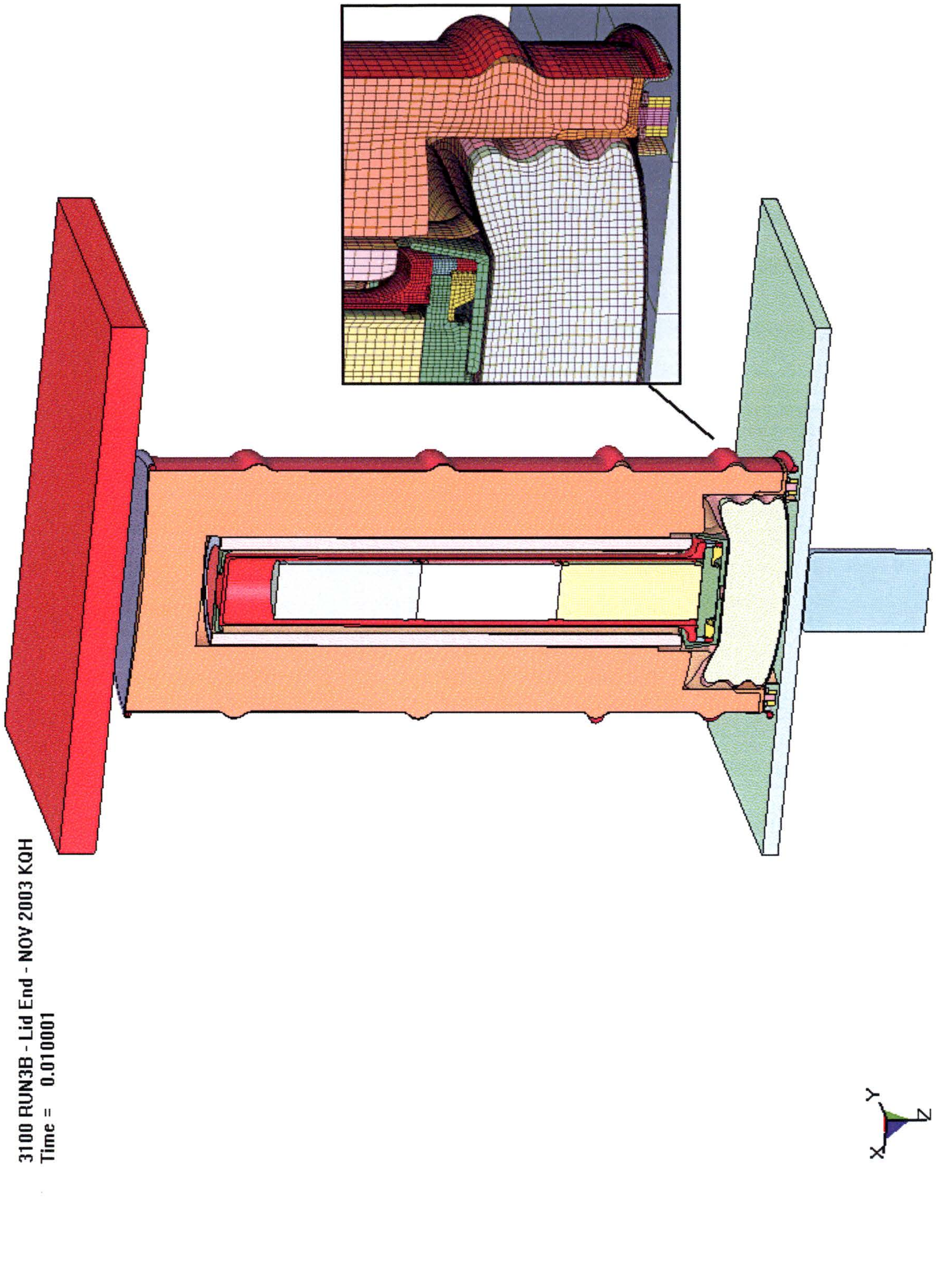

Figure 3.6.1 - Run3b, Configuration After the 30-Foot Impact

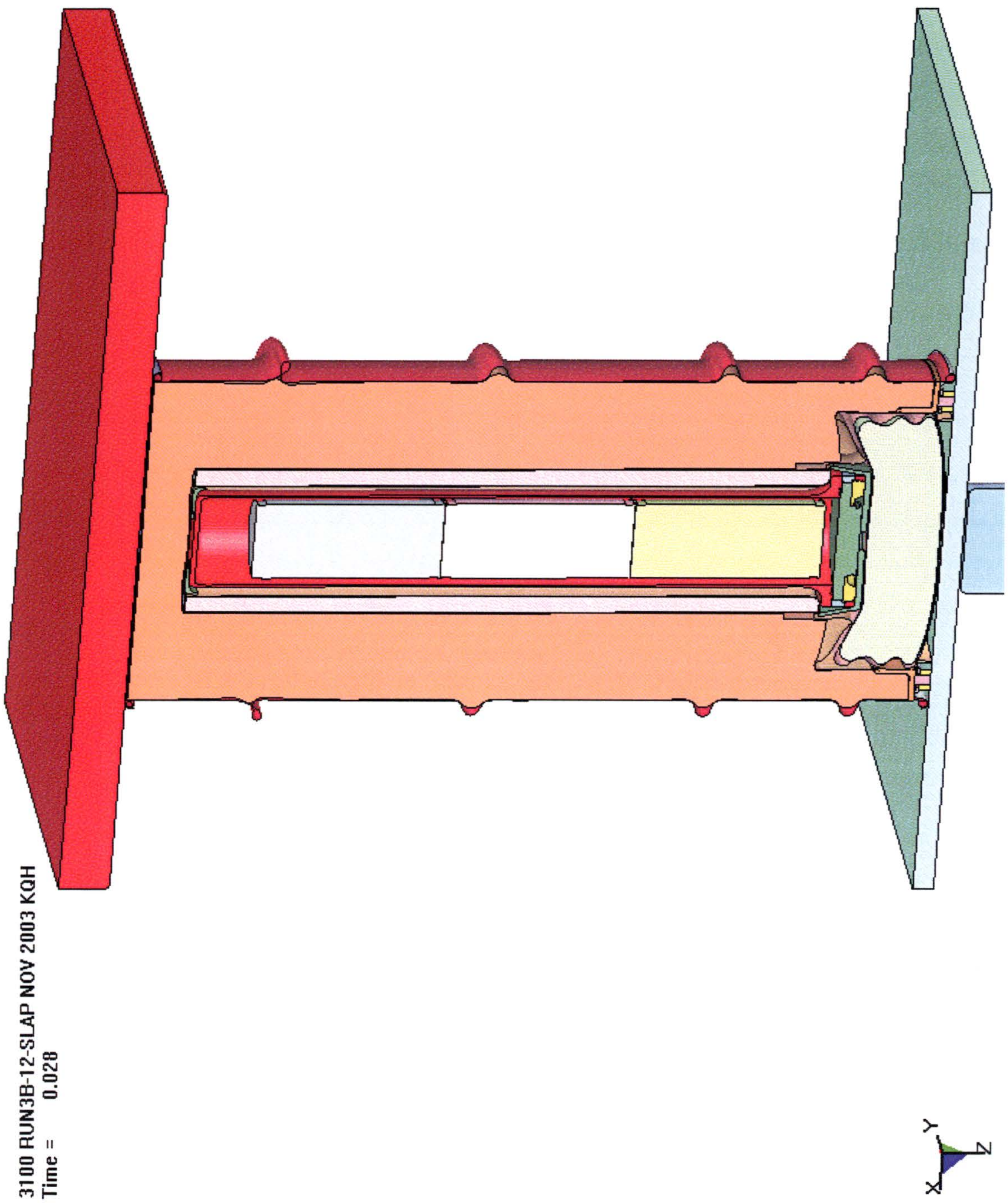

Figure 3.6.2 - Run3b, Crush Impact, Final Configuration

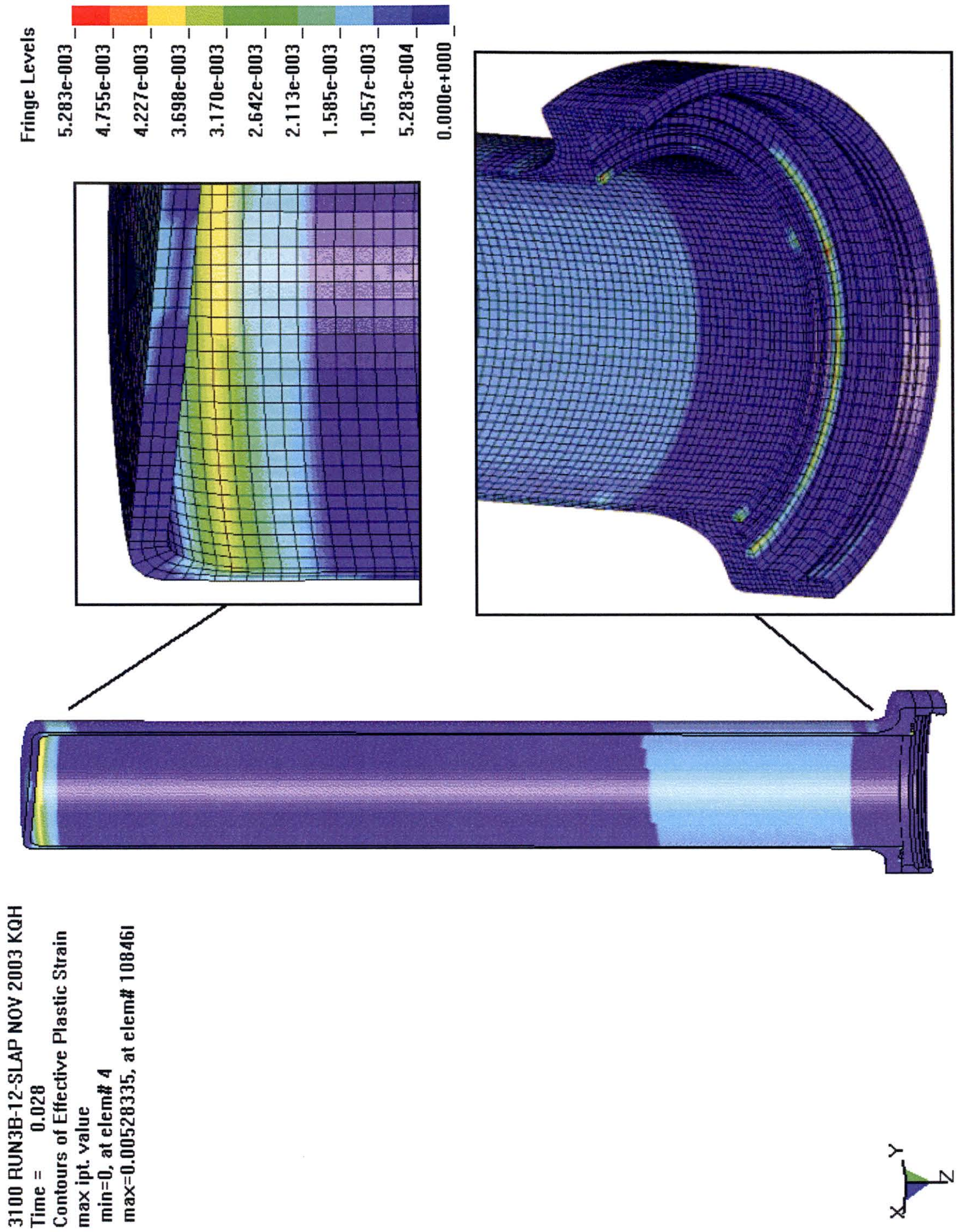

Figure 3.6.3 - Run3b, Crush Impact, Effective Plastic Strain in the CV Body

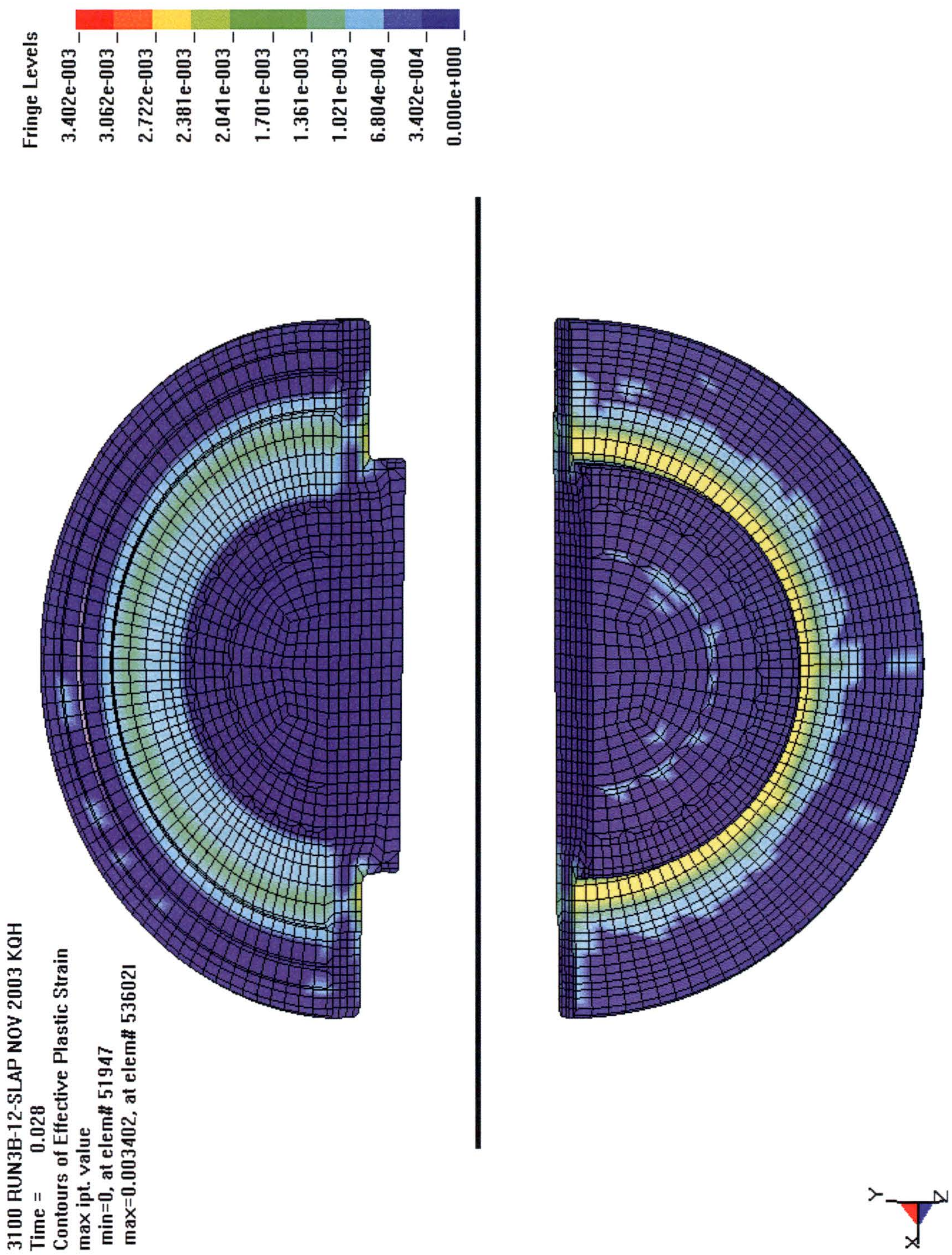

Figure 3.6.4 - Run3b, Crush Impact, Effective Plastic Strain in the CV Lid

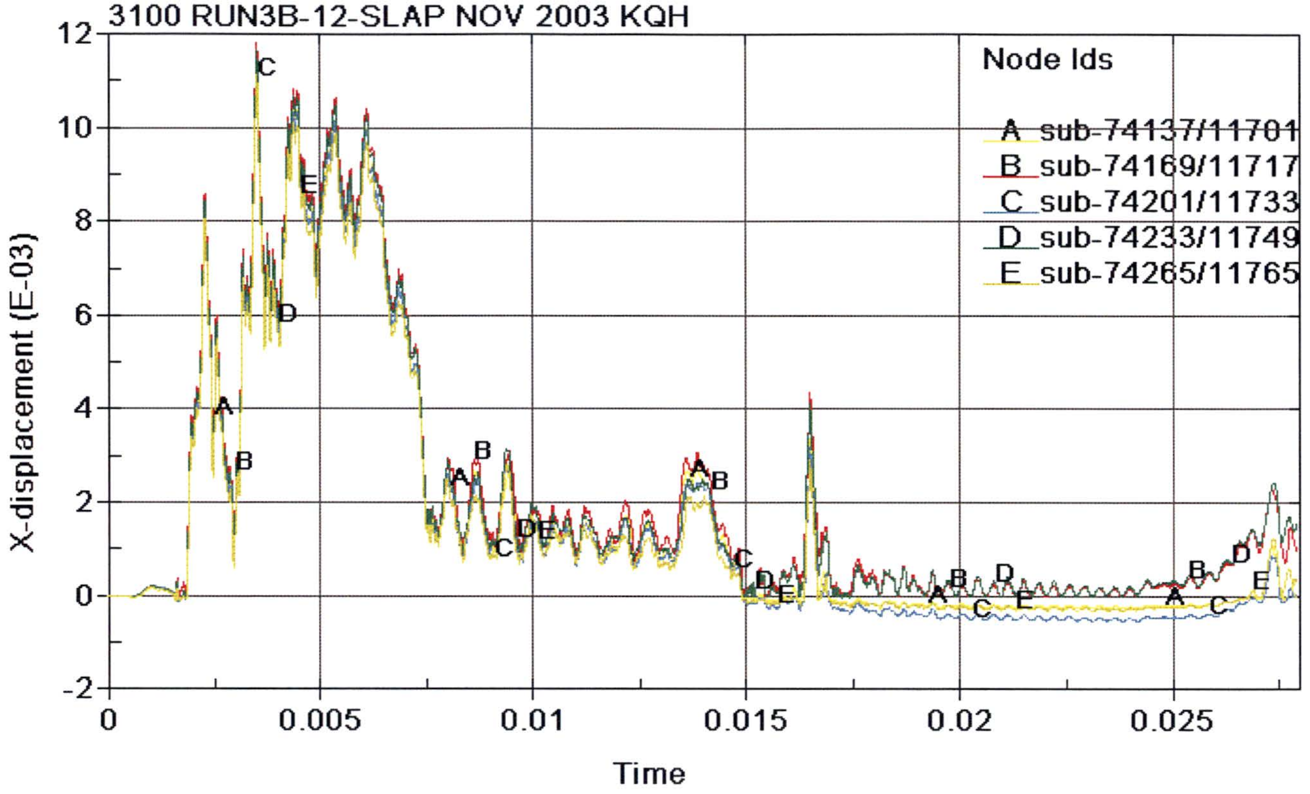

Figure 3.6.5 - Run3b, CV Lid Separation Time History

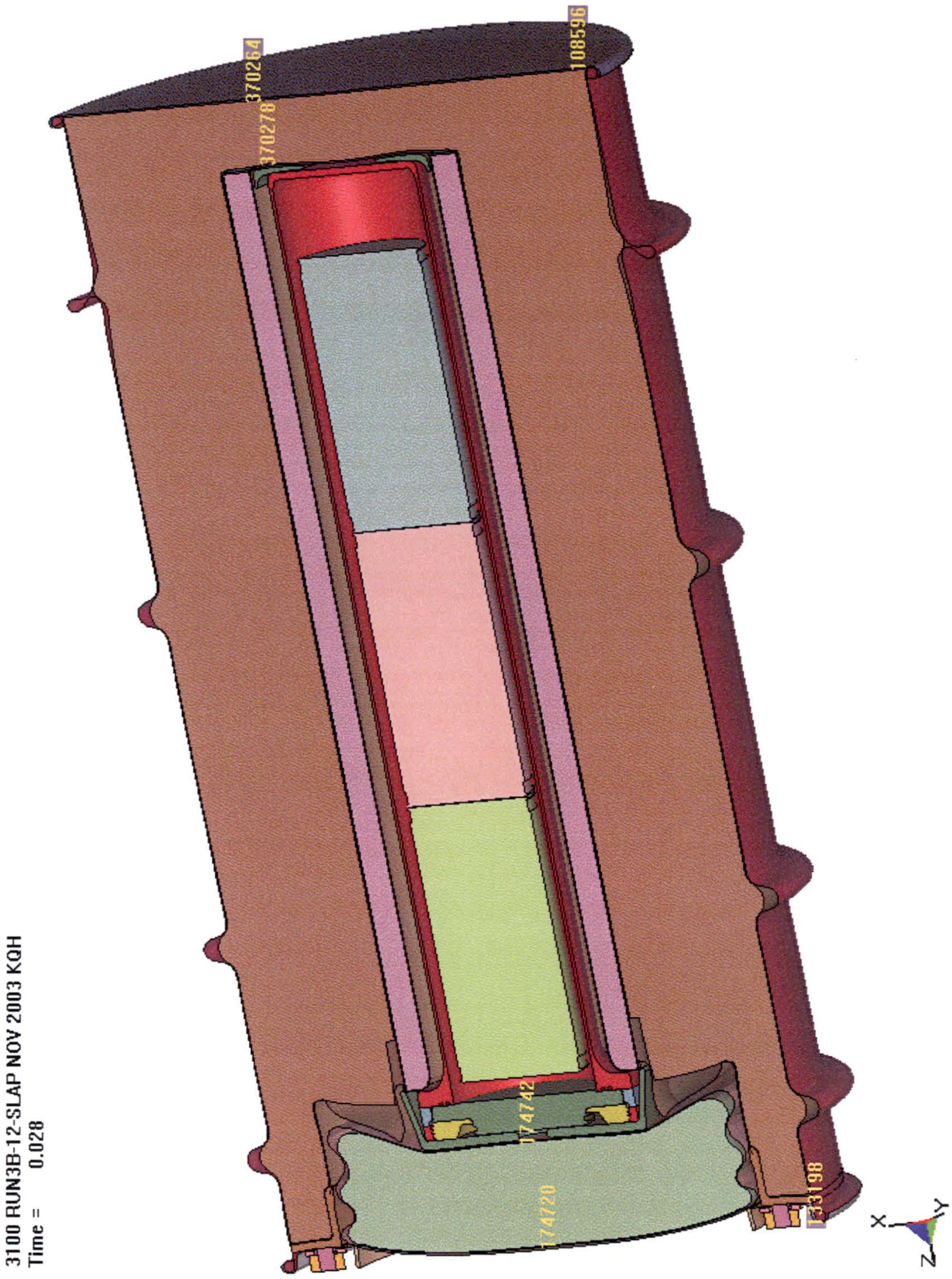

Figure 3.6.6 - Run3b, Nodes Chosen for Displacement Time Histories

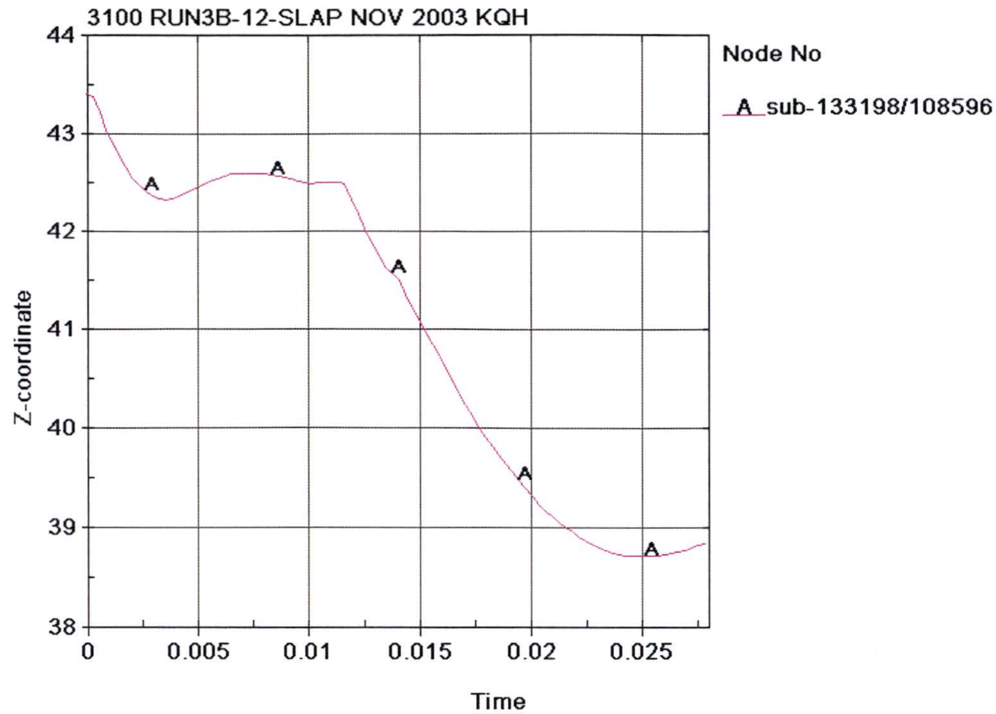

Figure 3.6.7 - Run3b, Drum Height Time History

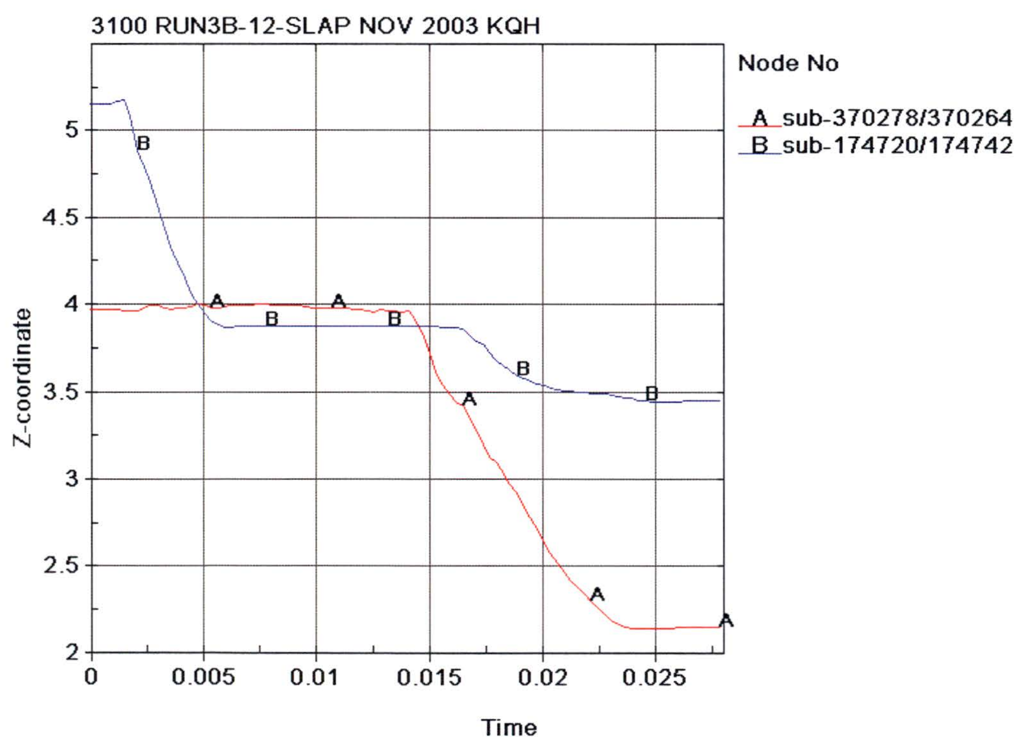

Figure 3.6.8 - Run3b, Kaolite Thickness Time History

3.7 Run4g - Slapdown

Run4g is a 12° slapdown, 30-foot impact (time 0 to 0.02 seconds) followed by a crush with the crush plate CG over the CV flange (0.02 to 0.04 seconds). A drum stud is located on the line of impact (0°) in this model.

The deflected shape of the package after the 30-foot impact is shown in Figure 3.7.1. The maximum effective plastic strain in the CV body for the 30-foot impact is 0.0445 in/in as shown in Figure 3.7.2 and occurs near the bottom head. The maximum effective plastic strain in other components for the 30-foot impact are listed in Table 3.7.1.

Table 3.7.1 - Run4g, 30-Foot Impact, Effective Plastic Strain Levels in Some Components

Component	Effective Plastic Strain, in/in
CV Lid	0.0003
CV Nut Ring	0.0000
Angle	0.0881
Drum	0.3017
Drum Bottom Head	0.2877
Liner	0.1234
Lid	0.5537
Lid Stiffener	0.0232
Lid Studs	0.1737
Lid Stud Nuts	0.0000
Lid Stud Washers	0.0597
Plug Liner	0.1290

Figure 3.7.3 shows the final configuration for the crush impact for run4g. The maximum effective plastic strain in the CV body is 0.0457 in/in as shown in Figure 3.7.4. The maximum effective plastic strain in the drum lid is 1.0797 in/in (surface strain) as shown in Figure 3.7.5. The maximum occurs near the stud at 90°, or initially along the Y axis. This high strain is caused by lid/stud reacting the ovalization response of the package due to the crush plate impact. The fringe range has been set such that the strain levels above 0.57 in/in are colored in red in Figure 3.7.5. The maximum membrane strain in the lid at

the same location (as the surface strain) is 0.8920 in/in. The region of elevated strain is localized to the hole at 90°, therefore any tearing of the lid would be localized. The large washers would restrain the lid.

Figure 3.7.6 shows the effective plastic strain in the drum studs. At the time shown the stud at the 90° position has failed (evident by removed element row at the base of the stud). All of the elements on the cross section reached the prescribed failure strain of 0.57 in/in and were deleted by LS-Dyna during the impact. Only one stud, the one at 90°, was shown to reach elevated strain levels and be severed for the crush impact. The plastic-kinematic model used for the studs allows a failure value to be used (0.57 in/in). The stud elements reach failure and elements begin to be deleted at about solution time = 0.0312 seconds. By 0.0332 seconds, all the elements on the cross section have been deleted by LS-Dyna.

The lid uses a power law model, which does not allow material failure in the model. Investigation shows that the lid reaches 0.57 in/in at about 0.0272 seconds, a time at which the stud maximum strain is about 0.28 in/in. This demonstrates that the lid reaches failure levels before the stud and at that time, the stud effective plastic strain is relatively low. Therefore, it would be expected that the lid would tear before the stud reaches failure. Due to the extent of the effective plastic strain fringe patterns in the lid plus the conservative modeling of the stud due to lid shear (Section 2.1 discussion), it is believed that the tearing would be local and that the lid (and by default the plug) would be restrained by the large washers. Table 3.7.2 shows the maximum effective plastic strain in the remainder of the package components for the crush impact.

Table 3.7.2 - Run4g, Crush Impact, Effective Plastic Strain Levels in Some Components

Component	Effective Plastic Strain, in/in
CV Body	0.0457
CV Lid	0.0005
CV Nut Ring	0.0000
Angle	0.1045
Drum	0.3972
Drum Bottom Head	0.2877
Liner	0.2702
Lid Stiffener	0.0838
Lid Stud Nuts	0.0086
Lid Stud Washers	0.1003
Plug Liner	0.2715

Figure 3.7.7 shows the lid separation time history for the nodal pairs shown in Figure 3.1.30. There are several spikes up to about 0.007 inches evident in the lid separation time history. However, most of the noise level is about 0.004 inches or less and is oscillatory in nature. Therefore, an average of 0.002 inches or less would be expected.

Figure 3.7.8 shows the drum diameter deformation in the X-direction. The nodes are those defined in Figure 3.1.34. Curve A in the figure shows that the final distance in at the lid, between the two flattened regions is about 13.5 inches. Figure 3.7.9 gives the radial deformation time history in the Y-direction.

Figure 3.7.10 gives the kaolite thickness time histories. The nodes are those defined in Figure 3.1.32.

Figure 3.7.11 shows the liner diameter time history at various locations along its length. Figure 3.1.37 and Table 3.1.3 show the locations of the nodal pairs along the liner.

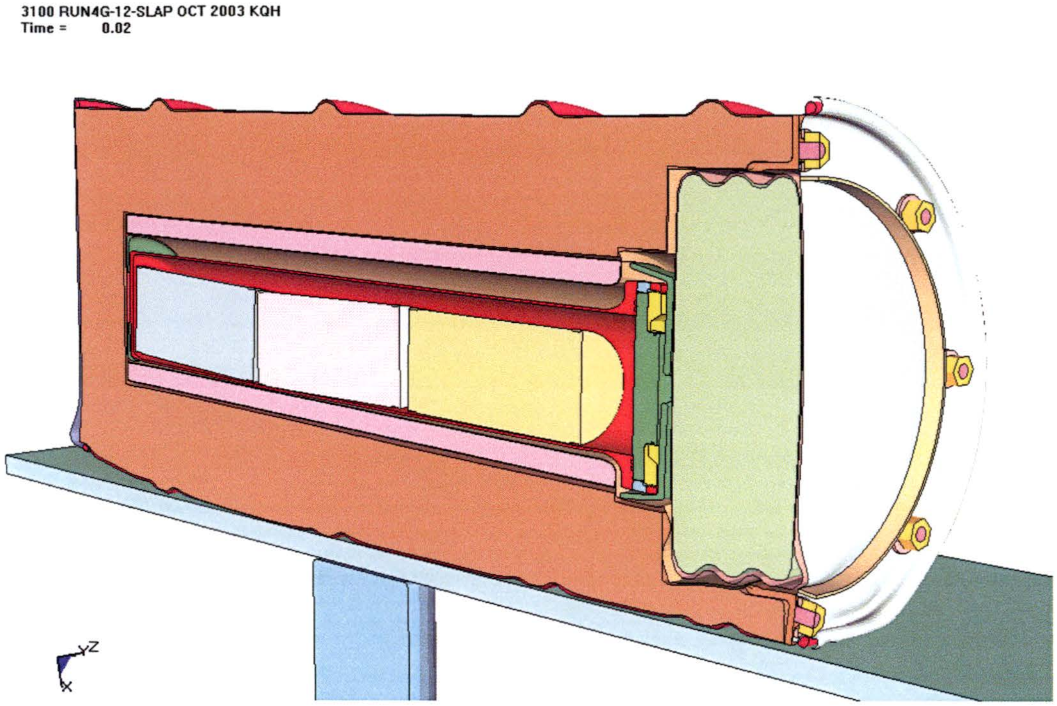

Figure 3.7.1 - Run4g, Slapdown Impact, Final Configuration

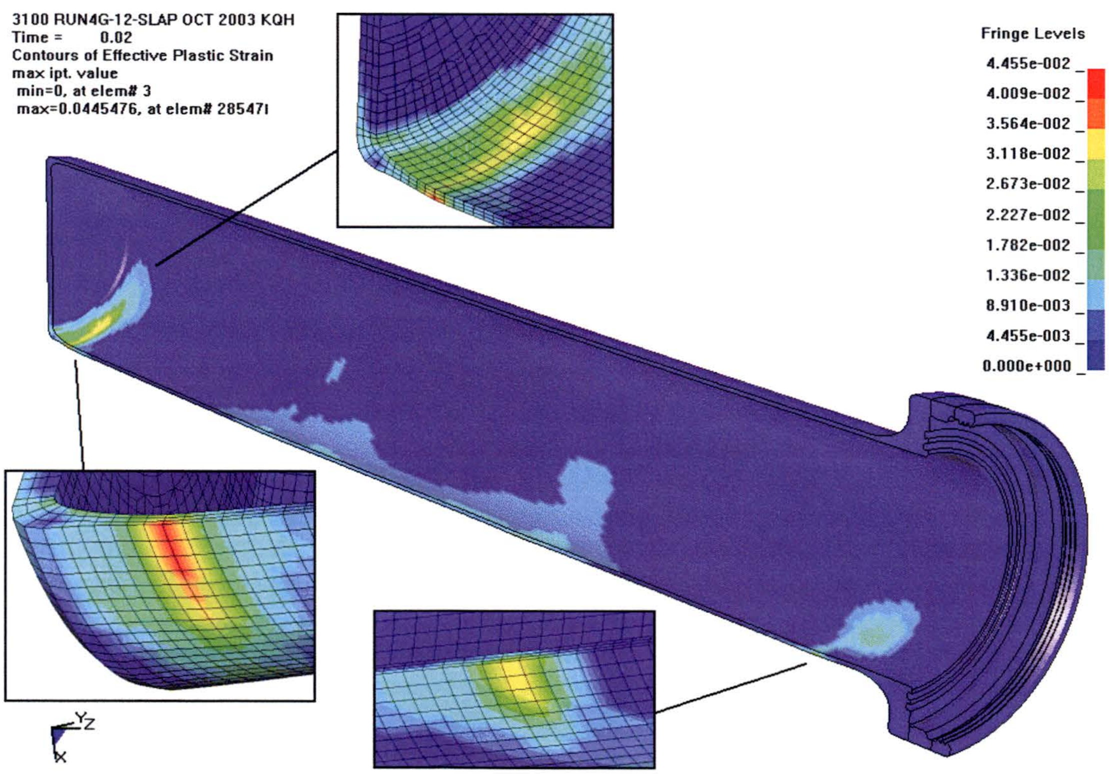

Figure 3.7.2 - Run4g, Slapdown Impact, Effective Plastic Strain in the CV Body

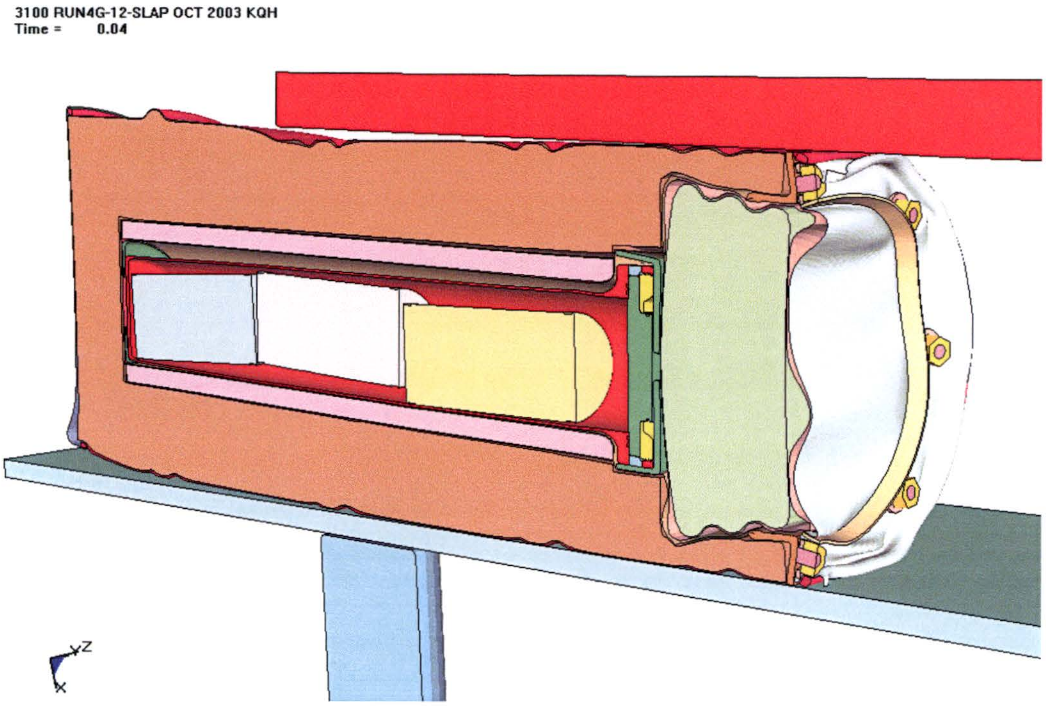

Figure 3.7.3 - Run4g, Crush Impact, Final Configuration

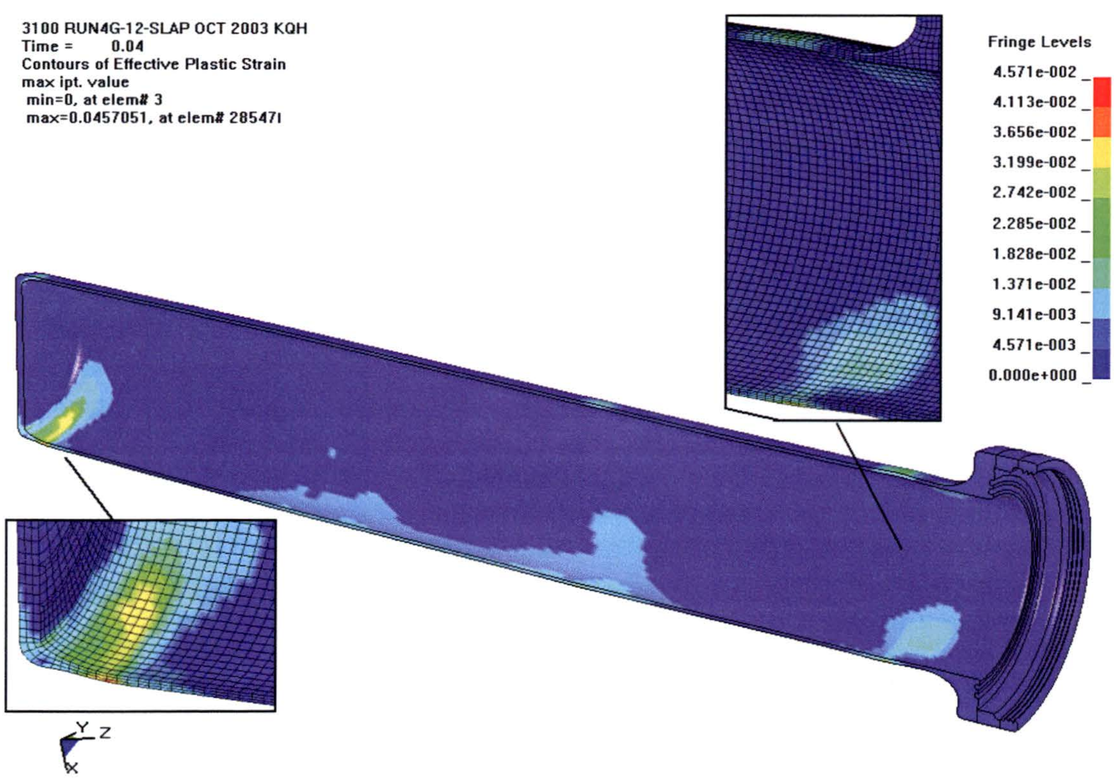

Figure 3.7.4 - Run4g, Crush Impact, Effective Plastic Strain in the CV Body

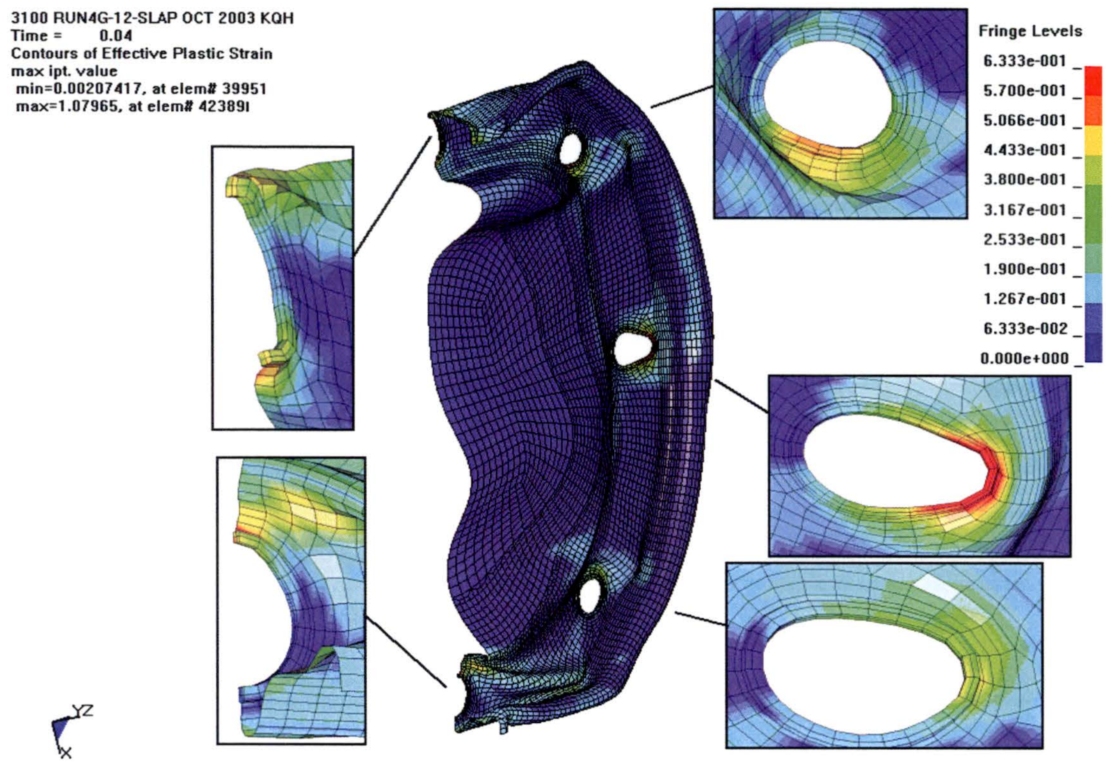

Figure 3.7.5 - Run4g, Crush Impact, Effective Plastic Strain in the Lid

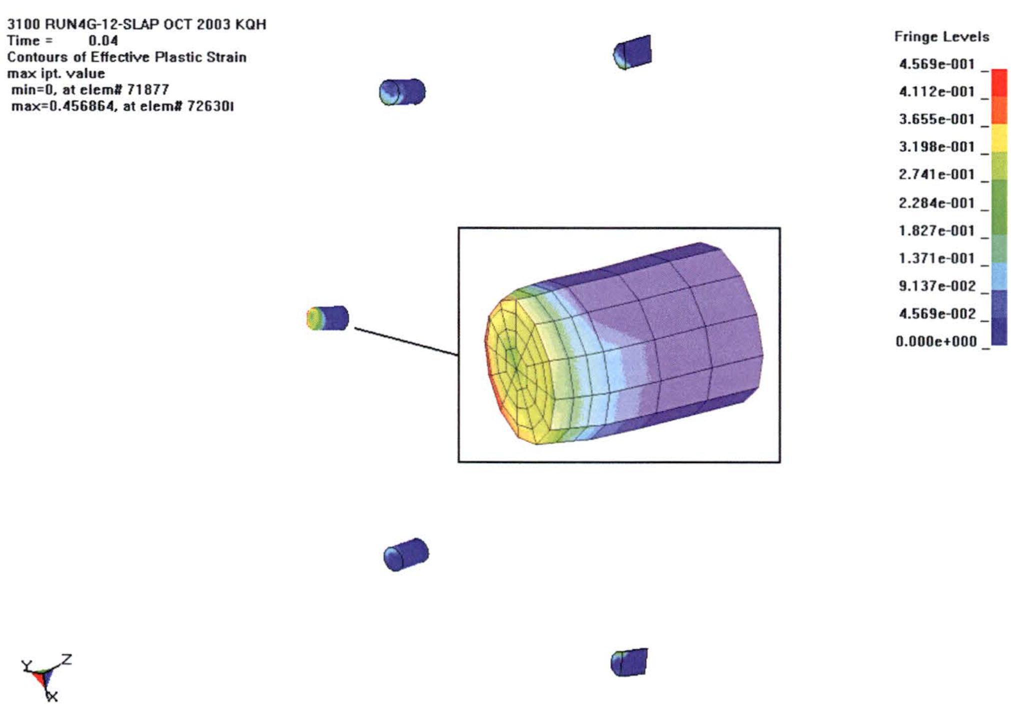

Figure 3.7.6 - Run4g, Crush Impact, Effective Plastic Strain in the Drum Studs

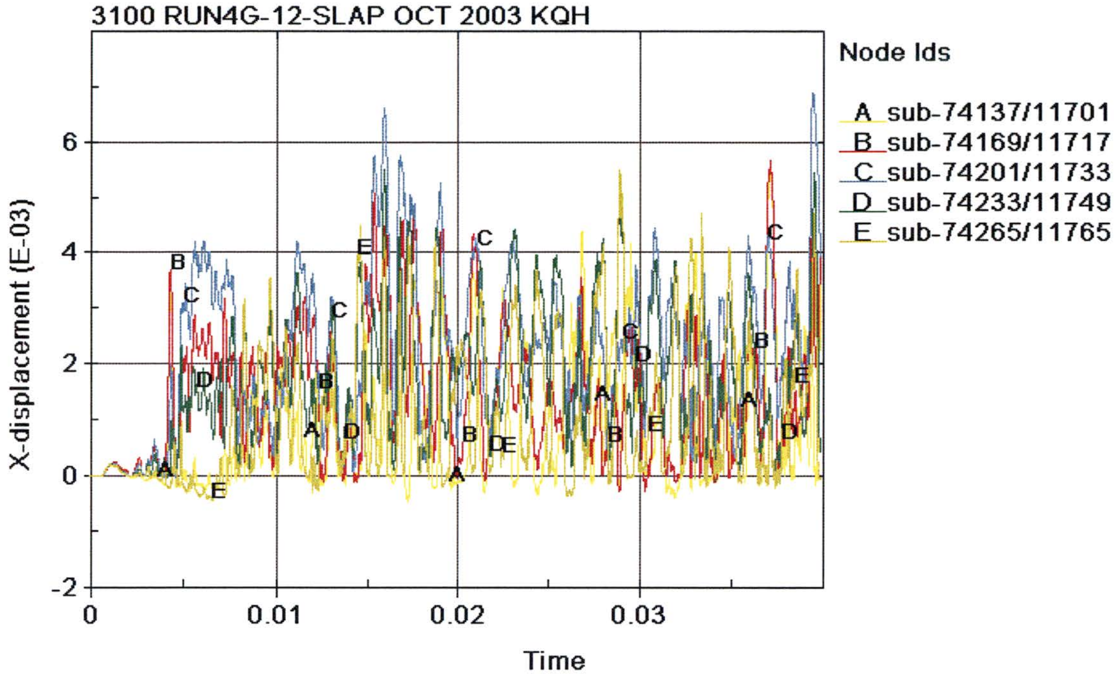

Figure 3.7.7 - Run4g, Lid Separation Time History

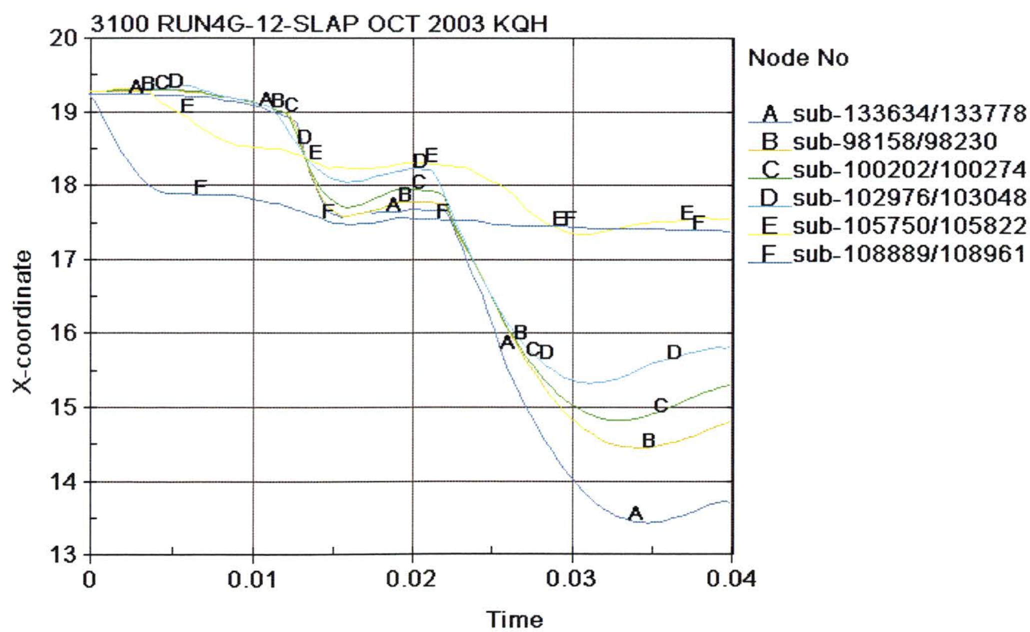

Figure 3.7.8 - Run4g, Drum Deformation in the Direction of the Impacts

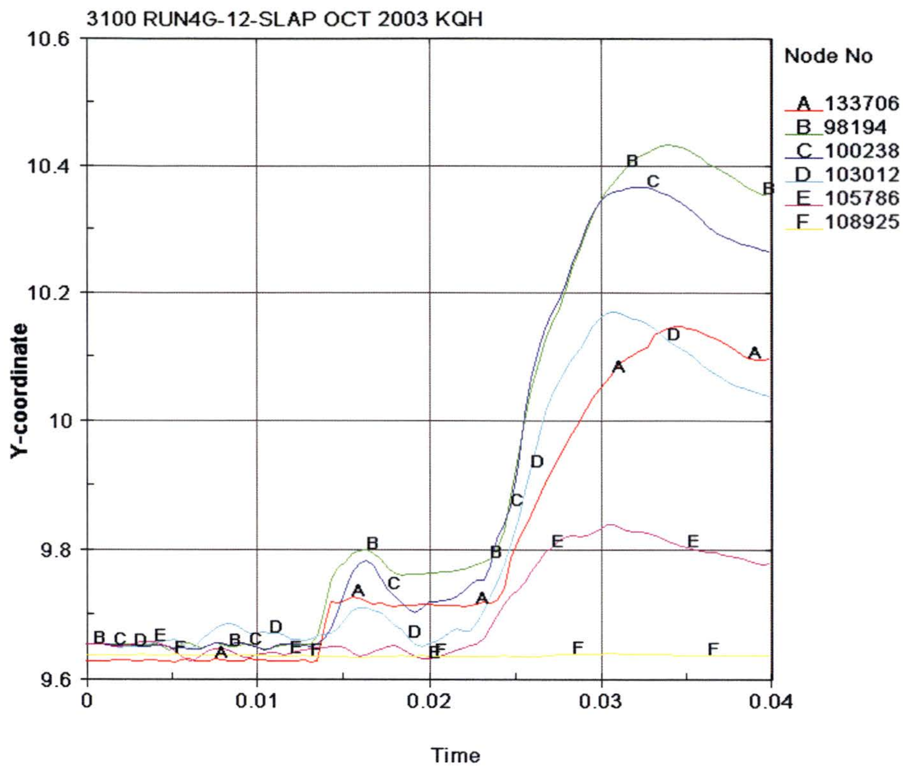

Figure 3.7.9 - Run4g, Drum Deformation Normal to the Impacts

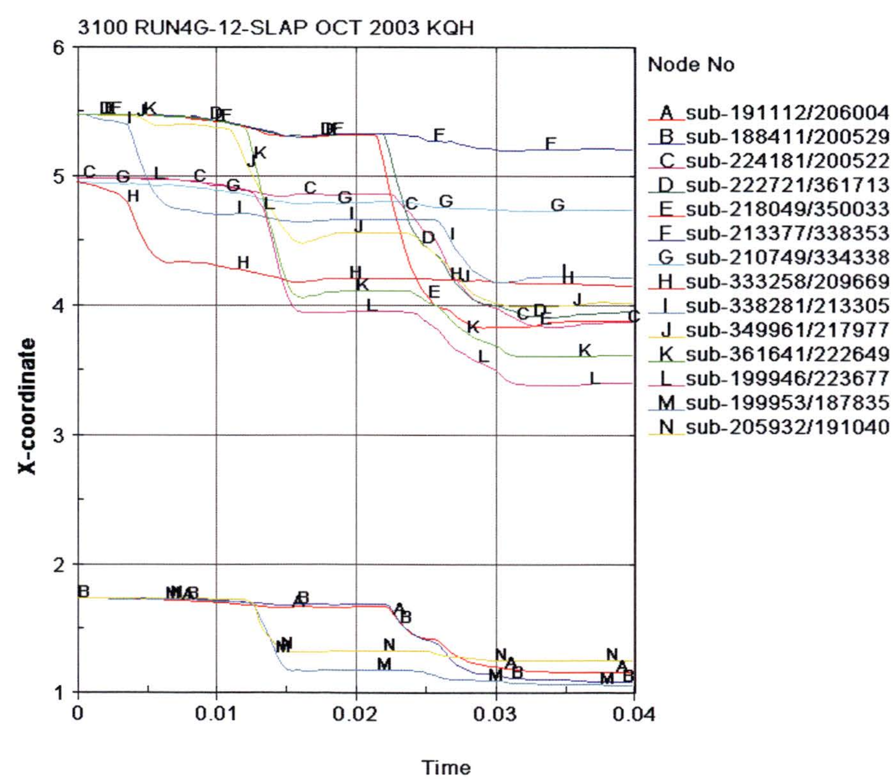

Figure 3.7.10 - Run4g, Kaolite Thickness Time Histories for the Impacts

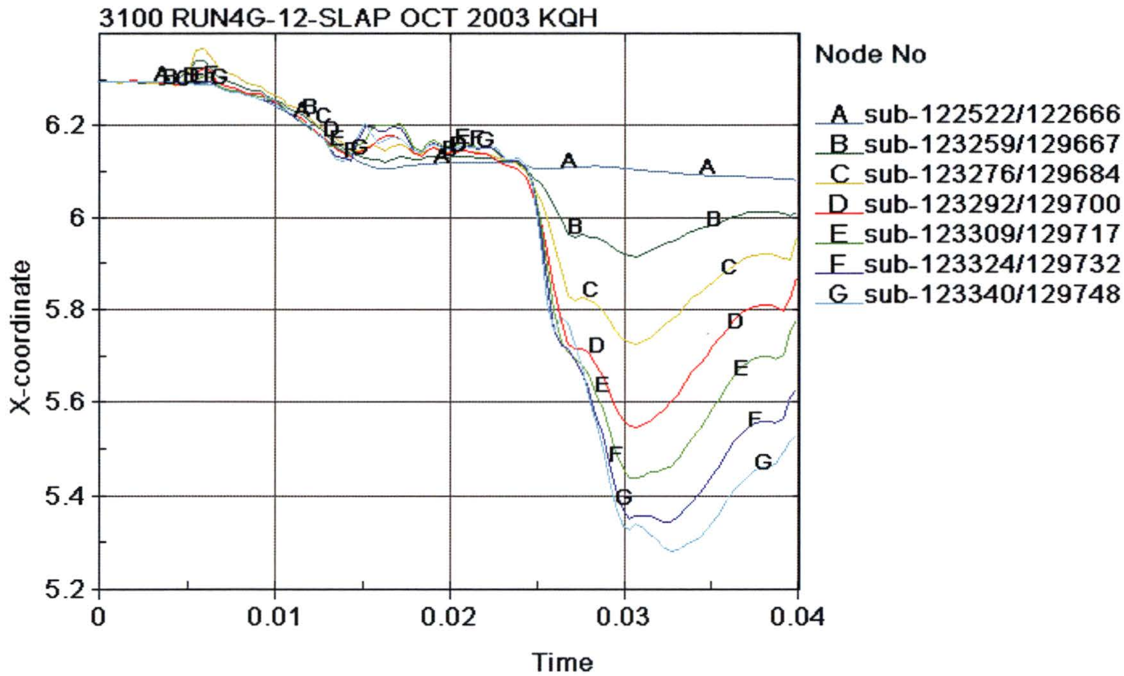

Figure 3.7.11 - Run4g, Liner Diameter Time History

3.8 Run4ga - Slapdown

Run4ga is a 30-foot, 12° slapdown impact (time - 0 to 0.02 seconds) followed by a crush impact with the crush plate centered on the drum (0.0201 to 0.04 seconds). The run4g 30-foot impact restart file was taken and the crush plate was moved by specifying nodal velocities so that it was centered on the drum. The translation occurred from time 0.02 to 0.0201 sec. Once the crush plate was centered, the run was halted and the crush impact was initiated. Therefore, the run4ga 30-foot impact is the run4g 30-foot impact. The 30-foot impact results for run1ga are presented in section 3.7 for run4g. The run4ga crush results are presented in this section.

The final configuration for the run4ga crush impact is shown in Figure 3.8.1. The maximum effective plastic strain in the CV body is 0.0741 in/in in the upper wall near the bottom head as shown in Figure 3.8.2.

The maximum effective plastic strain in the drum lid is 1.0795 in/in as shown in Figure 3.8.3. The regions of elevated strain are quite localized at the upper and lower stud holes in the lid. The value of 1.0795 in/in is a surface strain. The value of membrane strain is 0.6005 in/in. Due to the relatively localized regions of high effective plastic strain, some localized tearing may occur. Extended tearing or failure of the lid is not predicted due to the localized elevated fringe ranges of effective plastic strain. The large washers would provide restraint of the lid. Table 3.8.1 presents the maximum effective plastic strain in other shipping package components for the run4ga crush impact.

Table 3.8.1 - Run4ga, Crush Impact, Effective Plastic Strain Levels in Some Components	
Component	Effective Plastic Strain, in/in
CV Lid	0.0006
CV Nut Ring	0.0003
Angle	0.0917
Drum	0.3537
Drum Bottom Head	0.2919
Liner	0.2363
Lid Stiffener	0.0303
Lid Studs	0.3174
Lid Stud Nuts	0.0000
Lid Stud Washers	0.0597
Plug Liner	0.1636

The CV lid separation time history is shown in Figure 3.8.4. A maximum spike of about 0.009 inches is shown for the nodal pairs shown in Figure 3.1.30. The average value at the end of the impact is about 0.002 inches or less.

The time history of the drum diameter in the direction of the impacts is shown in Figure 3.8.5. Figure 3.8.6 shows the radial changes in the direction normal to the impacts. The location of the nodes is shown in Figure 3.1.34.

Figure 3.8.7 shows the kaolite thickness time histories for the run4ga crush impact. The nodes are shown in Figure 3.1.32.

Figure 3.8.8 shows the diameter time history at various locations along the liner. Figure 3.1.37 and Table 3.1.3 show the locations of the nodal pairs.

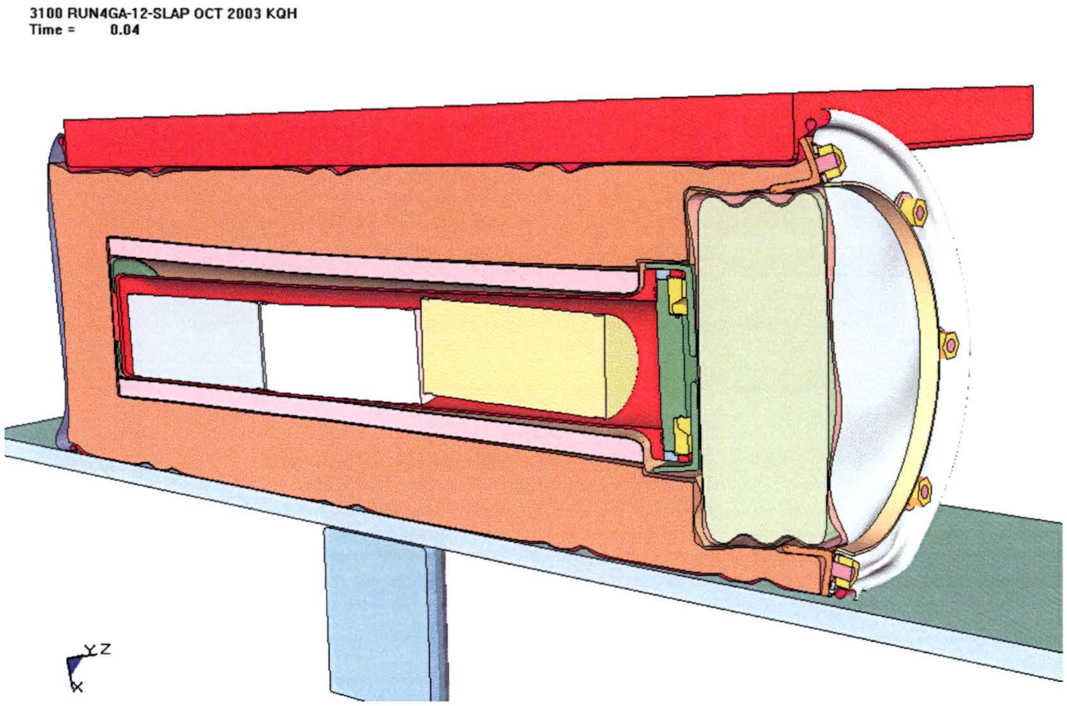

Figure 3.8.1 - Run4ga, Crush Impact, Final Configuration

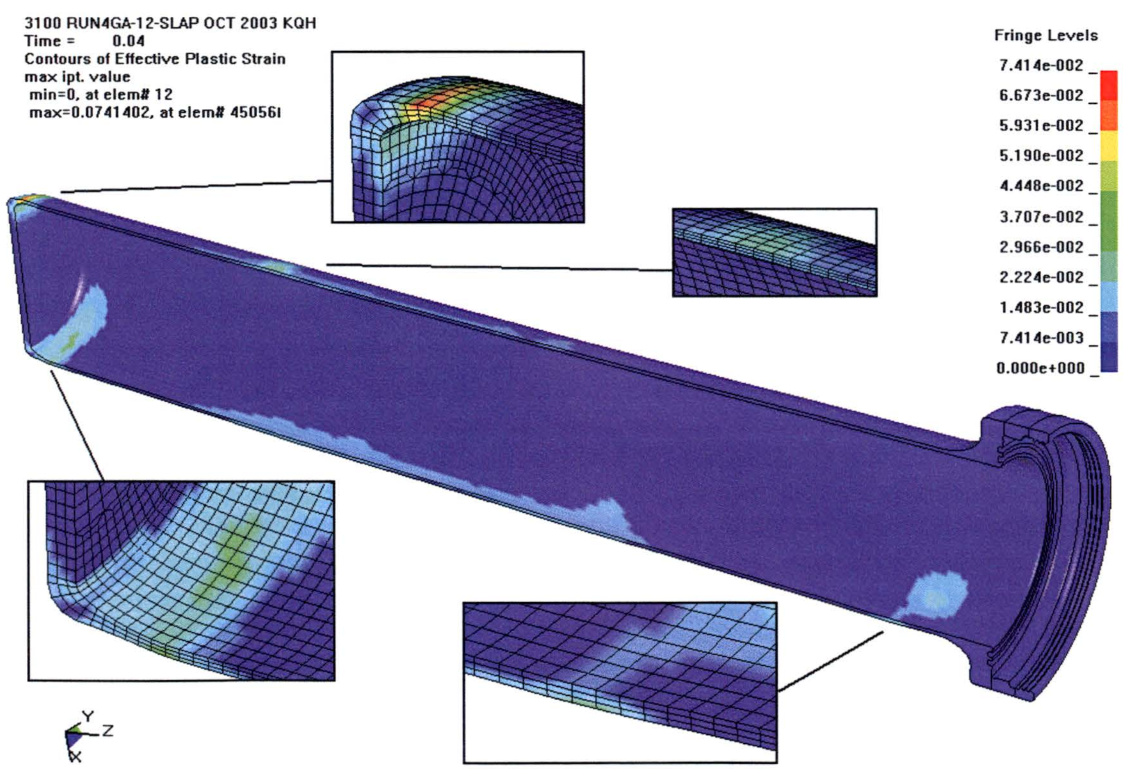

Figure 3.8.2 - Run4ga, Crush Impact, Effective Plastic Strain in the CV Body

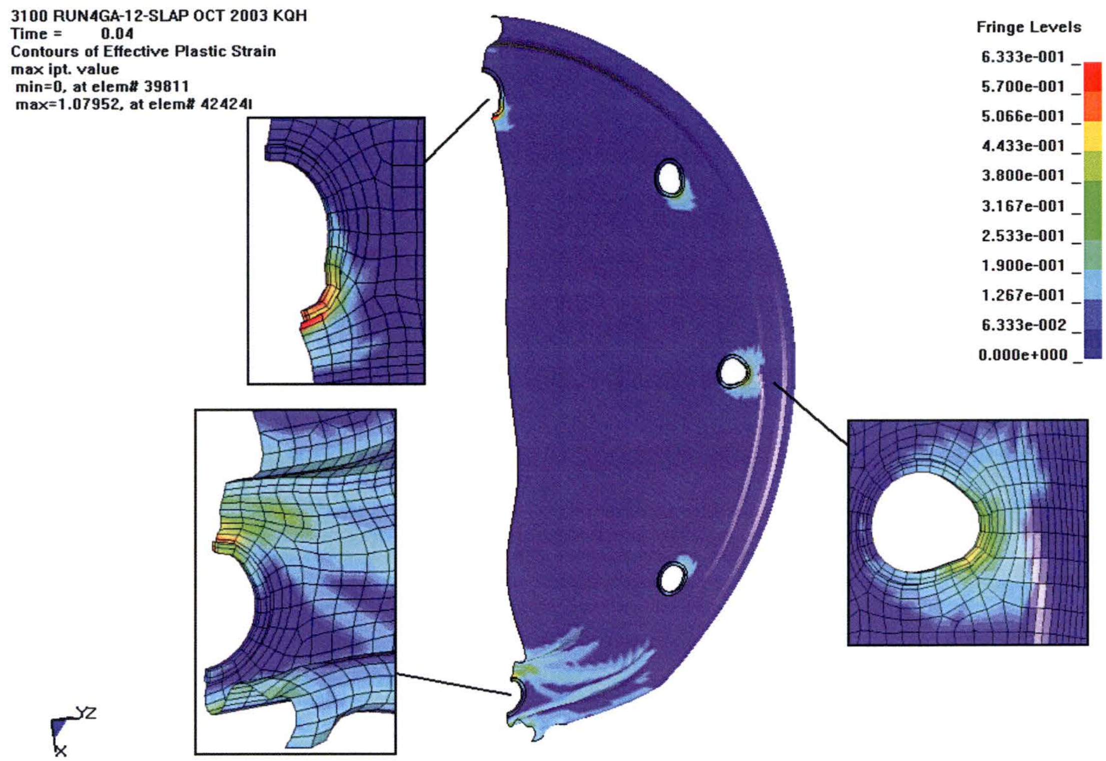

Figure 3.8.3 - Run4ga, Crush Impact, Effective Plastic Strain in the Lid

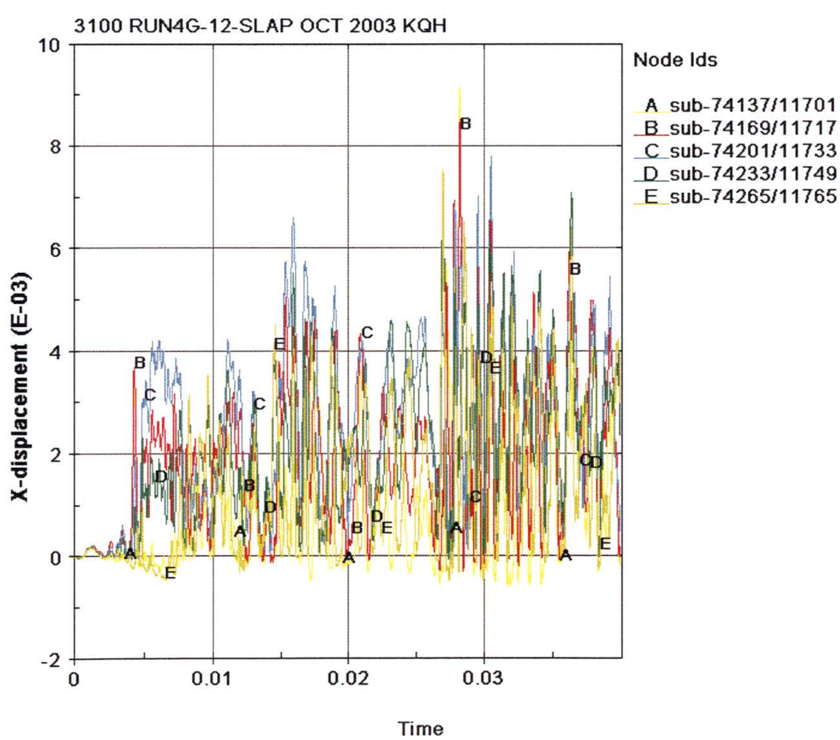

Figure 3.8.4 - Run4ga, Crush Impact, Lid Separation Time History

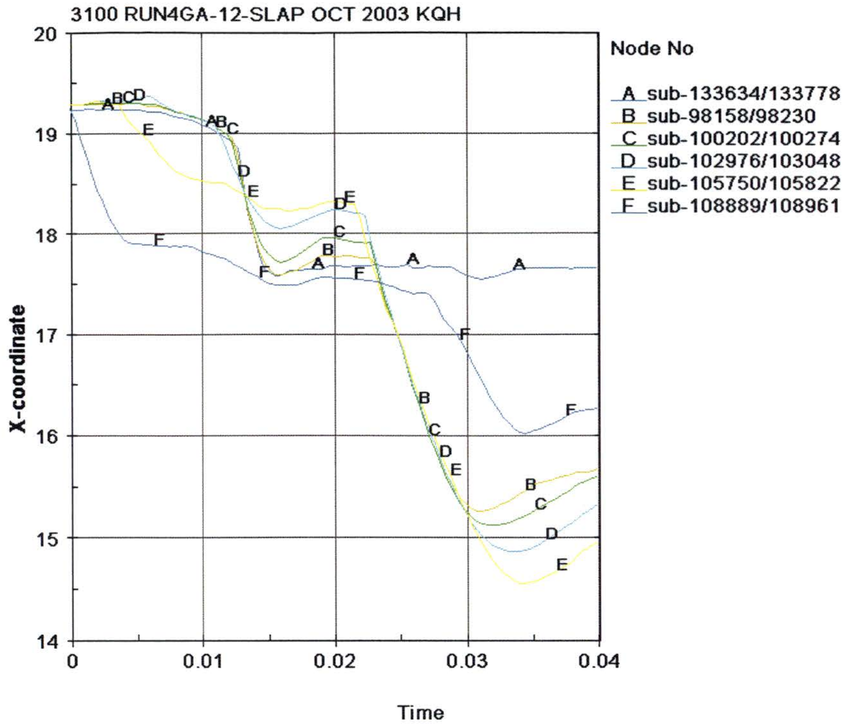

Figure 3.8.5 - Run4ga, Drum Deformation in the Direction of the Impacts

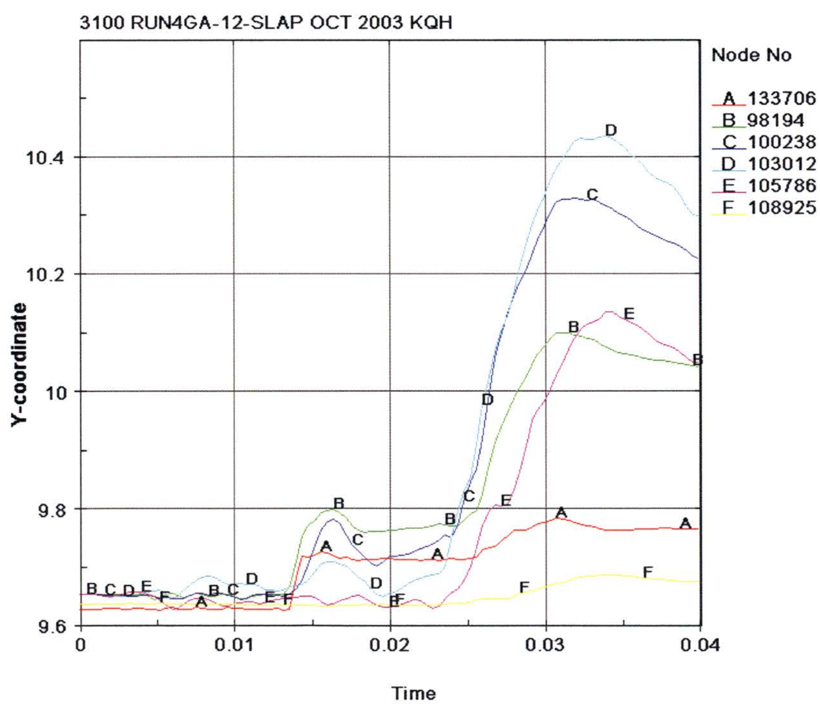

Figure 3.8.6 - Run4ga, Drum Deformation Time History in the Y-Direction

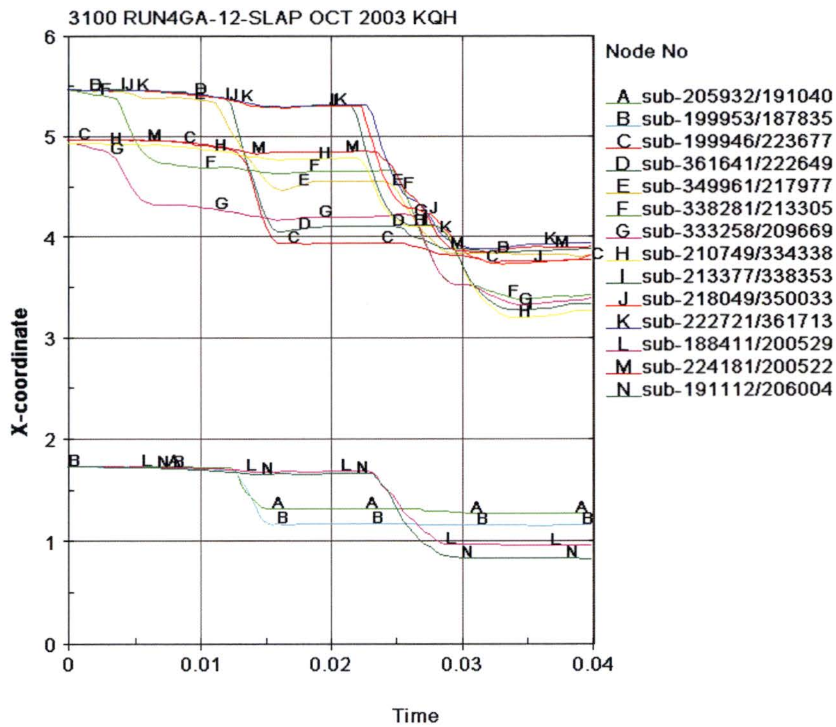

Figure 3.8.7 - Run4ga, Thickness in the Drum Kaolite in the Direction of the Impacts

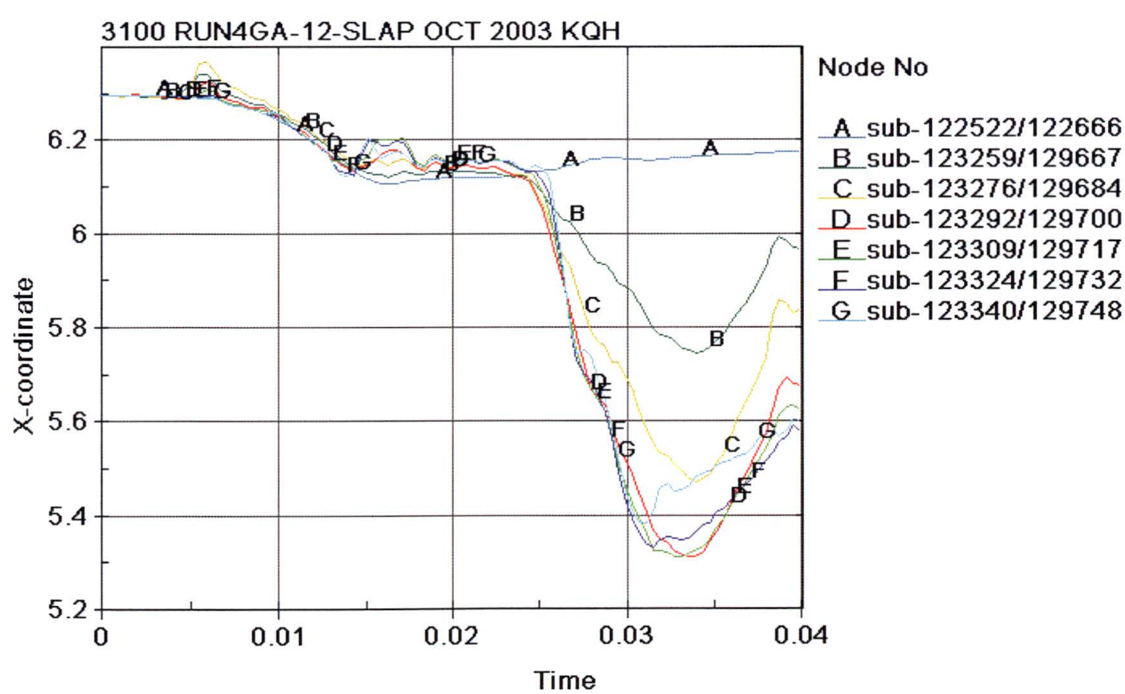

Figure 3.8.8 - Run1ga, Liner Diameter Time History

3.9 Run4h - Slapdown

Due to the minimal number of studs securing the lid, a model with the impact centered between the studs is made. Run4h is similar to run4g, except that the drum studs are rotated, such that the plane of symmetry is centered between two studs. Run4h is a 30-foot, 12° slapdown impact (time = 0 to 0.02 seconds) followed by a crush impact with the crush plate centered over the CV flange (0.02 to 0.04 seconds).

Figure 3.9.1 shows the final configuration for the 30-foot impact. Figure 3.9.2 shows the configuration in the lid region near the rigid plate. The effective plastic strain contours in the package components for the 30-foot impact are similar to strain patterns already presented. Therefore, no strain contour plots are presented for the 30-foot impact and the maximum strains are listed in Table 3.9.1.

Table 3.9.1 - Run4h, 30-Foot Impact, Effective Plastic Strain Levels in Some Components

Component	Effective Plastic Strain, in/in
CV Body	0.0450
CV Lid	0.0000
CV Nut Ring	0.0000
Angle	0.0861
Drum	0.3017
Drum Bottom Head	0.2877
Liner	0.1181
Lid	0.3831
Lid Stiffener	0.0184
Lid Studs	0.0891
Lid Stud Nuts	0.0000
Lid Stud Washers	0.0782
Plug Liner	0.1592

The final configuration for the run4h crush is shown in Figure 3.9.3. Figure 3.9.4 shows the lid configuration for the crush impact. The maximum effective plastic strain in the drum lid is 0.9830 in/in, which is a surface strain. The maximum membrane strain is 0.7225 in/in and is localized around the stud holes in the lid at the 67.5° and the 112.5° positions. The regions of high strain are localized at all the stud holes in the lid, therefore extended tearing is not predicted. Some localized tearing of the lid may be experienced, but the lid will be retained by the large washers.

The maximum effective plastic strain in the studs is 0.5364 in/in and occurs at the outer radius of the stud. The nominal effective plastic strain through the stud shank is about 0.300 in/in. Therefore, the studs would not be expected to fail. The maximum effective plastic strain in other components are listed in Table 3.9.2.

Table 3.9.2 - Run4h, Crush Impact, Effective Plastic Strain Levels in Some Components

Component	Effective Plastic Strain, in/in
CV Body	0.0461
CV Lid	0.0004
CV Nut Ring	0.0000
Angle	0.1071
Drum	0.3881
Drum Bottom Head	0.2877
Liner	0.2475
Lid Stiffener	0.1083
Lid Stud Nuts	0.0052
Lid Stud Washers	0.0885
Plug Liner	0.2719

The lid separation time history is similar to those presented in Sections 3.7 and 3.8. A maximum lid separation spike of approximately 0.007 inches is reached during the impacts and is oscillatory in nature. An average value of 0.003 inches or less is shown at the end of the crush impact.

Figure 3.9.7 shows the X-diameter time history for drum nodes shown in Figure 3.1.34. Figure 3.9.8 shows the radial time history for nodes normal to the direction of impact.

Due to the rotation of the studs on the lid, the nodes for the kaolite changed for the run4h model. The nodes used to obtain the kaolite thickness time histories for run4h are shown in Figure 3.9.9. The time histories for the kaolite thickness on the plane of symmetry is shown in Figure 3.9.10. Figure 3.9.11 shows the liner diameter time history at location shown in Figure 3.1.37 and Table 3.1.3.

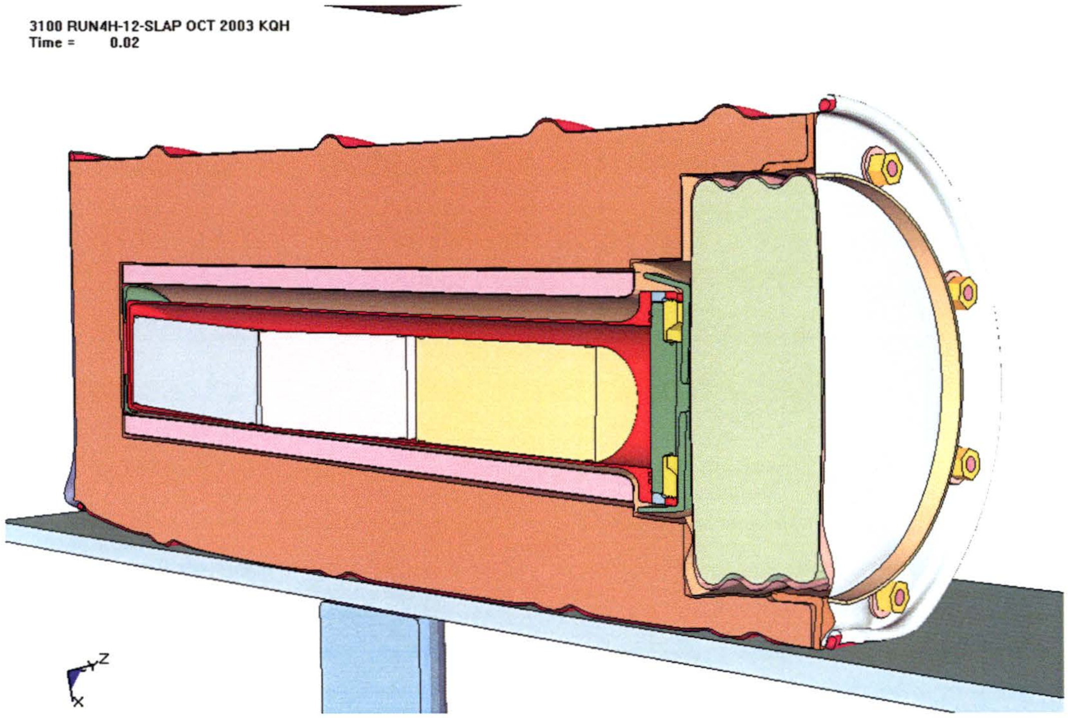

Figure 3.9.1 - Run4h, 30-Foot Impact, Final Configuration

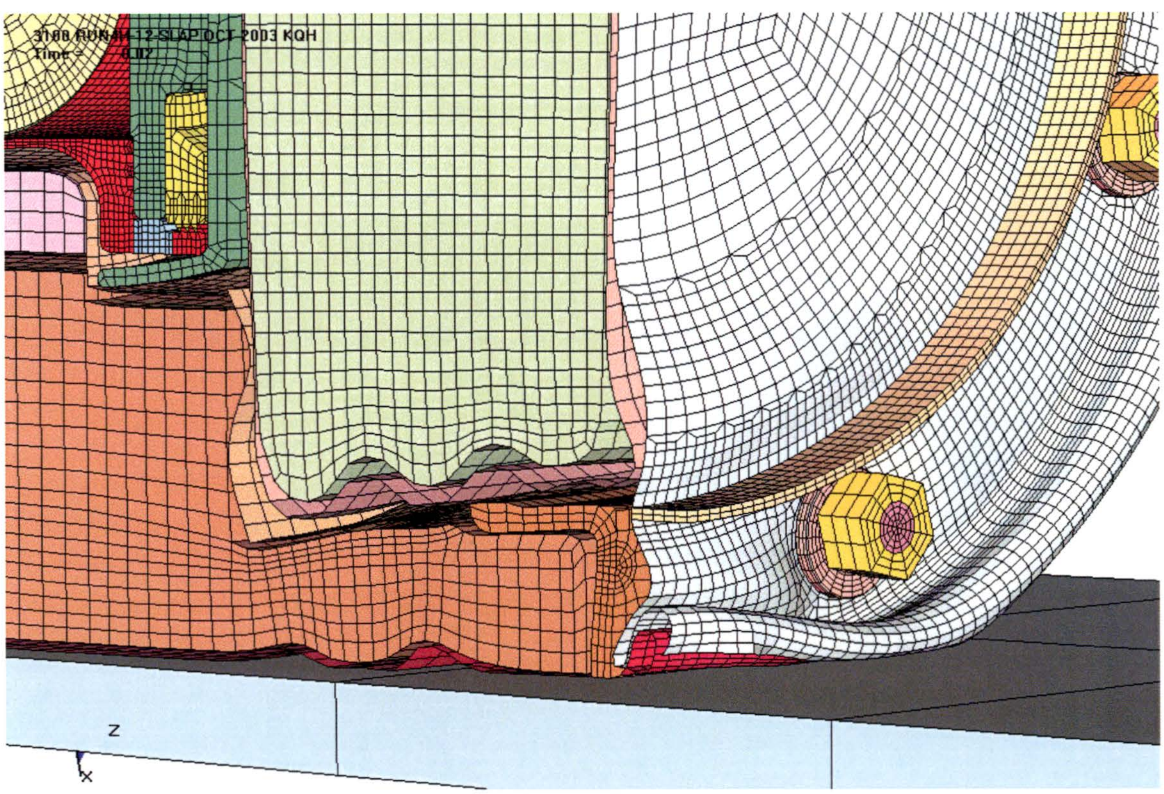

Figure 3.9.2 - Run4h, 30-Foot Impact, Configuration in the Lid

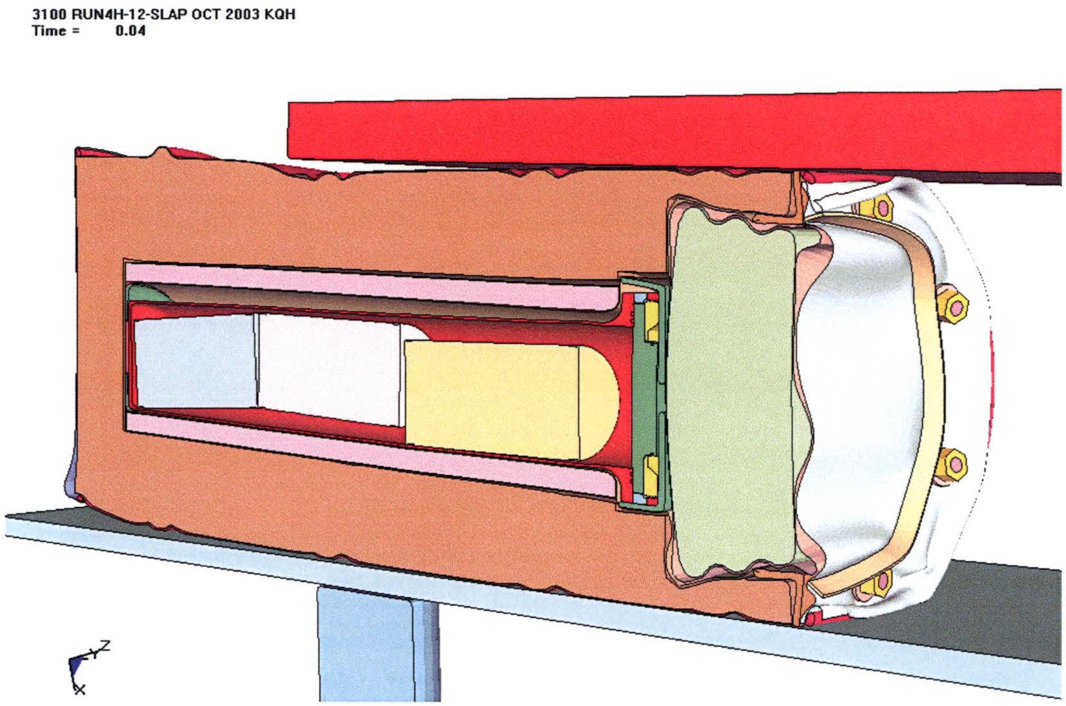

Figure 3.9.3 - Run4h, Crush Impact, Final Configuration

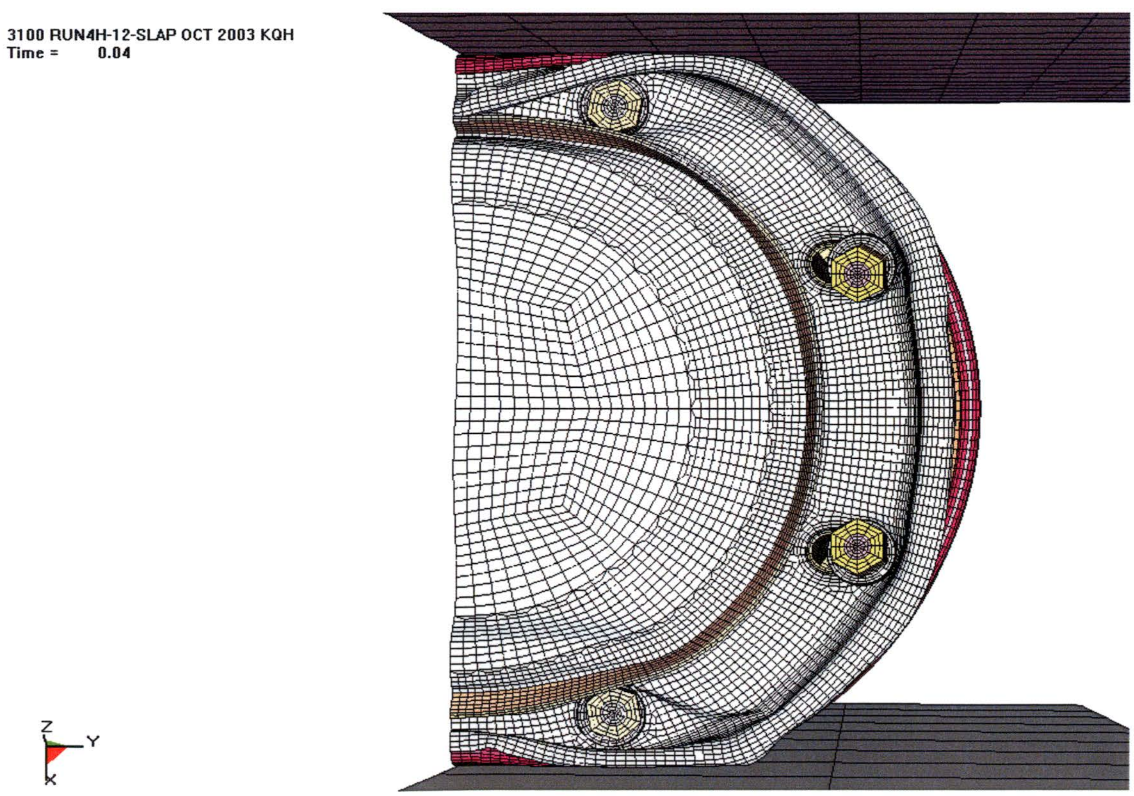

Figure 3.9.4 - Run4h, Crush Impact, Configuration of the Lid

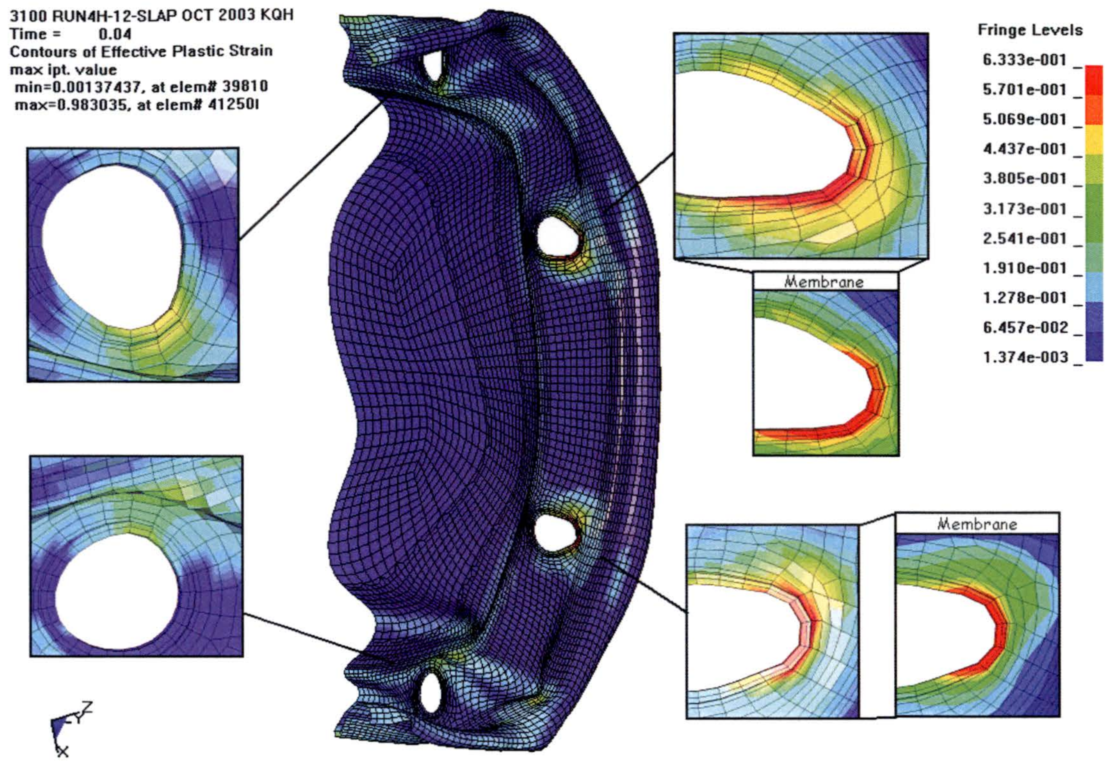

Figure 3.9.5 - Run4h, Crush Impact, Effective Plastic Strain in the Lid

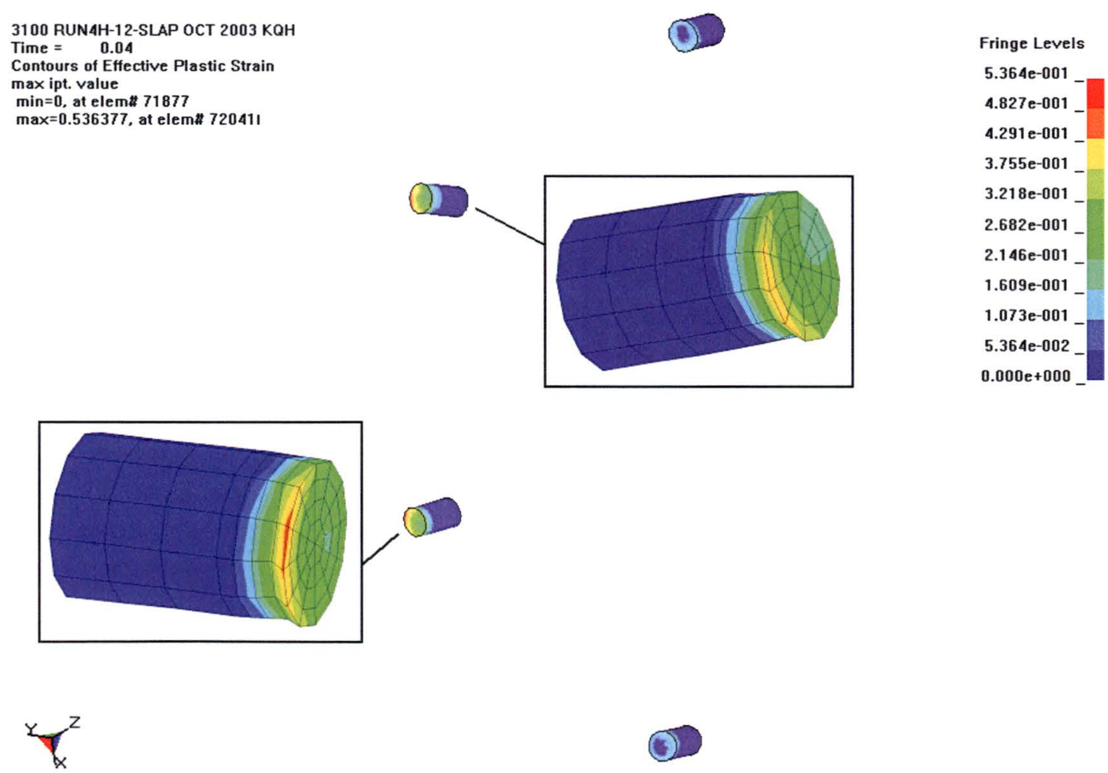

Figure 3.9.6 - Run4h, Crush Impact, Effective Plastic Strain in the Studs

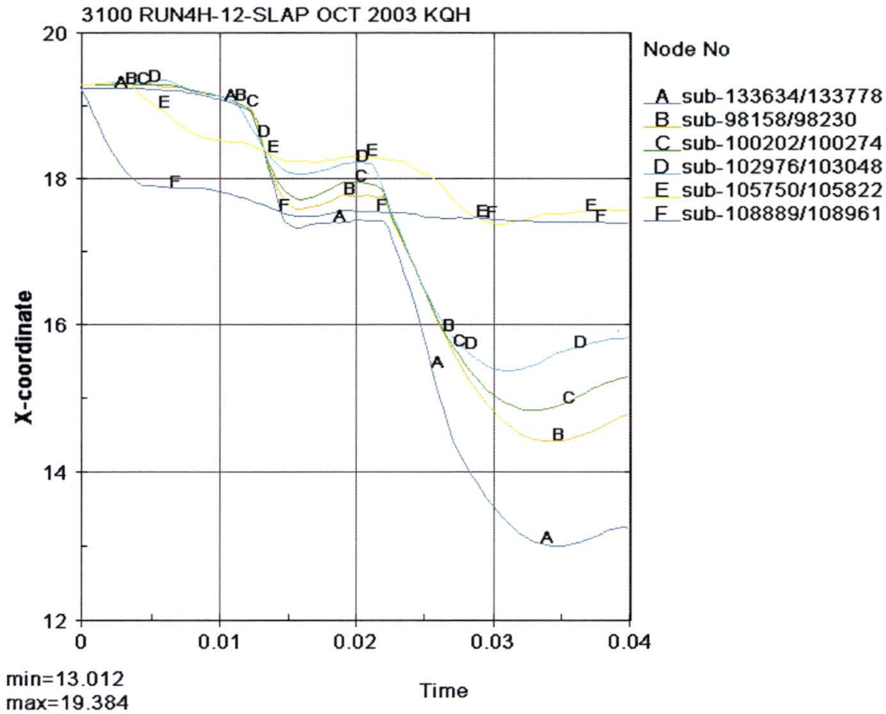

Figure 3.9.7 - Run4h, Drum Diameter in the Direction of the Impacts

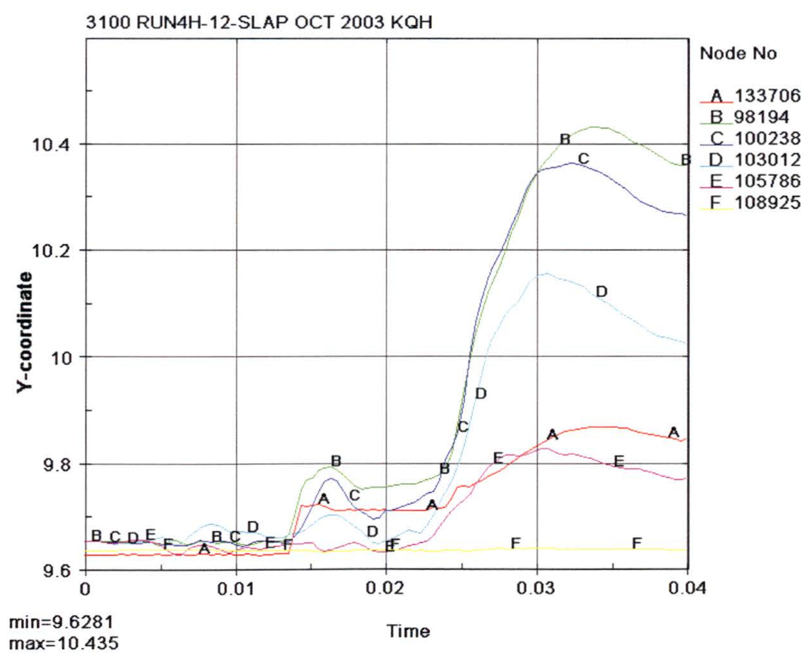

Figure 3.9.8 - Run4h, Drum Radius Normal to the Direction of the Impacts

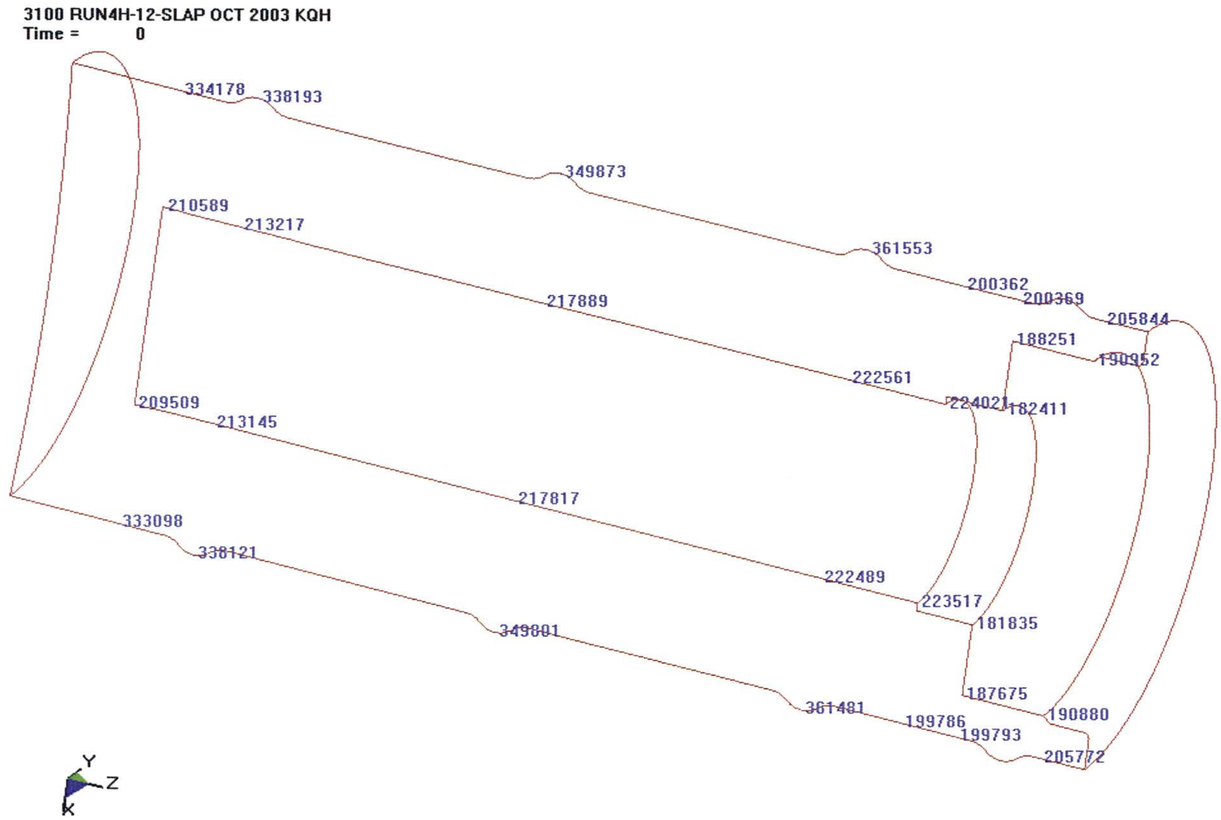

Figure 3.9.9 - Run4h, Drum Kaolite Nodes

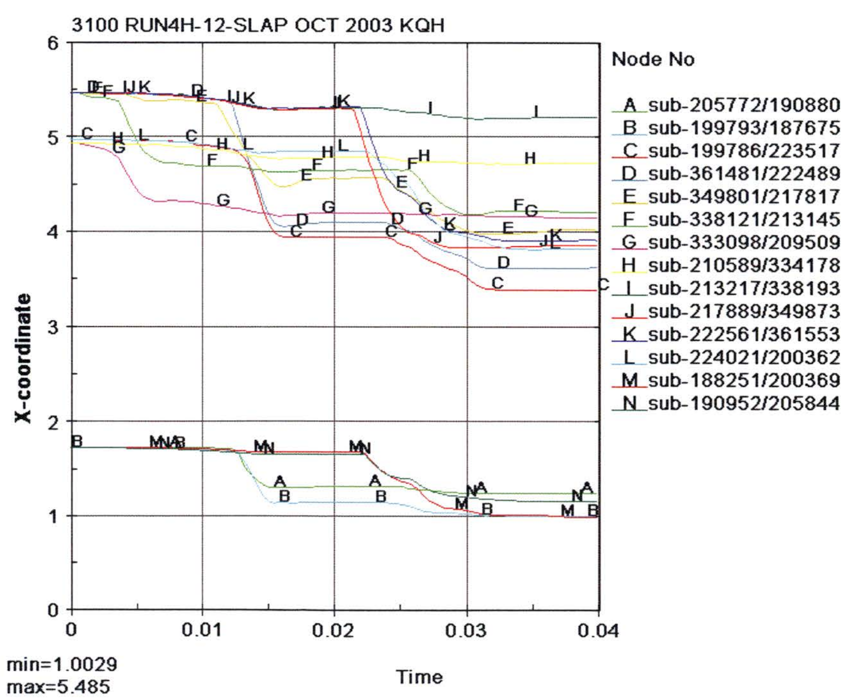

Figure 3.9.10 - Run4h, Thickness of the Drum Kaolite in the Direction of the Impacts

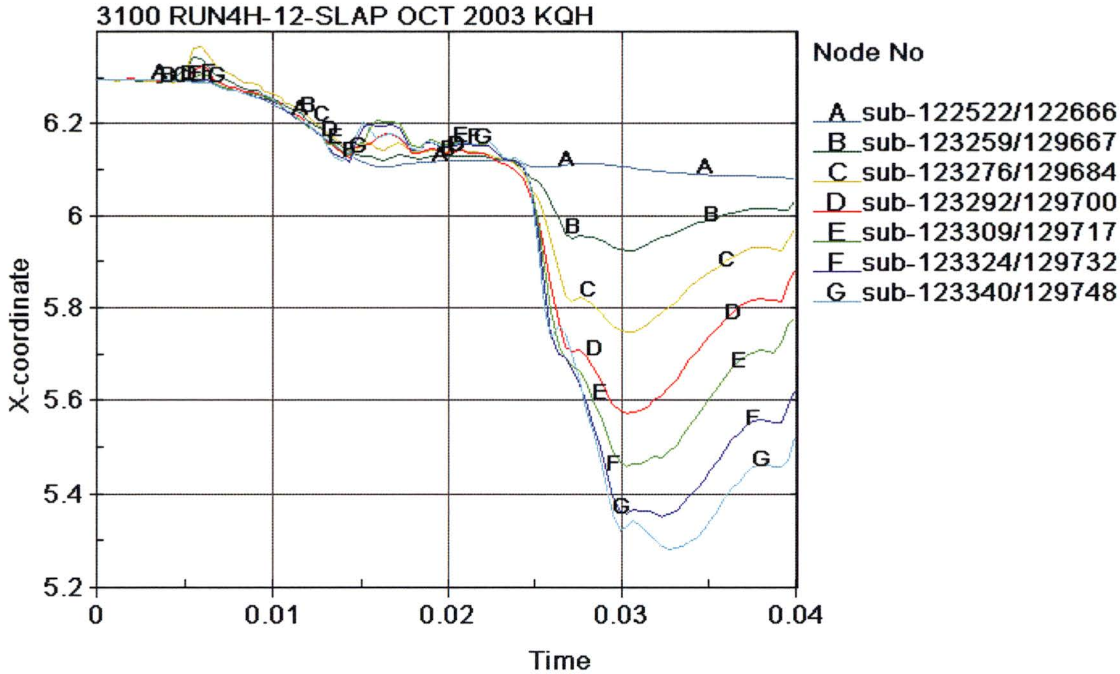

Figure 3.9.11 - Run4h, Liner Diameter Time History

3.10 Run4ha - Slapdown

Run4ha is similar to run4h except that the crush impact is with the crush plate centered on the drum. For run4ha, the restart file at the end of the run4h, 30-foot impact is used to initiate a run which moves of the crush plate such that it is centered on the drum (crush impact from 0.0201 to 0.04 seconds). The translation of the crush plate occurs at the end of the 30-foot impact, or time = 0.02 sec and lasts till 0.0201 sec. The restart file written at the end of the translation of the crush plate, becomes the restart file used to initiate the run4ha crush impact. Therefore, the 30-foot impact results from run4ha are presented in the run4h results. The results presented in this section are those of the centered crush impact for run4ha.

The final configuration for the crush impact is shown in Figure 3.10.1. The maximum effective plastic strain in the drum lid is 0.6335 in/in as shown in Figure 3.10.2. The maximum membrane strain is 0.5249 in/in and is highly localized at the stud hole nearest the crush plate (157.5°). If failure were to occur in the lid, it would be localized and the large washers would restrain the lid. The effective plastic strain in other components is shown in Table 3.10.1.

Table 3.10.1 - Run4ha, Crush Impact, Effective Plastic Strain Levels in Some Components

Component	Effective Plastic Strain, in/in
CV Body	0.0839
CV Lid	0.0013
CV Nut Ring	0.0000
Angle	0.0881
Drum	0.3848
Drum Bottom Head	0.2922
Liner	0.2633
Lid Stiffener	0.0338
Lid Studs	0.1705
Lid Stud Nuts	0.0000
Lid Stud Washers	0.0782
Plug Liner	0.1832

The lid separation time history is similar to that shown in Section 3.8. A maximum spike of 0.009 inches is shown to occur for the CV lid separation. The average separation at the end of the crush impact is 0.002 inches or less due to the oscillatory nature of the gap response.

Figure 3.10.3 gives the diameter time history in the X-direction for drum nodes shown in Figure 3.1.34. Figure 3.10.4 shows the radial time history in the Y-direction for the nodes normal to the direction of the impact.

Figure 3.9.9 shows the nodes used to obtain the kaolite thickness time history for the impact. Figure 3.10.5 shows the thickness time history for the kaolite.

Figure 3.10.6 show the liner diameter time histories in the liner. Figure 3.1.37 and Table 3.1.3 give the locations of the nodal pairs along the length of the liner.

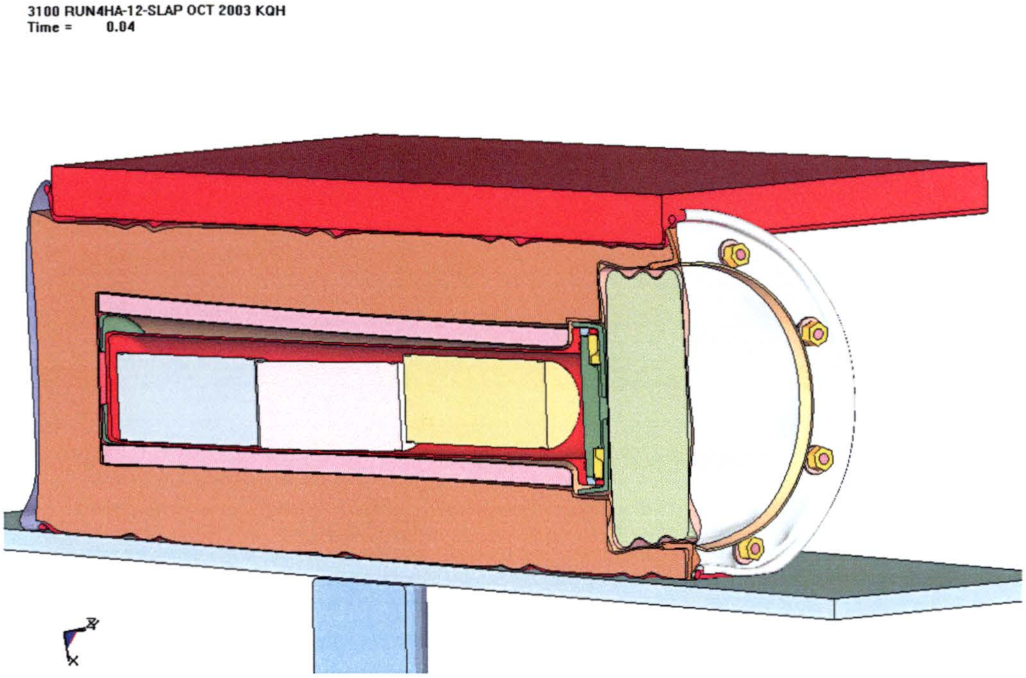

Figure 3.10.1 - Run4ha, Crush Impact, Final Configuration

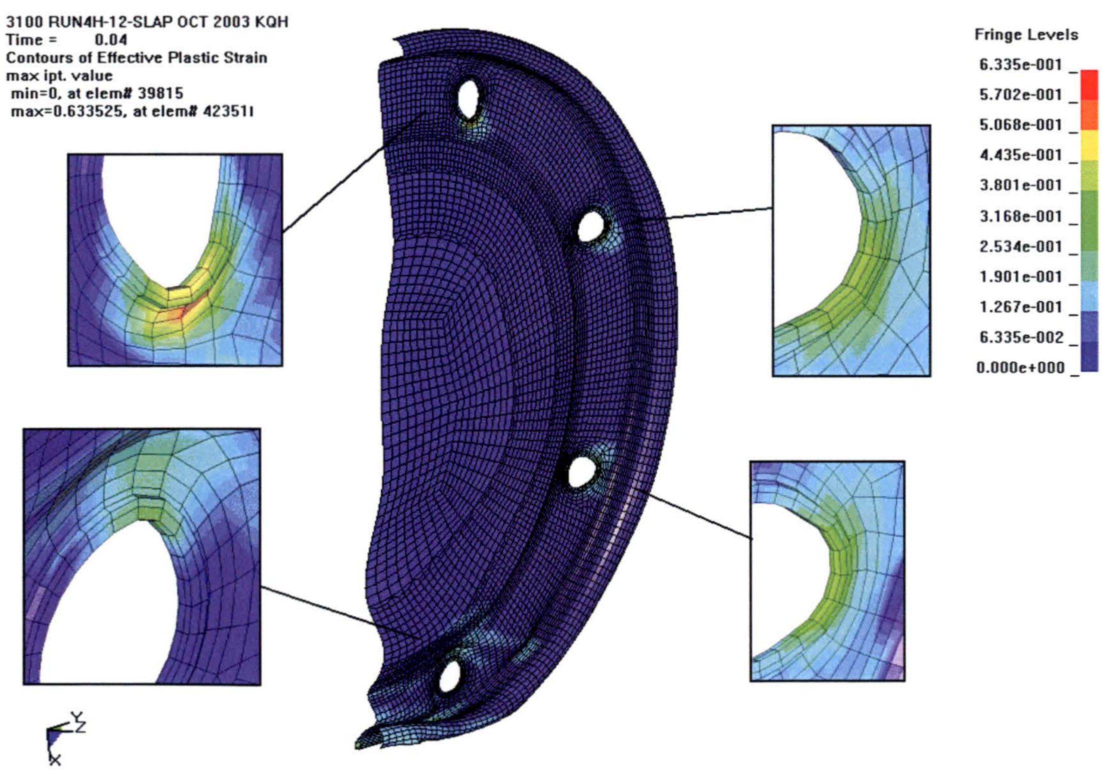

Figure 3.10.2 - Run4ha, Crush Impact, Effective Plastic Strain in the Lid

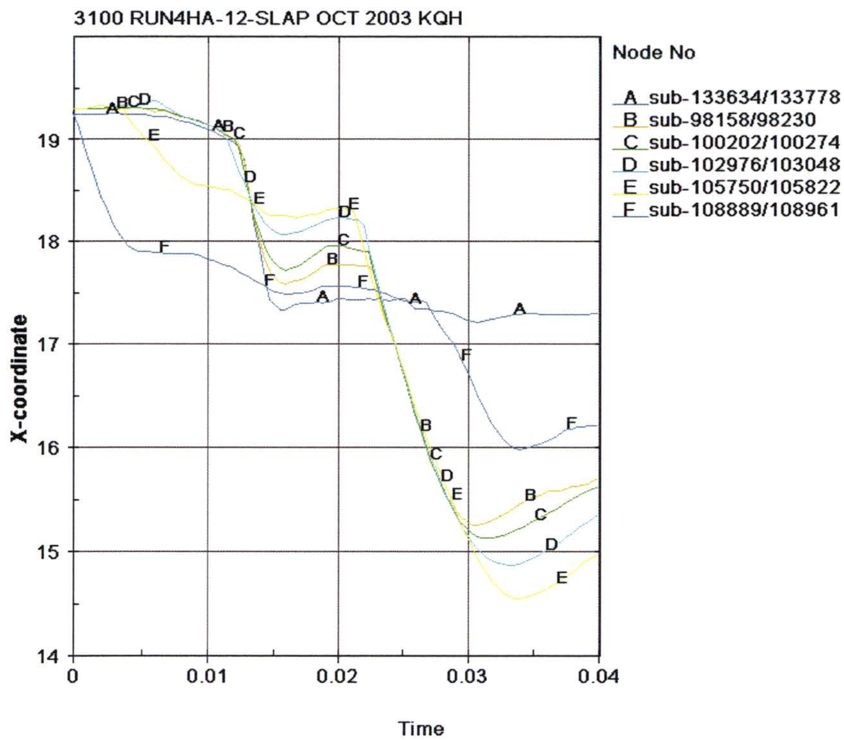

Figure 3.10.3 - Run4ha, Drum Diameter Time History in the Direction of the Impacts

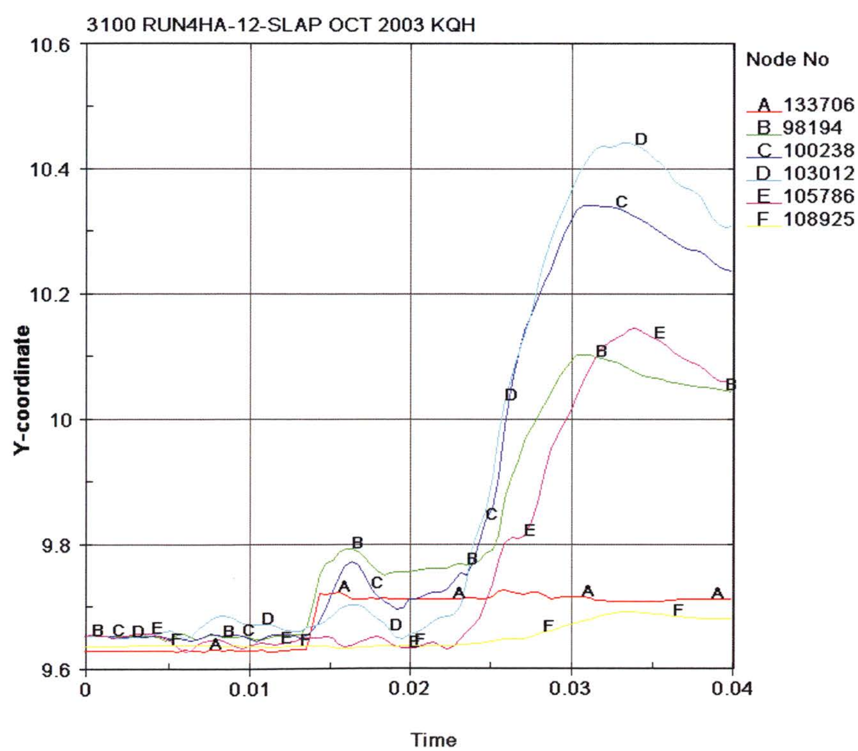

Figure 3.10.4 - Run4ha, Drum Radius Time History Normal to the Direction of the Impacts

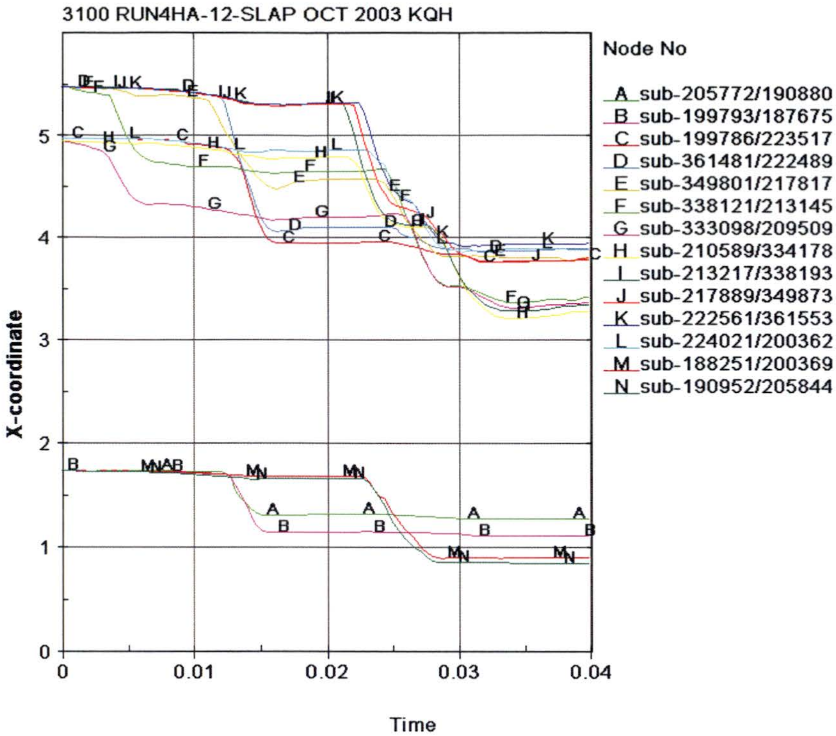

Figure 3.10.5 - Run4ha, Drum Kaolite Thickness in the Direction of the Impacts

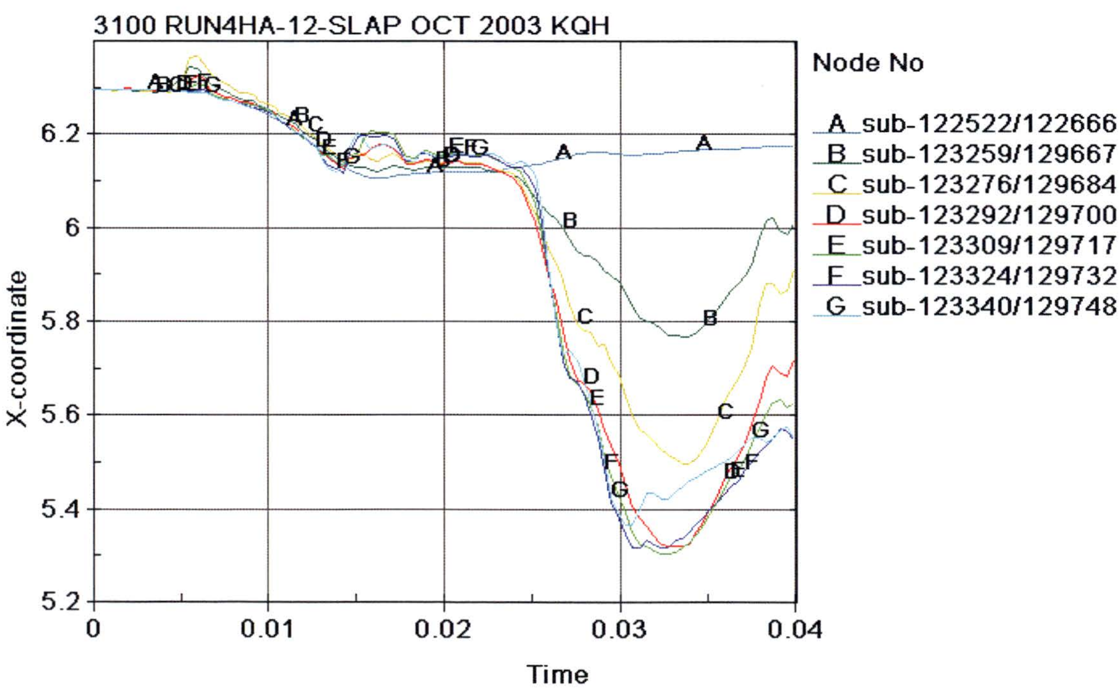

Figure 3.10.6 - Run4ha, Liner Diameter Time History

3.11 Punch Runs

The punch impacts were made with the simple model described in Section 2.2. The final configuration for the punch at 0° is shown in Figure 3.11.1. The surface effective plastic strain in the drum is shown in Figure 3.11.2 to be a maximum of 0.2030 in/in. The maximum membrane strain fringe plot is not shown, but is a maximum of 0.1385 in/in with a contour pattern similar to the surface strain.

Fringe plots of effective plastic surface strain for punch impacts at 40, 50, 60 and 63.6 are shown in Figures 3.11.3 through 3.11.6. Table 3.11.1 summarizes the maximum surface and membrane strain for all the punch impacts.

Table 3.11.1 - ES-3100 Summary of Punch Impacts

Punch Angle (degrees)	Maximum Effective Plastic Strain in the Drum (in/in)	
	Surface	Membrane
0	0.2030	0.1385
10	0.1204	0.0633
20	0.1100	0.0529
30	0.1551	0.0951
40	0.1632	0.1115
50	0.3340	0.1238
60	0.1844	0.0646
63.6	0.3895	0.1858

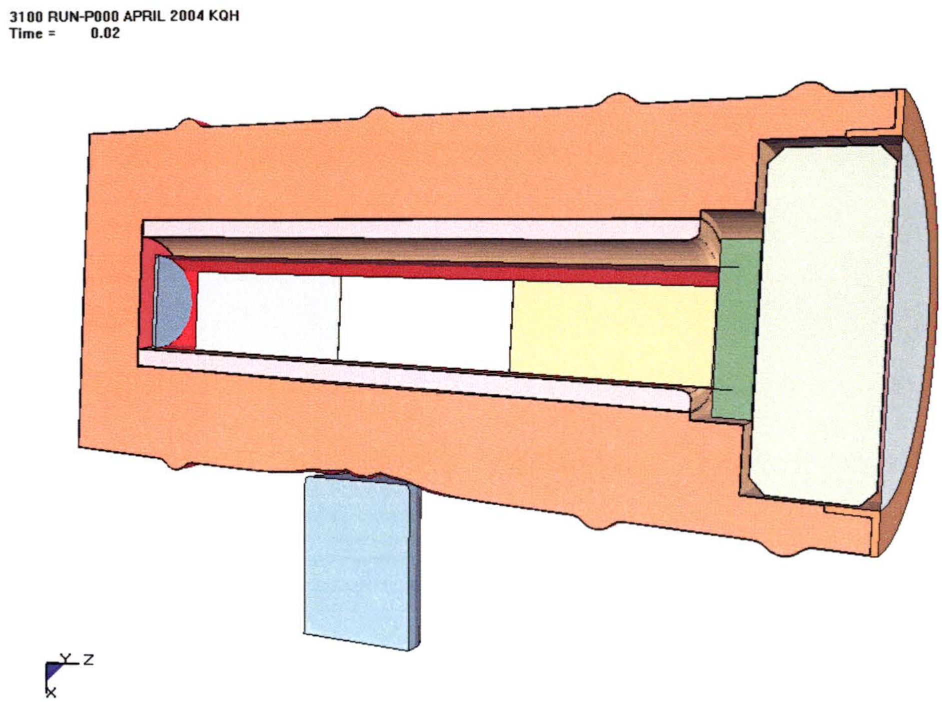

Figure 3.11.1 - Punch at 0°, Final Configuration

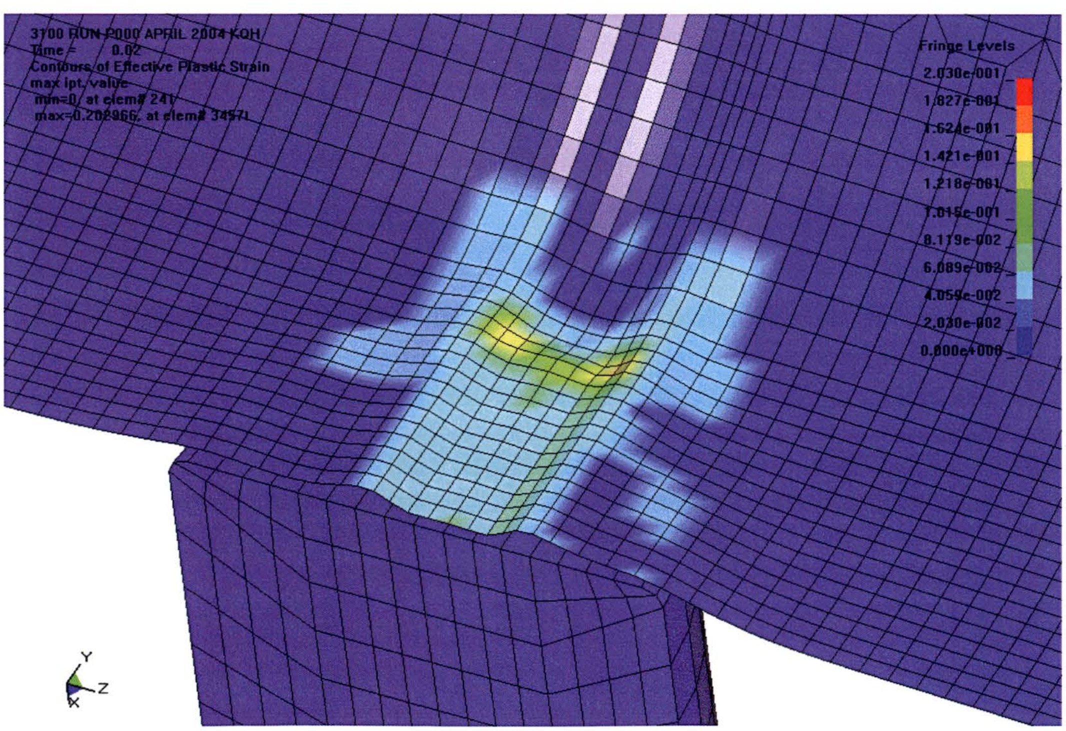

Figure 3.11.2 - Punch at 0°, Surface Strain in the Drum Liner

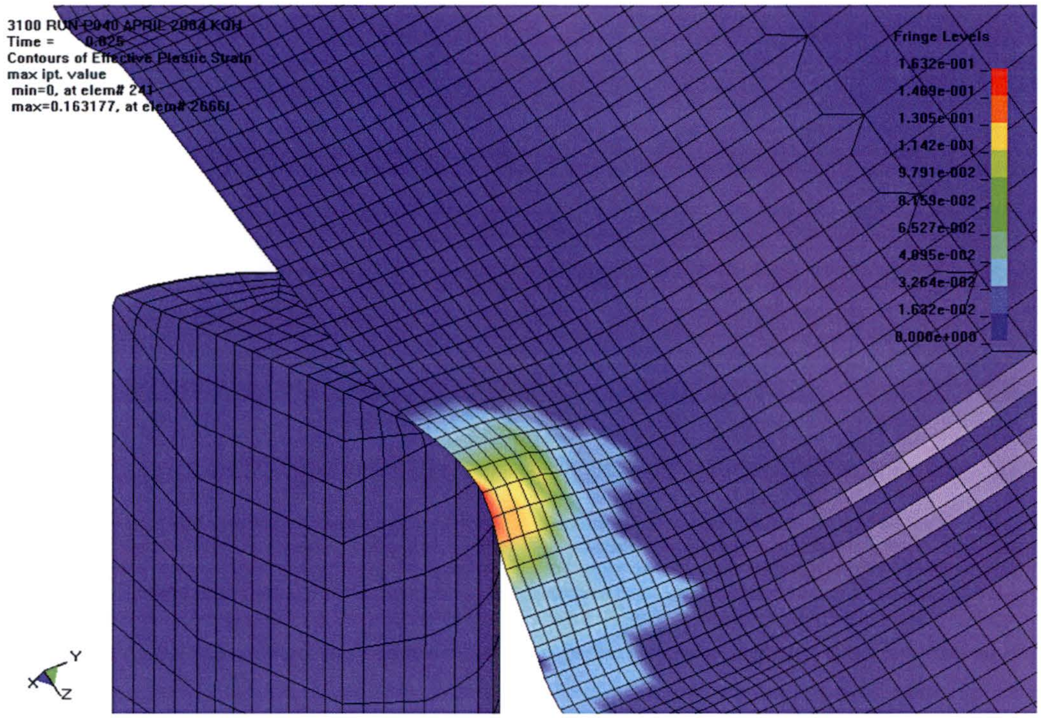

Figure 3.11.3 - Punch at 40°, Surface Strain in the Drum Liner

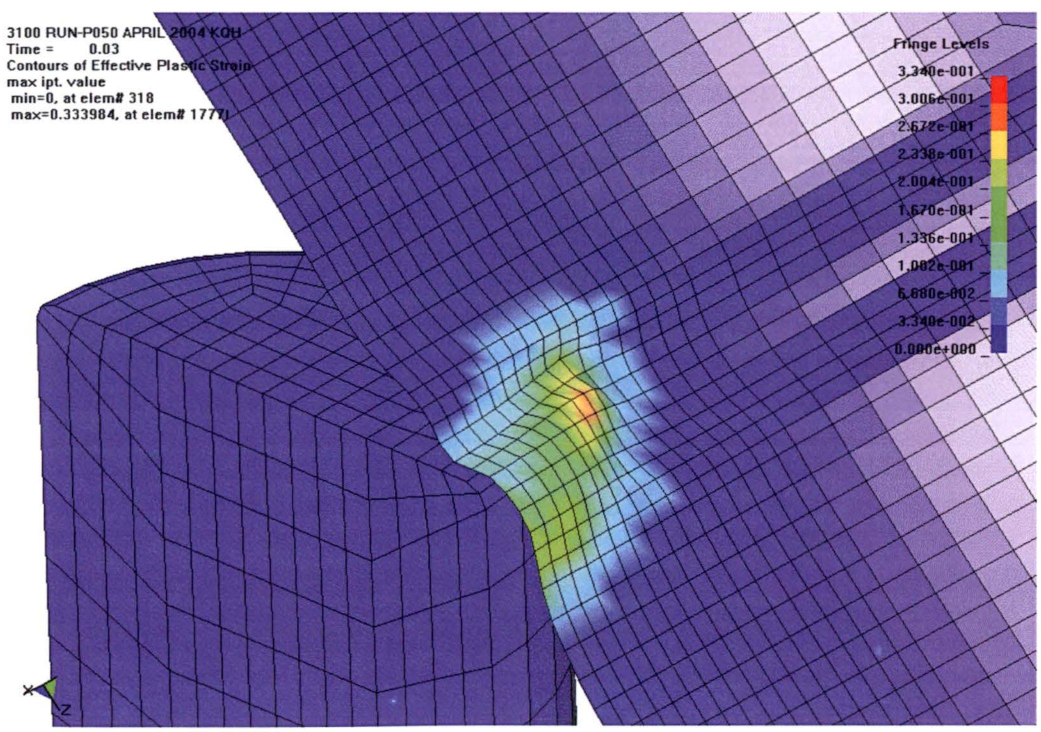

Figure 3.11.4 - Punch at 50°, Surface Strain in the Drum Liner

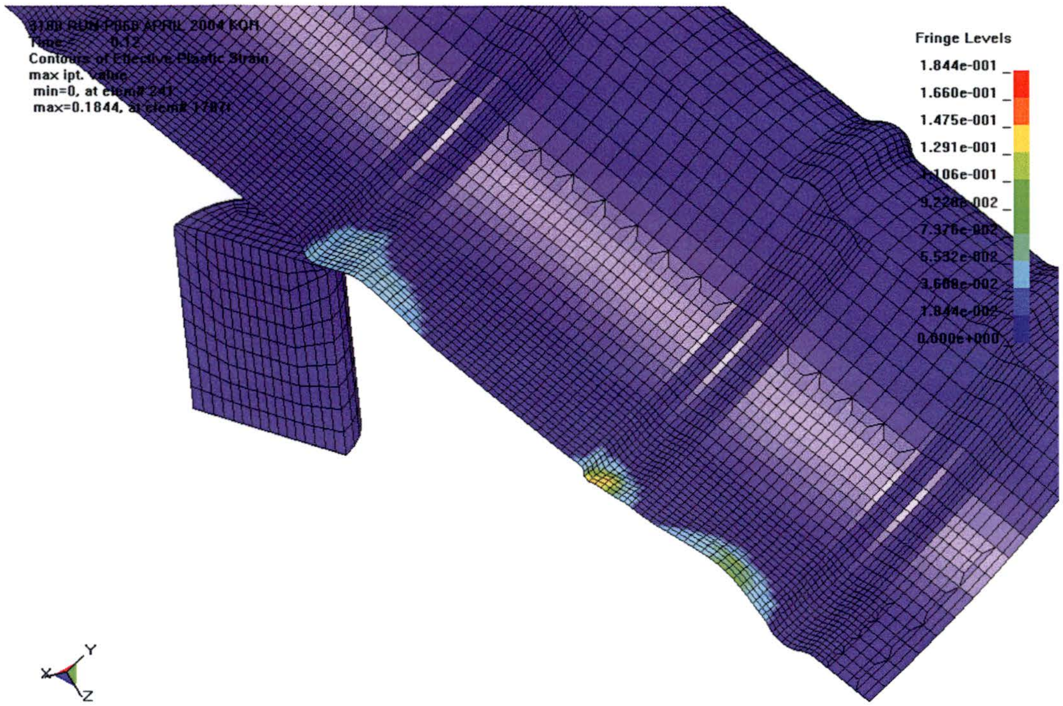

Figure 3.11.5 - Punch at 60°, Surface Strain in the Drum Liner

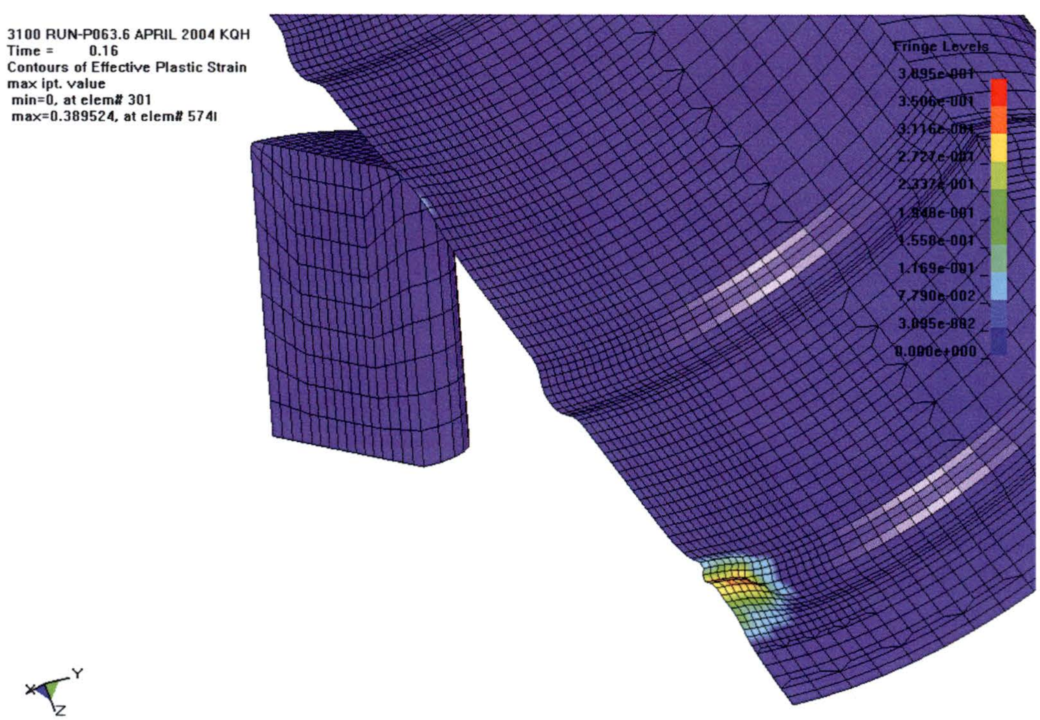

Figure 3.11.6 - Punch at 63.6°, Surface Strain in the Drum Liner

3.12 Comparison of Test vs Analysis

Physical testing of the ES-3100 shipping container to the 4-foot, 30-foot, 30-foot crush and 40-inch punch impacts were carried out in late May, 2004 at the Oak Ridge National Lab (ORNL), National Transportation Research Center (NTRC) facility in Oak Ridge.

The test specimen were subject to the entire series of impacts (4-foot, 30-foot, crush and punch), however the analytical impacts were not all subject to the entire series. Typically, the analysis was a design run which was subjected to a 30-foot impact followed by a crush impact. So the 30-foot analysis comparison was made to a test specimen that had experienced a 4-foot and a 30-foot impact. And likewise for the crush impact comparisons, the analysis results are lacking the initial 4-foot impact.

The comparisons are made for TU1 (Test Unit #1), TU2, TU3 and TU4. TU1 is the 12° slapdown, TU2 is the cold package side impact, TU3 is the corner impact and TU4 is the end impact. The nodes in the analysis model shell elements lie on the thickness centerline. Therefore, where appropriate, half thickness dimensions are included to render surface to surface comparisons with the test data. Figure 3.12.1 shows locations for which test diameters were obtained.

Dimensions in the tables are inches, unless otherwise noted. The analysis model was reflected with the post processor so that it appears as a full model. This was done to aid in the visual comparison between the test specimen and the model results. The background in the test photos has been erased, also to aid visual comparisons.

The "flats" is the region of relative flatness in the drum liner due to the impact. The analysis flats dimensions are obtained by knowing the element width (whole widths used) and judging which elements are dominantly in a relatively flat plane. The test flat dimensions are taken by visually judging when the drum deviates from a permanent, relatively flat region.

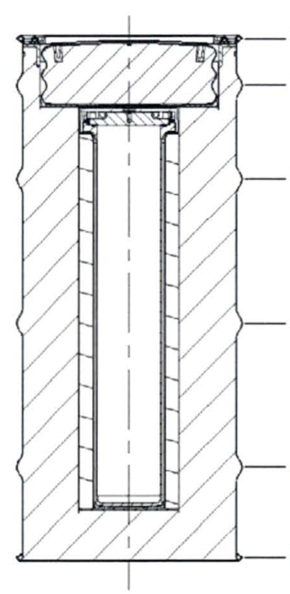

Figure 3.12.1 - Locations of Test Diameter Measurements

3.12.1 Comparison of Run4g to TU1

Run4g is a 30-foot, 12° slapdown impact followed by an offset crush (crush plate centered over the CV flange). TU1 is a 12° slapdown with a 4-foot impact, 30-foot impact, offset crush, and punch test specimen. The following Table 3.12.1.1 shows the initial diameter comparisons (pre-impact) using test data compared to the analysis results.

Table 3.12.1.1 - Run4g vs TU1, Comparison of Initial Diameters (Pre-Impact)				
Location	0°- 180°		90°-270°	
	Test	Analysis	Test	Analysis
Top Chime	19.25	19.32	19.25	19.32
Top Hoop	19.25	19.37	19.25	19.37
Top CG Hoop	19.25	19.37	19.25	19.37
CG Hoop	19.25	19.37	19.25	19.37
Bottom Hoop	19.25	19.37	19.25	19.37
Bottom Chime	19.25	19.38	19.25	19.38

The Table 3.12.1.2 shows the digital results of the 30-foot impact. The test diameters are after the 4 and 30-foot impacts, while the analysis is after the 30-foot impact.

Table 3.12.1.2 - Run4g vs TU1, Diameter Results After the 30-Foot Impact				
	0°-180°		90°-270°	
	Test	Analysis	Test	Analysis
Top Chime	18-1/2	18.1	19-3/8	19.5
Top Hoop	18-1/2	18.2	19-3/8	19.6
Top CG Hoop	18-1/2	18.5	19-3/8	19.5
CG Hoop	18-5/8	18.8	19-3/8	19.4
Bottom Hoop	18-5/8	18.9	19-1/4	19.3
Bottom Chime	17-13/16	18.1	19-3/8	19.4

Figure 3.12.1.1 shows the final configuration of the test specimen after the 4 and 30-foot impacts. Figure 3.12.1.2 shows the analytical model configuration after the 30-foot impact.

Figure 3.12.1.1 - TU1, Results of 30-Foot Impact

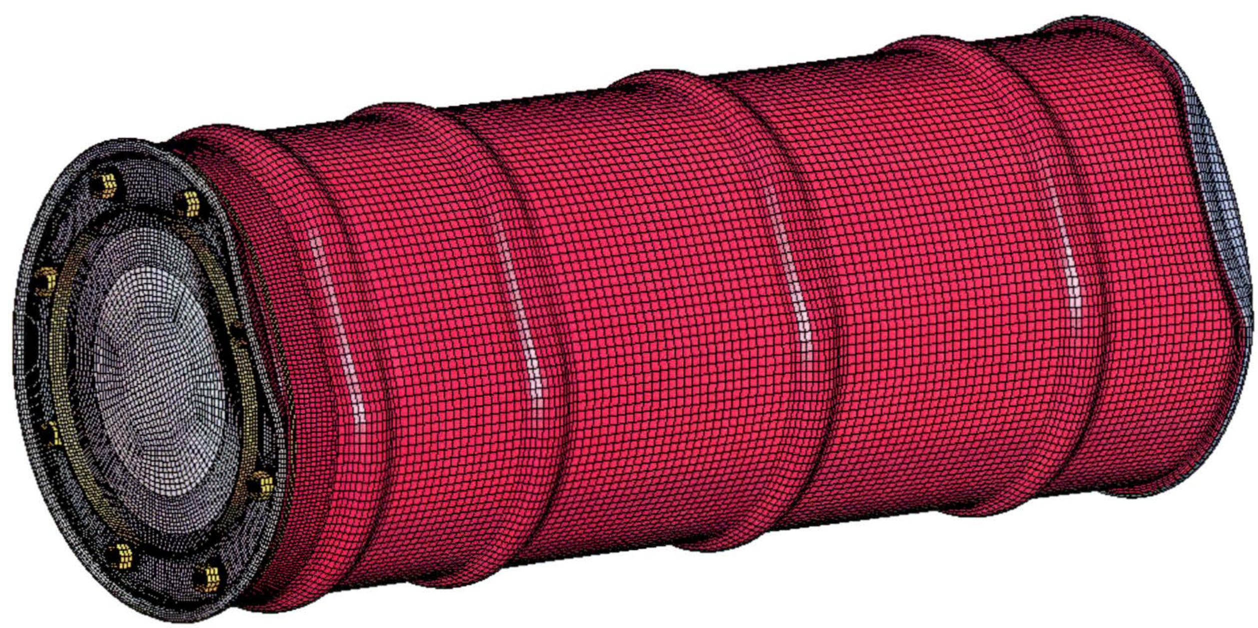

Figure 3.12.1.2 - Run4g, Results of the 30-Foot Impact

Table 3.12.1.3 shows the comparison of the digital results of the crush impact. The test data is for the cumulative effects of a 4-foot, 30-foot, and crush impact. The analysis data is for a cumulative 30-foot impact and crush impact.

Table 3.12.1.3 - Run4g vs TU1, Diameter Results After the Crush Impact

	0°-180°		90°-270°	
	Test	Analysis	Test	Analysis
Top Chime	15-5/8	15.0	20-5/8	20.7
Top Hoop	16	15.3	20-7/16	20.8
Top CG Hoop	16-1/4	15.9	20-1/4	20.6
CG Hoop	16-1/2	16.4	19-7/8	20.1
Bottom Hoop	18-1/4	18.3	19-1/2	19.6
Bottom Chime	17-13/16	18.1	19-1/4	19.4

Figure 3.12.1.3 shows an isometric view of the test specimen with the crush side up. Figure 3.12.1.4 shows a similar view for the analysis results.

Figure 3.12.1.3 - TU1, View of Crush Damage with the Crush Side Up

Figure 3.12.1.4 - Run4g, View of the Crush Damage With the Crush Side Up

Table 3.12.1.4 shows the results of a comparison of the "flats" measurements on the drum for the 30-foot impact and Table 3.12.1.5 compares the crush impact test measurements and analysis results.

Table 3.12.1.4 - Run4g vs TU1, Comparison of Flats for the 30-Foot Impact

	Test	Analysis
Top Chime	8	8.8
Top Hoop	7-3/8	8.4
Top CG Hoop	7-1/8	7.6
CG Hoop	6-3/8	5.9
Bottom Hoop	6-3/4	5.9
Bottom Chime	10	10.1

Table 3.12.1.5 - Run4g vs TU1, Comparison of Flats for the Crush Impact

Location	Rigid Surface Side		Crush Plate Side	
	Test	Analysis	Test	Analysis
Top Chime	9	10.5	8-1/2	10.5
Top Hoop	10	11.0	10	11.0
Top CG Hoop	10	10.1	10-1/8	10.1
CG Hoop	9	8.4	10-5/8	10.1
Bottom Hoop	8-1/4	7.6	- - -	0.0
Bottom Chime	9-7/8	10.1	- - -	0.0

The stud at the 90° position was severed in the model (reference Section 3.7, Figure 3.7.6), however arguments were made that the lid would tear first, relieving the loading on the stud. This was verified in the test results where tears were noted at both stud holes at 90° to the impacts/crush.

Table 7.7.1.3 shows the comparison of the results of the crush impacts. The test data is for the cumulative effects of a 4-foot, 30-foot, and crush impact. The analysis data is for a cumulative 30-foot impact and crush impact.

Table 7.7.1.3 - Run4g vs TU1, Diameter Results After the Crush Impact				
	0°-180°		90°-270°	
	Test	Analysis	Test	Analysis
Top Chime	15-5/8	14.9	20-5/8	20.7
Top Hoop	16	15.1	20-7/16	20.8
Top CG Hoop	16-1/4	15.7	20-1/4	20.7
CG Hoop	16-1/2	16.2	19-7/8	20.4
Bottom Hoop	18-1/4	18.1	19-1/2	19.8
Bottom Chime	17-13/16	18.0	19-1/4	19.4

Figure 7.7.1.3 shows an isometric view of the test specimen with the crush side up. Figure 7.7.1.4 shows a similar view for the analysis results.

Figure 7.7.1.3 - TU1, View of Crush Damage with the Crush Side Up

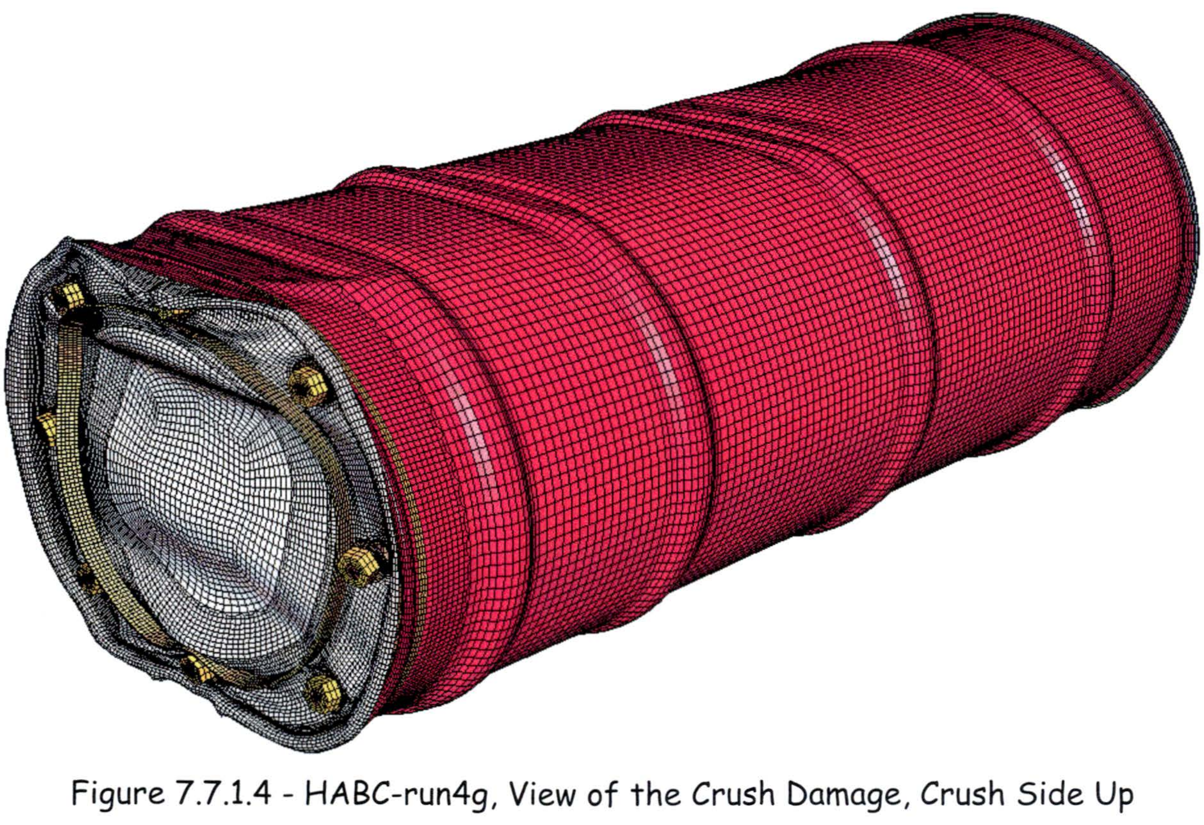

Figure 7.7.1.4 - HABC-run4g, View of the Crush Damage, Crush Side Up

Table 7.7.1.4 shows the results of a comparison of the "flats" measurements from the test after the 30-foot impacts and Table 3.12.1.5 compares the crush impact results.

Table 7.7.1.4 - HABC-run4g vs TU1, Comparison of Flats for the 30-Foot Impact		
	Test	Analysis
Top Chime	8	8.8
Top Hoop	7-3/8	8.4
Top CG Hoop	7-1/8	7.6
CG Hoop	6-3/8	5.9
Bottom Hoop	6-3/4	5.9
Bottom Chime	10	10.1

Table 7.7.1.5 - HABC-run4g vs TU1, Comparison of Flats for the Crush Impact				
Location	Rigid Surface Side		Crush Plate Side	
	Test	Analysis	Test	Analysis
Top Chime	9	10.5	8-1/2	10.9
Top Hoop	10	11.0	10	11.0
Top CG Hoop	10	10.1	10-1/8	10.1
CG Hoop	9	8.4	10-5/8	10.1
Bottom Hoop	8-1/4	7.6	- - -	0.0
Bottom Chime	9-7/8	10.1	- - -	0.0

7.7.2 Comparison of HABC Run2e vs TU3

The HABC-run2e is a CG over lid corner 30-foot impact, followed by a bottom corner crush. TU3 is a similar test impact configuration with a 4-foot impact, 30-foot impact on the lid corner, then a crush impact on the bottom corner followed by a punch.

The test results show that there is 1.125 inches between the top chime and the top hoop in the test. Similar measurements in the analysis show that the distance is about 1.7 inches. This would be a somewhat judgmental comparison due to points chosen for measurement on the test specimen might not be the same as those chosen in the analysis. The analysis measurement is from the top of the crimped drum roll to the center of the flattened region in the lid roll, on the plane of symmetry.

Table 7.7.2.1 shows the comparison of the TU3 test unit and the computer run2e drum diameter changes after the 30-foot impact.

Table 7.7.2.1 - Run2e vs TU3, Diameter Results After the 30-Foot Impact

	0°-180°		90°-270°	
	Test	Analysis	Test	Analysis
Top Chime	19-1/4	19.0	19-3/16	19.2
Top Hoop	18-5/8	19.1	19-7/8	20.0
Top CG Hoop	19-1/8	19.3	19-3/8	19.5
CG Hoop	19-1/8	19.4	19-3/8	19.4
Bottom Hoop	19-1/8	19.4	19-1/4	19.4
Bottom Chime	19-1/8	19.4	19-3/8	19.4

Figure 7.7.2.1 is an image of the damage after the 30-foot impact of TU3. The test photo shows the cumulative damage from the 4-foot and 30-foot impacts. Figure 7.7.2.2 shows a similar view after the 30-foot impact in run2e. The analysis image is the damage from only the 30-foot impact.

Figure 7.7.2.1 - TU3, Deformed Shape After the 30-Foot Impact

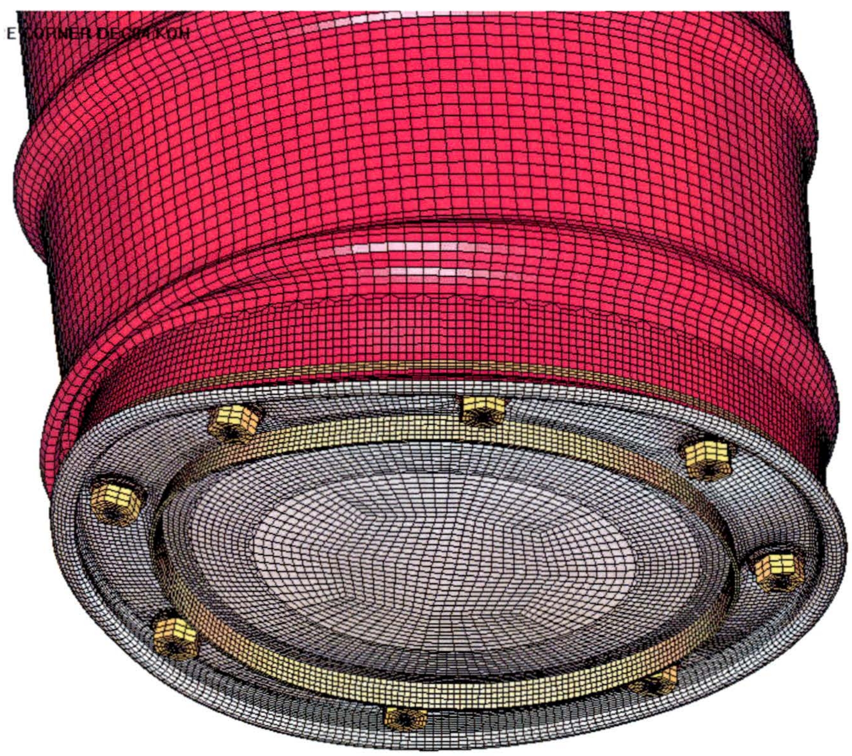

Figure 7.7.2.2 - HABC-run2e, Deformed Shape After the 30-foot Impact

The package drum diameters after the crush impact are compared in Table 7.7.2.2.

Table 7.7.2.2 - Run2e vs TU3, Diameter Results After the Crush Impact

	0°-180°		90°-270°	
	Test	Analysis	Test	Analysis
Top Chime	19-1/4	19.0	19-1/16	19.0
Top Hoop	18-3/4	18.9	20-1/4	20.6
Top CG Hoop	19-1/4	19.4	19-3/4	19.8
CG Hoop	19-1/8	19.3	19-1/4	19.4
Bottom Hoop	19-1/8	19.3	19-3/4	20.4
Bottom Chime	18	18.6	19-3/8	19.4

The final images after the crush impact are shown for the test and the analysis. Figure 7.7.2.3 shows the final shape of the crushed bottom on the test specimen (4ft + 30ft + crush) and Figure 7.7.2.4 shows a similar view of the analysis (30ft + crush).

Figure 7.7.2.3 - TU3, Damage to the Bottom Head in the Crush Impact

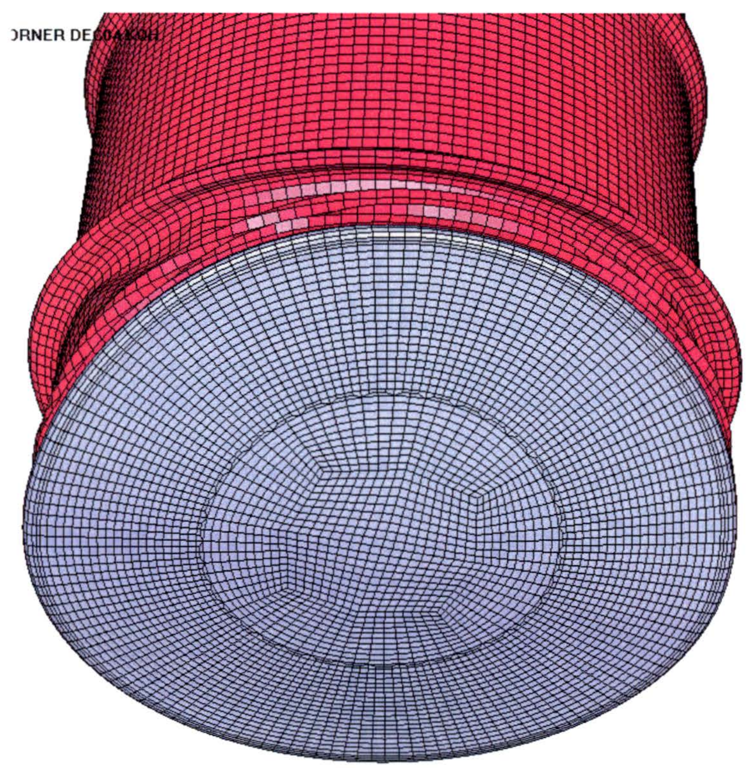

Figure 7.7.2.4 - HABC-run2e, Damage to the Bottom Head in the Crush Impact

The damage to the lid region at the end of the crush impact is shown in Figure 7.7.2.5 for the TU3. The damage to the lid region in the analysis run2e is shown in Figure 7.7.2.6.

Figure 7.7.2.5 - TU3, Lid Damage from the Crush Impact

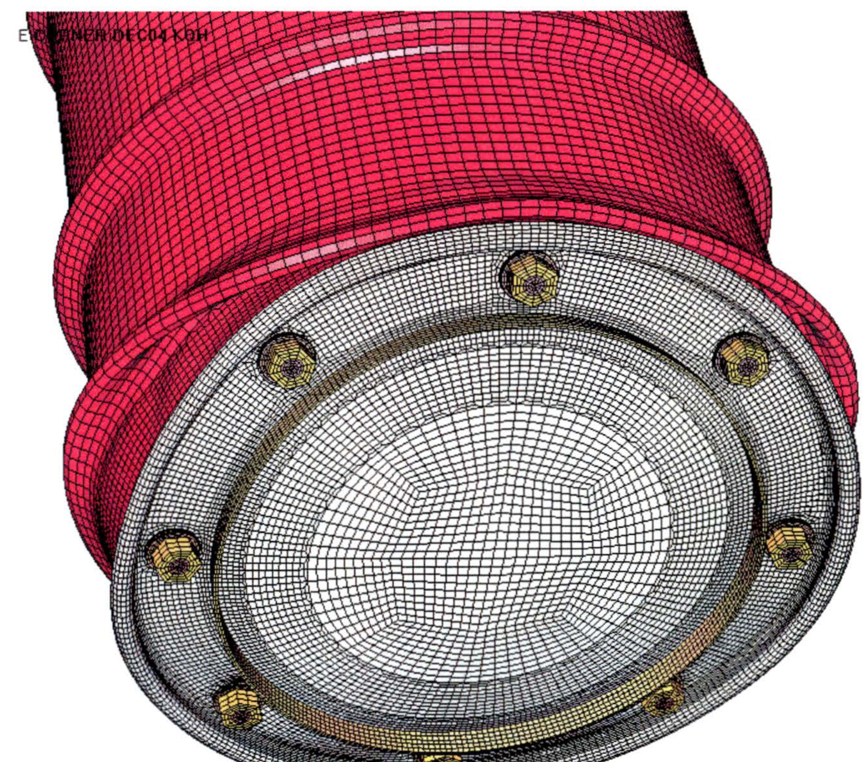

Figure 7.7.2.6 - HABC-run2e, Damage to the Bottom Head from the Crush Impact

7.7.3 Comparison of HABC-Run3b vs TU4

The HABC-run3b is a 30-foot lid down impact onto the rigid surface, followed by a crush impact onto the container bottom. The diameter measurements after the 30-foot impact are given in Table 7.7.3.1.

Table 7.7.3.1 - HABC Run3b vs TU4, Diameter Results After the 30-Foot Impact

	0°-180°		90°-270°	
	Test	Analysis	Test	Analysis
Top Chime	19-1/4	19.3	19-3/8	19.3
Top Hoop	19-1/8	19.7	19-7/8	19.7
Top CG Hoop	19-13/16	20.0	19-3/8	20.0
CG Hoop	19-1/8	19.5	19-1/4	19.5
Bottom Hoop	19-1/4	19.4	19-1/4	19.4
Bottom Chime	19-1/4	19.4	19-1/4	19.4

The overall height measurements were compared between the test and the analysis. For the 30-foot impact, the test results vary around the circumference: 43.0 inches at 0°, 43.125 inches at 90°, 42.875 inches at 180° and 42.625 inches at 270°. The analysis is symmetrical, and the height from the top of the lid drum roll to the bottom head surface after the 30-foot impact is about 42.6 inches.

Figure 7.7.3.1 shows the configuration of the TU4 after the 30-foot impact (4ft + 30ft). Figure 7.7.3.2 shows the analysis model configuration after the 30-foot impact in a similar orientation to the test unit.

Figure 7.7.3.1 - TU4, 4-Foot + 30-Foot Impact Damage

Figure 7.7.3.2 - HABC-Run3b, 30-Foot Impact Damage

The drum height measurement after the test crush impact is 39-3/8 inches at 0°, 40-3/8 inches at 90°, 40-5/8 inches at 180°, and 39-3/4 inches at-270°. The analytical value for the height is about 39.0 inches.

The drum diameters after the crush impact are compared in Table 7.7.3.2.

Table 7.7.3.2 - HABC Run3b vs TU4, Diameter Results After the Crush Impact				
	0°-180°		90°-270°	
	Test	Analysis	Test	Analysis
Top Chime	19-1/4	19.3	19-3/8	19.3
Top Hoop	20	20.1	20-1/8	20.1
Top CG Hoop	20	20.2	20-1/16	20.2
CG Hoop	19-7/16	20.1	19-1/2	20.1
Bottom Hoop	19-15/16	20.5	20	20.5
Bottom Chime	19-1/4	19.4	19-1/4	19.4

Figure 7.7.3.3 shows the TU4 at the end of the crush impact (4ft + 30ft + crush), while Figure 7.7.3.4 shows the configuration of the HABC-run3b model (30ft + crush).

Figure 7.7.3.3 - TU4, Crush Damage

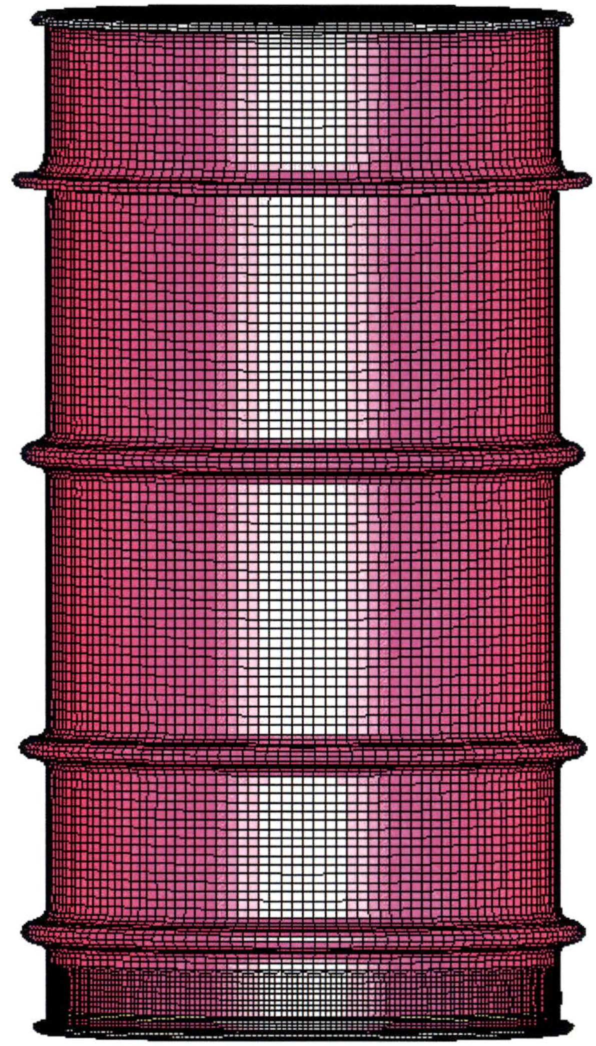

Figure 7.7.3.4 - HABC Run3b, Crush Damage

7.7.4 Comparison of HABC Run1hh vs TU2

HABC-run1hh was the upper bounding kaolite run which included a 4-ft, 30-foot and crush impacts. The test results are for the cumulative damage from the 4-ft, 30ft, crush and punch impacts. The table 7.7.4.1 shows the results for the diameter changes due to all the impacts for the test and the analysis.

Table 7.7.4.1 - Run1hh vs TU2, Cumulative Diameter Results				
	0°-180°		90°-270°	
	Test	Analysis	Test	Analysis
Top Chime	17-5/8	18.0	19-13/16	19.6
Top Hoop	17-3/8	16.6	19-3/4	20.1
Top CG Hoop	17	16.5	20	20.4
CG Hoop	16	16.3	20-1/4	20.5
Bottom Hoop	15-1/2	16.1	20-1/8	20.0
Bottom Chime	18	17.6	19-3/8	19.4

Table 7.7.4.2 shows the comparison of the "flats" dimensions for the test and the analysis.

Table 7.7.4.2 - Run1hh vs TU2, Cumulative Flats Results†				
	180° - Crush Plate Side		0° - Rigid Surface Side	
	Test‡	Analysis	Test	Analysis
Top Chime	6-1/4	0	8.0	9.2
Top Hoop	8-7/8	10.1	9.0	9.3
Top CG Hoop	9-5/8	9.3	10-1/8	8.4
CG Hoop	12	9.3	9-7/8	9.3
Bottom Hoop	14-7/8	10.1	9-7/8	9.3
Bottom Chime	0	0	9-3/8	10.1
† - Note - The reported test results for the 0 and the 180 sides are reversed in the test report (evidence Figure 7.7.4.3 below). ‡ - Note - The crush plate edge was 4.75 inches from bottom of package.				

A visual comparison of the cumulative damage on the rigid surface side after the impacts is shown in Figures 7.7.4.1 (test) and Figure 7.7.4.2 (analysis).

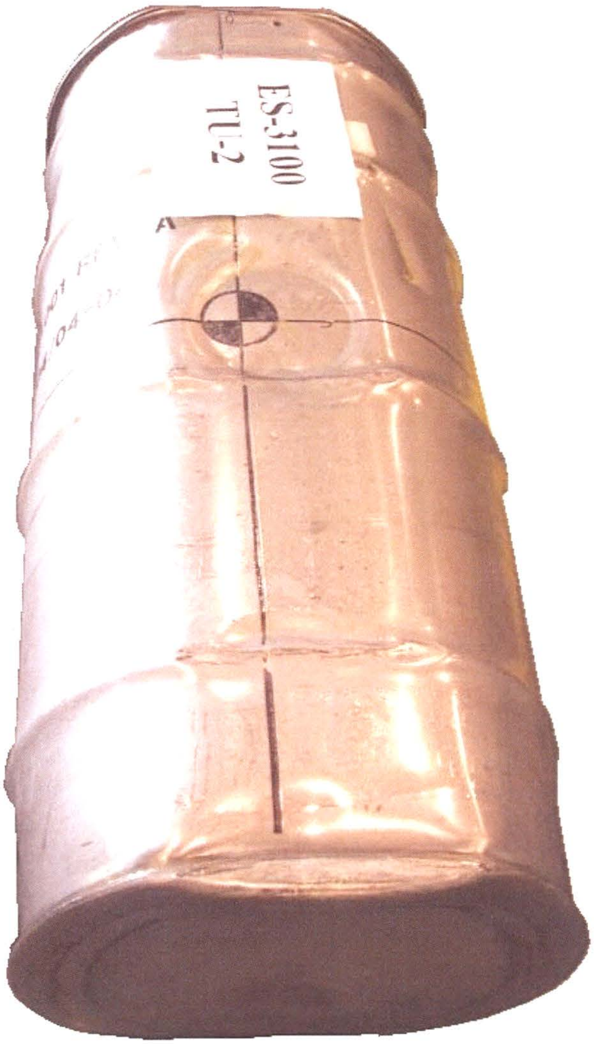

Figure 7.7.4.1 - TU2, Cumulative Damage After the Punch Impact, Rigid Surface Side

Figure 7.7.4.2 - HABC-run1hh, Cumulative Damage, Rigid Surface Side

A visual comparison of the cumulative damage on the crush side after the four impacts is shown in Figures 7.7.4.3 (test) and Figures 7.7.4.4 (analysis).

Figure 7.7.4.3 - TU2, Cumulative Damage After the Punch Impact, Crush Plate Side

Figure 7.7.4.4 - HABC-run1hh, Cumulative Damage, Crush Plate Side

8.0 Summary

The computer simulation impacts for the HABC re-design of the ES-3100 shipping container are presented in Sections 7.1 to 7.6. The comparison of the HABC re-design container to the physical tests is presented in Section 7.7. The effective plastic strain for the components are summarized in Table 8.0.1. The punch impact is not included in the HABC runs, due to the fact that the drum shell capability is demonstrated in the initial borobond models, and the tested specimen.

Maximum strains in excess of 0.5 in/in are near the 304L strain limit of 0.57 in/in and are highlighted in red in Table 8.0.1. The components which are highlighted included the drum , lid, studs and liner. Evidence from looking at the Table 8.0.1 summary, a high demand is placed on the lid and the studs in the side and slapdown impacts.

In runs HABC-runs1hl, 1hh, 4g and 4ga a high demand is placed on the lid/studs. In runs 1hh, 1hl, 4g and 4ga, the region of plastic strain is very localized at the stud holes. Runs 1hl and 4g also have relatively high demands placed on the studs. In runs1hl and 4g, it is shown that the times at which the lid strains become excessive in membrane, the stud strains are relatively low. Hence, it is predicted that the lid will locally tear, thereby relieving loading on the studs. The tearing associated with the lid is expected to be local due to the localized fringes of extreme strain shown in the Section 7 fringe plots. The large washers provided on the packages would restrain the lid.

In runs HABC-run1hl, 2e and 4g, the studs reach high levels of effective plastic strain. In HABC-run1hl, the lid was shown to tear before the studs reached an elevated level of plastic strain.

HABC-run2e shows that the stud at the impact reaches extreme levels of plastic strain near the 0.57 in/in failure strain in the 30-foot impact and the subsequent crush impact. The level of high strain is throughout the cross section of the stud in HABC-run2e. Due to this high level of strain and the direct load path between the shipping package and the rigid surface, any slight changes in length, friction, localized deformations (stud "digging" into the relatively rigid plate in the test) could cause the stud to fail.

In HABC-run4g, the stud reached its failure strain and the cross section row of elements failed (removed by LS-Dyna). A time study shows that the lid reaches its levels of elevated strain in membrane before the stud. Therefore, the lid is expected to tear before the stud fails, thus relieving loading on the stud. However, the model does show the shipping container response if the lid were not to tear, and the stud were to fail.

The relatively high level of plastic strain in the HABC-run2e liner is a surface strain. Investigation shows that the membrane strain is about 0.2205 in/in, or well below the expected failure level. The deformation/fringe plot shows that the region of high strain is relatively local at the attachment of the liner to the angle. The plot also shows that it is the result of crimping or folding of the liner due to the relatively stiffer angle. Any tearing that might take place would be limited, evidence the local concentration of fringe levels.

Table 8.0.1 - ES-3100 HABC Shipping Package Summary of Component Maximum Effective Plastic Strain (in/in)

Material	Description	HABC-run1hl Side - Lower Bound Kaolite (Section 7.1)			HABC-run1hh Side - Upper Bound Kaolite (Section 7.2)		
		4-foot	30-foot	Centered Crush	4-foot	30-foot	Centered Crush
1	CV Body	0.0185	0.0195	0.0206	0.0238	0.0347	0.0525
3	CV Lid	0.0001	0.0002	0.0002	0.0000	0.0001	0.0004
4	CV Nut Ring	0.0000	0.0000	0.0000	0.0000	0.0000	0.0005
5	Angle	0.0055	0.0780	0.1142	0.0061	0.0632	0.0845
6	Drum	0.1599	0.2251	0.5139	0.1207	0.2296	0.2814
7	Drum Bottom	0.1033	0.2126	0.3562	0.1252	0.2517	0.2827
10	Liner	0.1045	0.1078	0.1593	0.0991	0.1184	0.2022
12	Lid	0.1393	0.5790	1.2580	0.1604	0.4063	0.6413
15	Lid Stiffener	0.0004	0.0093	0.0515	0.0006	0.0076	0.0171
16	Lid Studs	0.0000	0.1140	0.5121	0.0000	0.1306	0.2364
17	Lid Stud Nuts	0.0000	0.0000	0.0005	0.0000	0.0004	0.0018
18	Lid Stud Washe	0.0194	0.0194	0.0693	0.0411	0.0424	0.0439
19	Plug Liner	0.0022	0.0958	0.1220	0.0045	0.1072	0.1286

Material	Description	HABC-run2e Corner (Section 7.3)		HABC-run3b End (Section 7.4)		HABC-run4g Slapdown (Section 7.5)		HABC-run4ga Slapdown (Section 7.6)	
		Impact	Crush	Impact	Crush	Impact	Offset Crush	Impact	Centered Crush
1	CV Body	0.0371	0.0371	0.0028	0.0083	0.0376	0.0564	Same as HABC-Run4g Impact Results	0.0643
3	CV Lid	0.0051	0.0051	0.0072	0.0072	0.0004	0.0013		0.0018
4	CV Nut Ring	0.0002	0.0002	0.0011	0.0011	0.0000	0.0001		0.0000
5	Angle	0.0394	0.0462	0.0287	0.0308	0.0900	0.1070		0.0944
6	Drum	0.3247	0.3830	0.0557	0.1237	0.3018	0.3920		0.3443
7	Drum Bottom	0.0000	0.0761	0.0031	0.0267	0.2879	0.2879		0.3000
10	Liner	0.3983	0.5254	0.0607	0.3812	0.1458	0.2060		0.2846
12	Lid	0.2791	0.3622	0.1082	0.1389	0.5278	0.9689		0.5828
15	Lid Stiffener	0.0272	0.0272	0.0069	0.0100	0.0213	0.0894		0.0288
16	Lid Studs	0.5233	0.5598	0.0962	0.1535	0.1892	0.4018		0.2390
17	Lid Stud Nuts	0.2260	0.2266	0.0166	0.0173	0.0000	0.0028		0.0000
18	Lid Stud Washe	0.1528	0.1528	0.0506	0.0506	0.0724	0.0790		0.0775
19	Plug Liner	0.1152	0.1166	0.0670	0.0960	0.1258	0.2665		0.1644

9.0 Comparison of Borobond Cylinder and HABC Cylinder Models

Part A of this calculation (Sections 2 through 5) apply to the initial, borobond neutron absorber model. Section 3.12 compared the borobond model results to the physical tested specimen. Part B (Sections 6 through 8) apply to the HABC redesigned neutron absorber model. Section 7.7 compares the HABC model to the physical tested specimen. The HABC model was derived from the initial borobond model, with changes detailed in Section 6. Section 6.1 gives the configuration changes and Section 6.2 gives the material model derivation for the HABC neutron absorber.

The borobond and the HABC materials are similar in nature in that they are castable, cement type materials. The LS-Dyna material model used in both analytical simulations was the *MAT_SOIL_AND_FOAM model. Similar approaches were taken for both the borobond and the HABC to match the material test results to the needed material properties in the analytical model. The approach is shown explicitly for the HABC material model in Section 6.2. The borobond model used in the Part A models, was also used in the Highly Enriched Uranium Materials Facility (HEUMF) storage pallet modeling, testing and qualification.

The CV body cylinder has an outside diameter of about 5.6 in. A minimum liner diameter of about 5.3 inches was found to occur in the borobond slapdown runs (4g, 4ga, 4h and 4ha). This minimum occurred at several locations along the liner length, and also near the CV flange. A somewhat similar response is noted for the HABC models, but with more deflection near the mid-height of the CV cavity. A minimum liner diameter of about 5.2 inches near the CV flange is noted in slapdowns HABC-run4g and 4ga. However, a minimum diameter of about 4.5 in is noted in HABC-run4ga near the mid-height of the CV body. This region of the CV body is remote from the bottom head or the flange and plastic strains in the body are relatively low (compare Figures 3.8.2 and Figure 7.6.4). The region of concern, near the CV flange, experiences about the same deformation (5.3 in vs 5.2 in).

A significant demand is placed on the lid and the studs in both the borobond and the HABC model side and slapdown impacts. This is a precipitate of the design attempt to minimize the number of studs securing the lid. The lid power law material model does not allow for element failure, whereas the model used for the studs (elastic-plastic) did allow element failure to be modeled. The effective plastic strain in bending and membrane reach significantly high levels (about 1.0 strain) in the lid. The regions of elevated plastic strain in the lid are shown to be localized at the stud holes. The studs also reached elevated levels of plastic strain. Investigation into the time history of the demand placed on the lid and the studs reveals that the lid reaches the elevated levels earlier in the impact, and therefore tearing of the lid would be expected. The tearing of the lid is expected to relieve the loading on the studs, such that the integrity of the studs would be maintained. The large washers will restrain the lid. This fact was verified in the test with some tearing at the 90°and 270° position stud holes and no loss of a stud.

Both models compared favorably with the test results and with each other. This can be seen in the tables in Section 3.12 for the borobond and 7.7 for the HABC material.

THIS PAGE INTENTIONALLY LEFT BLANK.

Appendix 2.10.3

KAOLITE PROPERTIES

Kaolite SuperLightweight Insulating Castables, Thermal Ceramics, Augusta, Ga., September 1999.

Material Safety Data Sheet, *Refractory Castable, Silicate Product, Kaolite*, Thermal Ceramics, Augusta, Ga., September 1999.

R. E. Oakes, Jr., *Mechanical Properties of a Low Density Concrete for the New ES-2 Shipping/Storage Container Insulation, Impact Mitigation Media and Neutron Absorber*, Y/DW-1661, Lockheed Martin Energy Systems, Inc., Oak Ridge Y-12 Plant, Apr. 10, 1997.

H. Wang, *Thermal Conductivity Measurements of Kaolite*, ORNL-TM-2003/49, UT-Battelle, Oak Ridge Natl. Lab., n.d.

B. F. Smith and G. A. Byington, *Water Content and Temperature-Dependent Impact Properties of an Inorganic Cast Refractory Material*, Y/DW-1890, BWXT Y-12, Y-12 Natl. Security Complex, Feb. 14, 2003.

B. F. Smith, *Low Temperature Impact Properties of an Inorganic Cast Refractory Material*, Y/DW-1972, BWXT Y-12, Y-12 Natl. Security Complex, Sept. 14, 2003.

Advantages of Using a Fireproof Inorganic Cast Refractory Material in Hazardous Content Shipping Packages, Y/LF-565, Lockheed Martin Energy Systems, Inc., Oak Ridge Y-12 Plant, Nov. 10, 1998.

K. Moody, Thermal Ceramics, Augusta, Ga., *RE: Coefficient of thermal expansion for Kaolite 1600*, email to P. A. Bales, BWXT Y-12, Oak Ridge, Tenn., Dec. 9, 2004.

KAOLITE SUPER LIGHTWEIGHT INSULATING CASTABLES

Super lightweight Kaolite castables reduce both the quantity of heat storage and heat transfer through the lining producing significant savings in furnace fuel consumption. The lower densities of these vermiculite based Kaolite castables reduce the amount of supporting furnace steel work required and provide more insulation with a thinner lining. These products can be cast, poured, or gunited.

Kaolite 1600 is a super lightweight, low thermal conductivity vermiculite based castable designed for backup insulation up to 1600°F. Kaolite 1600 contains portland cement which limits use temperature to 1600°F; however, this makes it an economical product based on cost per cubic foot.

Kaolite 1800 is a super lightweight, low thermal conductivity vermiculite castable designed for both backup insulation and hot face applications up to 1800°F. Kaolite 1800 contains a calcium-aluminate cement which gives it better high-temperature stability when compared to Kaolite 1600. Typical applications would be low-temperature lining for ovens and ductwork lining.

Kaolite 2000 is a super lightweight, low thermal conductivity castable designed for backup insulation and hot face applications up to 2000°F. Typical applications would be low-temperature lining for ovens and ductwork lining.

Instructions For Using

Casting

Highest strength is obtained with castable refractory by using the least amount of clean mixing water. This will allow thorough working of material into place by lightly vibrating or rodding. A mechanical mixer is required for proper placement (paddle-type mortar mixers are best suited). After achieving a ball-in-hand consistency, mix for 6 minutes. Place material within 20 minutes after mixing.

Gunning

Use suitable gunite equipment. Material should be predampened uniformly with approximately 10 - 12% by weight of clean water in mechanical mixer before placing into gun. This will reduce rebound and dust. Add required water at nozzle for effective placement. Suggested air pressure at the nozzle is between 15 and 25 psi.

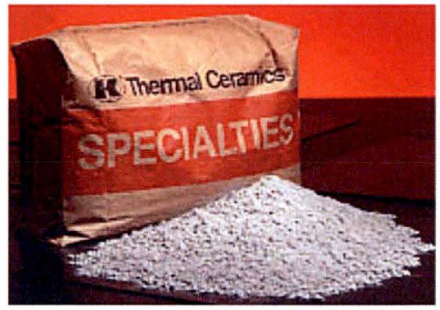

Precautions

Store bagged castables in a dry place, off the ground and, when possible, with the original shrink wrapping intact.

Watertight forms must be used when placing material. All porous surfaces that will come into contact with the material must be waterproofed with a suitable coating or membrane. For maximum strength, cure 24 hours under damp conditions before initial heat-up. Keep freshly placed castable warm during cold weather, ideally between 70°F and 80°F. New castable installations must be heated slowly the first time.

Freshly placed lightweight castables are prone to a deteriorating condition called alkali hydrolysis when they are kept in a non-dried state for a sustained period of time in a warm, humid environment. Under these conditions, the castables should be force dried soon after placement or coated with Kao-Seal™ to resist the possible deterioration effects.

For mor information on castable placement, consult your Thermal Ceramics representative or call 1-800-329-7444 to receive faced instruction manuals.

Kaolite	**1600**	**1800**	**2000**
Specifications	cast, gunned	cast, gunned	cast, gunned
Recommended use limit, °F	1600	1800	2000
Melting point, °F,	2300	2400	2400
Average lb required to place one cubic ft[1]	23, 36*	23, 35*	25, 35*
Nominal density, pcf, fired	20 - 25, 31 - 39	20 - 25, 29 - 38	21 - 26, 29 - 35
Pounds per bag	50	50	50
Method of installation[2]	C,G,P	C,G,P	C,G,P
Recommended water ranges, % by weight			
Casting (by vibrating)	120 - 145	145 - 165	155 - 180
Pouring	150 - 180	175 - 190	175 - 190

*Note: For overhead gunning applications, pounds required to place one ft³ should be increased to 40-50 pcf. Does not include rebound loss.

Physical Properties[3]			
Modulus of rupture, psi (ASTM C 133)	cast, gunned	cast, gunned	cast, gunned
Dried 18-24 hrs. @ 220°F	45 - 75, 70 - 120	25 - 40, 50 - 100	18 - 26, 50 - 100
Fired 5 hrs. @ 1500°F	25 - 40, 35 - 55	30 - 50, 40 - 60	28 - 36, 40 - 65
Fired 5 hrs. @ use limit	25 - 40, 35 - 50	25 - 40, 35 - 55	–
Cold Crushing strength			
Dried 18-24 hrs. @ 220°F	80 - 120, 125 - 175	35 - 50, 70 - 120	55 - 64, 75 - 85
Fired 5 hrs. @ 1500°F	50 - 70, 90 - 120	50 - 80, 80 - 110	70 - 120, 80 - 110
Fired 5 hrs. @ use limit	50 - 70, 90 - 120	40 - 60, 60 - 80	–
Perm. linear change, % (ASTM C 113)[4]			
Fired 5 hrs. @ 1500°F	-1.0 to -2.0	-0.5 to -1.5	-0.5 to -1.5
Fired 5 hrs. @ use limit	-1.5 to -2.5	-1.5 to -2.5	-1.5 to -3.0

Chemical Analysis (Nominal, %)			
Alumina, Al_2O_3	11	29	34
Silica, SiO_2	33	32	26
Ferric oxide, Fe_2O_3	7.9.	7.0	7.0
Titanium oxide, TiO_2	1.4	2.3	1.0
Calcium oxide , CaO	30	14	17
Magnesium oxide, MgO	12.1	12	10
Alkalies, as, Na_2O	3.7	3.5	2.5

Thermal Conductivity, Btu•in./hr•ft²•°F (ASTM C 417)			
Mean temperature			
@ 500°F	0.87, 1.03	0.79, 0.93	0.79, 0.93
@ 1000°F	1.02, 1.11	0.95, 1.06	0.95, 1.06
@ 1500°F	1.19, 1.20	1.11, 1.26	1.11, 1.27
@ 2000°F	–	–	1.28, 1.49

1. Gunite installation may require 10-30% overage due to rebound and on-site loss.
2. Installation key: C-cast, G-gun, P-pour
3. Properties indicated are for vibratory cast materials unless specified otherwise.
4. Fired linear change values reflect samples taken from a dried to fired state.

Consult Thermal Ceramics for specific curing and heat-up recommendations.

Data are average results of tests conducted under standard procedures and are subject to variation. Results should not be used for specification purposes.

Refer to the Material Safety Data Sheet (MSDS) for recommended work practices and other product safety information.

For further information, contact your nearest Thermal Ceramics technical sales office or your local Thermal Ceramics authorized distributor. You may also fax us toll-free at 1-800-KAOWOOL or write to Thermal Ceramics, P. O. Box 923, Dept. 140, Augusta, GA 30903.

AUGUSTA, GA
(800) 338-9284
Fax: (706) 796-4324

CHICAGO, IL
(888) 649-2442
Fax: (630) 527-0285

DETROIT, MI
(800) 590-4338
Fax: (734) 459-7860

LOS ANGELES, CA
(800) 990-5264
Fax: (714) 521-4662

INTERNATIONAL
(706) 796-4216
Fax: (706) 796-4262

BATON ROUGE, LA
(877) 722-2866
Fax: (504) 292-4082

CLEVELAND, OH
(877) 787-3385
Fax: (216) 831-4485

HOUSTON, TX
(800) 824-6878
Fax: (713) 680-9070

TRANSPORTATION
(888) 205-2358
Fax: (219) 296-3585

THERMAL CERAMICS
BURLINGTON, ONTARIO, CANADA
(905) 335-3414
Fax: (905) 335-5145

Thermal Ceramics

MATERIAL SAFETY DATA SHEET

MSDS No: 154	Date Prepared: 09/06/1993	Current Date: 2/3/2003 Last Revised: (01/16/2003)

1. PRODUCT AND COMPANY IDENTIFICATION

Product Group: **REFRACTORY CASTABLE**
Chemical Name: Silicate Product
Intended Use: High Temperature Thermal Insulation
Trade Names: Kaolite® 1600; Kaolite® 1600 RFT; Kaolite® 1800; Kaolite® 1800 RFT; Kaolite® 2000; Therm-O-Flake Coating

Manufacturer/Supplier:
Thermal Ceramics Inc.
P. O. Box 923; Dept. 300
Augusta, GA 30903-0923

For Product Stewardship and Emergency Information -
Hotline: 1-800-722-5681
Fax: 706-560-4054

For additional MSDSs and to confirm this is the most current MSDS for the product, visit our web page [*www.thermalceramics.com*] or call our automated FaxBack: 1-800-329-7444

2. COMPOSITION/INFORMATION ON INGREDIENTS

INGREDIENT & CAS NUMBER	% BY WEIGHT	OSHA PEL	ACGIH TLV
Vermiculite 01318-00-9	52 - 78	15 mg/m^3 (total dust); 5 mg/m^3 (respirable dust)	10 mg/m^3 (inhalable dust) 3 mg/m^3 (respirable dust)
Cement, alumina, chemicals 65997-16-2	15 - 50	15 mg/m^3 (total dust); 5 mg/m^3 (respirable dust)	10 mg/m^3 (inhalable dust) 3 mg/m^3 (respirable dust)
Crystalline silica 14808-60-7 or 14464-46-1	0.5 - 7	See notes[1]	0.05 mg/m^3 (respirable dust)

NOTES:

[1] Depending on the percentage and type(s) of silica in the mineral, the OSHA Permissible Exposure Limit (PEL) for respirable dust containing crystalline silica (8 HR TWA) is based on the formula listed in 29 CFR 1910.1000, "Air Contaminants" under Table Z-3, "Mineral Dust". For quartz containing mineral dust, the PEL = 10 mg/m^3 / (% of silica + 2); for cristobalite or tridymite, the PEL = 5 mg/m^3/ (% of silica + 2); for mixtures, the PEL = 10 mg/m^3 / (% of quartz + 2 (% of cristobalite) + 2 (% of tridymite) + 2).

(See Section 8 "Exposure Controls / Personal Protection" for exposure guidelines.)

MATERIAL SAFETY DATA SHEET

3. HAZARDS IDENTIFICATION

EMERGENCY OVERVIEW

WARNING!

Respirable dust from these products may contain crystalline silica, which is known to cause respiratory disease. (See Section 11 for more information)

POSSIBLE HEALTH EFFECTS

Target Organs:	Eyes, skin, nose and/or throat
Primary Entry Route:	Inhalation
Acute effects:	May cause temporary, mild mechanical irritation to the eyes, skin, nose and/or throat. Pre-existing skin and respiratory conditions may be aggravated by exposure.
Chronic effects:	Prolonged/repeated inhalation of respirable crystalline silica may cause delayed lung injury (e.g.: silicosis, lung cancer).

HAZARD CLASSIFICATION

Dust samples from these products have not been tested for their specific toxicity, but may contain more than 0.1% crystalline silica, for which the following apply:

The **International Agency for Research on Cancer (IARC)** has classified crystalline silica inhaled in the form of quartz or cristobalite from occupational sources as carcinogenic to humans (Group 1).

The Ninth Annual Report on Carcinogens (2000), prepared by the **National Toxicology Program (NTP),** classified silica, crystalline (respirable size), as a substance known to be a human carcinogen.

The **American Conference of Governmental Industrial Hygienists (ACGIH)** has classified crystalline silica (quartz) as "A2-Suspected Human Carcinogen."

The **State of California,** pursuant to Proposition 65, The Safe Drinking Water and Toxic Enforcement Act of 1986, has listed "silica, crystalline (airborne particles of respirable size)" as a chemical known to the State of California to cause cancer.

The **Canadian Workplace Hazardous Materials Information System (WHMIS) –** Crystalline silica [quartz and cristobalite] is classified as Class D2A - Materials Causing Other Toxic Effects.

The **Hazardous Materials Identification System (HMIS) –**
Health: 1* Flammability: 0 Reactivity: 0 Personal Protection Index: X (Employer determined)
(* denotes potential for chronic effects)

4. FIRST AID MEASURES

EYE IRRITATION:
Flush with large amounts of water for at least 15 minutes. Do not rub eyes.

SKIN IRRITATION:
Wash affected area gently with soap and water. Skin cream or lotion after washing may be helpful.

INGESTION:
Unlikely route of exposure.

INHALATION:
Remove affected person to dust free location. See Section 8 for additional measures to reduce or eliminate exposure.

- If symptoms persist, seek medical attention. -

5. FIRE FIGHTING MEASURES

NFPA CODES: **Flammability:** 0, **Health:** 1, **Reactivity:** 0, **Special:** 0

NFPA Unusual Hazards:	None
Flash Point:	None
Extinguishing Media:	Use extinguishing media suitable for type of surrounding fire.
Explosion Hazards:	None
Hazardous Decomposition Products:	None

6. ACCIDENTAL RELEASE MEASURES

SPILL/LEAK PROCEDURES:
Avoid creating airborne dust. Follow routine housekeeping procedures. Vacuum only with HEPA filtered equipment. If sweeping is necessary, use a dust suppressant and place material in closed containers. Do not use compressed air for clean-up. Personnel should wear gloves, goggles and approved respirator.

7. HANDLING AND STORAGE

HANDLING
Limit the use of power tools unless in conjunction with local exhaust. Use hand tools whenever possible. Frequently clean the work area with HEPA filtered vacuum or wet sweeping to minimize the accumulation of debris. Do not use compressed air for clean-up.

STORAGE
Store in original factory container in a dry area. Keep container closed when not in use.

EMPTY CONTAINERS
Product packaging may contain residue. Do not reuse.

8. EXPOSURE CONTROLS/PERSONAL PROTECTION

ENGINEERING CONTROLS
Use engineering controls, such as ventilation and dust collection devices, to reduce airborne particulate concentrations to the lowest attainable level.

RESPIRATORY PROTECTION
When it is not possible or feasible to reduce airborne crystalline silica or particulate levels below the PEL through engineering controls, or until they are installed, employees are encouraged to use good work practices together with respiratory protection. Before providing respirators to employees (especially negative pressure type), employers should **1)** monitor for airborne crystalline silica and/or dust concentrations using appropriate NIOSH analytical methods and select respiratory protection based upon the results of that monitoring, **2)** have the workers evaluated by a physician to determine the workers' ability to wear respirators, and **3)** implement respiratory protection training programs. Use NIOSH-certified particulate respirators (42 CFR 84), in compliance with OSHA Respiratory Protection Standard 29 CFR 1910.134 and 29 CFR 1926.103, for the particular hazard or airborne concentrations to be encountered in the work environment. For the most current information on respirator selection, contact your supplier.

PROTECTIVE CLOTHING

Wear full body clothing, gloves, hat, and eye protection as necessary to prevent skin irritation. Washable or disposable clothing may be used. If possible, do not take unwashed work clothing home. If soiled work clothing must be taken home, employers should ensure employees are trained on the best practices to minimize or avoid non-work dust exposure (e.g., vacuum clothes before leaving the work area, wash work clothing separately, rinse washer before washing other household clothes, etc.).

EYE PROTECTION

Wear safety glasses with side shields or other forms of eye protection in compliance with appropriate OSHA standards to prevent eye irritation. The use of contact lenses is not recommended, unless used in conjunction with appropriate eye protection. Do not touch eyes with soiled body parts or materials. If possible, have eye-washing facilities readily available where eye irritation can occur.

9. PHYSICAL AND CHEMICAL PROPERTIES

ODOR AND APPEARANCE:	Coarse brown powder.
CHEMICAL FAMILY:	Silicate
BOILING POINT:	Not applicable
WATER SOLUBILITY (%):	Slight
MELTING POINT:	> 2300°F
SPECIFIC GRAVITY:	Not applicable
VAPOR PRESSURE:	Not applicable
pH:	Not applicable
VAPOR DENSITY:	Not applicable
VOLATILE BY VOLUME (%):	Not applicable
MOLECULAR FORMULA:	Not Applicable

10. STABILITY AND REACTIVITY

HAZARDOUS POLYMERIZATION:	Will not occur
CHEMICAL INCOMPATIBILITIES:	Powerful oxidizers; fluorine, manganese trioxide, oxygen disulfide
HAZARDOUS DECOMPOSITION PRODUCTS:	None

11. TOXICOLOGICAL INFORMATION

TOXICOLOGY

Dust samples from these products have not been tested. They may contain respirable crystalline silica.

Crystalline silica

Some samples of crystalline silica administered to rats by inhalation and intratracheal instillation have caused fibrosis and lung cancer. Mice and hamsters, similarly exposed, develop inflammatory disease including fibrosis but no lung cancer.

Vermiculite

This product contains vermiculite. Some vermiculite deposits may contain other naturally occurring substances such as crystalline silica or asbestiform materials. Thermal Ceramics has relied upon supplier MSDSs to conclude that crystalline silica or asbestiform materials are not present, in regulated quantities, in the vermiculite used in this product.

EPIDEMIOLOGY

No studies have been undertaken on humans exposed to these products in occupational environments.

Crystalline silica

Exposure to crystalline silica can cause silicosis, and exacerbate pulmonary tuberculosis and bronchitis. IARC (Monograph vol. 68, 1997) concluded that "crystalline silica from occupational sources inhaled in the form of quartz or cristobalite is carcinogenic to humans (Group 1)", and noted that "carcinogenicity in humans was not detected in all industrial circumstances studied" and "may be dependent on inherent characteristics of the crystalline silica or on external factors affecting its biological activity".

12. ECOLOGICAL INFORMATION

Adverse effects of this material on the environment are not anticipated.

13. DISPOSAL INFORMATION

WASTE MANAGEMENT

To prevent waste materials becoming airborne during waste storage, transportation and disposal, a covered container or plastic bagging is recommended. Comply with federal, state and local regulations.

DISPOSAL

If discarded in its purchased form, this product would not be a hazardous waste under Federal regulations (40 CFR 261) Any processing, use, alteration or chemical additions to the product, as purchased, may alter the disposal requirements. Under Federal regulations, it is the waste generator's responsibility to properly characterize a waste material, to determine if it is a hazardous waste. Check local, regional, state or provincial regulations to identify all applicable disposal requirements.

14. TRANSPORT INFORMATION

U.S. DEPARTMENT OF TRANSPORTATION (DOT)

Hazard Class:	Not Regulated	United Nations (UN) Number:	Not Applicable
Labels:	Not Applicable	North America (NA) Number:	Not Applicable
Placards:	Not Applicable	Bill of Lading:	Product Name

INTERNATIONAL

Canadian TDG Hazard Class & PIN: Not regulated
Not classified as dangerous goods under ADR (road), RID (train) or IMDG (ship).

15. REGULATORY INFORMATION

UNITED STATES REGULATIONS

SARA Title III:	This product does not contain any substances reportable under Sections 302, 304, 313 (40 CFR 372). Sections 311 and 312 apply.
OSHA:	Comply with Hazard Communication Standards 29 CFR 1910.1200 and 29 CFR 1926.59 and Respiratory Protection Standards 29 CFR 1910.134 and 29 CFR 1926.103.
TSCA:	All substances contained in this product are listed in the TSCA Chemical Inventory
California:	"Silica, crystalline (airborne particles of respirable size)" is listed in Proposition 65, The Safe Drinking Water and Toxic Enforcement Act of 1986 as a chemical known to the State of California to cause cancer.

MATERIAL SAFETY DATA SHEET

Other States:	Crystalline silica products are not known to be regulated by states other than California; however, state and local OSHA and EPA regulations may apply to these products. Contact your local agency if in doubt.

INTERNATIONAL REGULATIONS

Canadian WHMIS:	Class D-2A Materials Causing Other Toxic Effects
Canadian EPA:	All substances in this product are listed, as required, on the Domestic Substance List (DSL).

16. OTHER INFORMATION

SARA TITLE III HAZARD CATEGORIES

Acute Health:	No	**Pressure Hazard:**	No
Chronic Health:	Yes	**Reactivity Hazard:**	No
Fire Hazard:	No		

MATERIAL SAFETY DATA SHEET

MSDS No: 154	Date Prepared: 09/06/1993	Current Date: 2/3/2003 Last Revised: (01/16/2003)

DEFINITIONS:

ACGIH:	American Conference of Governmental Industrial Hygienists
ADR:	Carriage of Dangerous Goods by Road (International Regulation)
CAA:	Clean Air Act
CAS:	Chemical Abstracts Service Registry Number
CERCLA:	Comprehensive Environmental Response, Compensation and Liability Act
EPA:	Environmental Protection Agency
EU:	European Union
f/cc:	Fibers per cubic centimeter
HEPA:	High Efficiency Particulate Air
HMIS:	Hazardous Materials Identification System
IARC:	International Agency for Research on Cancer
IATA:	International Air Transport Association
IMDG:	International Maritime Dangerous Goods Code
mg/m^3 :	Milligrams per cubic meter of air
mppcf:	Million particles per cubic meter
MSHA:	Mine Safety and Health Administration
NFPA:	National Fire Protection Association
NIOSH:	National Institute for Occupational Safety and Health
OSHA:	Occupational Safety and Health Administration
PEL:	Permissible Exposure Limit
PNOC:	Particulates Not Otherwise Classified
PNOR:	Particulates Not Otherwise Regulated
RCRA:	Resource Conservation and Recovery Act
RID:	Carriage of Dangerous Goods by Rail (International Regulation)
SARA:	Superfund Amendments and Reauthorization Act
Title III:	Emergency Planning and Community Right to Know Act
...Section 302:	Extremely Hazardous Substances
...Section 304:	Emergency Release
...Section 311:	MSDS/List of Chemicals
...Section 312:	Emergency and Hazardous Inventory
...Section 313:	Toxic Chemicals Release Reporting
STEL:	Short-Term Exposure Limit
TCLP:	Toxicity Characteristics Leaching Procedures (EPA)
TLV:	Threshold Limit Values (ACGIH)
TSCA:	Toxic Substance Control Act
WHMIS:	Workplace Hazardous Materials Information System (Canada)
29 CFR 1910.134 & 1926.103:	OSHA Respiratory Protection Standards
29 CFR 1910.1200 & 1926.59:	OSHA Hazard Communication Standards

Revision Summary:
1) MSDS revised in its entity with updated information.
2) Product "Therm-O-Flake Coating" added (see Section 1).

MSDS Prepared By: THERMAL CERAMICS ENVIRONMENTAL, HEALTH & SAFETY DEPARTMENT

DISCLAIMER

The information presented herein is presented in good faith and believed to be accurate as of the effective date of this Material Safety Data Sheet. Employers may use this MSDS to supplement other information gathered by them in their efforts to assure the health and safety of their employees and the proper use of the product. This summary of the relevant data reflects professional judgment; employers should note that information perceived to be less relevant has not been included in this MSDS. Therefore, given the summary nature of this document, Thermal Ceramics does not extend any warranty (expressed or implied), assume any responsibility, or make any representation regarding the completeness of this information or its suitability for the purposes envisioned by the user.

THIS PAGE INTENTIONALLY LEFT BLANK.

Y/DW-1661

Y-12

OAK RIDGE
Y-12
PLANT

MECHANICAL PROPERTIES OF A LOW DENSITY CONCRETE FOR THE NEW ES-2 SHIPPING/STORAGE CONTAINER INSULATION, IMPACT MITIGATION MEDIA AND NEUTRON ABSORBER

Raymon E. Oakes, Jr.
Development Division
Oak Ridge Y-12 Plant

April 10, 1997

Prepared by the
Oak Ridge Y-12 Plant
Oak Ridge, Tennessee 37831
managed by
LOCKHEED MARTIN ENERGY SYSTEMS, INC.,
for the
U.S. DEPARTMENT OF ENERGY
Under contract DE-AC05-84OR21400

MANAGED BY
LOCKHEED MARTIN ENERGY SYSTEMS, INC.
FOR THE UNITED STATES
DEPARTMENT OF ENERGY

UCN-13672 (2 11-97)

INTRODUCTION

The design, analysis and testing of new Shipping/Storage container design for enriched uranium, labeled ES-2, is underway at the Oak Ridge Y-12 Plant. To assure greater containment during an accidental impact or fire, a better insulating/energy-absorbing material is being sought for the outermost filler. A replacement for the presently used Celotex(R), a low density wood product, and plywood is desirable. A more fire retardant material with otherwise equal or better impact energy and neutron absorption is being sought.

Kaolite(R) 1600, a castable Portland cement-based product by Thermal Ceramics, contains vermiculite (expanded mica) instead of gravel or other high density aggregates. It is a low density, high temperature insulating material with non-recoverable impact energy absorption capabilities. The major components of Kaolite 1600 according to the manufacturers Product Information sheet are:

Alumina	Al_2O_3	9.6%
Silica	SiO_2	31.5%
Ferric Oxide	Fe_2O_3	6.7%
Titanium Oxide	TiO_2	1.0%
Calcium Oxide	CaO	29.8%
Magnesium Oxide	MgO	11.9%
Alkalies, as	Na_2O	1.8%

The purpose of this work is to quantify the mechanical properties of this product for a variety of thermal cures, test temperatures and neutron absorbing additives in a form useable for data input for finite element analysis of a variety of potential accident scenarios.

EXPERIMENTAL WORK

Test Types_ Four properties tests are conducted on the Kaolite 1600 material, Flexural Tensile Strength, Unconstrained Compressive Strength, Constrained Compressive Strength and Density.

All specimens are cast in containers the shape of the desired specimen. The vendors wet mix ratio of water/Kaolite, 36 quarts water to 50 lb Kaolite 1600 is used exclusively (473 cc water/315 g Kaolite used in laboratory size specimens). After mixing and packing in the molds, mild impacts from a plastic hammer against the mold sides are made until air bubbles ceased to rise to the top.

An electrically heated, liquid nitrogen cooled convection oven with +/-2EF control is used for elevated temperature cures and testing.

Tensile Strength_ Nine tensile strength values are obtained from cast and tested quarter-point, four-point bend specimens, 1 in wide x 1 in high x 8 in long. Each are tested over a 6-in support span and 3-in compression span, having the following very low outer fiber tensile strength and density:

average tensile strength = 19.4 psi, standard deviation 4.7 psi, and
average density = 21.2 lb/ft^3, standard deviation 1.0 lb/ft^3.

Low tensile strengths should not be detrimental in this application where the predominate failure mode is constrained compression.

Cure for the tensile specimens is 24 hr at 72EF plus 24 hr at 220EF, high enough to drive off free water but retain the water of hydration. Water of hydration is loosely bound to a number of cement components and can be driven off at elevated temperatures either by using elevated temperature curing or could occur in a hypothetical long term fire environment.

Unconstrained Compressive Strength_ Unconstrained or uniaxial compression test specimens are molded, cured and tested in 3-in diam polyurethane coated paper mailing tubes cut to 6-in heights with one end sealed. The cure is 24 hr at 72EF + 24 hr at 220EF. The tubes are thin and weak enough to add little strength to the specimen. Figure 1 shows the stress-strain curves and initial densities for three tests each at different test rates, including impact conditions (200 in/s). The increased strength values of the two highest test rates probably result from air entrapment in the cells. Also shown is the minor strength contribution of an empty paper mold.

Three deformation stages are associated with compression of low density materials containing voids (vermiculite is considered to be a void as well as any remaining air entrapments). First, the matrix surrounding the voids buckles, shown as the steep initial portion of the curves in Figure 1. The buckling stage is followed by a large strain region of compaction with minor stiffness increase. In the unconstrained compression tests large-scale shear failures occur across the sample prior to full compaction. Specimen buckling and gross shear failures forced the tests to be terminated. Constrained compression tests will show the steeper rise of more densified material.

Figure 2 is the integrated area under each of the three stress-strain curves of Figure 1, the cumulative work or energy per unit volume absorbed by the material as a function of strain.

Constrained, Hydrostatic Compression Tests_ Constrained compression tests simulate the deformation mode of accident conditions in the material as it is used in the ES-2 container. The material is constrained by filling the outer stainless steel drum. In the event of an accident the inner container and its contents must remain intact. In the absence of vacant volume compaction or hydrostatic compression is the only deformation mode available. Laboratory simulations require compressing a specimen in a rigid, tight closed-ended cylinder with a tight fitting piston. A 20k pound testing machine loads the piston. The cylinders are four-inch ID thick-walled pipe and the specimens are cast, cured and tested in the cylinder. The specimen height is 4.5 in.

This test is used to provide primary input to the Finite Element Analysis as well as a relevant means to evaluate repeatability, cures , test temperature and additive effects on properties.

Note that percent compressive strain and percent volume change values are equivalent for all constrained compression tests.

Repeatability_The five stress-strain curves of Figure 3 represent material cured for 24 hr at 72EF + 24 hr at 220EF + 48 hr at 500EF. Each specimen is individually mixed and cast. Initial measured densities are shown for each specimen. Repeatability of density and the stress-strain curves are good for this type material. Note the three stages of deformation, cell buckling , densification and the beginning of compression of densified material are present. Load limitations of the test machine prevent reaching full compaction, a near vertical rise in the curve.

Cure Effects_Both cure time and temperature have major effects on the constrained compressive properties of Kaolite 1600, Figures 4 and 5. Cures at higher temperatures and/or longer cure times remove the most water as noted by decreasing density. Material strength increases in proportion to the degree of water loss. Cure time/temperature would be volume dependent so these cures may only represent the limiting cure for the much larger ES-2 container.

Test Temperature Effects_Decreasing test temperature in well cured specimens, Figures 6 and 7, lowers both strength and energy absorption only slightly.

Neutron Absorbing Additives_Residual water, free or as hydrates, is the primary neutron absorber in Kaolite. Adequate water or other neutron absorber must be present before, during and after all ES-2 container accident scenarios. The 500EF cure should eliminate most of the free water and part of the water of hydration, at least in specimen sized lots where equilibrium temperatures are reached throughout the material. Higher temperatures are required to release all the water of hydration of two of the basic Portland cement components:

$$Fe_2O_3 \cdot xH_2O \quad (660\text{-}750^0F)$$
$$CaO_2 \cdot 8H_2O \quad (400^0F).$$

These hydrates during curing actually form very complex and unique hydrates. The disassociation temperatures for these complex hydrates are unique for each cement formulation and are unknown for Kaolite 1600. One requirement for the ES-2 container is survival in a fire environment of 1470EF for 0.5 hr without loss of seal of the inner container. Certainly loss of criticality protection must be assured in the same scenario.

Measured Kaolite densities cast and cured in ES-2 containers is about 29 lb/ft^3 when cured at 200EF for 48 hr. followed by 500EF for 48 hr. This is much higher than 21-22 lb/ft^3 in similarly cured laboratory samples, indicating either considerable residual water is retained in the ES-2 containers or large differences in compaction exist or both. Under long term fire conditions the amount of residual water and its distribution throughout the container is unknown.

Boron is a nonvolatile neutron absorber available in numerous chemical forms. Two forms, borax ($Na_2B_4O_7 \cdot 10H_2O$) and boron carbide (B_4C), are investigated as potential neutron absorbers. The required amount according to criticality calculations is 2.5% natural boron. Weight percentages of 11.3% borax or 3.0% boron carbide meet this requirement. Note that natural boron implies the isotopic ratio found in nature. Not all boron in the market meets this criteria.

Figure 8 and 9 show that borax degrades both the strength and energy absorption an unacceptable amount. Due to the high molecular weight of borax the amount of material needed to provide adequate boron is excessive.

Unlike borax, boron carbide is predominately boron and Figures 8 and 9 show that the needed amount and even double the needed amount does not degrade the Kaolite and would be an acceptable, nonvolatile neutron absorbing additive.

Bibliography

(1) *Handbook of Chemistry and Physics*, 60th Edition, Robert C. Weast, ed., CRC Press, Inc., Boca Raton, Florida 33431.

(2) *Concrete Admixtures Handbook, Properties, Science, and Technology*, V. S. Ramachandran, ed., Noyes Publications, Park Ridge, New Jersey.

Ka16fig1.xls

Figure 1_Kaolite 1600 Compressive Stress-Strain vs Strain Rate

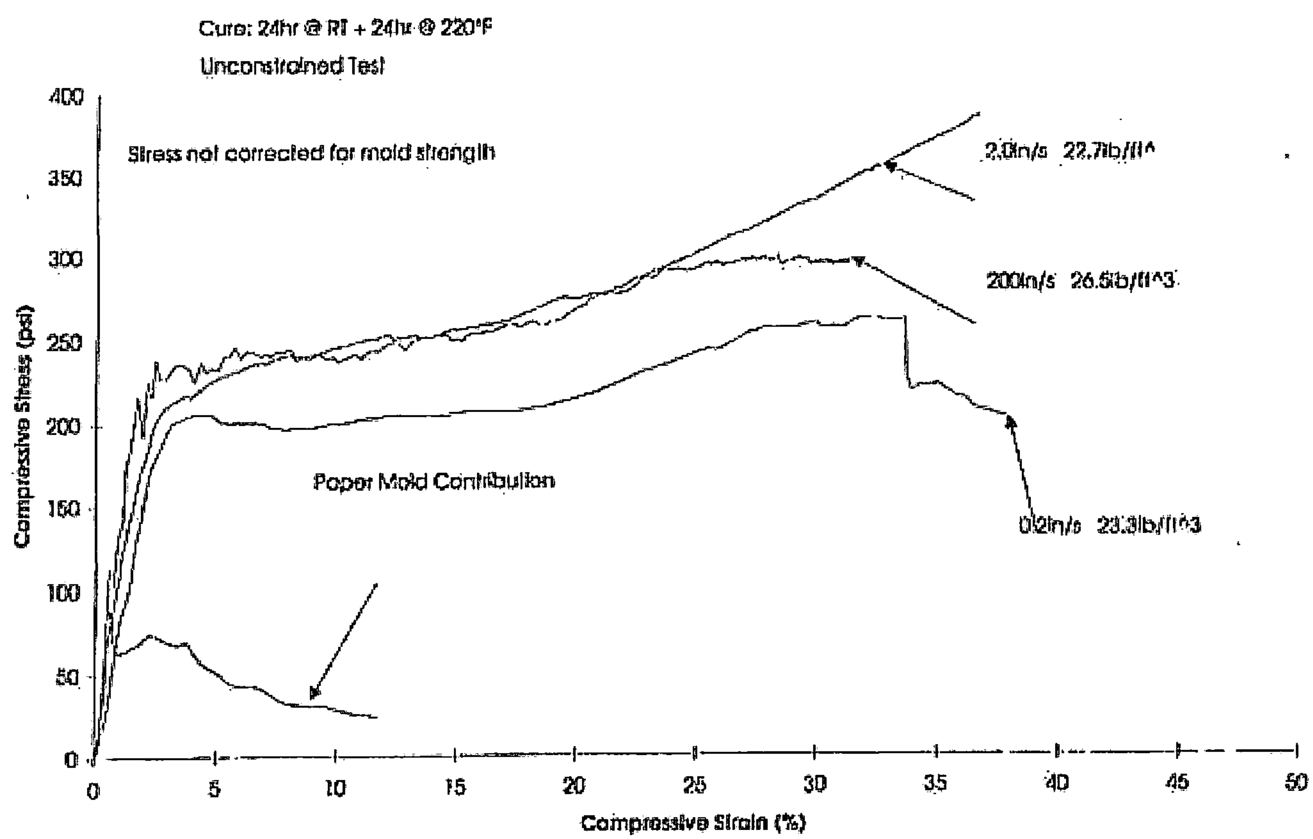

Ka16fig2.xlc

Figure 2_Kaolite 1600 Energy/Unit Volume vs Strain and Strain Rate

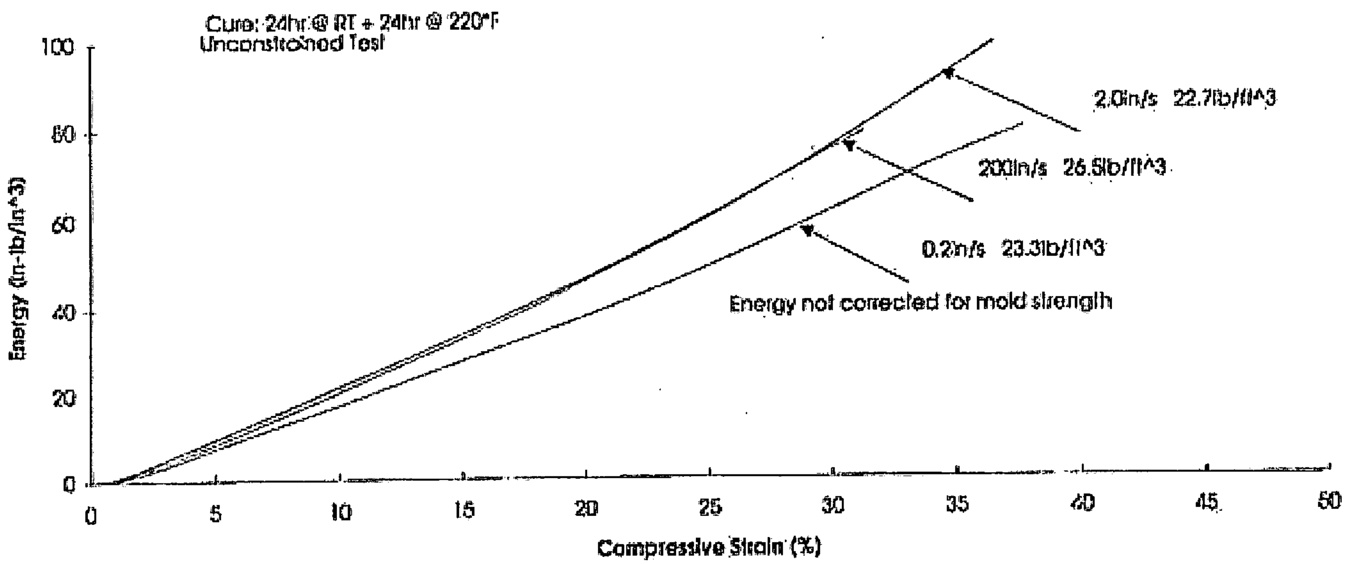

Ka16fig3.xlc

Figure 3_Kaolite 1600 Stress-Strain Curves, Repeatability Tests

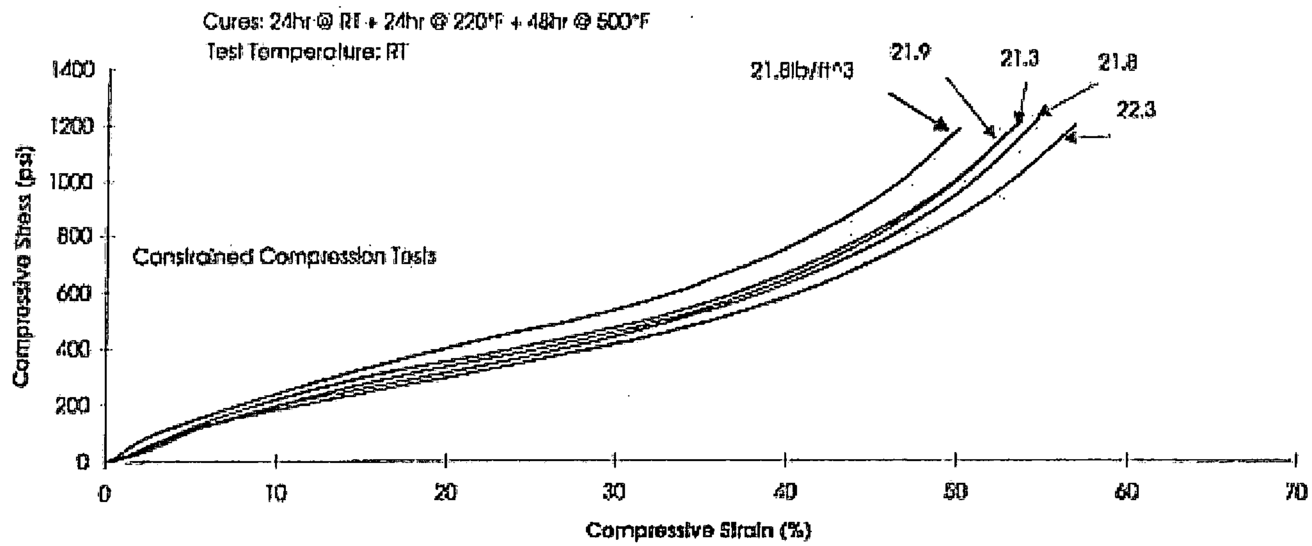

Ka16bg4.xlc

Figure 4_Kaolite 1600 Stress-Strain Curves for Different Cures

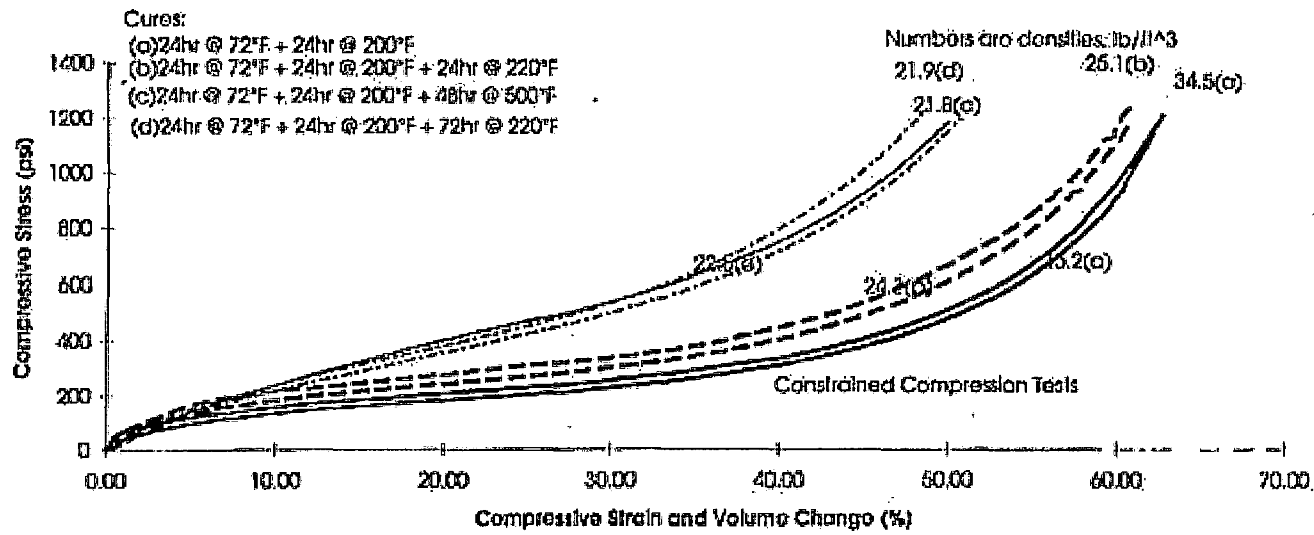

Ka16fig5.xls

Figure 5_Kaolite 1600 Energy-Strain Curves for Different Cures

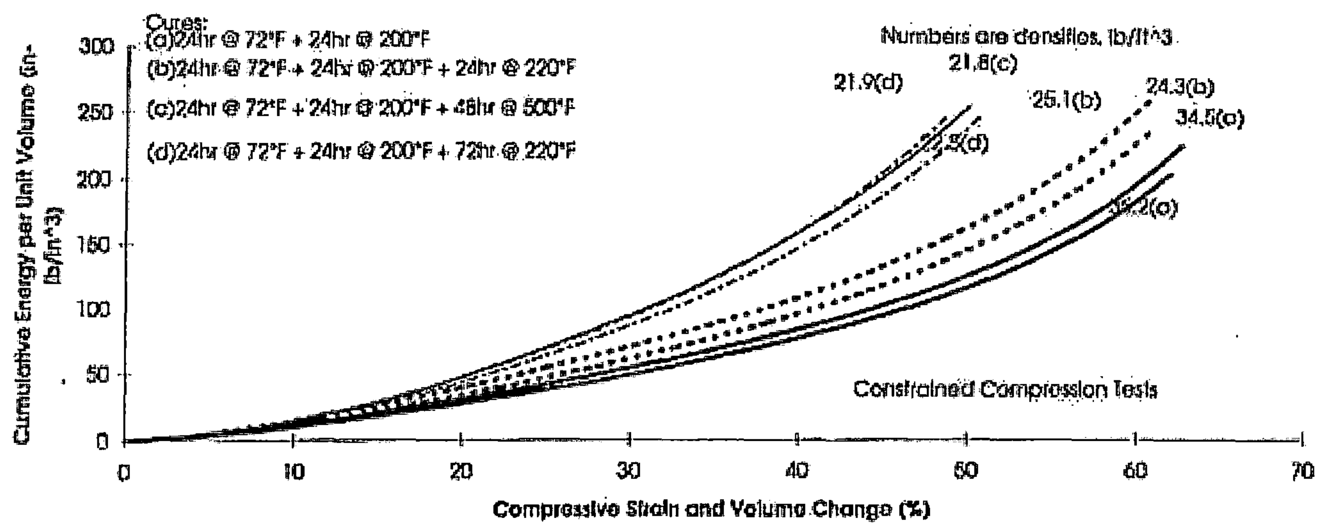

6

Figure 6_Kaolite 1600 Stress-Strain Curves for Different Test Temperatures

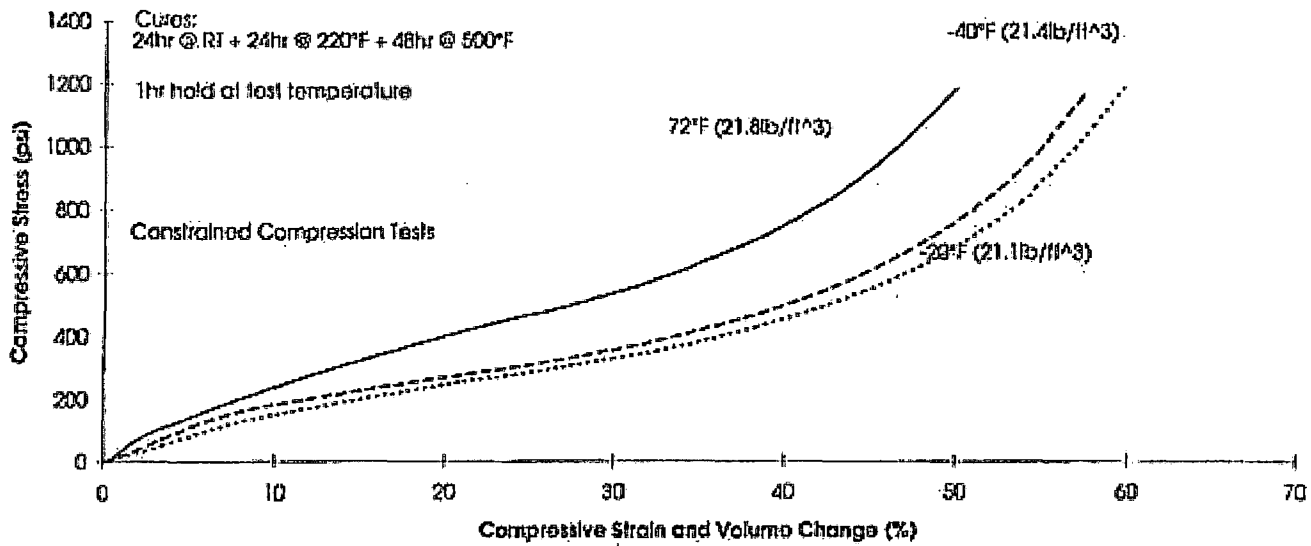

10

Ka16fig7.xlc

Figure 7_Kaolite 1600 Energy-Strain Curves for Different Test Temperatures

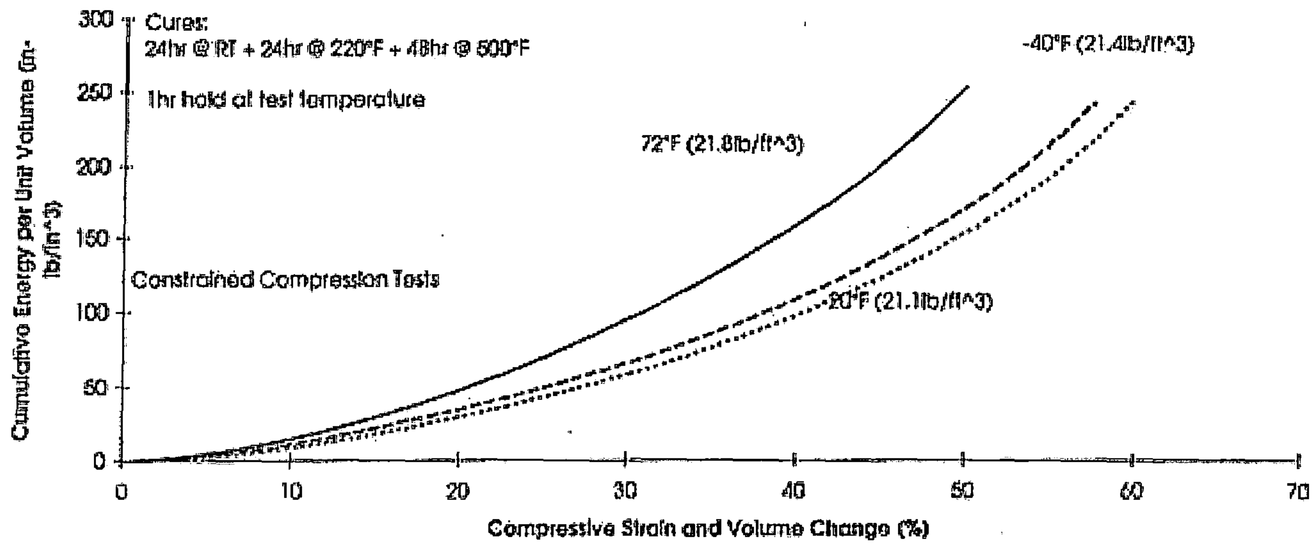

ORNL-TM-2003/49

Thermal Conductivity Measurements of Kaolite

Hsin Wang

Prepared by the
Thermophysical Properties User Center
High Temperature Material Laboratory
Metal and Ceramics Division

Oak Ridge National Laboartory
Oak Ridge, TN 37831-6064
Managed by UT-BATTELLE LLC.
For the
U.S. DEPARTMENT OF ENERGY
Under contract DE-AC05-00OR22725

Introduction

Testing was performed to determine the thermal conductivity of Kaolite 1600, which primarily consists of Portland cement and vermiculite. The material was made by Thermal Ceramics for refractory applications. Its combination of light weight, low density, low cost, and noncombustibility made it an attractive alternative to the materials currently used in ES-2 container for radioactive materials.

Mechanical properties and energy absorption tests of the Kaolite have been conducted at the Y-12 complex. Heat transfer is also an important factor for the application of the material. The Kaolite samples are porous and trap moisture after extended storage. Thermal conductivity changes as a function of moisture content below 100° C. Thermal conductivity of the Kaolite at high temperatures (up to 700° C) are not available in the literature. There are no standard thermal conductivity values for Kaolite because each sample is somewhat different. Therefore, it is necessary to measure thermal conductivity of each type of Kaolite. Thermal conductivity measurements will help the modeling and calculation of temperatures of the ES-2 containers. This report focuses on the thermal conductivity testing effort at ORNL.

Experimental

Thermal conductivity of the Kaolite was measured using a Hot Disk Thermal Constants Analyzer. A picture of the system is shown in Figure 1. A box furnace, with

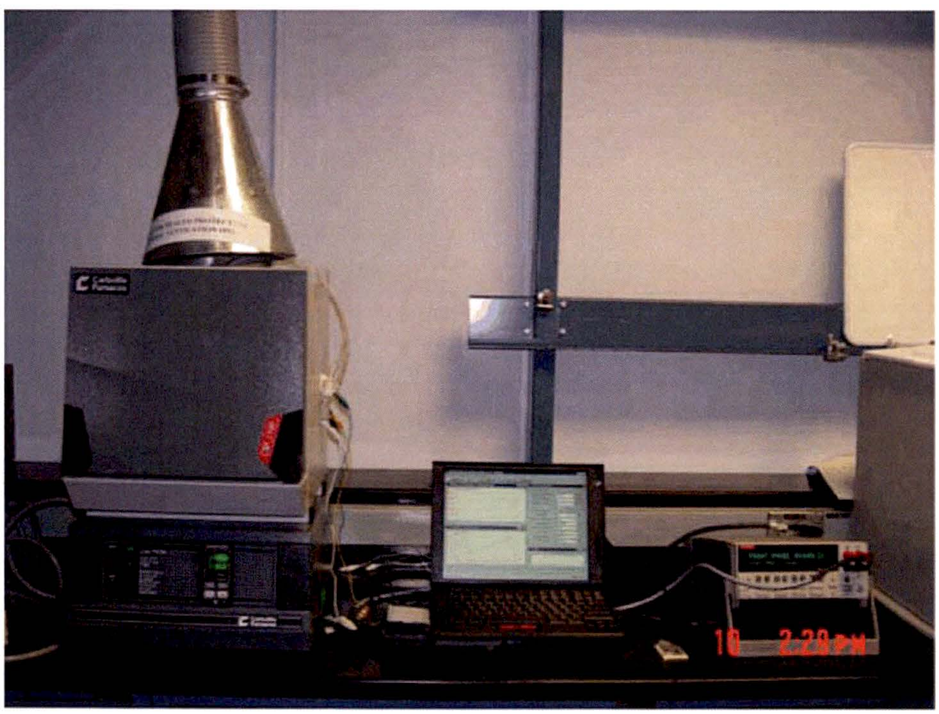

Figure 1. Experimental set up for thermal conductivity measurements.

maximum temperature of 1050° C, was used for high temperature tests. The Hot Disk sensor is a flat, thin, double-spiral nickel wire sandwiched between two mica sheets. The sensor is placed between two identical hockey-puck Kaolite samples (2" in diameter and 1" thick). During the measurement, the mica sensor acts as both a heater and a temperature sensor.

A typical test for Kaolite uses 0.05-watt constant-power heating for 80 seconds. The sensor temperature is recorded as a function of time. Thermal conductivity is then calculated directly from the experimental data. Detailed theory and experimental descriptions of the Hot Disk technique can be found in the references [1-3].

In order to perform high temperature measurements, special contacts were made from stainless steel. Four high temperature wires with insulation were connected to the mica sensor with the wires being fed through an opening on top of the furnace. A rectangular mica sheet with four screw holes was used as the support for the sensors. The four wires were connected to the contacts as shown in Figure 2. The mica sensor can be delaminated due to high temperature exposure, therefore, the sensor has to be replaced after a 600° C measurement. A heavy alloy block was placed on top of the sample to ensure good contact at the interface.

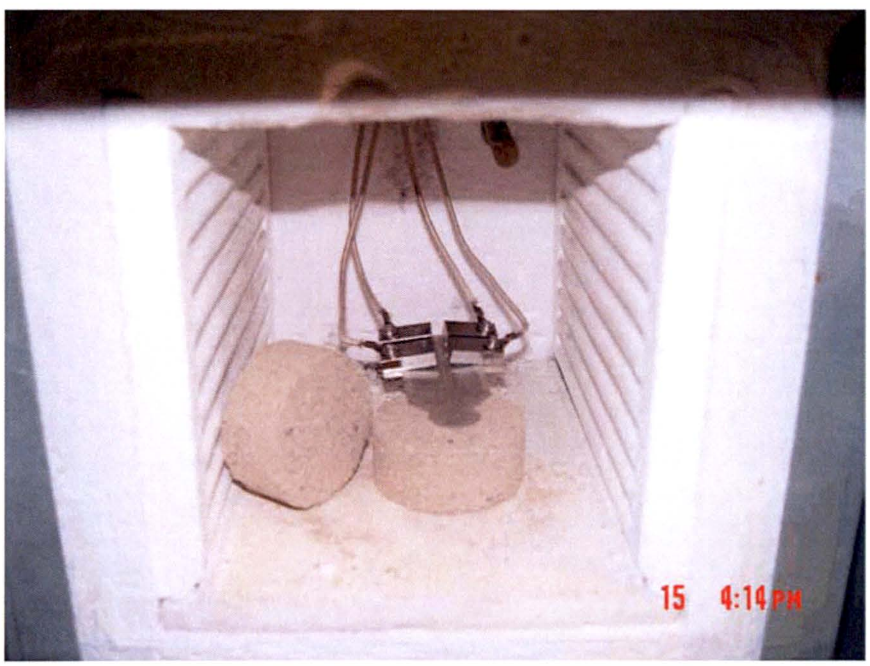

Figure 2. Kaolite samples and mica sensor used for high temperature testing.

Results and Discussion:

Thermal conductivities of six Kaolite samples were tested using the mica sensor. Since high temperature tests can destroy the sensor and only one set of samples was tested in the furnace, all the samples were tested at room temperature and then at 100° C. but only one sample was tested up to 600° C.

At room temperature and 100° C, the thermal conductivity values of the 6 Kaolite samples are similar, although the densities of the samples are grouped in 3 pairs at high, medium and low. The test results are shown in Table 1 for room temperature and Table 2 for 100° C. During the tests the humidity was not controlled in the laboratory or in the furnace. The samples did not have the same thermal history. For example, one set of sample was heated up from room temperature to 100° C, but the other 5 sets of samples had to wait outside the furnace. In addition, the local density of the sampling volume, i.e. ¾" diameter semi sphere, can also vary due the existence of large pores and

Table 1. Thermal conductivity of six Kaolite at 20° C (unit: W/mK)

Density (lb/ft3)	H 23.690	H 23.541	M 22.055	M 22.011	L 20.407	L 20.281
Test 1	0.188	0.183	0.152	0.198	0.165	0.172
Test 2	0.188	0.185	0.157	0.182	0.168	0.192
Test 3	0.191	0.181	0.167	0.198	0.169	0.181
Average	**0.189**	**0.183**	**0.158**	**0.192**	**0.167**	**0.181**
	High Density	**0.186**	**Medium Density**	**0.176**	**Low Density**	**0.175**

Table 2. Thermal conductivity of six Kaolite at 100° C (unit: W/mK)

Density ρ (lb/ft3)	H 23.690	H 23.541	M 22.055	M 22.011	L 20.407	L 20.281
Test 1	0.165	0.172	0.157	0.179	0.163	0.177
Test 2	0.152	0.172	0.157	0.191	0.163	0.179
Test 3	0.161	0.179	0.156	0.194	0.152	0.178
Average	**0.159**	**0.174**	**0.156**	**0.188**	**0.159**	**0.178**
	High Density	**0.166**	**Medium Density**	**0.172**	**Low Density**	**0.168**

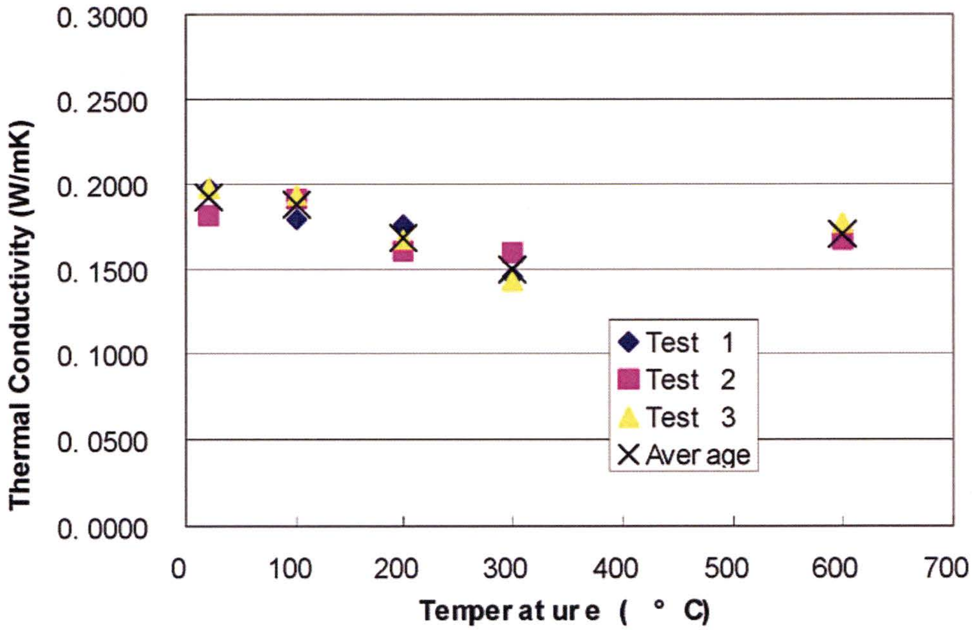

Figure 3. Thermal conductivity of Kaolite from room temperature to 600° C

Table 3. High Temperature Thermal Conductivity of Kaolite (unit: W/mK)

No. 323011258	Test 1	Test 2	Test 3	Average
20	0.1978	0.1815	0.1976	0.1923
100	0.1792	0.1913	0.1936	0.1880
200	0.1758	0.1601	0.1673	0.1677
300	0.1452	0.1592	0.1427	0.1490
600	0.1676	0.1665	0.1771	0.1704

density variation. Thermal conductivity results showed some scatter at these two temperatures.

The high temperature tests were performed on one medium density Kaolite sample. The thermal conductivity data are shown in Table 3. As shown in Figure 3, thermal conductivity values decreased as a function of temperature up to 300° C. This trend is consistent with ceramics and other insulating materials. At 600° C, thermal conductivity started to increase. This is also consistent with the fact that thermal radiation effect takes place in this temperature range. As temperature goes up, thermal conductivity of most insulating materials also goes up.

References:

[1] S.E. Gustafsson, E. Karawacki and M.N., Khan, *J. Phys.D.: Appl. Phys*, **1979**, 12, 1411.
[2] S.E. Gustafsson, *Rev. Sci. Instrum.*, **1991**, 62, 797
[3] V. Bohac, M.K. Gustavsson, L. Kubicar and S.E. Gustafsson, *Rev. Sci. Instrum.*, **2000**, 71, 2452

Distribution List:

Name	Bldg.	Mail Stop	#
C. N. Heatherly	9113	8206	1
J. L. Heck	9111	8201	1
S. T. Holder	9113	8206	1
G. A. Byington	9111	8201	1
M. R. Feldman	9113	8206	1
M. L. Goins	9112	8201	1
S. E. McClanahan	9113	8206	2
J.C. Walls	9201-2	8073	1
K. H. Luk	9201-2	8073	1
K. D. Handy	9201-2	8073	1
J. C. Anderson	9113	8206	1
J. H. Doyle	9113	8206	1
Jacob Y. Neal	9201-2	8073	1

BWXT Y-12
A BWXT/Bechtel Enterprise

Y-12 NATIONAL SECURITY COMPLEX

MANAGED BY BWXT Y-12, LLC FOR THE UNITED STATES DEPARTMENT OF ENERGY

UCN-13672 (10-00)

Y/DW-1890

Water Content and Temperature-Dependent Impact Properties of an Inorganic Cast Refractory Material

B. F. Smith
Technology Development

G. A. Byington
Mechanical, Manufacturing, and Specialty Engineering

February 14, 2003

LIMITED DISTRIBUTION

DISCLAIMER

Y/DW-1890

WATER CONTENT AND TEMPERATURE-DEPENDENT IMPACT PROPERTIES OF AN INORGANIC CAST REFRACTORY MATERIAL

B. F. Smith
Technology Development

G. A. Byington
Mechanical, Manufacturing, and
Specialty Engineering

Date of Issue: February 14, 2003

LIMITED DISTRIBUTION

Prepared by the
Y-12 National Security Complex
P.O. Box 2009
Oak Ridge, Tennessee, 37831-8169
Managed by BWXT Y-12, L.L.C.
for the
U.S. DEPARTMENT OF ENERGY
under contract DE-AC05-00OR22800

THIS PAGE INTENTIONALLY LEFT BLANK.

CONTENTS

FIGURES

TABLES

INTRODUCTION

Impact-absorbing media used in radioactive material packaging systems have historically left much to be desired. Common materials included woods, papers, cardboards, foams, and other hydrocarbons. While relatively easy to install, these types of materials generate toxic gases, are flammable, and are prone to rupture the container in an overheating scenario.[1]

Kaolite 1600 primarily consists of portland cement and vermiculite.[2] This ceramic was originally intended for use in refractory applications by its manufacturer, Thermal Ceramics. Its combination of light weight, low density, low cost, and noncombustibility made Kaolite an attractive alternative to the materials mentioned above for use in shipping packages.[3] A variety of mechanical property tests were performed in the past on Kaolite specimens to gage its selection and effectiveness as an impact absorber in the ES-2 shipping package container. The mechanical properties included tensile strength, unconstrained compressive strength, and constrained compressive strength. Since the ES-2 will primarily contain radioactive materials, the neutron-absorbing properties of Kaolite are important. Since boron is a good neutron absorber, the addition of boron-containing compounds to Kaolite was proposed, but their effect on the mechanical properties of Kaolite had to be measured. For this reason, the strength and energy absorption of Kaolite that contained borax and boron carbide were also measured. If boron-containing compounds are not mixed with standard Kaolite, the only compound present that can absorb neutrons is the water of hydration.[4]

The ES-2 shipping package design was modified and renamed the ES-2100. During the production of 100 ES-2100 shipping containers, 280 insulation samples were taken. An insulation sample was taken for each 50-lb bag of material mixed. These constrained compressive production-run test samples were cast approximately 4 in. tall in a 4-in. schedule 40 steel pipe 6.5 in. long.

All of the samples were statically evaluated on the basis of their density. The upper and lower densities were statically rejected based upon the normal distribution probability of 90%, which rejected 11 high- and 13 low-density specimens. Three small groups' high, middle, and low densities containing eight samples each were made from the remaining samples. Each of the density groups was divided into three testing sets. Two of the test sets of four specimens were used for temperature-dependent constrained compressive testing and for dehydration testing. The third sample set of two specimens was used for temperature-dependent thermal conductivity testing performed at Oak Ridge National Laboratory.

This work follows up on the mechanical property testing previously performed on Kaolite but concentrates on constrained compression testing and measuring the water of hydration and latent water reabsorbed from air. No further tensile tests or unconstrained compression tests were performed. No investigations into the effects of boron-containing compounds were done, either. Previous mechanical testing was performed on specimens that were mixed in very small batches in a laboratory environment. The main purpose of this work is to ensure that Kaolite mixed according to Manufacturing Process Specification No. Y/EN-5984[5] in a production environment is as strong as that mixed in a lab.

EXPERIMENTAL PROCEDURE

It was determined that 24 Kaolite 1600 specimens would be impact tested; 12 tested at 100°F and 12 tested at –40°F. Each set would contain four each of high-, medium-, and low-density specimens. All specimens would be subsequently heated to 1600°F to drive off the water of hydration and the latent water reabsorbed from air. The difference between the initial weight and the final weight would be the water of hydration and reabsorbed from air weight. Densities were calculated for each specimen and compared to the manufacturer's calculated values.

IMPACT TESTING

Each specimen consisted of a Kaolite plug, measuring 4-in. in diameter by 4 in. tall, inside a 6.5-in.-long, 4-in. schedule 40 steel pipe. One end of the plug was flush with the end of the pipe. The steel pipe of each specimen was engraved with its mix control number (MCN). A 4-in. schedule 40 pipe was specified in order to withstand the anticipated pressure generated during a constrained compression test. All impact testing was to be performed at the fastest readily obtainable speed. The machine that met this requirement was a 20,000-lb_f-capacity servohydraulic load frame with an actuator (hydraulic piston) that can reach 200 in./s. Compression platens of 3⅞-in. diameter were used. Test fixtures were designed and fabricated. The standard load cell used during slow-speed tests could not be used with high-speed tests, so a Kistler quartz force transducer was used in its place. The test fixtures were designed such that each specimen would be compressed to 50% strain. Typically, the deformation of a specimen is measured with an external sensor such as an extensometer, strain gage, or external linear variable differential transformer (LVDT). Measurements of extension or compression can be taken using the LVDT that is inside the hydraulic actuator, but this is not usually done since it introduces the overall deflection of the load frame into the deflection reading of the specimen. The maximum deflection of the load frame is about 0.040 in., which is negligible compared to the 2-in. deflection of the specimen. Thus, the LVDT internal to the actuator would be used to measure the compression of the specimen. Figure 1 shows that several extenders had to be used to allow for the height of the environmental chamber in which all tests were performed. Calculations showed that the extenders would buckle under a load of approximately 74,000 lb_f, which is significantly more than the 20,000-lb_f maximum capacity of the load frame. Since testing would be done at elevated and lowered temperatures, each specimen would need to soak until the interior of the specimen reached its test temperature. Rough calculations showed that a soak time of 39 h would get the specimen to within 10% of the test temperature. All specimens were soaked significantly longer than 39 h. The 100°F specimens were soaked for approximately 100 h, and the –40°F specimens were soaked for approximately 300 h. Tables 1 and 2 summarize these testing conditions.

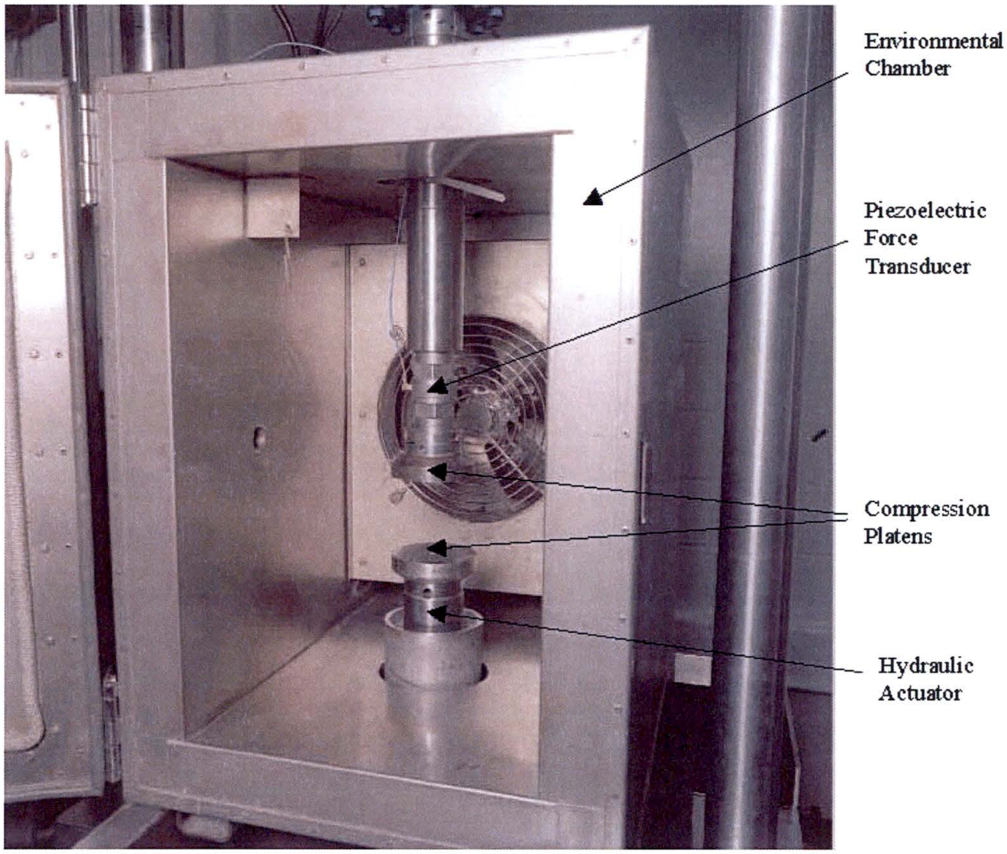

Fig. 1. Impact testing apparatus.

Table 1. Test conditions for Kaolite specimens tested at 100°F

MCNID	Heating time (h)	Density group	Documented density (lb/ft^3)	Density gain[a] (lb/ft^3)	Density before heating (lb/ft^3)	Heating density change (lb/ft^3)	Density after heating (lb/ft^3)	Average test velocity (in./s)
411011216	101.25	Low	20.27	1.43	21.70	−0.15	21.55	192.9
402011246	120.42	Low	20.35	1.82	22.17	−0.20	21.97	190.6
419011046	93.92	Low	20.42	2.74	23.16	−0.08	23.08	189.7
406011219	98.80	Low	20.47	3.07	23.54	−0.06	23.48	194.6
222011053	100.85	Mid	21.98	1.46	23.44	−0.17	23.27	191.7
309011000	102.25	Mid	22.06	1.04	23.10	−0.16	22.94	192.3
406011232	93.67	Mid	22.06	2.44	24.50	−0.09	24.41	192.6
425011101	96.90	Mid	22.06	2.34	24.40	−0.09	24.31	195.3
316011054	94.40	High	23.49	-0.78	22.71	−0.07	22.64	186.8
425011046	93.00	High	23.53	3.44	26.97	−0.10	26.87	183.5
118010847	101.65	High	23.68	1.48	25.16	−0.16	25.00	185.1
425011329	53.72	High	23.71	3.17	26.88	−0.25	26.63	

[a] It is assumed that the change in density is latent water.

Table 2. Test conditions for Kaolite specimens tested at −40°F

MCNID	Cooling time (h)	Density group	Documented density (lb/ft^3)	Density gain[a] (lb/ft^3)	Density before cooling (lb/ft^3)	Cooling density change (lb/ft^3)	Density after cooling (lb/ft^3)	Average test velocity (in./s)
508010845	338.48	Low	20.28	2.64	22.92	0.08	23.00	192.3
316011150	362.03	Low	20.40	1.71	22.11	0.09	22.20	187.7
425010912	340.38	Low	20.41	2.33	22.74	0.09	22.83	191.7
508010830	364.87	Low	20.47	2.65	23.12	0.11	23.23	192.4
326011220	337.45	Mid	21.99	1.78	23.77	0.11	23.88	185.6
301010815	361.40	Mid	22.06	2.20	24.26	0.10	24.36	188.7
326011239	339.62	Mid	22.06	2.20	24.26	0.10	24.36	185.8
426011155	364.23	Mid	22.06	1.88	23.94	0.09	24.03	185.7
425011235	339.02	High	23.53	3.16	26.69	0.11	26.80	182.0
425010941	363.58	High	23.53	2.71	26.24	0.07	26.31	183.7
323010953	360.85	High	23.56	1.93	25.49	0.08	25.57	174.6
425011007	337.13	High	23.71	3.57	27.28	0.09	27.37	189.9

[a] It is assumed that the change in density is latent water.

DEHYDRATION TESTING

The water content of Kaolite determines the neutron-absorbing properties. Properly cured Kaolite should have very little latent water, but may have a significant amount of water of hydration. This water of hydration can be driven off by heating the specimens above a critical temperature, 1600°F. Each specimen was heated at this temperature until consecutive measurements differed by <0.1%. Each plug was removed from its metal sleeve using a larger, 200,000-lb$_f$ capacity load frame. This load frame was used instead of the 20,000-lb$_f$ capacity machine since its larger actuator area and load cell area simplified setting up fixturing. During heating, each compacted Kaolite plug was placed into an Inconel crucible, which was placed in a small lab furnace. A metal crucible had to be used because ceramic ones would not withstand the thermal shock associated with repeated removal from the furnace into cool, room-temperature air.

RESULTS

IMPACT TESTING

Figure 2 shows average compressive stress-strain curves for specimens tested at 100°F. Each curve is the average of the specimens in a density group, high, medium, or low. Using the average density group values dampened some of the noise in the gathered data. The average density of the high-density group was documented as 23.6 lb/ft^3. The average density of the medium density group was documented as 22.0 lb/ft^3. The average density of the low-density group was documented as 20.4 lb/ft^3. These curves were generated by averaging the stresses at discrete strain points at intervals of 1% strain. Figure 3 shows the average compressive stress-strain curves for specimens tested at −40°F. Figure 4 repeats the average compressive stress-strain curves shown in Figs. 2 and 3 and adds to them upper, lower, and average bounding curves.

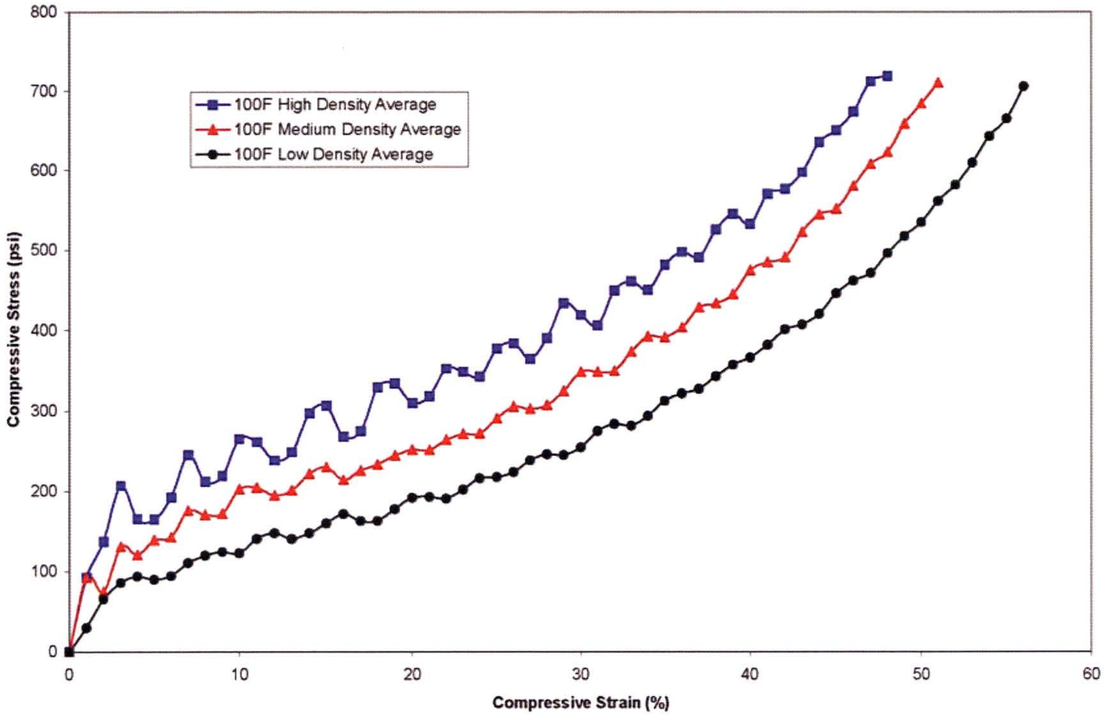

Fig. 2. Average stress-strain curves for Kaolite specimens tested at 100°F.

5

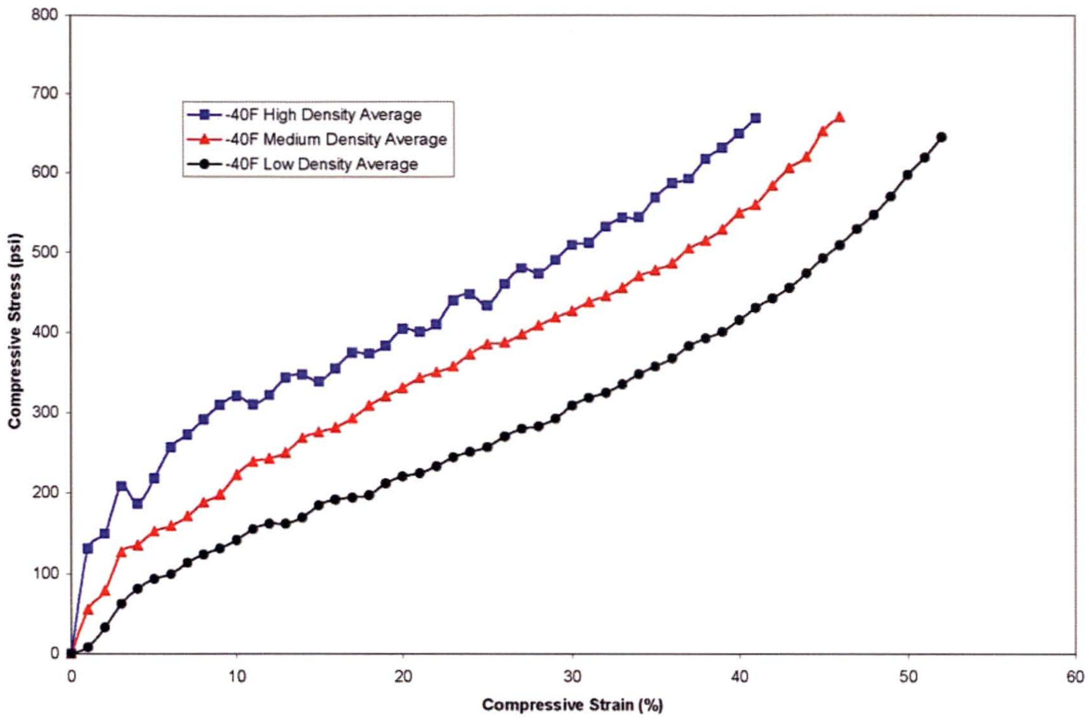

Fig. 3. Average stress-strain curves for Kaolite specimens tested at -40°F.

6

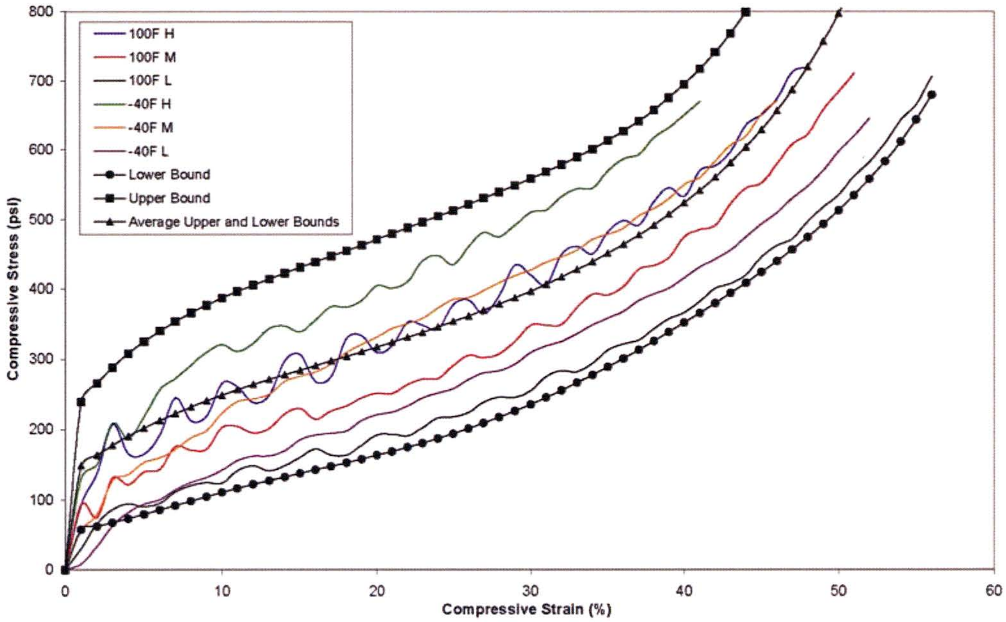

Fig. 4. Average stress-strain curves, upper and lower bounding curves, and average of upper and lower bounding curves.

7

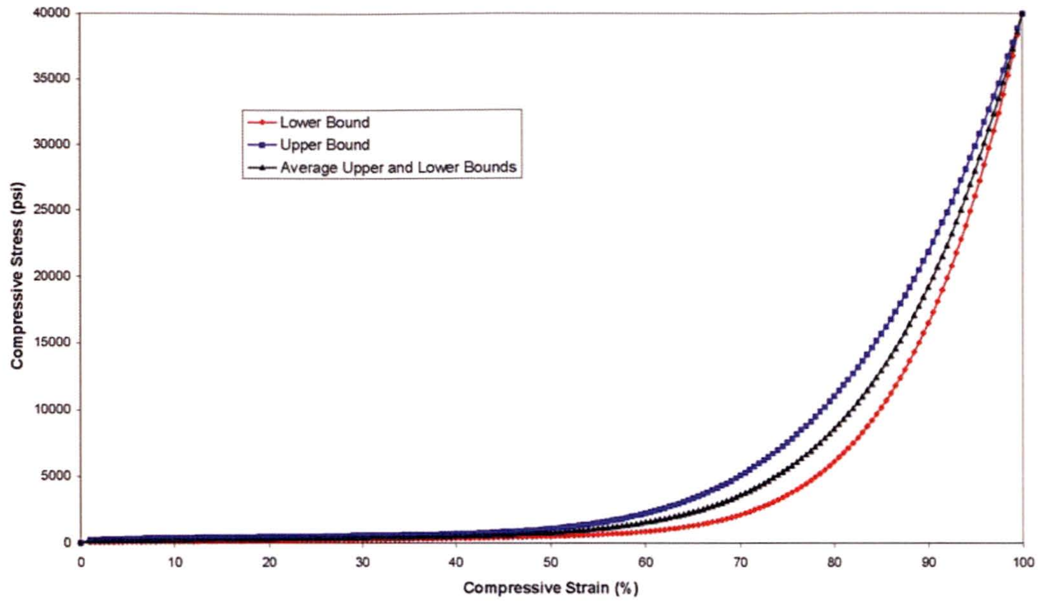

Fig. 5. Upper and lower bounding curves, average of upper and lower bounding curves, all extrapolated to 100% compressive strain.

8

The bounding curves were generated at the extreme noise peaks. The strongest material created the upper bound, and it was the –40°F high-density group. The weakest material generated the lower bounding curve, and it was the 100°F low-density group. Table 3 shows the coefficients for the equations of the bounding curves between 1 and 100% strain. A value of 40,000 psi at 100% strain was used with the collected data to create a smooth curve beyond the tested values for computer drop test simulations. A straight line is assumed to be from zero stress and strain to the curve value at 1% strain.

Table 3. Coefficients to upper and lower bounding equations

$\sigma = a + b\varepsilon + c\varepsilon^2 + d\varepsilon^3 + e\varepsilon^4 + f\varepsilon^5 + g\varepsilon^6$							
	a	**b**	**c**	**d**	**e**	**f**	**g**
Upper	209.2	31.96	–2.244	0.1050	–0.00253	2.78×10^{-5}	7.06×10^{-8}
Average	131.5	17.29	–0.7443	0.01878	4.31×10^{-5}	-8.36×10^{-6}	1.06×10^{-7}
Lower	53.86	2.613	0.7550	–0.06748	0.002618	-4.45×10^{-5}	2.83×10^{-7}

DEHYDRATION TESTING

Tables 4, 5, and 6 show the initial weight of each specimen and total water loss after heating at 1600°F. The percent of the initial weight of water is given in the third column. No data are included for MCNIDs 0425011007 and 0425011329 since their initial weights were mistakenly not measured. Without the initial weight, it is impossible to know how much water was lost through heating.

Table 4. High-density dehydration data

MCNID	Initial weight (lb)	Water loss (lb)	Initial weight (%)	Documented density (lb/ft^3)	Density before dehyd (lb/ft^3)	Dehyd water lost (lb/ft^3)	Water gained (lb/ft^3)	Initial water (lb/ft^3)
0316011054	0.6189	0.0842	13.60	23.49	22.64	3.08	-0.85	3.93
0425010941	0.7098	0.0982	13.83	23.53	26.31	3.64	2.78	0.86
0425011046	0.7135	0.0934	13.09	23.53	26.87	3.52	3.34	0.18
0425011235	0.7190	0.0961	13.37	23.53	26.80	3.58	3.27	0.31
0323010953	0.7250	0.0996	13.74	23.56	25.57	3.51	2.01	1.50
0118010847	0.7022	0.0946	13.47	23.68	26.63	3.59	2.95	0.64
0425011007								
0425011329								
Average	0.6981	0.0944	13.52	23.55	25.80	3.49	2.25	1.24

Table 5. Medium-density dehydration data

MCNID	Initial weight (lb)	Water loss (lb)	Initial weight (%)	Documented density (lb/ft^3)	Density before dehyd (lb/ft^3)	Dehyd water lost (lb/ft^3)	Water gained (lb/ft^3)	Initial water (lb/ft^3)
0222011053	0.6104	0.0844	13.83	21.98	23.27	3.22	1.29	1.93
0326011220	0.6851	0.0928	13.55	21.99	23.88	3.24	1.89	1.35
0309011000	0.6612	0.0879	13.29	22.06	22.94	3.05	0.88	2.17
0301010815	0.6800	0.0978	14.38	22.06	24.36	3.50	2.30	1.20
0326011239	0.6849	0.0945	13.80	22.06	24.36	3.36	2.30	1.06
0406011232	0.6586	0.0879	13.35	22.06	24.41	3.26	2.35	0.91
0426011155	0.6651	0.0876	13.17	22.06	24.03	3.16	1.97	1.19
0425011101	0.6772	0.0950	14.03	22.06	24.31	3.41	2.25	1.16
Average	0.6653	0.0910	13.68	22.04	23.95	3.28	1.90	1.37

Table 6. Low-density dehydration data

MCNID	Initial weight (lb)	Water loss (lb)	Initial weight (%)	Documented density (lb/ft^3)	Density before dehyd (lb/ft^3)	Dehyd water lost (lb/ft^3)	Water gained (lb/ft^3)	Initial water (lb/ft^3)
0411011216	0.5180	0.0710	13.71	20.27	21.55	2.95	1.28	1.67
0508010845	0.6320	0.0897	14.19	20.28	23.00	3.26	2.72	0.54
0402011246	0.6025	0.0825	13.69	20.35	21.97	3.01	1.62	1.39
0316011150	0.6348	0.0876	13.80	20.40	22.20	3.06	1.80	1.26
0425010912	0.6299	0.0888	14.10	20.41	22.83	3.22	2.42	0.80
0419011046	0.6391	0.0909	14.22	20.42	23.08	3.28	2.66	0.62
0508010830	0.6404	0.0912	14.24	20.47	23.23	3.31	2.76	0.55
0406011219	0.6418	0.0825	12.85	20.47	23.48	3.02	3.01	0.01
Average	0.6173	0.0855	13.85	20.38	22.67	3.14	2.28	0.86

Additional evaluations of the water loss and density changes need to be examined further. On the average the samples gained about 1.9 lb/ft^3 in density after manufacturing and lost 3.28 lb/ft^3 during the dehydration testing. The difference between these average density values is assumed to be water, and the as-cast manufactured water content is 1.37 lb/ft^3. Therefore, the cast insulation Kaolite specimens used for this testing tends to absorb water from the air if it is available.

DISCUSSION

IMPACT TESTING

Generally, the constrained compressive strength of Kaolite is proportional to its density and inversely proportional to its temperature. For each temperature group and for each strain point, the stress in the specimen was higher at the next higher density group. Also, for a given density group, the specimens tested at low temperatures displayed higher stress levels than those tested at high temperatures. (Refer to Figs. 2 and 3.)

DEHYDRATION TESTING

During heating at 1600°F, the Kaolite specimens lost between 12.85% and 14.38% of their initial weight as water. The high-density group lost an average of 13.52% of its initial weight as water. The medium-density lost an average of 13.67% and the low-density group lost an average of 13.85%. In general, the percentage of water loss by weight is inversely proportional to the density. The less dense specimens lost a larger percentage of their starting weight as water.

REFERENCES

1. *Advantages of Using a Fireproof Inorganic Cast Refractory Material in Hazardous Content Shipping Packages*, Y/LF-565, compiled by Y-12 Nuclear Package Systems, Lockheed Martin Engineering Systems, Inc., Manufacturing Engineering, Engineering Analysis, Lockheed Martin Energy Systems, Inc., Oak Ridge Y-12 Plant, Oak Ridge, Tennessee, November 1998.

2. Thermal Ceramics, *Kaolite Super Lightweight Insulating Castables*, Augusta, Georgia, http:/www.thermalceramics.com.

3. Byington et al., "Fireproof Impact Limiter Aggregate Packaging Inside Shipping Containers," U.S. Patent No. US 6,299,850 B1, October 9, 2001.

4. Oakes, R., *Mechanical Properties of a Low Density Concrete for the New ES-2 Shipping/Storage Container Insulation, Impact Mitigation Media and Neutron Absorber*, Y/DW-1661, Lockheed Martin Energy Systems, Inc., Oak Ridge Y-12 Plant, Oak Ridge, Tennessee, April 1997.

5. *For Casting Kaolite 1600™ into ES Shipping Containers*, Manufacturing Process Specification No., Y/EN-5984, Rev. A, February 11, 2000.

DISTRIBUTION

Y-12 National Security Complex

Anderson, J. C., 9113, MS-8206
Byington, G. A., 9111, MS-8201 (2)
Doyle, J. H., 9113, MS-8206
Feldman, M. R., 9113, MS-8206
Goins, M. L., 9112, 8201
Handy, K. D., 9201-2, MS-8073 (2)
Heatherly, C. N., 9113, MS-8206
Heck, J. L., 9111, MS-8201
Holder, S. T., 9113, MS-8206
Kitzke, K. A., 9203, MS-8084
Luk, K. H., 9201-2, MS-8073
McClanahan, S. E., 9113, MS-8206 (2)
Neal, J. Y., 9201-2, MS-8073
Smith, B. F., 9203, MS-8084
Walls, J.C., 9201-2, MS-8073
Y-12 Plant Records—RC